



COPYRIGHT AND USE OF THIS THESIS

This thesis must be used in accordance with the provisions of the Copyright Act 1968.

Reproduction of material protected by copyright may be an infringement of copyright and copyright owners may be entitled to take legal action against persons who infringe their copyright.

Section 51 (2) of the Copyright Act permits an authorized officer of a university library or archives to provide a copy (by communication or otherwise) of an unpublished thesis kept in the library or archives, to a person who satisfies the authorized officer that he or she requires the reproduction for the purposes of research or study.

The Copyright Act grants the creator of a work a number of moral rights, specifically the right of attribution, the right against false attribution and the right of integrity.

You may infringe the author's moral rights if you:

- fail to acknowledge the author of this thesis if you quote sections from the work
- attribute this thesis to another author
- subject this thesis to derogatory treatment which may prejudice the author's reputation

For further information contact the University's Director of Copyright Services

sydney.edu.au/copyright

Learning and Reacting with Inaccurate Prediction: Applications to Autonomous Excavation

Guilherme Jorge Maeda MSc (Tokyo Inst. Tech.)

A thesis submitted in fulfillment
of the requirements of the degree of
Doctor of Philosophy



Australian Centre for Field Robotics
School of Aerospace, Mechanical and Mechatronic Engineering
The University of Sydney

Submitted March 2013; revised September 2013

Declaration

I hereby declare that this submission is my own work and that, to the best of my knowledge and belief, it contains no material previously published or written by another person nor material which to a substantial extent has been accepted for the award of any other degree or diploma of the University or other institute of higher learning, except where due acknowledgement has been made in the text.

 Guilherme Maeda
2013.09.23
18:40:32 +10'00'

Guilherme Jorge Maeda

September 23, 2013

Abstract

Motivated by autonomous excavation, this work investigates solutions to a class of problem where disturbance prediction is critical to overcoming poor performance of a feedback controller, but where the disturbance prediction is intrinsically inaccurate. Poor feedback controller performance is related to a fundamental control problem: due to causality there is only a limited amount of disturbance rejection that feedback compensation can provide. It is known, however, that the use of predictive compensation can improve the disturbance rejection of a control system beyond the limitations of feedback. While prediction is desirable in a controller, the problem in excavation is that disturbance predictions are prone to error due to the variability and complexity of soil-tool interaction forces.

This work proposes the use of iterative learning control to map the repetitive components of excavation forces into feedforward predictive compensation commands. Although experimental results show that preemptive disturbance compensation improves excavation performance, the non-repetitive nature of soil-tool interaction forces when digging is a source of inaccurate predictions. To explicitly address the use of imperfect predictive compensation, a disturbance observer is used to estimate the prediction error rather than the disturbance. To quantify inaccuracy in prediction, a feedforward model of excavation disturbances is interpreted as a communication channel that transmits corrupted disturbance previews, for which metrics based on the sensitivity function exist.

During field trials the proposed method demonstrated the ability to iteratively achieve a desired dig geometry, independent of the initial feasibility of the excavation passes in relation to hydraulic actuator flow saturation. Under this iterative method predictive commands adapted to different soil conditions and passes were repeated autonomously until a pre-specified finish quality of the trench was achieved. Evidence of improvement in disturbance rejection is presented as a comparison of sensitivity functions of systems with and without the use of disturbance compensation given by feedforward action, also referred to as disturbance previews.

Autonomous excavation is one of the oldest challenges in field robotics; despite almost three decades of research no commercial deployment of a fully autonomous excavator has been reported to date. In the literature, proposed solutions have required stringent preconditions, such as laser scanning of terrain profiles in dusty and harsh environments and the design of behaviour-based control actions using knowledge from skilled operators. These requirements increase the difficulty of implementing the controller. Control solutions in this work focused on simplicity of implementation: general and straightforward reference-tracking control methods were preferred over excavation-tailored formulations. The benefit is that the proposed controller has potential applications to other processes where a plant is subject to large and approximately repetitive disturbances.

Acknowledgements

First and foremost, I would like to thank my supervisors David Rye and Ian Manchester for their support and guidance. David always made time to meet, discuss and give me feedback. His experience and guidance have been invaluable to me not only as a researcher but also as a person. I would like to thank Ian for his guidance in dynamics and control theory. His advice brought a new direction and a new level to my research.

I would like to thank Surya Singh whose enthusiastic approach and passion for robotics and teaching are admirable. As my past supervisor, the meetings and discussions I had with Surya were always exciting and had a huge influence on my research. I also would like to thank Hugh Durrant-Whyte for giving me freedom when advising and for sharing his experience and vision of field robotics.

I would like to thank the past and present technical staff of the Field Robotics Lab for their support with the experimental platform: Pak Hung (Victor) Chan, Mark Calleja, Dharmapriva C. (DC) Bandara, Craig Rodgers, and Tim Miller. I would also like to thank Stephen Burgun for supporting the experiments at the farm, Bruce Crundwell for assisting with the crane and for assembling the load pins on the excavator arm, and Ross Barker from the School of Civil Engineering for providing and explaining the use of the soil penetrometer.

In particular I would like to thank Javier Martinez and Seong Ho Lee for their support during the several field trials—for standing outside from 7 am in wet and cold weather so that I could do the experiments that are now part of this document. I will always be indebted to you for that. I also would like to thank Hadrien Vbra for the long hours we spent in the Field Lab trying to implement our first controllers.

I would like to thank Vitor Guizilini and Victor Cano who, despite being busy with their own research, more than once were “voluntarily selected” to have the privilege of being in charge of the radio emergency stop. I want to thank Sildomar Monteiro for introducing me to the ACFR, and for the nice chats about research and life.

Finally, I would like to thank my family and especially my wife, Yoshiko, to whom I dedicate this thesis.

This work was supported by the Rio Tinto Centre for Mine Automation and the Australian Centre for Field Robotics, funded in part by the New South Wales State Government.

To Yoshiko.

Contents

Declaration	i
Abstract	ii
Acknowledgements	iv
Contents	vi
List of Figures	x
List of Tables	xiv
List of Theorems	xv
Nomenclature	xvi
1 Introduction	1
1.1 Approach to the Problem	2
1.2 Fundamental Limitation	3
1.3 Inaccurate Prediction	7
1.4 Contributions	9
1.5 Thesis Outline	10

2 Background	12
2.1 Autonomous Excavation	13
2.1.1 Behaviour-based Control and Task Decomposition	13
2.1.2 Impedance and Admittance Control	18
2.1.3 Predictive Excavation	20
2.1.4 Other Approaches to Excavation	25
2.1.5 Hydraulic Arm Control	29
2.2 Fundamental Limitations	32
2.2.1 The Bode Integral	33
2.2.2 Controllers with Preview	34
2.2.3 Information Metrics in Preview Control	38
2.3 Iterative Learning Control	47
2.3.1 Convergence Properties	52
2.3.2 Plant Inversion as Learning Function	56
2.3.3 Related Work: Inaccurate Prediction in ILC	58
2.3.4 Related Work: ILC and H_∞ Control Design	62
2.4 Conclusion	64
3 Experimental Platform and Excavation Strategy	66
3.1 Experimental Platform	67
3.1.1 Original Modifications (1996–2000)	67
3.1.2 Current Configuration (2009–)	70
3.1.3 Differences in Approach to Previous Work at ACFR	70
3.1.4 Excavator Joint Dynamics with Servo-Valves	72
3.2 Scope and Approach to Excavation	76
3.2.1 Proposed Excavation Strategy	76
3.2.2 Path and Trajectory Generation	79
3.3 Definition of Performance Metrics	82
3.4 Limitations of a Position-Based Approach	84
3.5 Conclusion	87

4 Feedback Disturbance Rejection	89
4.1 Proportional Control in Excavation	90
4.2 Increasing Disturbance Rejection	101
4.2.1 Disturbance Observation	103
4.2.2 Stability Properties	109
4.2.3 Excavation with Disturbance Estimation	113
4.3 Disturbance Rejection Beyond Feedback Limits	116
4.4 Conclusion	120
5 A Predictive-Reactive Controller in Excavation	122
5.1 Disturbances in Excavation	123
5.2 Proposed Method	125
5.2.1 General Properties	128
5.2.2 Properties in Excavation	131
5.3 Simulations in 1D	137
5.4 Discussions of the Method	146
5.4.1 Relation to Other Approaches	146
5.4.2 A Note on Implementation	149
5.5 Conclusion	153
6 Field Experiments	154
6.1 Experimental Procedure and Soil Conditions	155
6.2 Results	157
6.2.1 General Results	158
6.2.2 Predictive and Reactive Compensation	163
6.2.3 Sensitivity-Like Function in Experiments	166
6.2.4 Trenching	174
6.3 Conclusion	176

7 Summary and Conclusions	178
7.1 Summary of Main Results	179
7.2 Limitations and Future Work	183
List of References	188
A Experimental Platform	201

List of Figures

1.1	Feedback controller with disturbance at the plant output.	4
1.2	A sequence of excavation passes using a linear proportional position controller.	5
1.3	The waterbed effect.	7
1.4	Typical disturbances as seen at each joint actuator input.	8
2.1	The LUCIE mini-excavator platform and the CARE 30 tonne wheel loader.	15
2.2	The Autonomous Loading System developed by CMU.	16
2.3	The experimental rope shovel developed by CSIRO.	18
2.4	The extended wedge model of soil-tool interaction based on the FEE.	23
2.5	The hybrid Mohr-Coulomb and Chen-Liu upper bound model.	25
2.6	Bucket trajectories commanded by skilled operators.	26
2.7	Empirical work at the Warsaw University of Technology, Poland.	27
2.8	The auto levelling controller developed by Hitachi.	29
2.9	A feedback system with disturbances at the plant input.	33
2.10	Waterbed effect for an open-loop-unstable plant	34
2.11	Examples of an aircraft pitch control system with and without side information.	36
2.12	A generic control system with side information.	37
2.13	Sensitivity of a system with preview.	44
2.14	Examples of sensitivity-like functions for Gaussian noise.	46
2.15	Iterative learning control concept in excavation.	49

2.16 Basic structure of iterative learning control.	50
2.17 Iterative learning control with plant inversion.	57
2.18 An illustration of coordinated ILC and H_∞ design proposed by Helfrich et al. (2010).	63
3.1 The 1.5 tonne excavator used for the experimental work.	67
3.2 A simplified schematic of the excavator system used in this work.	69
3.3 Command to flow characteristics of the Moog D633 servo-valve used in the experimental platform	73
3.4 Bucket dynamics approximated by a first-order model.	75
3.5 The path defining an 80 cm deep cut used for evaluating controllers.	79
3.6 Joint commands in free motion.	81
3.7 Definition of performance metrics based on bucket tip tracking error and bucket orientation error.	83
3.8 Swept volume of material as a function of tracking error.	86
4.1 Three conventional manipulator control methods based on a linear PD controller.	91
4.2 Sensitivity of the first-order approximation of the joint dynamics to variation in the value of K_v	93
4.3 The basic proportional controller for each joint of the excavator arm.	94
4.4 Visual inspection of the opened trenches shows that the dominant material was clay.	98
4.5 Initial experiments using the basic proportional controller with a feed-forward input based on the estimated internal dynamics of the plant.	99
4.6 Control effort decreases as the end-effector approaches the trajectory.	100
4.7 Structure of a controller with feedforward reference compensation and a disturbance observer	104
4.8 Structure of the Luenberger observer as an estimator of disturbances.	105
4.9 The simulated response of the linear DOB and robust DOB (VSO) to step disturbances for each joint controller of the arm.	108
4.10 Joint controller with DOB and unknown soil reactions.	110
4.11 Rearrangement of the excavator joint controller for Popov analysis.	111

4.12 The Popov plot where disturbances enter the system at the servo-valve input.	113
4.13 The experiment with a proportional controller reported in Section 4.1 is repeated with the proportional controller augmented with the robust DOB.	115
4.14 The frequency response of the linear disturbance observer for each joint of the arm shows that the estimated value is a low-pass filtered version of the true disturbance.	116
4.15 Prediction of excavation forces as side information.	118
4.16 Prediction of excavation forces as side information.	120
5.1 Disturbances at the three servo-valves of the excavator arm during field experiments.	123
5.2 Proposed predictive-reactive controller structure.	126
5.3 Evaluating the validity of Equation (5.8) using real excavation data. .	134
5.4 A comparison of typical disturbances when the prediction from the previous pass is used and is not used.	136
5.5 Attenuation of the disturbance prediction error by the sensitivity function of the feedback controller.	137
5.6 Comparison of compensation error using only the predictive ILC and the proposed predictive-reactive controller.	138
5.7 Examples of different disturbance fields for 1D simulation.	141
5.8 Simulated results of the 1D case.	144
5.9 The power spectrum of excavation disturbances and ILC prediction error.	148
5.10 The use of the observer in the reactive and predictive cases.	150
5.11 Implementations of an ILC structure with a disturbance observer. . .	151
6.1 Location of field experiments.	155
6.2 Heterogeneous soil conditions during experiments.	156
6.3 Measurements of the soil shear resistance made using a penetrometer. .	157
6.4 Comparison of the performance of the Proportional, PI, P-DOB, P-ILC, and P-DOB-ILC controllers in terms of the distance error and orientation error metrics.	161

6.5	Flow saturated servo-valve commands when iteratively cutting a desired profile.	163
6.6	Motion of the bucket tip with the P-DOB, P-ILC, and P-DOB-ILC controllers.	165
6.7	Tracking error per pass. Comparison between the experimental performance of controllers with and without preview.	166
6.8	Tracking error per pass. Comparison between the P-ILC and the P-DOB-ILC to quantify the attenuation provided by the reactive part of the controller.	167
6.9	Sensitivity attenuation achieved experimentally with the ILC feedforward action as a disturbance preview.	168
6.10	In excavation the ILC regarded as a remote preview system presents coloured noise.	169
6.11	Disturbance attenuation provided by the empirical FEE-based model.	172
6.12	Trenching with the P-ILC and P-DOB-ILC controllers.	175
7.1	The excavation strategy proposed in this work, compared to a strategy used by skilled operators.	180
7.2	The use of a disturbance observer as a form of virtual sensor of excavation disturbances was used as an alternative to integral action.	181
7.3	Quantification of the disturbance rejection provided by ILC in terms of the sensitivity function (a) and the tracking distance error (b).	182
7.4	The use of the observer to estimate inaccurate predictions resulted in less overshooting of the reference trajectory as shown by the bucket tip motion.	183
7.5	Examples of potential use of high-level excavation planners with the controller proposed for autonomous excavation.	186
A.1	Excavator dimensions and location of encoders and load pins.	202
A.2	General schematic of the robotic excavator control and hydraulic systems.	204

List of Tables

1.1	Maximum load to mass ratios of different manipulators.	6
2.1	Attenuation and channel capacity values.	47
3.1	Parameter values of the joint dynamics	74
4.1	Proportional gains	97
4.2	Parameters of the disturbance observer.	108
4.3	Parameters of the joint controller	112
5.1	Controllers evaluated in 1D simulation	142
5.2	1D simulation results in terms of tracking error.	146
6.1	Controllers evaluated in field trials	157
6.2	Experimental ILC sensitivity attenuations in bits/message	170
6.3	Attenuation of sensitivity function using the FEE-based empirical model and ILC.	173
A.1	Arm link parameters of interest.	202
A.2	Experimental platform values of interest.	205

List of Assumptions and Theorem

3.1	Assumption (Experimental Soil Conditions)	76
4.1	Assumption (Feedforward Reference Compensation)	94
5.1	Assumption (Ideal Disturbance Estimate)	129
5.1	Theorem (One-Iteration Convergence)	129
5.2	Assumption	132
5.3	Assumption	132
5.4	Assumption	132
5.5	Assumption	132
5.2	Theorem (Convergence to Zero Tracking Error)	132

Nomenclature

Notation

a	a scalar quantity
\mathbf{a}	a vector quantity
	stochastic process $\mathbf{a}_0^\infty = [\mathbf{a}(0), \dots, \mathbf{a}(\infty)]^T$
j	pass number
	iteration number
\mathbf{x}_j	signal history $[\mathbf{x}_j(0), \mathbf{x}_j(1) \dots \mathbf{x}_j(N-1)]^T$ during iteration j
\hat{F}_x or $\text{PSD}(x)$	power spectral density of signal x
M	last iteration number
J	Jacobian
X	Laplace transform of variable x
	z -transform of variable x

Acronyms

ACFR	Australian Centre for Field Robotics
ALS	Autonomous Loading System
CAN	controller area network
CSIRO	Commonwealth Scientific and Industrial Research Organisation
DOB	disturbance observer
FEE	fundamental equation of earthmoving
FSM	finite state machine
IMP	internal model principle
ILC	iterative learning control
LTI	linear time-invariant
PI	proportional-integral
P-DOB	proportional controller with disturbance observer
P-ILC	proportional controller with ILC prediction
P-DOB-ILC	proportional controller with disturbance observer and ILC prediction
PD	proportional-derivative

PID	proportional-integral-derivative
PD-DOB	proportional-derivative with disturbance observer
PD-DOB-ILC	proportional-derivative with disturbance observer and ILC prediction
PD-ILC	proportional-derivative with ILC prediction
PLC	programmable logic controller
PSD	power spectral density
RMS	root-mean-square
RNR	repetitive to non-repetitive
RPS	remote preview system
SISO	single-input/single-output
SNR	signal-to-noise ratio
SMC	sliding mode control
VSO	variable structure observer

Chapter 1

Introduction

The great majority of robotic manipulators are designed and used for handling known loads under limited perturbations. Control methods for robotic manipulators have therefore focused mainly on modeling and control of the dynamics of the arm, rather than on counteracting external disturbances. In an industrial scenario manipulators work in highly structured environments where disturbances are minimised and tasks are repetitive. Although feedforward action is used to achieve high tracking performance in such manipulators, disturbance rejection usually relies on high-reduction gearing in the drive train and high-gain feedback.

On the other hand, the use of heavy-duty robotic manipulators in the field, or “field manipulators”, has long been contemplated for improving capability in sectors like mining, agriculture and construction. More recently, the Fukushima nuclear accident in 2011 has triggered an urgent review of the availability of heavy-duty manipulators for disaster response. An issue with manipulation in the field is that the magnitude of external disturbance forces can not be foreseen, nor are they often repeatable. Large disturbance magnitudes mean that the actuators of the manipulator arm often saturate, and the controller loses margin for correction. Poor repeatability means that predictive methods are inaccurate.

This work addresses the problem of controlling field manipulators with practical applications in autonomous excavation. Although the demand for autonomous excavation

is quite obvious—conditions to which excavator operators are exposed are dirty, repetitive, uncomfortable, and sometimes unsafe—designing a controller for a manipulator under forceful contact with an uncertain environment is challenging. Counteraction of the large excavation forces requires high feedback gains for disturbance rejection, but counteraction is often unachievable due to the limited bandwidth and saturation of heavy hydraulic arms. While feedforward action may compensate poor feedback performance, attempts to predict excavation forces are prone to inaccuracy due to the complicated nature of soil-tool interaction.

From a control perspective, the excavation problem translates to a need to resolve two fundamental issues. First, that a conventional feedback controller for a robotic manipulator can not achieve complete disturbance rejection due to causality of the feedback action and limits on feedback gains. Second, that a predictive controller for a field manipulator is expected to receive erroneous compensation commands due to inaccurate prediction. This work investigates the combination of predictive and reactive (feedback) disturbance compensation to improve the disturbance rejection of a controller used in tasks where disturbances are large and approximately repetitive between consecutive iterations.

1.1 Approach to the Problem

In industry the automation of heavy-duty robotic manipulators is limited to remotely-operated equipment for de-mining and waste removal, and assistive controllers that automate the digging motion on wheel loaders for scooping loose materials (e.g. “Autodig” (Rocke, 1995, 1996)). In the latter, digging parameters are manually selected and an operator is required to supervise and complete the rest of the cycle. This requirement is in contrast to the variety of methods found in the literature for autonomous excavation: for example, behaviour-based control (Bradley and Seward, 1998), impedance control with robust sliding mode (Ha et al., 2000b), control with soil-tool interaction force prediction (Cannon and Singh, 2000), fuzzy-logic control (Wang, 2004), admittance control (Marshall et al., 2008), and so on. Despite the

large number of different approaches proposed over almost three decades of research, to date there is no reported commercial deployment of a fully-autonomous excavator in any mine or construction site around the world.

Here it is argued that one of the reasons for the low level of automation in excavation is the difficulty in implementing advanced control methods. The same is true in factory automation where proportional-integral-derivative (PID) controllers are still widely used to control manipulators despite the availability of more sophisticated, higher-performance nonlinear controllers reported in the literature.

This work therefore begins with experimental investigations of the limitations of a simple proportional controller subject to large force disturbances during excavation. The controller is then augmented systematically, with a focus on general control tracking methods rather than on approaches tailored specifically to excavation. The problem of adapting bucket motion to changing soil conditions will be assigned to a low-level motion controller, as opposed to the behavioural, sensor-based supervisory controllers that are more usual in excavation.

1.2 Fundamental Limitation

A linear controller structure for independent joint position control of a robotic arm is shown in Figure 1.1. In that figure P represents the joint dynamics, C is the feedback controller and q is the actual joint position. The reference input is not shown since the task of the controller is to regulate the joint to its initial position. The disturbance d is the exogenous force that arises from the interaction between the arm and the environment.

The sensitivity of the controller to disturbances is characterised by the transfer function

$$\frac{Q}{D} = \left(\frac{1}{1 + CP} \right) = S \quad (1.1)$$

where Q and D are the Laplace transforms of the joint angle and the disturbance, respectively. The transfer function $S = (1+CP)^{-1}$ is known as the sensitivity transfer

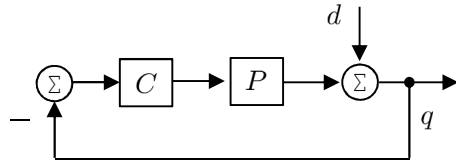


Figure 1.1 – Feedback controller with disturbance at the plant output. As a convention adopted in this work all signals entering summation circles are positive unless marked explicitly with the negative sign.

function.

Figure 1.2 (a) shows a sequence of experimentally-measured bucket tip trajectories that resulted from a proportional position controller ($C = K_p$) commanding flow-control servo-valves, thereby effectively implementing a proportional-derivative control law on position. The controller used the desired cut¹ as a fixed reference trajectory. The first pass², shown as the lightest grey curve, did not achieve the desired cut because, as shown in Figure 1.2 (b), the first link actuator was severely saturated. This form of output limitation is a characteristic of the excavator, and is thus a limitation also encountered by human operators.

While an operator’s strategy on encountering saturation is to repeat passes until the final cut is reached, the simple linear controller fails in doing so: convergence decreases to the point that the last two passes (darkest curves) barely differ while still being far from the desired cut. Note from Figure 1.2 (b), however, that the corresponding actuator commands are not saturated indicating that poor tracking is now due to a lack of control effort. Excavation involves both the problem of *saturation*, evident during initial passes, and lack of control effort due to *bandwidth limitations*, which is dominant during the latter passes.

From a control design perspective it is intriguing that a position tracking proportional controller that is widely used in industrial robotic applications performs poorly in excavation. The reason is that disturbances in excavation are “large” in relation to the

¹ A *cut* is defined here as the final profile of a hole that is opened by several passes of the excavator bucket using only the motion of the arm while the excavator body maintains the same position.

² A *pass* is one “scoop” of an excavator bucket.

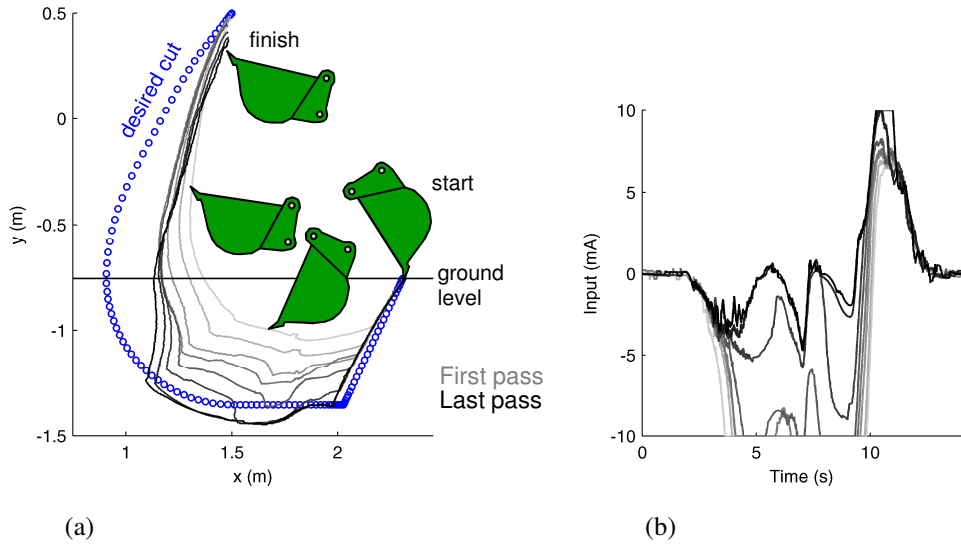


Figure 1.2 – A sequence of excavation passes using a linear proportional position controller commanding flow-control servo-valves. (a) Trace of the bucket tip. (b) Commands to the first link actuator.

disturbance rejection capacity of the controller. To quantify what “large” disturbances are in the context of this work, Table 1.1 shows the ratio of the maximum payload mass to the arm mass for several different types of manipulators.

For the Kuka KR 30-3 electric industrial robot used for medium payloads, the maximum payload represents 9.8% of the arm mass. In a hydraulic excavator such as the Komatsu PC05-7 the maximum payload represents 303% of arm mass. Assuming that the rated load mass is an approximate indication of the maximum expected disturbance, the ratio of masses indicates the relative disturbance magnitudes that different types of manipulators are expected to encounter under maximum load. Since $Q = SD$, the magnitude of the sensitivity transfer function must be inversely proportional to the disturbance to maintain the same position control performance. In a proportional controller the magnitude of S can be decreased only by increasing feedback gains; an unrealistic requirement for low-bandwidth heavy-duty hydraulic manipulators.

The present work will then explore methods that do not rely on feedback gains to improve disturbance rejection. One such approach is to estimate the value of the

Table 1.1 – Maximum load to mass ratios of different manipulators.

Manipulator	Max. load (kg)	Arm mass (kg)	ratio(%)
Kuka KR 3	3	53	5.7
Kuka KR 30-3	65	665	9.8
DLR arm III	14	14	100
Komatsu PC05-7 (1.5 ton)	455	150	303.3
Komatsu PC8000 (777 ton)	203,943	65,700	310.4

disturbance at the plant input, and feed the estimated value back to the controller as a compensation command. Experimental results will show that such estimation based on feedback can significantly improve tracking performance. There is, however, a fundamental limitation of linear closed-loop systems that incorporate feedback. For an open-loop stable plant, such as an excavator, the limitation is given by the fact that the integral of the log of the sensitivity transfer function, also simply referred to as the sensitivity function, must be zero (Bode, 1956; Seron et al., 1997). This integral, known as the Bode integral, is

$$\int_0^\infty \log |S(j\omega)| d\omega = 0. \quad (1.2)$$

The Bode integral shows that a feedback controller can not decrease the gain of the sensitivity transfer function $S = (1 + CP)^{-1}$ at all frequencies. If a controller is designed to compensate disturbances at lower frequencies, this will cause amplification of the higher frequency disturbances, and vice versa. This effect—the “waterbed effect”—is illustrated in Figure 1.3 (a).

A recent result based on the fundamental limits of feedback control show that non-causal knowledge of the disturbance, that is, when the system is provided with a preview of the disturbance, can decrease the value of the Bode integral (Martins et al., 2007). That is, for an open-loop-stable plant, the Bode integral of a controller with preview can have a negative value. This suggests that if the controller is given predicted values of incoming disturbances in advance of the disturbances affecting the plant, the disturbance rejection characteristics can be improved beyond feedback

limitations. This improvement is illustrated in Figure 1.3 (b). Note that decreasing the magnitude of the sensitivity function diminishes the effect of disturbances. In terms of excavation, this suggests that bucket passes will be closer to the desired cut, thus finishing a cut with fewer passes.

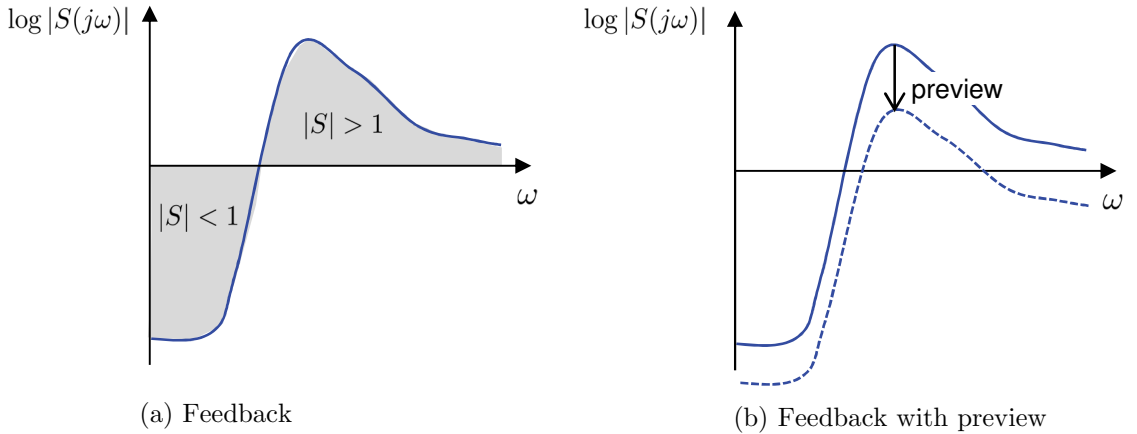


Figure 1.3 – The waterbed effect. (a) For a feedback controller the negative and positive areas must sum to zero. (b) For a controller with a disturbance preview the integral can be reduced, potentially improving disturbance rejection over a larger range of frequencies.

1.3 Inaccurate Prediction

As disturbance preview seems to be a key factor in improving disturbance rejection a feedforward model of the disturbance must be designed.

Figure 1.4 shows the sequence of disturbances at each joint actuator of the excavator arm, obtained from digging experiments with the proportional controller. Despite the first and last passes being quite different, disturbances of consecutive passes show that there is some form of consistency which may be amenable to prediction.

This work makes use of iterative learning control (ILC) (Arimoto et al., 1984) as an efficient method of learning better input commands for compensating iteration-repetitive disturbances. In the context of excavation, ILC has the advantage that it

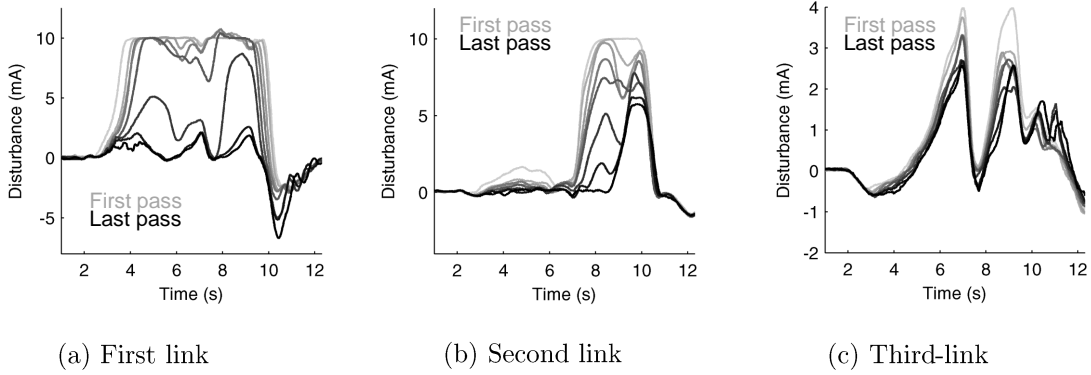


Figure 1.4 – Typical disturbances as seen at the input of each joint actuator of the three-link excavator arm. The first link (a) is attached to the excavator frame, the third link (c) is the end-effector.

does not require explicit modeling of the complicated soil-tool interaction forces. The disadvantage, however, is that the non-repetitive components of the disturbances will become a source of inaccurate prediction.

This work proposes a predictive-reactive controller that uses the accurate parts of prediction and at the same time accounts for the fact that prediction inaccuracies are inevitable. The proposed controller provides two complementary mechanisms for counteracting disturbances during excavation. The first compensation is *predictive* and is attempted between iterations when ILC is used to predict the disturbance to be encountered in the next pass. The second compensation is *reactive* and occurs during the execution of the controller when the output of a time-domain disturbance estimator is used to compensate for the error in prediction.

Using the proposed predictive-reactive controller, the experimental platform will demonstrate the ability to autonomously and iteratively excavate a deep cut, independent of the feasibility of the desired trajectory in relation to actuator saturation. Commands will be adapted to different soil conditions while disturbances will be compensated preemptively, and passes will be repeated if necessary, based on a specified finish quality of the cut and without the need of operator decisions.

1.4 Contributions

The principal contributions of this work are:

- An empirical evaluation of the limitations of a widely-used linear proportional controller when exposed to large excavation disturbances, and the proposition of general methods based on disturbance observation and iterative learning control to overcome those limitations in the excavation scenario.
- A general control method that learns the repetitive components of disturbances and explicitly compensates for inaccurate predictions. Since all excavation-related assumptions are contained in the trajectory design, but not in the controller structure itself, the method is open to other processes where a manipulator undergoes large disturbances in an approximately repetitive manner.
- An interpretation of the work of Martins et al. (2007), which shows that disturbance attenuation can be achieved through the presence of side information transmitted by a communication channel. Here, this form of preview is interpreted as a feedforward model of excavation disturbances. This interpretation not only suggests the use of predictive action in excavation but also offers metrics that quantify the attenuation limits of an inaccurate predictive method in the form of a “sensitivity-like” function.
- Extensive field experiments where the experimental platform is used to dig in realistic undisturbed and heterogeneous soil conditions. An experimental comparison of the performance of controllers based on proportional, proportional-integral (PI), proportional control with disturbance observer (P-DOB), proportional control with ILC prediction (P-ILC), and proportional control with a combination of disturbance observer and iterative learning control (P-DOB-ILC) is made. This work introduces the iterative strategy where the excavator achieves a desired cut independent of the initial feasibility (in the sense of actuator saturation) of the reference trajectory.

- A flexible re-organisation and re-commissioning of the control hardware and software of the experimental platform, allowing the implementation of different control methods with minimum programming.

During the course of the present work the following related publications were made, or are in preparation:

- G. Maeda, I. Manchester and D. Rye. ILC with Observer for Rejection of Near-Repetitive Disturbances, with Application to Excavation. In preparation, 2013.
- G. Maeda, D. Rye, and S. Singh. Iterative autonomous excavation. In *Field and Service Robotics: Results of the 8th International Conference*, Springer, in press 2013.
- G. Maeda and D. Rye. Learning disturbances in autonomous excavation. In *Proceedings of the 2012 IEEE/RSJ International Conference on Intelligent Robots and Systems*, 2012, pp. 2599–2605.
- G. Maeda, S. Singh, and D. Rye. Improving operational space control of heavy manipulators via open-loop compensation. In *Proceedings of the 2011 IEEE/RSJ International Conference on Intelligent Robots and Systems*, 2011, pp. 725–731.
- G. Maeda, S. Singh, and H. Durrant-Whyte. A tuned approach to feedback motion planning with RRTs under model uncertainty. In *Proceedings of the 2011 IEEE International Conference on Robotics and Automation*, pp. 2288–2294.

1.5 Thesis Outline

The remainder of this thesis is arranged as follows. **Chapter 2** presents background on the three principal areas of knowledge used in this work. Section 2.1 reviews related work in autonomous excavation with a focus on low-level motion/force control. Section 2.2 introduces the Bode integral and preview control, also detailing the work of Martins et al. (2007) regarding systems with side information. Finally, Section 2.3 presents ILC in the context of autonomous excavation.

In **Chapter 3** the experimental platform used in field trials is introduced and the arm joint dynamic model is presented. Differences in approach between the present work and previous work using the same experimental platform are discussed. An excavation strategy is proposed based on the characteristics of the platform and on how human excavator operators dig, as reviewed in Chapter 2. This chapter also introduces two metrics that quantify excavation performance.

Chapter 4 introduces and experimentally evaluates a simple proportional feedback controller on the hydraulic excavator arm. A disturbance observer is introduced as form of virtual sensor of excavation forces to increase the disturbance rejection of the proportional controller.

In **Chapter 5** a predictive-reactive controller is introduced based on ILC prediction. The proposed controller has the property of using the accurate parts of prediction to improve disturbance rejection while using a disturbance observer to attenuate the inaccuracies in prediction. Assumptions under which the method is effective will be made and the applicability of the assumptions will be evaluated with real excavation data.

Chapter 6 reports the results of extensive field trials in real excavation conditions. The experimental results will support the hypotheses suggested throughout this work.

Chapter 7 summarises the main results of this work and discusses limitations of the proposed methods and directions for future work.

Chapter 2

Background

This review chapter is comprised of three sections. Section 2.1 reviews related work in autonomous excavation. The literature is categorised according to the three main approaches that have been adopted: behaviour-based control, impedance control and predictive excavation. Approaches to controlling an arm in free motion are also discussed.

Section 2.2 introduces the fundamental feedback limitation and the “waterbed effect” on the Bode integral. The section also reviews the work of Martins et al. (2007) where side information in preview control is shown to overcome the waterbed effect.

Section 2.3 introduces iterative learning control (ILC) and motivates its use in the context of excavation. The assumptions that are required for iterative learning control (ILC) convergence are also reviewed. This section introduces a particular form of learning function that makes use of the inverse model of the plant and is shown ideally to achieve convergence in one iteration. Finally, methods proposed to address the problem of non-repetitive disturbances in ILC are reviewed.

2.1 Autonomous Excavation

This section reviews the literature relating to the low-level control of excavators under soil contact, organised according to the three main approaches used. One category of work is related to the use of behaviour-based actions, motivated mainly by the difficult problem of excavating fragmented rock. This first approach has been used with success in wheel loader applications in hard rock mining. A second approach adopts the use of impedance or admittance control to adapt bucket motion to the large resistive forces without requiring explicit modelling of soil-tool interaction forces. A third approach is to use predictions of excavation forces to plan feasible trajectories and, more recently, for on-line force compensation.

Two related sub-areas in autonomous excavation are teleoperation and high-level planning. Exemplars of teleoperation work are found in Parker et al. (1993); Salcudean et al. (1997); Tafazoli et al. (2002); Westerberg et al. (2008); Kim et al. (2009); Duff et al. (2010). High-level planning relates to the proper partitioning of an excavation into a sequence of smaller sectors; see Romero-Lois et al. (1989); Schmidt et al. (2010); Seo et al. (2011) for example. Although important, these areas are omitted from this review as they are not within the focus of the present work.

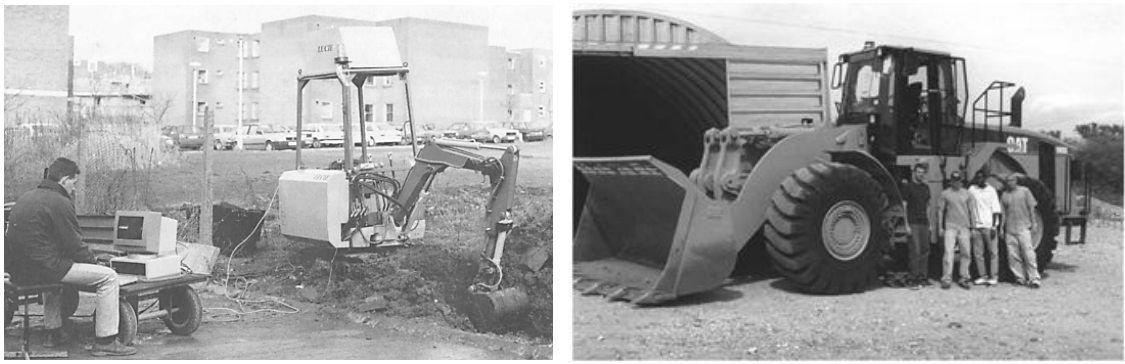
2.1.1 Behaviour-based Control and Task Decomposition

In pioneering work on autonomous excavation, the concept of “dig by feel” was introduced by civil engineers motivated by the promise of automation in civil construction. Bullock and Oppenheim (1989) argued that it was impossible to characterise excavation forces until forceful contact is made. They proposed a strategy where a supervisory controller responded to the interaction as it occurs, by means of a “force-

cognitive” excavation controller. The method was based on a conventional low-level motion controller where a reference trajectory was modified by a supervisory outer loop on the basis of force feedback measurements. Although experiments were conducted with an industrial manipulator digging only in a sandbox, the authors showed that simple rules like “reverse the scooping” could effectively adjust a digging trajectory to maintain soil strain levels up to a desired value.

Aiming to imitate the actions of an expert operator, the LUCIE excavator project (Bradley and Seward, 1998) lasted nine years and used a control idea somewhat similar to the supervisory control of Bullock and Oppenheim. A high-level rule-based “activity manager” was used to define velocity set points for a lower-level velocity controller depending on the conditions of the excavation. By the end of the project, the activity manager contained approximately 80 heuristic rules, most of them based on empirical observations. A photograph of the mini-excavator used as the experimental platform during the project is shown in Figure 2.1 (a). The project also led to a detailed study of the bucket motion commanded by expert and novice operators. Part of these results will be used in the present work to design reference trajectories. A similar behaviour-based approach has been recently suggested by Schmidt and Berns (2010) for simulated excavation of granular material.

Motivated by excavation scenarios where large rocks were encountered, Shi et al. (1996) emphasised the use of artificial intelligence techniques in control. The authors investigated the problem of digging in the presence of large rocks hidden beneath the soil surface, a much more difficult problem than excavation in homogeneous soil. This has also been referred to as the “iceberg problem” (Huntsberger et al., 2005). The controller proposed by Shi et al. was based on the decomposition of an excavation task into a sequence of several sub-tasks in the form of primitive actions. One sequence example is “under-particle-follower”; another is “horizontal-digger” (Shi et al., 1996).



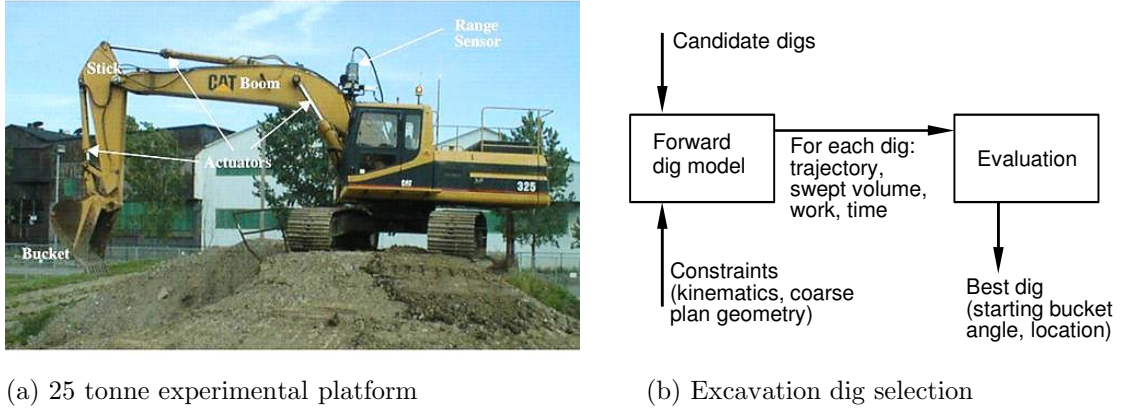
(a) The LUCIE mini-excavator platform (b) The CARE 30 tonne wheel loader platform

Figure 2.1 – Earlier works in autonomous excavation based on artificial intelligence.

(a) The LUCIE project used 80 heuristic rules as a high-level supervisory controller. From Bradley and Seward (1998). (b) Work by Lever developed behaviour-based strategies for large rock excavation. From Lever (2001).

A finite state machine (FSM) designed with skilled operator expertise took the form of a supervisory control where decisions were made by neural networks. A fuzzy-logic controller was used to determine a new reference position and orientation of the bucket during digging whenever forces surpassed a threshold limit, similar to Bullocks's "dig-by-feel". Using a PUMA arm as a proxy for an excavator, experimental results showed that the controller could autonomously follow the contour of a large rock buried in soil. The behaviour-based fuzzy controller was later used as part of the Control Architecture for Robotic Excavation (CARE), a project developed at the University of Arizona and supported by Caterpillar Inc. Within this project Lever (2001) reported experiments with a 30 tonne wheel loader, shown in Figure 2.1 (b), where performance comparable to an expert human operator was achieved. Later, Wang (2004) proposed substituting the FSM with Petri nets as a systematic approach to rule generation. Validation was done by experiments on a PUMA arm.

Also aiming at encoding expert human knowledge, Rowe and Stentz (1997) proposed the use of parameterised scripts to break complex excavation tasks into smaller motion



(a) 25 tonne experimental platform

(b) Excavation dig selection

Figure 2.2 – The Autonomous Loading System developed by CMU. (a) The 25 tonne hydraulic excavator used as the experimental platform. From Cannon and Singh (2000). (b) Candidate trajectories were selected through forward simulation with soil-tool prediction models and ranked according to their ability to optimise a desired cost function. After Stentz et al. (1999).

primitives. An example of a script fragment extracted from Rowe and Stentz (1997) is “... *move joint 0 up to 20 deg.; when joint 0 passes 10 deg. then move joint 1 down to 0 deg.; ...*”. Experiments using simple PD controllers were conducted on the 25 tonne hydraulic excavator shown in Figure 2.2 (a). This work was later extended and presented in Stentz et al. (1999) as the Autonomous Loading System (ALS); a complete system that automated the full excavation cycle. The system used data from laser range finders to map the terrain to be excavated and identify trucks, and planned excavator motion with collision avoidance. At the low level, closed-loop force controllers were used and digging trajectories were selected to locally optimise a cost function (e.g. volume, energy, time) whose computation was based on forward simulation (Figure 2.2 (b)). The simulator used a soil-tool interaction force model which will be reviewed in Section 2.1.3. The system was reported to achieve a loading cycle as fast as expert human operators.

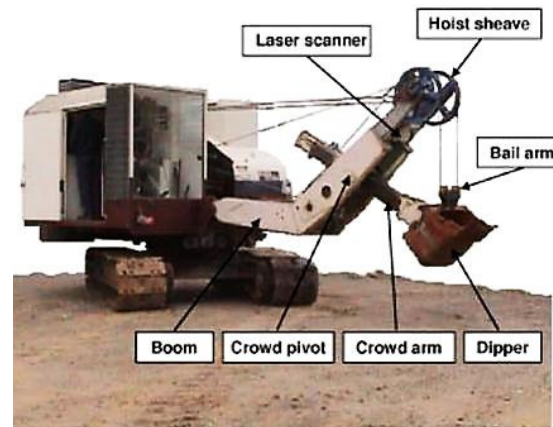
Under a framework of cognitive force control, Vähä (1993) proposed a single rule where the bucket penetration was decreased when excavation forces exceeded the arm actuation limits, or some other threshold. The results were reported only in simulation, but introduced the principle that a single rule can account for the whole of excavation control. Recently, a similar approach based on crowd arm retraction was reported by Dunbabin and Corke (2006) for rope shovel control¹. The rule proposed was

$$R_{k+1} = R_k + \eta_{stalled}, \quad (2.1)$$

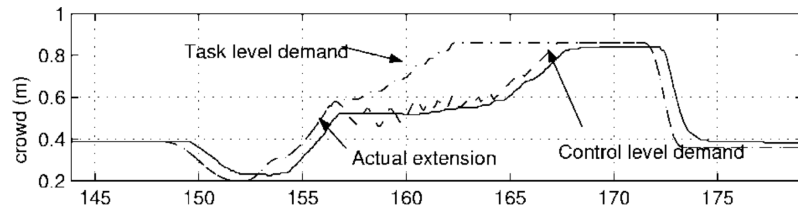
where $\eta_{stalled}$ is a fixed amount that is added to the retraction counter R and k increments each time a drive stalls. Despite the simple rule, field trials using the one-seventh scale electric rope shovel shown in Figure 2.3 (a) showed over 100 excavation cycles that the approach was successful. The simple control rule achieved cycle times comparable to a human operator, but with lower average motor loading. One excavation pass is shown in Figure 2.3 (b).

Another investigation of simple rules for bucket trajectory shaping was reported by Sarata et al. (2004). By means of analytical investigation of the kinematics and soil-tool friction models for the bucket of a wheel loader the authors proposed dividing the bucket motion into three phases separated by thresholds given by the horizontal force acting on the bucket. The critical phase of shearing and dislodging material was accomplished by an alternating bucket tilt motion. Experimental results were later reported by Sarata et al. (2008) for excavation of loose piles of soil.

¹The crowd arm is the link that sets the depth of the dipper into the excavation face.



(a) Rope shovel experimental platform



(b) An example of crowd retraction

Figure 2.3 – (a) The experimental rope shovel developed by CSIRO. (b) Experimental result showing position accommodation produced by the simple crowd retraction rule given by Equation 2.1. The initial task level demand signal is modified to the control level demand in response to drive stall. From Dunbabin and Corke (2006).

2.1.2 Impedance and Admittance Control

Impedance control and admittance control are strategies used to achieve a desired dynamic relationship between the end-effector and the environment. As defined by Hogan (1984), a control system that emulates impedance accepts motion commands and outputs force. In excavation this represents the usual material removal case where the excavator arm is commanded by position. Also following Hogan's definition, a control system that emulates admittance accepts force commands and outputs motion. A simplistic example in excavation is the case where the controller adjusts

bucket motion to contour around a large, immovable rock.

The use of impedance control has been widely accepted in excavation. In distinction from the behaviour-based approaches, impedance control has the advantage of being a simpler framework that is already mature as a manipulation control method. Impedance control seems suitable for excavation under actuation limits and force thresholds due to its natural ability to adjust the applied force in response to the large resistive forces from excavation. Moreover, the majority of heavy-duty hydraulic machines are actuated by proportional or flow-control servo-valves which aligns well with impedance controllers designed with inner position- and outer force-control loops. Impedance control, however, may not suit applications where human-like discrete actions are required, such as excavation of fragmented rock.

In 1993 Bernold proposed impedance control of an excavator, motivated by difficulties in predicting excavation motion due to large uncertainties in digging force as a function of soil cohesion. Bernold investigated differences in cutting forces as a function of soil constitution. The work reported an increase of 60% in the required cutting moment when water representing up to 7% of soil mass content was added to dry sand. Another mixture showed that the addition of 20% clay with 4% water to dry sand would further increase the required cutting moment by 20%.

Salcudean et al. (1997) and Tafazoli et al. (2002) used position-based impedance control for teleoperating a mini-excavator. The impedance was emulated at the cylinder with a PD controller with valve dead-band compensation. A second-order mass-damper-spring was used as a model of the environment from which the reference commands for the position controller could be computed to achieve a specified compliant behaviour.

A low-level impedance control approach was proposed by Ha et al. (2000b) whereby

target impedances were emulated at the cylinder level with feedback on differential cylinder pressures. The cylinder position was controlled with a sliding mode controller incorporating a fuzzy tuning approach. The controller was initially proposed in Ha et al. (1999) with the particular characteristic of rotating and shifting sliding surfaces. A sliding mode controller was also reported in Ha et al. (2000a) as a feedback controller and as its dual in the form of a friction observer. Experimental results were reported in Ha et al. (2002) where the trajectory was defined by means of a state chart that encoded discrete phases of a digging motion based on expert operator heuristics. Transitions between behaviours were managed by verifying the current state of the arm, and new states were added to the desired reference trajectory as step inputs.

Based on the analysis of operator measurements when digging fragmented rocks with a wheel loader, Marshall et al. (2008) proposed the use of admittance control to adjust the velocity of the bucket in response to the resistance from the environment. Motivated by excavation in planetary exploration Richardson-Little and Damaren (2008) proposed admittance control for excavation as an adaption to unknown off-world soil conditions. The same work also relaxed conventional analytical soil-tool models to a rheological mass-spring-damper model. Results, however, have only been reported by means of simulation, and the use of rheological models to represent soil-tool interaction forces lacks experimental validation.

2.1.3 Predictive Excavation

Using a mechanics-based formulation, Singh (1995) presented a learning framework for force prediction. Singh proposed and compared different basis functions containing the depth, distance and orientation of the bucket. The learning part accounted for the extraction of the parameter values of the model based on experimental data.

Several methods were compared: global regression, nearest neighbours, local weighted regression and neural networks. Although prediction accuracies were somewhat similar among the different methods, a large discrepancy was observed in training time. Brute force search of parameters took days, while training a neural network took hours. This work is an indication that, while learning may be a feasible approach in excavation, some training methods may be unsuitable for real-time purposes.

Modelling of soil-tool interaction forces has been investigated in autonomous excavation as a predictive tool with two main purposes. Firstly, interaction force modelling allows for feasible bucket trajectories to be planned, which can then be used for strategic planning as in the body of work from CMU. Secondly, if done on-line, prediction of forces allows for the immediate compensation of excavation forces by a low-level controller, which can be incorporated as an adaptive control law. Although prediction may be impractical in excavation of fragmented rock (Shi et al., 1996), several authors have shown that prediction is possible when homogeneous conditions are dominant. On-line algorithms may also handle the case where heterogeneity occurs through smooth transitions; for example when soil cohesion changes gradually over the excavation area.

In autonomous excavation, successful attempts to predict excavation forces were made with the use of physics models provided by the classical soil-mechanics literature. This literature is very rich: it has been reported (Blouin et al., 2001) that more than 50 empirical models are available solely for describing the bucket penetration phase of excavation.

Blouin et al. (2001) summarised and compared the principal soil-tool interaction models proposed for excavation. Such models are usually referred by the names of their author. The “Osman, Gill and Vanden Berg”, “Swick and Perumpral”, and “McKyes”

(also known as the universal or fundamental equation of earthmoving (FEE)) models represent excavation in two dimensions as a flat blade dragging soil in the horizontal direction. Other models consider the trajectory and the geometry of the bucket during the scooping motion. Some models of this type are known as “Alekseeva”, “Zelenin”, “Hemami”, “Balovnev” and “Korzen” after their authors. While it is not within the scope of the present work to review soil-tool interaction models the reader should be aware that the selection of an interaction model is a non-trivial task. This task is worsened by a lack of experimental validation and significant disagreement amongst the various models as was reported by Hemami and Hassani (2009).

Amongst the two-dimensional models, the FEE has successfully been applied in autonomous excavation for the purposes of trajectory prediction and tactical planning. The FEE was initially proposed (Reece, 1964; McKyes and Desir, 1984) as a basic soil-mechanics model for predicting forces during agricultural tillage. The FEE was introduced in excavation by Malaguti (1994a) and Singh (1995) by approximating the bucket as a two-dimensional flat blade as shown in Figure 2.4.

The model in Figure 2.4 is also referred to as the “wedge model” due to the assumption that the failure surface is planar. To improve prediction accuracy, Malaguti (1999) replaced the single failure surface with two surfaces having different inclinations, naming the model the “double-wedge”.

The FEE model was also extended by Luengo et al. (1998) to address terrain slopes. The general soil-tool interaction force equation proposed by Luengo et al. is

$$F = d^2 w \gamma g N_w + cwd N_c + V_s \gamma g N_q, \quad (2.2)$$

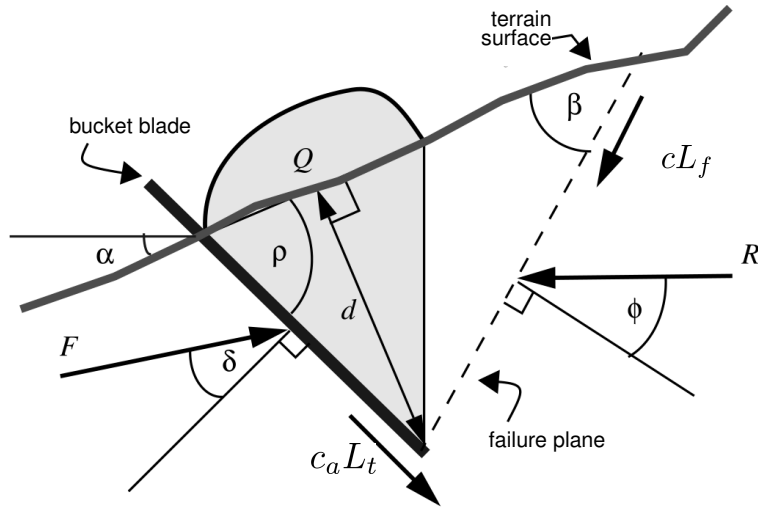


Figure 2.4 – A soil-tool interaction model based on the FEE approximates the bucket bottom as a flat blade, and the failure surface as a plane; d is the depth of the pass, α is the terrain slope, β is the angle of the failure surface, ρ is the rake angle, c_a is the soil-tool friction pressure, L_t is the length of the tool, c is the soil-soil cohesion pressure, and L_f is the length of the failure surface. After Luengo et al. (1998).

where the triple N_w, N_c, N_q is

$$\begin{aligned} N_w &= \frac{(\cot \beta - \tan \alpha)(\cos \alpha + \sin \alpha \cot(\beta + \phi))}{2[\cos(\rho + \delta) + \sin(\rho + \delta) \cot(\beta + \phi)]} \\ N_c &= \frac{1 + \cot \beta \cot(\beta + \phi)}{\cos(\rho + \delta) + \sin(\rho + \delta) \cot(\beta + \phi)} \\ N_q &= \frac{\cos \alpha + \sin \alpha \cot(\beta + \phi)}{\cos(\rho + \delta) + \sin(\rho + \delta) \cot(\beta + \phi)}, \end{aligned}$$

and d is the depth of the pass, α is the terrain slope, β is the angle of the failure surface, ρ is the rake angle, c_a is the soil-tool friction pressure, L_t is the length of the tool, c is the soil-soil cohesion pressure, and L_f is the length of the failure surface.

The solution of Equation (2.2) is the main problem for the purpose of on-line force estimation. In agricultural tillage, the terms N_w, N_c, N_q are constant and the literature provides empirical results that tabulate the relations between parameters; see for example McKyes and Desir (1984). The difficulty in excavation is that the triple

is nonlinear in relation to the varying bucket angle ρ . As a consequence the assumed geometry of the soil failure surface constantly changes during a pass; that is, β and ϕ are nonlinear functions of bucket angle ρ . Luengo et al. (1998) proposed a combination of global and local optimisation. Malaguti (2005) proposed a gradient descent approach to estimating the parameters N_w , N_c and N_q for the double-wedge FEE.

Cannon and Singh (2000) introduced a simplified empirical model in the form

$$F = \Psi_1 \Gamma_1 + \Psi_2 \Gamma_2 + \dots \quad (2.3)$$

where the basis $\Gamma = (d^2, \cos(\rho), \alpha, V_s)$ was selected using physical insight to eliminate part of the nonlinearity. The resulting linear nature of Equation (2.3) offers the advantage that parameters can be estimated by simple linear regression. Since the selected basis Γ is clearly inspired by the FEE model, this model will be referred to as the “FEE-based empirical model”. In the same work Cannon and Singh compared the empirical method with the method in Luengo et al. (1998) in terms of prediction accuracy and training time. Both methods presented the same prediction error of approximately 20%, however the empirical method could estimate the linear parameters 425 times faster than the optimisation of the parameters of the nonlinear FEE model.

Motivated by a need for on-line prediction of soil-tool interaction forces, Tan et al. (2005) investigated soil-soil frictional forces using the Mohr-Coulomb and the Chen-Liu upper bound (CLUB) models. The CLUB model has a detailed three-region shear surface, illustrated in Figure 2.5 (a). The envisioned controller used an on-line estimator as a feedforward predictor for excavation control as shown in Figure 2.5 (b). The soil-soil friction angle and density parameters were estimated using Newton-Raphson optimisation.

Tan et al. concluded that errors in the estimation of soil parameters in the range of 20% to 30% are to be expected. Althoefer et al. (2009) designed a hybrid method that switched between the Mohr-Coulomb and the CLUB models as a function of the bucket orientation. In the same work the authors augmented the estimation to account for soil-tool friction and cohesion. Estimation was achieved within one second with inaccuracies of 20% in the worst case. Yousefi Moghaddam et al. (2012) has recently applied the same method under laboratory conditions using a bench-scale excavating apparatus to dig in cohesive materials. Although showing promise as an on-line predictor, the hybrid method lacks validation with real excavators.

2.1.4 Other Approaches to Excavation

Several other researchers have investigated excavation from a purely empirical perspective. In empirical approaches it is hypothesised that measurement of the main variables of the excavator when driven by human operators can lead to correlations

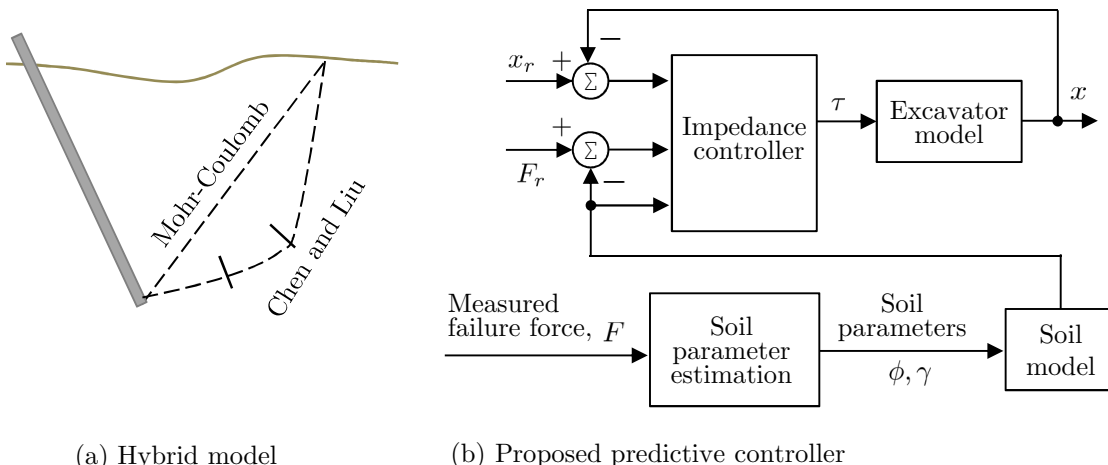


Figure 2.5 – (a) The hybrid model used by Althoefer et al.. (b) The controller with on-line disturbance compensation envisioned by Tan et al.. From Althoefer et al. (2009) and Tan et al. (2005).

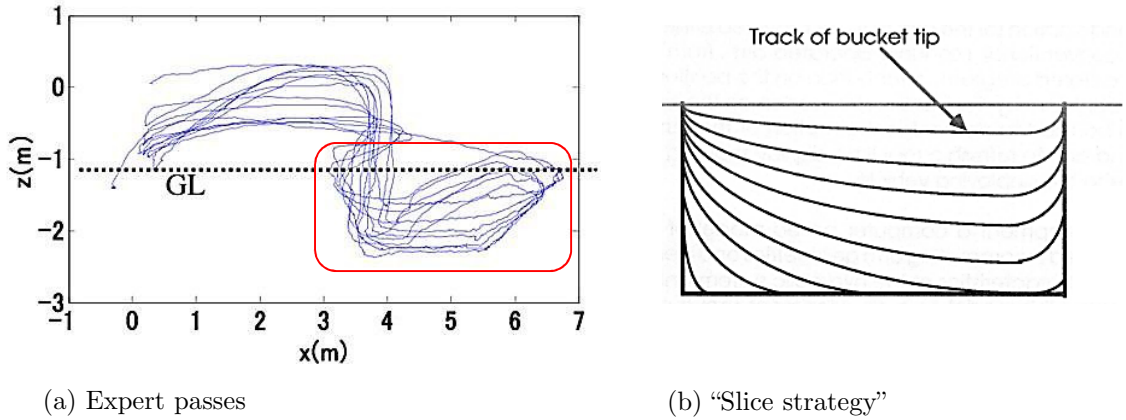


Figure 2.6 – Bucket trajectories commanded by skilled operators. (a) Actual measurements reported by Shao et al. (2008). (b) Slice strategy proposed by Bradley et al. (1989). Note the similarity between the measured operator passes and the proposed slicing strategy. From Shao et al. (2008) and Bradley et al. (1989).

and findings that will help to devise better control strategies.

Yamaguchi and Yamamoto (2006) reported the differences in values of bucket positions and cylinder pressures of a backhoe excavator when trenching² was done by novice, intermediate, and skilled operators. This work was extended in Sakaida et al. (2008) with additional experiments with skilled operators. The same group reported field trials (Shao et al., 2008) where excavation trajectories were planned based on the conclusions from their empirical investigations. The skilled operator strategy consisted of opening a trench by repeated passes of increasing depths using trapezoidal trajectories. Figure 2.6 (a) shows an example of an expert cut. A similar conclusion was reported by Bradley et al. (1989) based on visual observation of expert passes, and was referred to by the authors as the “slice approach”, shown in Figure 2.6 (b).

Marshall (2001) reported extensive analysis of data collected from motion transducers, wheel encoders and pressure sensors on a wheel loader during excavation of fragmented rock. Controlled and aggressive excavation trials were conducted with different op-

² A *trench* is a long hole achieved by the concatenation of several cuts, formed by moving the excavator backwards once each cut is finished.

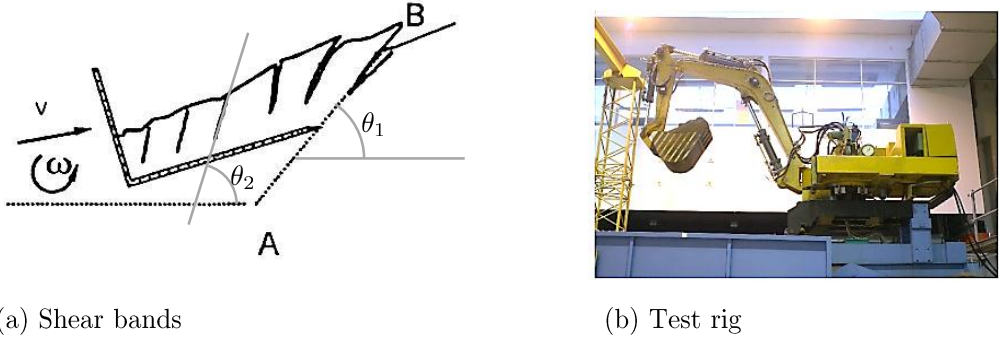


Figure 2.7 – Empirical work at the Warsaw University of Technology, Poland. (a) The optimum digging strategy aligns the lifting angle θ_1 with the angle of the direction of shear bands θ_2 . After Jarzebowski et al. (1995). (b) Test rig on soil with controlled parameters. From Kuśmierczyk and Szlagowski (2008).

erators to correlate differences in approach with sensor measurements. Those results were later used to propose admittance control in excavation.

Laboratory experiments aimed at optimising bucket passes in autonomous excavation were conducted by Jarzebowski et al. (1995) and Maciejewski and Jarzebowski (2002). The authors investigated the effect of the occurrence of shear bands when scooping with a flat blade, and their relation to bucket filling. Shear bands are the sequence of cracks that form on the surface of a cohesive material when cut by a tool, as shown in Figure 2.7 (a). The authors concluded that in terms of energy consumption, the optimum digging strategy is given by a trajectory where the tool lifts parallel to the shear band, since material cohesion decreases to values close to zero in that direction. Experiments showed that the energy efficiency could be increased by 50% using the proposed strategy. The same group also investigated digging strategies with a hydraulic excavator arm mounted on the top of a bin with designed soil, shown in Figure 2.7 (b). A initial report on the use of the test rig is found in Kuśmierczyk and Szlagowski (2008).

Several other advances in autonomous excavation are related directly to industrial

research and patented technology. Caterpillar Inc. has been granted the majority of patents in this area. The body of work related to the Autonomous Loading System developed at the Carnegie Mellon University Robotics Institute has generated eleven patents related to autonomous excavation. Some of those patents that are relevant to automation of excavation are summarised next.

The patents granted to Rocke (1995, 1996) and Rocke et al. (1996) introduced the Autodig system. The system is in the form of a supervisory controller that regulates actuation based on look-up tables. The look-up tables contain ideal values of commands obtained from a skilled operator. Pressure measurements on each link actuator are monitored and compared to the ideal tabulated values, and adjustments are made by feedback. Each tabulated curve represents a different soil type which is selected by an operator prior to excavation commencing.

The dependence on pressure/force feedback and the requirement that the correct soil type be selected by a user has motivated a velocity approach for the Autodig system. A patent by Clark et al. (2011) claims improved adaptability of the system in comparison to force-based methods. The velocity profile is adapted according to the hardness of the material being excavated without requiring the use of force or pressure sensors.

Several other patents assume the existence of the Autodig system as the controller that executes the interaction part of the cycle. A patent granted to Kale et al. (2011) describes a higher-level system that adjusts the Autodig system, correcting the inefficiency of unskilled operators by measuring the speed of their operation. Finally, a patent by Mintah et al. (2011) describes a system that decreases the burden on the operator by transferring parts of the digging cycle to segments that are fully controlled by Autodig.

Hitachi has developed an assistive controller whereby the excavator is used for precisely level digging operations. This controller assists in underground sewer construction or when the operator cannot see the bottom of the cut (Figure 2.8). This work was published in the excavation literature by Haga et al. (2001). The controller requires an initial operator input to define the maximum depth of the cut which is then regulated by feedback control using the boom link while the operator controls the stick and bucket links.

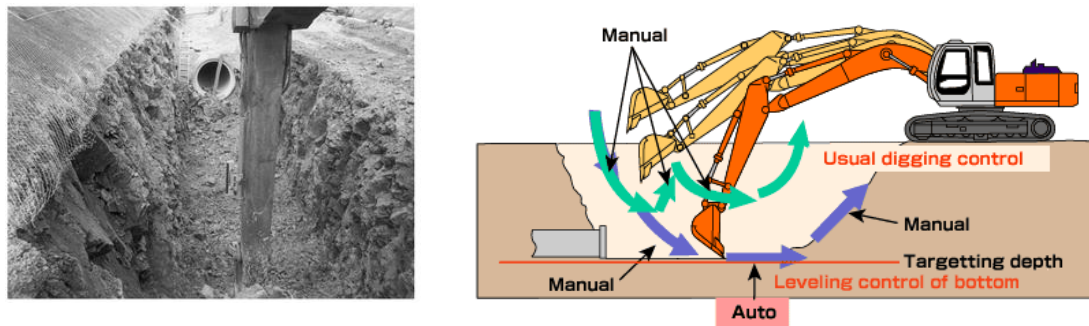


Figure 2.8 – The auto levelling controller developed by Hitachi provides assistive control for level digging operations and when the operator cannot see the bottom of the cut. From Haga et al. (2001).

2.1.5 Hydraulic Arm Control

Control of a hydraulic excavator arm in free motion is a required step before any attempt at digging is made. During the early 90's several authors reported detailed analyses of the kinematics (Koivo, 1994) and rigid-body dynamics (Vähä and Skibniewski, 1993) of a hydraulic excavator arm, including the nonlinear relations between cylinder lengths and joint angles.

While the kinematics and rigid-body dynamics equations of the excavator arm were quickly formulated, the low-level control of the cylinders remains a current challenge.

One difficulty arises from nonlinearities due to the dead zone often found in valves used to control cylinder flow. While the dead zone is a designed feature for minimising leakage through spool overlap, the same overlap introduces non-linearities in flow control that must be compensated. Another difficulty is related to high friction of cylinder seals due to the tight sealing required by the internal pressure of the hydraulic circuit. Lischinsky et al. (2002) reported that joint friction in a Schilling Robotics Titan 2 hydraulic manipulator accounted for 30% of the total nominal actuator commands.

Model-based control laws for the hydraulic cylinders in an excavator can become extremely complex due to the governing equations and parameter variations. For example, Sohl and Bobrow (1999) suggests that accurate measurement of fluid bulk modulus is essential for proper linearisation. However, identification of parameters can be difficult in the excavation scenario due to the large and varying loads and consequent changes in hydraulic oil temperature which may cause uncertainty and fluctuations in the effective bulk modulus of the oil. Moreover, while the majority of experimental investigations of control methods have focused on single cylinders, a real excavator arm presents flow coupling due to simultaneous motion of multiple cylinders together with limited hydraulic pump and accumulator capacity. Nonlinearities in flow rates, friction, and dead zones usually require some form of robust control method (Bu and Yao, 2000; Sorouspour and Salcudean, 2001).

To avoid those dynamical complexities Song and Koivo (1995) proposed the use of a feedforward neural network to learn the inverse dynamics of a hydraulic excavator arm. For the same reasons, neural networks were used as a forward excavator model in Cannon (1999) and in Cannon and Singh (2000). The use of a free-motion fuzzy controller to position the arm for digging and to swing the arm during dumping also appeared in a patent by Gay (2004).

Zhang et al. (2005) proposed a look-up table nonlinear mapping to model the flow rate and a robust feedback for model error compensation. By means of system identification La Hera et al. (2008) derived a fourth-order linear time-invariant (LTI) model relating command to cylinder force, which was then used to implement an H_∞ inner loop force controller. In the same work, friction was compensated by an approximate model based on a static velocity-current mapping obtained experimentally.

Lischinsky et al. (2002) used the LuGre friction model (Åström and Canudas de Wit, 2008) to compensate friction in an industrial hydraulic arm with rotary actuators. The same model was used to compensate friction in a single cylinder by Zeng and Sepehri (2006).

A popular friction compensator in hydraulic systems is the Friedland-Park observer (Friedland and Park, 1992). This observer provides an estimator of the magnitude of Coulomb friction and was introduced for excavator hydraulic control by Tafazoli et al. (1998). A variable structure observer (VSO) was proposed as a robust alternative to the Friedland-Park observer with a switching action on the correction in Ha et al. (2000a), who also tested this observer on an excavator arm. Bonchis et al. (2001) experimentally investigated the performance of several friction compensation methods using a single-cylinder experimental setup. The experimental results showed that while all compensation methods improved in relation to a PD controller, a VSO achieved better robustness against parameter variation. An alternative model for friction compensation of hydraulic cylinders was also proposed in Bonchis et al. (1999) by making direct use of cylinder differential pressure.

The use of sliding mode control (SMC) for robust control of hydraulic actuators has been investigated and proposed by several authors (e.g. Alleyne and Liu (2000); Perruquetti and Barbot (2002); Bessa et al. (2010)). Sliding mode control in exca-

vation was introduced by Malaguti (1994b) to overcome uncertainty in the values of hydraulic parameters and load variations. Experiments in Nguyen (2000) using the same experimental platform as the present work showed that the robustness provided by SMC could properly compensate for friction in cylinders, thus suppressing the need for a friction observer. This work was also reported in Ha et al. (2002). Experiments with SMC on a 13 tonne excavator were reported by Lee and Chang (2002). Bonchis (2001) reported by means of experiments with a single hydraulic cylinder that, although SMC achieved better positioning performance than a VSO, SMC implementation was more difficult due to the large number of required parameters.

Following this brief survey of control methods and load models in excavation, the next section will discuss the effects of disturbance force prediction on the sensitivity function of a feedback controller. In excavation, prediction will be shown to be useful in overcoming the limitations of a feedback controller in rejecting the large disturbance forces generated during contact. The principal theoretical results of section 2.2 will be used in Chapter 6 to quantify and compare the inaccuracy of predictive methods in excavation.

2.2 Fundamental Limitations

Consider initially the generic linear feedback control system shown in Figure 2.9 (a), where C is the feedback controller and P represents the dynamics of the plant free from loads or interaction with the environment: that is, in free motion. The dynamics that arise during interaction with the environment are assumed to enter the plant as load disturbances $d(t)$ generating feedback action and changing the total input $e(t)$ to the plant. In excavation, $d(t)$ can be thought of as the force produced by soil-tool interaction. The relation between the disturbance $d(t)$ and its effect on the plant

input $e(t)$ is given by the sensitivity transfer function $S = (1 + CP)^{-1}$ as shown in Figure 2.9 (b). To attenuate the effects of the disturbance at the plant input it is desired to decrease the magnitude of S which is usually achieved by designing the controller C . Note that when $|S| < 1$, or equivalently when $\log |S| < 0$, the effect of the disturbance is decreased, indicating that the feedback improves the disturbance rejection of the system. When $|S| > 1$, or equivalently when $\log |S| > 0$, the presence of the feedback, in fact, *increases* the effect of the disturbance at the plant input.

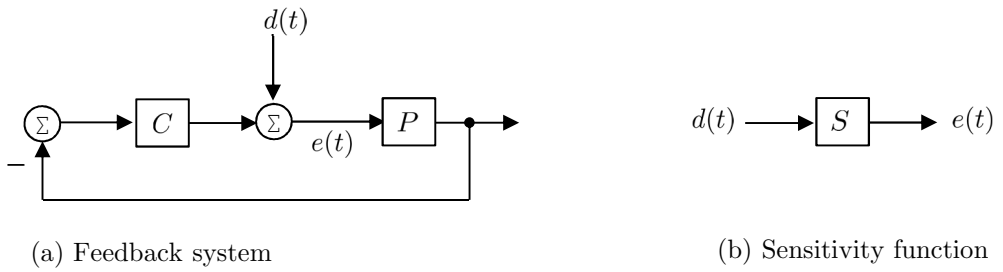


Figure 2.9 – (a) A feedback system with disturbances at the plant input. (b) The sensitivity function.

2.2.1 The Bode Integral

A fundamental property of linear feedback systems is that the integral of the logarithm of the magnitude of the sensitivity transfer function S can not be changed by feedback action (Bode, 1956; Seron et al., 1997). In other words, the Bode integral has a constant value given by the frequency response of the discrete sensitivity function

$$\frac{1}{2\pi} \int_{-\pi}^{\pi} \log |S(e^{j\omega})| d\omega = \sum_{i=1}^n \log |\lambda_i(A)| , \quad (2.4)$$

where the integral is evaluated over the unit circle and λ_i are the unstable poles of the open-loop plant with state-matrix A . For an open-loop-stable plant where all poles are stable the integral is zero. The Bode integral is regarded as a conservation

law of feedback control. This conservation law, also known as the “waterbed effect”, is illustrated in Figure 2.10. The figure graphically shows that the Bode integral in Equation (2.4) computes the area of the logarithm of the sensitivity function of the feedback system. Designing a controller to increase the negative area, which increases disturbance rejection at lower frequencies, inevitably increases the positive area, amplifying disturbances at higher frequencies. This is a fundamental limitation of feedback control.

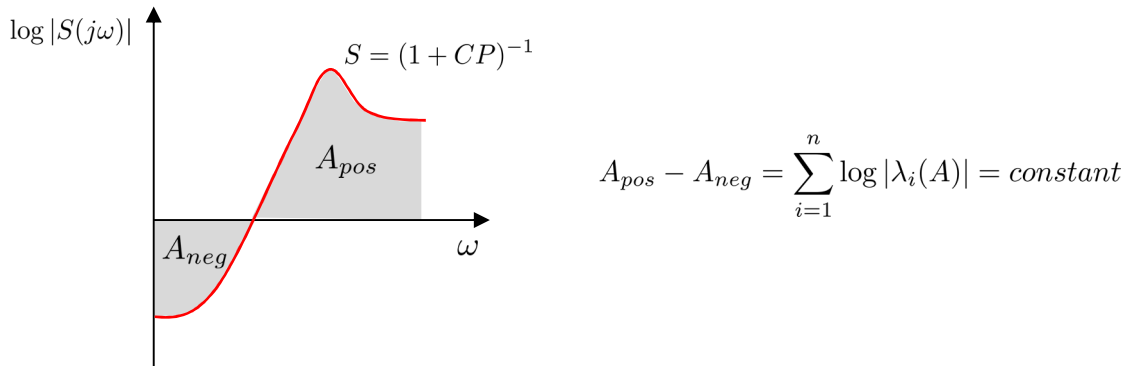


Figure 2.10 – Illustration of the waterbed effect for an open-loop-unstable plant.

2.2.2 Controllers with Preview

A recent result from Martins et al. (2007) shows that the fundamental feedback limit can be overcome in a system where the controller has a finite-horizon preview of the disturbance, also referred to as a system with side information.

Feedback control with side information is usually treated under the framework of preview control. One of the first authors to introduce preview control (Tomizuka, 1975) motivates the problem in a very simple way:

“If a driver cannot look ahead, he will not be able to drive a car. By seeing the road shape, adjacent vehicles, etc., and by planning ahead, one can decide what kind of action should be taken to overcome the limited rate of response of human and vehicle dynamics.”

Preview control differs from traditional feedforward control as it investigates the best possible use of disturbance information, rather than transmitting it as an additional time-indexed feedforward signal. In preview control the feedback controller is designed to process the preview information to improve control actions—for example, by considering the lookahead time for which the best performance improvement can be achieved (Seiler et al., 2012) or by augmenting an H_∞ feedback controller with the preview information (Takaba, 2003).

The prototypical case of a controller with side information is a networked control system where a sensor node that is physically distant from the plant provides information through a communication network to the controller about incoming disturbances before they reach the plant. As an example of such system consider an aircraft controller that attempts to regulate the pitch angle despite the presence of headwinds. A cartoon is shown in Figure 2.11. In Figure 2.11 (a) the aircraft controller has no information about the disturbance such that disturbance rejection is provided solely by the feedback controller whose sensitivity is indicated by S . In an idealised opposite case, Figure 2.11 (b) shows an aircraft controller that has access to the disturbance m units before it arrives at the plant via a remote preview system (RPS). Assuming that the controller makes appropriate use of this perfect information, complete disturbance rejection becomes possible and the sensitivity of such controller, here indicated by $S_{d,e}$, is zero. In practice, sensing, transmission and use of disturbance information is not perfect and the output of the remote preview system is an estimated value of the true disturbance as shown in Figure 2.11 (c). In this case complete rejection is

not possible. It is expected, however, that the proper use of partial information leads to a sensitivity that is lower than the sensitivity of a pure feedback controller, that is $|S| > |S_{d,e}| \neq 0$.

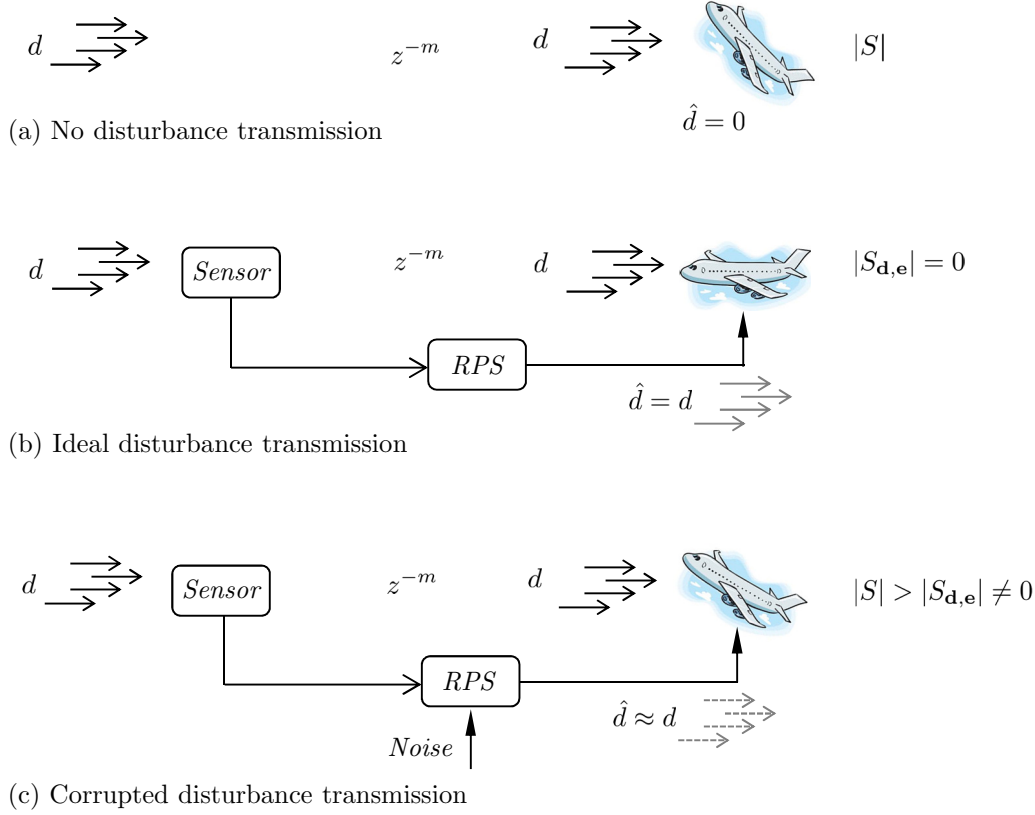


Figure 2.11 – Examples of an aircraft pitch control system with and without side information. The sensor could be a Doppler radar. (a) The case of a feedback controller without side information. (b) The idealised case where disturbances from a wind gust is perfectly transmitted to the controller. (c) The non-ideal case where the disturbances from a wind gust is partially transmitted to the controller.

A control structure for a generic system with side information is shown in Figure 2.12. In the figure G is a linear time-invariant filter that represents a model of the disturbance that relates the physical phenomena \mathbf{w} to the disturbance signal \mathbf{d} through a time delay. To quantify the limitations of the remote preview system a possible interpretation is to treat the RPS as a communication channel with limited capacity. The output of the RPS is used by the controller K to generate compensation

with non-causal action. The delay z^{-m} indicates that the controller has access to the imperfect disturbance preview m units before the disturbance enters the plant.

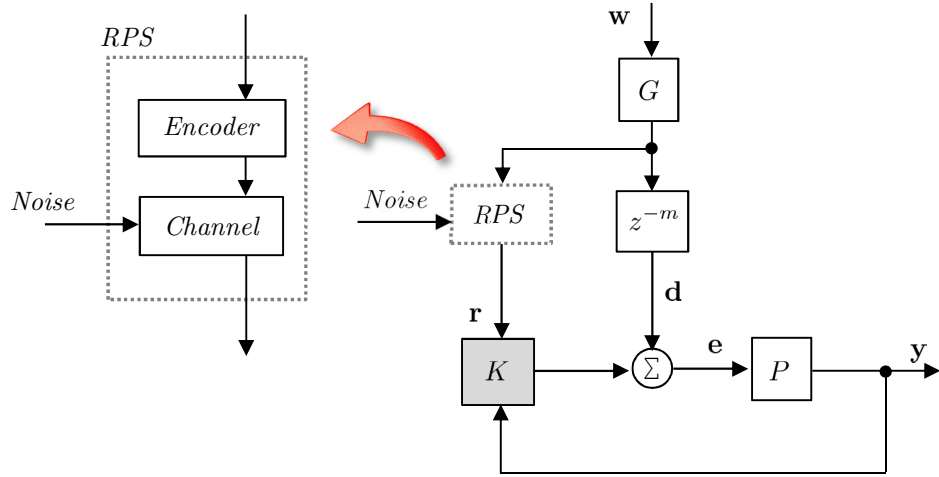


Figure 2.12 – A generic control system with side information where K is the controller, P is the plant, G is the disturbance model, and RPS is a remote preview system that transmits the encoded disturbance through a channel with limited capacity, w is the source of physical phenomena, d is the disturbance that reaches the plant m units later than the preview r , e is the plant input and y is the plant output.

In contrast to a predictive control problem with an inaccurate feedforward model, in preview control the inaccuracy is not on the model but on the information that is being transmitted to the controller, which can be limited in horizon and/or integrity. In feedforward control the main issue is to improve the model accuracy for better prediction, while in preview control the main challenge is to make use of the limited preview information by means of feedback design. Control design with preview has motivated a formal treatment of performance stability and limitations. Analyses of the performance of systems with preview have been investigated as a function of a variety of design methods, such as linear quadratic and both H_2 and H_∞ synthesis approaches. Such analyses are found, for example, in Cohen and Shaked (1997); Kojima and Ishijima (1999, 2003), Middleton et al. (2004); and Seiler et al. (2012).

Limitations of controllers with preview have also been investigated by means of entropy measures. Such an information-theoretic approach is mostly used in the feedback context where the loop is closed on communication channels. Initial results in this area are attributed to Iglesias (2001) and are based on the observation that the sensitivity integral of a feedback controller is related to the differences of entropy rate between the exogenous signal and the control action. Investigation of this relation shows, for example, how the constrained information rates of the control loop change the fundamental limits of a feedback controller. Here, the work of Martins et al. (2007) is of particular interest because it relates the entropy rate of a system with preview to limits on the attenuation of the magnitude of the sensitivity integral.

2.2.3 Information Metrics in Preview Control

This section introduces some of the basic definitions and an informal derivation based on the work of Martins et al. (2007) that leads to two results of interest for the present work: a bound of the maximum achievable decrease of the magnitude of the sensitivity function by means of side information; and the concept of a “sensitivity-like” function, a term defined by Martins et al. (2007), which is the sensitivity of a system provided with side information.

Basic Definitions

The basic quantity in this section is the entropy of a random variable X defined as

$$H(X) = - \sum p(x) \log_2 p(x) \quad (2.5)$$

where p is the probability distribution of x . In information theory the concept of entropy can be described in different ways: as a measure that quantifies “choice” and the uncertainty of an outcome (Shannon, 2001) or as the average uncertainty of a variable (Cover and Thomas, 2006). For the purposes of this section, perhaps the most natural interpretation of entropy is the one given in Papoulis and Pillai (2002), where entropy is said to quantify the amount of information that one gains when the value of a variable is known. From Figure 2.12 it is intuitively seen that if a control system has access to a corrupted version \mathbf{r} of the incoming disturbance \mathbf{d} that the plant will encounter, not only will this information have an influence on the disturbance rejection performance (for example, as a preemptive compensation) but this gain in information is quantifiable in terms of its entropy. In fact, the principal result in Martins et al. (2007) is that the rate at which information \mathbf{r} arrives at the system via the communication channel is directly related to the decrease in the magnitude of the sensitivity function S of the control system.

In the continuous case, the entropy of a random variable \mathbf{a} is defined as

$$h(\mathbf{a}) = - \int_{\mathcal{X}} p_a(\gamma) \log_2 p_a(\gamma) d\gamma, \quad (2.6)$$

and the conditional differential entropy is defined as

$$h(\mathbf{a}|\mathbf{b}) = - \int_{\mathcal{X}'} \left(\int_{\mathcal{X}} p_{a|b}(\gamma_a, \gamma_b) \log_2 p_{a|b}(\gamma_a, \gamma_b) d(\gamma_a) \right) d\gamma_b \quad (2.7)$$

where $\mathcal{X}, \mathcal{X}'$ are the support sets of \mathbf{a} and \mathbf{b} respectively, and $p_{a|b}$ is the conditional probability of \mathbf{a} given \mathbf{b} .

The mutual information rate is defined (Martins and Dahleh, 2008, Definition 1.3) as

$$I_{\infty}(\mathbf{a}; \mathbf{b}) = \lim_{N \rightarrow \infty} \sup \frac{I(\mathbf{a}_0^{N-1}; \mathbf{b}_0^{N-1})}{N} \quad (2.8)$$

where $\mathbf{a}_0^{N-1} = [\mathbf{a}(0), \mathbf{a}(1), \dots, \mathbf{a}(N-1)]^T$ is a stochastic process and

$$I(\mathbf{a}; \mathbf{b}) = h(\mathbf{a}) - h(\mathbf{a}|\mathbf{b}) \quad (2.9)$$

is the mutual information where the convention $\mathbf{a} = \mathbf{a}_0^{\infty}$ is adopted. The mutual information indicates the dependency between the variables \mathbf{a} and \mathbf{b} in the form of the reduction in the uncertainty of \mathbf{a} given knowledge of \mathbf{b} . In the context of Figure 2.12 a large mutual information rate $I(\mathbf{r}; \mathbf{d})$ indicates that \mathbf{r} and \mathbf{d} have a large entropy overlap; that is, the partial preview given by \mathbf{r} contains significant information about the true disturbance \mathbf{d} .

The capacity of a channel represents the maximum value $I_{\infty}(\mathbf{a}; \mathbf{b})$ achieved as \mathbf{a} ranges over all possible inputs

$$C_p = \max_{p_a} I_{\infty}(\mathbf{a}; \mathbf{b}). \quad (2.10)$$

The entropy rate $h_{\infty}(\mathbf{x})$ is defined as

$$h_{\infty}(\mathbf{x}) = \lim_{N \rightarrow \infty} \frac{h(\mathbf{x}_0^{N-1})}{N}. \quad (2.11)$$

For a normal process \mathbf{x} the entropy rate is related to its power spectrum $F_{\mathbf{x}}$ through Equation 14-130 of Papoulis and Pillai (2002):

$$h_{\infty}(\mathbf{x}) = \frac{1}{4\pi} \int_{-\pi}^{\pi} \log(2\pi e F_{\mathbf{x}}(\omega)) d\omega. \quad (2.12)$$

Although a normal process is being used here to simplify the derivation, a recurrent

strategy for generalisation of the results to an arbitrary process relies on the fact that a normal distribution has the maximum entropy amongst all process under the same covariance. Based on this argument, it can be shown (Martins et al., 2007) that Equation 2.12 generalises for a non-Gaussian process to the inequality

$$h_\infty(\mathbf{x}) \leq \frac{1}{4\pi} \int_{-\pi}^{\pi} \log(2\pi e F_{\mathbf{x}}(\omega)) d\omega. \quad (2.13)$$

Considering that the normal process \mathbf{x} is the input of a linear system with transfer function $L(z)$, then the output \mathbf{y} is also normal and the relation between their power spectra is given by

$$F_{\mathbf{y}}(\omega) = F_{\mathbf{x}}(\omega) |L(e^{j\omega})|^2. \quad (2.14)$$

From Equations (2.12) and (2.14) we obtain

$$\begin{aligned} h_\infty(\mathbf{y}) &= \frac{1}{4\pi} \int_{-\pi}^{\pi} \log(2\pi e F_{\mathbf{x}}(\omega) |L(e^{j\omega})|^2) d\omega \\ h_\infty(\mathbf{y}) &= h_\infty(\mathbf{x}) + \frac{1}{2\pi} \int_{-\pi}^{\pi} \log |L(e^{j\omega})| d\omega \end{aligned} \quad (2.15)$$

The equality in Equation (2.15) represents the entropy rate of the response of a linear system, which also extends to arbitrary processes (Papoulis and Pillai, 2002, p. 663) where the distribution is not necessarily normal.

Sensitivity Reduction Due to Preview

Note from Equations (2.15) and (2.4) that both integrals are identical, and therefore if $L(z)$ represents the sensitivity transfer function $S(z)$ of the control system shown

in Figure 2.9, then it follows that

$$h_\infty(\mathbf{e}) - h_\infty(\mathbf{d}) = \frac{1}{2\pi} \int_{-\pi}^{\pi} \log |S(e^{j\omega})| d\omega = \sum_{i=1}^n \log |\lambda_i(A)|. \quad (2.16)$$

The central result in Martins et al. (2007) is that for a system with a remote preview system (RPS), the entropy rates of the plant input \mathbf{e} and the disturbance \mathbf{d} are related by

$$h_\infty(\mathbf{e}) - h_\infty(\mathbf{d}) \geq \sum_{i=1}^n \max\{0, \log |\lambda_i(A)|\} - I_\infty(\mathbf{r}; \mathbf{d}). \quad (2.17)$$

Notice that for a system without preview—that is, when \mathbf{e} is a function only of \mathbf{d} and $I_\infty(\mathbf{r}; \mathbf{d}) = 0$ —the summation in Equation 2.17 is recognised as the Bode integral, Equation (2.4). With an RPS block available, the term $I_\infty(\mathbf{r}; \mathbf{d})$ is non-zero and represents the flow of information between the disturbance and the preview input.

Since, by definition, the maximum information rate is the channel capacity, Equation (2.17) can be rewritten as

$$h_\infty(\mathbf{e}) - h_\infty(\mathbf{d}) \geq \sum_{i=1}^n \max\{0, \log |\lambda_i(A)|\} - C_p. \quad (2.18)$$

Using Equation (2.13) in the previous Equation (2.18), we obtain

$$\begin{aligned} \frac{1}{4\pi} \int_{-\pi}^{\pi} \log(\hat{F}_\mathbf{e}(\omega)) d(\omega) - h_\infty(\mathbf{d}) &\geq \\ \sum_{i=1}^n \max\{0, \log |\lambda_i(A)|\} - C_p - \frac{1}{2} \log(2\pi e). \end{aligned} \quad (2.19)$$

Returning to Equation (2.15), the entropy rate of the system response applied to the

model of the disturbance G in Figure 2.12 is

$$h_\infty(\mathbf{d}) = \frac{1}{4\pi} \int_{-\pi}^{\pi} \log(\hat{F}_\mathbf{d}(\omega)) d(\omega) + h_\infty(\mathbf{w}), \quad (2.20)$$

and from Equations (2.19) and (2.20),

$$\begin{aligned} \frac{1}{4\pi} \int_{-\pi}^{\pi} \log \left(\frac{\hat{F}_\mathbf{e}(\omega)}{\hat{F}_\mathbf{d}(\omega)} \right) d(\omega) &\geq \\ \sum_{i=1}^n \max\{0, \log |\lambda_i(A)|\} - C_p - \frac{1}{2} \log(2\pi e) + h_\infty(\mathbf{w}). \end{aligned} \quad (2.21)$$

The ratio $\hat{F}_\mathbf{e}(\omega)/\hat{F}_\mathbf{d}(\omega)$ gives rise to a function similar to the sensitivity transfer function of a feedback controller. Notice, however, that $\hat{F}_\mathbf{e}$ is a signal that also contains the information provided by the RPS that transmits information in a feedforward manner. Martins et al. (2007) defines the “sensitivity-like function” of a stochastic system with an RPS as

$$S_{\mathbf{d}, \mathbf{e}} = \sqrt{\hat{F}_\mathbf{e}(\omega)/\hat{F}_\mathbf{d}(\omega)}. \quad (2.22)$$

In the case where \mathbf{w} is a normal process $h_\infty(\mathbf{w}) = (1/2) \log(2\pi e)$ and Equation (2.21) becomes

$$\frac{1}{2\pi} \int_{-\pi}^{\pi} \log |S_{\mathbf{d}, \mathbf{e}}(\omega)| d\omega \geq \sum_{i=1}^n \max\{0, \log |\lambda_i(A)|\} - C_p. \quad (2.23)$$

Since the entropy rate of a normal distribution is maximal for a given variance, assuming \mathbf{w} to be normal leads to a conservative estimate of the lower bound, and Equation (2.23) is valid for non-Gaussian disturbances as well.

A graphical interpretation of Equation (2.23) is given in Figure 2.13 where the grey area equals the channel capacity of the RPS. The effect of the preview is to decrease the sensitivity to disturbances, relaxing the original limitation of the conventional Bode integral of a pure feedback system ($S = (1 + CP)^{-1}$). Figure 2.13 suggests that

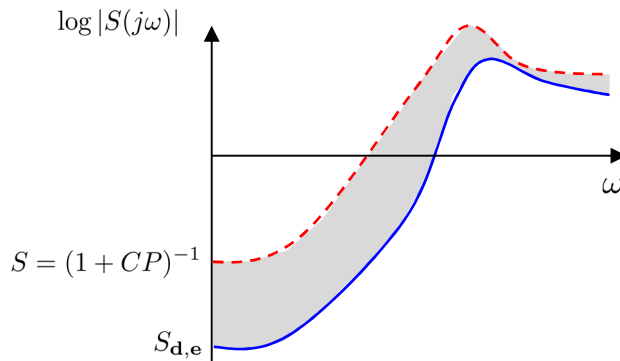


Figure 2.13 – The sensitivity of a system with preview is lower than that of a system where disturbance rejection is achieved purely by feedback control action.

for a control system that has access to disturbance values by means of a non-causal RPS, the disturbance rejection can be improved beyond feedback limitations.

Notice that the channel capacity as defined in Equation (2.10) is the maximum information rate which is dependent only on the RPS, and not on the limitations of the plant. If the system can not make full use of the preview information, for example because of limited actuation bandwidth or noisy actuators, the sensitivity will not be reduced to the bound C_p . The achievable reduction will lie between S and $S_{d,e}$ and will not reach $S_{d,e}$. Using the driving analogy from Tomizuka (1975), although the driver may have very good eyesight and reflexes, the information contained in the driver's view of the road can not necessarily be fully used if the car does not respond as commanded due, for example, to a defective steering system. Intuitively, in this situation the attenuation of the disturbances (resulting in effective driving performance) does not make full use of the channel capacity (the sensorimotor capability of the driver). This discrepancy between the achieved attenuation and channel capacity is illustrated in the following example.

Example: Attenuation with a Noisy Channel

To illustrate the effect of side information transmitted by a remote preview system (RPS) on the original sensitivity function, consider the following example where the control system in Figure 2.12 has a plant and controller given as

$$P(s) = \frac{25}{(s^2 + 7s + 25)(0.01s + 1)}, \quad K(s) = -4. \quad (2.24)$$

The plant is open-loop-stable and therefore Equation (2.23) becomes

$$\int_{-\pi}^{\pi} \log |S_{\mathbf{d}, \mathbf{e}}(\omega)| d\omega \geq -2\pi C_p. \quad (2.25)$$

For simplicity, consider that the RPS has a noisy channel such that $\mathbf{r} = \mathbf{d} + \mathbf{n}$, where \mathbf{n} is Gaussian noise. The capacity of a channel with additive white noise is

$$C_p = \frac{1}{2} \log_2 \left(1 + \frac{\bar{\sigma}_d^2}{\sigma_n^2} \right), \quad (2.26)$$

where $\bar{\sigma}_d^2$ is the variance of the disturbance, representing the power of the input signal such that $\bar{\sigma}_d^2 = \text{Var}(d)$. The value of σ_n^2 is the variance of the additive noise. Figure 2.14 shows the sensitivity-like function for four different values of noise variance.

The results were computed with the power spectral density (PSD) ratios in Equation (2.22) by simulating the controller in Figure 2.12 with known disturbances \mathbf{d} to obtain the plant input \mathbf{e} , and therefore the PSD $\hat{F}_{\mathbf{e}}$. The values of the attenuated sensitivity-like functions obtained from the PSD ratios and the channel capacities obtained from Equation (2.26) are listed in Table 2.1. As shown by the simulated

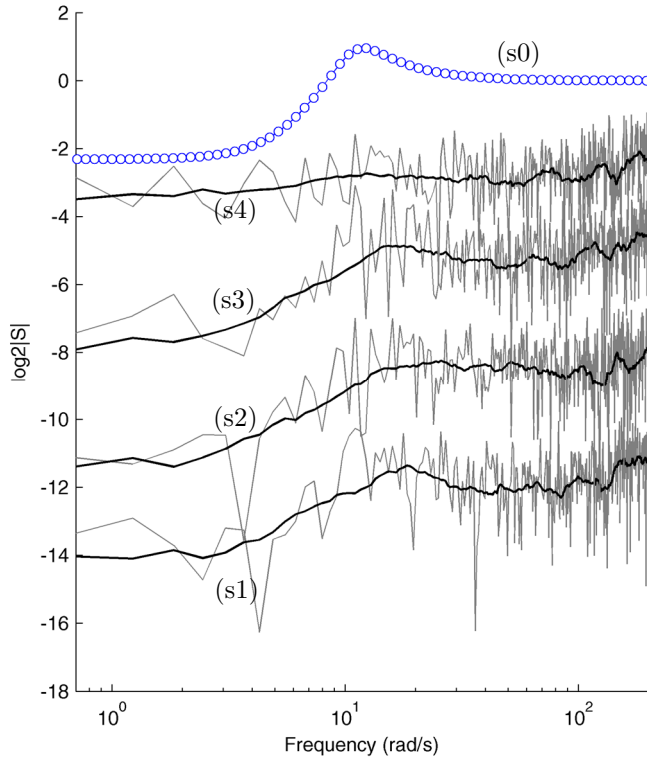


Figure 2.14 – Examples of sensitivity-like functions for four different Gaussian noise variances. The grey curves represent the true values. The black curves are smoothed versions used only to facilitate visualisation. In simulations (s1) to (s3) the system is ideal and the preview is fully used for disturbance compensation, thus the attenuation value is similar to the lower bound defined by the capacity (refer to Table 2.1). In (s4) noise in the actuator decreases the attainable sensitivity attenuation despite the capacity of the channel being large. The circles (s0) show the feedback sensitivity function when the system has no RPS.

cases s1, s2, and s3, smaller noise variances in the channel lead to larger sensitivity reductions.

As mentioned, the communication capacity of the remote preview system provides an upper bound on the attenuation of disturbances. This upper bound can be achieved only if the transmitted preview value can be fully utilised by the controller and reproduced by the actuators. This is indicated by the values of simulation (s4) on Table 2.1 where Gaussian noise with variance of 0.25 was added to the actuator input. The

Table 2.1 – Attenuation and channel capacity values.

	Attenuation $\int_{-\pi}^{\pi} \log S_{\mathbf{d}, \mathbf{e}}(\omega) d\omega$	Channel capacity $2\pi C_p$	Noise variance	
			Channel	Actuator
s0	0	0	—	—
s1	69.35	69.91	0.001	0
s2	48.09	49.08	0.01	0
s3	27.57	28.06	0.1	0
s4	13.08	28.31	0.1	0.25

noise compromises the effectiveness of the preview, causing disparity between the capacity of the communication channel (28.31 bits/message) and the attained sensitivity attenuation (13.08 bits/message). In Figure 2.14 this disparity can be seen by comparing the (s3) and (s4) curves. Both simulations have the same channel capacity, however, (s4) does not achieve the lower bound while (s3) does.

Note from this example that only the disturbance \mathbf{d} and the plant input signal \mathbf{e} were required to compute the attenuation values in Table 2.1. In Chapter 6, field trials with the excavator will allow for the recording of the plant input signal \mathbf{e} and an estimation method will be devised so that \mathbf{d} can be recovered from experiments. Experimental values of \mathbf{d} and \mathbf{e} will allow plotting of the sensitivity of an excavator controller provided with predictive action. Similar to this example, in Chapter 6 the signal-to-noise ratio (SNR) will be used to compute the channel capacity of the predictive method, allowing for a comparison between the actual attenuation achieved and its theoretical bound.

2.3 Iterative Learning Control

In the present work iterative learning control (ILC) will be used as a straightforward method for predicting excavation forces, with the main advantage that it does not require an explicit model of the soil-tool interaction.

Iterative learning control is a data-driven technique that uses previous tracking errors to improve input commands at the next iteration of a repetitive process. The main difference of ILC in comparison to classical adaptive control approaches is that ILC does not adapt parameter values or the feedback controller structure; instead, ILC directly modifies the input command.

As a technique that was focused initially on industrial robotic manipulators, performance improvement in ILC is usually considered to be in the form of precise tracking and fast transient performance. Precisely tracking a desired cut with a bucket is of little importance in excavation, and ILC may initially seem inappropriate. The aspect of ILC that is of interest to excavation is that ILC decreases tracking error by preemptively compensating disturbances. Recall from Figure 2.9 that the relation between position and disturbance in a feedback system is $Y = SD$. ILC adds a feedforward signal u to the loop such that $Y = S(D - U)$ and $(d - u) \rightarrow 0$ iteratively.

In excavation the use of ILC should not be viewed as a method of improving trajectory tracking accuracy. Instead, it should be regarded as an algorithm that generates preemptive disturbance compensation commands that increase the aggressiveness of intermediate passes and, as a consequence, also decreases tracking error. In fact, it can be shown that using a specific type of learning (plant inversion), ILC uses the disturbance of the previous pass to exactly compensate for the next pass.

The difference between using ILC in an industrial scenario and in excavation is illustrated in Figure 2.15, where an industrial manipulator attempts to achieve precise tracking with a potentially large number of iterations. In excavation, the critical passes are the intermediate passes, and precise tracking during the last passes is of lesser importance.

The basic ILC algorithm is illustrated in Figure 2.16 (a). The algorithm records the

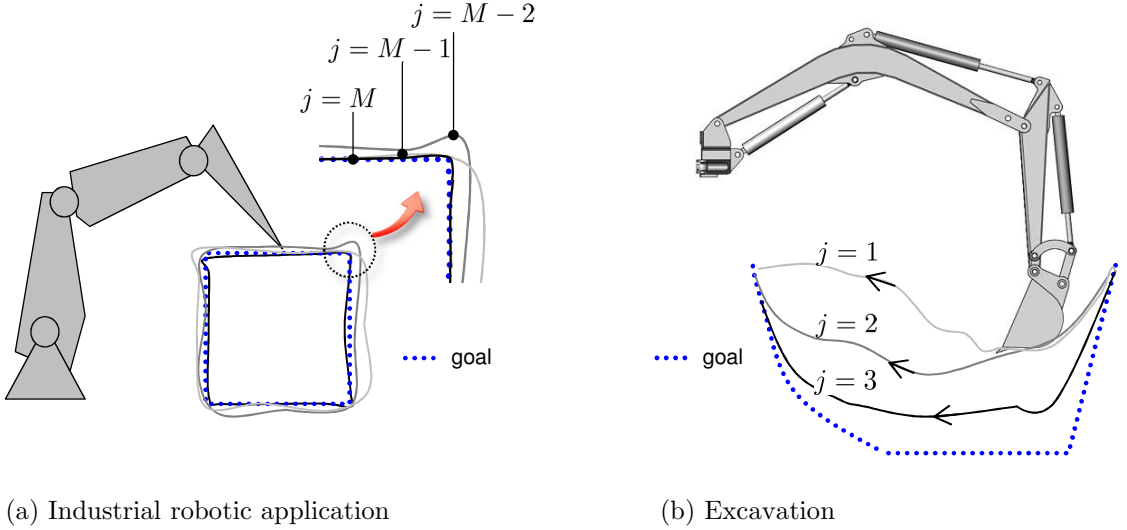
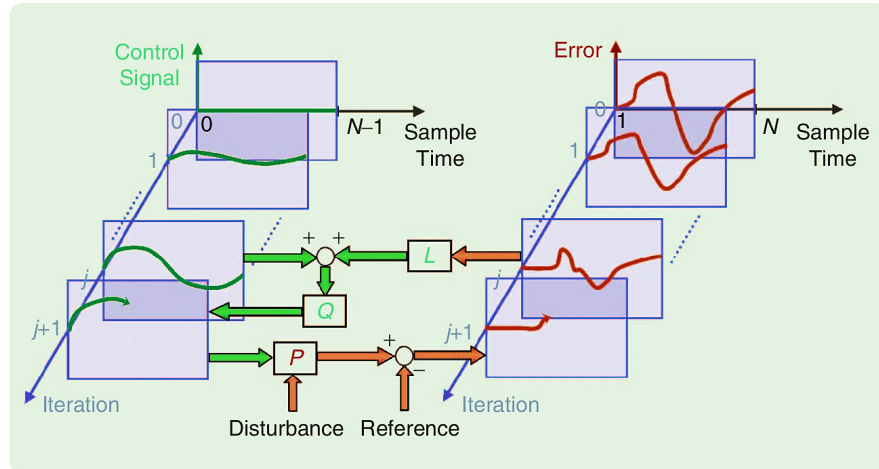


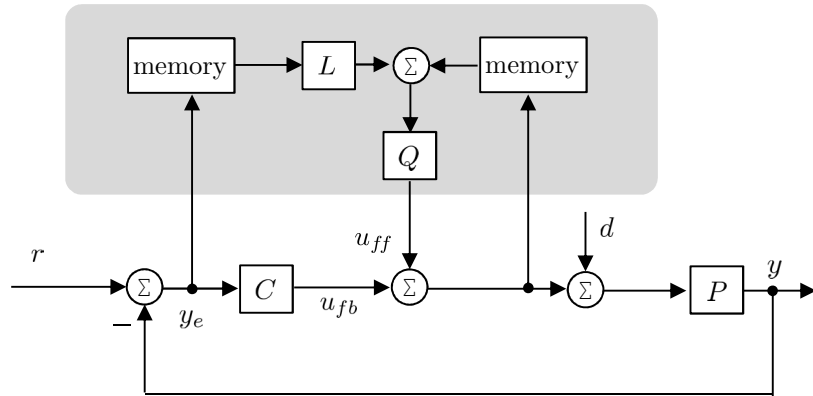
Figure 2.15 – (a) ILC is used in industrial robotics to achieve precise tracking after a potentially large number of passes M ; the number of iterations is usually of secondary importance. (b) ILC is used in excavation to increase the aggressiveness of intermediate passes to achieve the final cut with the least number of passes; the precision of the final pass is of secondary importance.

control signals u and the tracking error y_e during an attempt to track a trajectory. The tracking error is then mapped off-line to feedforward control commands by means of a learning function L . The resulting updated action $u + Ly_e$ is filtered with Q and used as an improved feedforward signal for the next tracking attempt. The controller structure is shown in Figure 2.16 (b) where the blocks on the grey background are implemented off-line. It will be shown that, given a sufficient number of iterations, this iterative process completely compensates repetitive disturbances through predictive action. An important point related to excavation is that the gain in performance provided by ILC is due to the fact that feedback action iteratively becomes predictive action: ILC transfers the disturbance compensation load to the predictive part of the controller, relying less and less on the possibly poor reactive action of the feedback controller.

As a flexible model-free approach, applications of ILC have been extended from in-



(a) ILC propagation in the time and iteration directions



(b) Control structure with ILC

Figure 2.16 – Basic structure of iterative learning control. The controller iteratively learns how to generate feedforward actions that compensate external disturbances and internal dynamics of the plant. (a) The ILC method consists of updating the feedforward input at the next iteration with the previous command plus a correction based on the tracking error. From Bristow et al. (2006). (b) The on-line part of the controller structure is a conventional feedback controller with feedforward input.

dustrial scenarios to several other areas ranging from insulin delivery (Wang et al., 2010) to traffic density control (Hou et al., 2007). Recent robotic applications are gait generation of hopping legs (Satoh et al., 2006), acquisition of writing skills with redundant manipulators (Tahara and Arimoto, 2011), control of surgical manipulators (Van

Den Berg et al., 2010) and quadrocopter control for acrobatic manoeuvres (Lupashin et al., 2010; Schoellig et al., 2012). An overview of ILC can be found in Moore et al. (2006) and Bristow et al. (2006), and extensive reviews of ILC results and applications can be found in Moore (1999) and Ahn et al. (2007).

The potential advantages of ILC in comparison to explicit modelling of soil-tool interaction forces in excavation are

- No explicit soil-tool interaction force modelling is required.
- Disturbances are estimated at the plant input, without the need for sensing of external forces and inner force-control loops.
- The learning also compensates for inaccurate modelling of the dynamics of the arm. In an approach that uses an analytical soil-tool model, unmodelled arm dynamics would erroneously be fitted by adjusting the soil-tool model parameters.

There are, however, three important assumptions required by ILC.

- The initial conditions are iteration-invariant. In excavation the start position of the arm must be the same at each iteration.
- Each iteration has the same pass length.
- For full compensation, disturbances must be iteration-invariant.

In Chapter 3 an excavation strategy will be proposed such that the first and second conditions are satisfied. The third assumption, however, needs special attention and will be discussed next in terms of algorithm convergence.

2.3.1 Convergence Properties

The following derivation introduces the conventional notation and some key properties of ILC. The derivation is useful to show the basic assumptions made to assure that ILC converges to zero tracking error or, equivalently, convergence to full disturbance rejection. More importantly, the derivation shows that the conditions for convergence are independent of the model of the interaction, which is the aspect of interest for autonomous excavation.

Consider the discrete system dynamics representation

$$\begin{aligned}\mathbf{x}_j(t+1) &= \mathbf{A}\mathbf{x}_j(t) + \mathbf{B}u_j(t) + \mathbf{B}d_j(t) \\ y_j(t) &= \mathbf{C}\mathbf{x}_j(t).\end{aligned}\tag{2.27}$$

where $j \in \{1, \dots, M\}$ indicates the iteration number, $t \in \{0, \dots, N-1\}$ is the time index sampled uniformly up to a fixed number of N samples. At each sampling \mathbf{x}_j is a n -dimensional state vector, y_j is the q -dimensional output vector and u_j and d_j are each m -dimensional, representing the control input and matched disturbance respectively. The matrices \mathbf{A} , \mathbf{B} and \mathbf{C} have dimensions $n \times n$, $n \times m$, and $q \times n$, respectively. Equation (2.27) could represent either an open- or closed-loop system. The output of the system during a pass j is

$$y_j(t) = \mathbf{C}\mathbf{A}^t\mathbf{x}_j(0) + \sum_{i=0}^{t-1} \mathbf{C}\mathbf{A}^{t-i-1}\mathbf{B}u_j(i) + \sum_{i=0}^{t-1} \mathbf{C}\mathbf{A}^{t-i-1}\mathbf{B}d_j(i).\tag{2.28}$$

Assumption 1. At the beginning of each iteration the system is returned to the same initial condition. Refer to Equation (2.28) and note that the difference between two iterations will cancel the first term on the right hand side; that is

$$\mathbf{C}\mathbf{A}^t\mathbf{x}_{j+1}(0) - \mathbf{C}\mathbf{A}^t\mathbf{x}_j(0) = 0.$$

Assumption 2. Disturbances are repetitive. Again, refer to Equation (2.28) and note that the difference between two iterations will cancel the third term on the right hand side; that is $\mathbf{CA}^{t-i-1}\mathbf{Bd}_{j+1}(i) - \mathbf{CA}^{t-i-1}\mathbf{Bd}_j(i) = 0$

Under Assumptions 1 and 2 the difference between two consecutive iterations is then

$$y_{j+1}(t) - y_j(t) = \sum_{i=0}^{t-1} \mathbf{CA}^{t-i-1}\mathbf{B}(u_{j+1}(i) - u_j(i)). \quad (2.29)$$

To simplify notation the t index will be omitted whenever it refers to the whole time history $t = \{0, \dots, N-1\}$, such that \mathbf{f}_j represents the whole history of time-indexed values

$$\mathbf{f}_j = [\mathbf{f}_j(0), \dots, \mathbf{f}_j(N-1)]^T. \quad (2.30)$$

Assumption 3. All iterations have the same length; that is N is fixed.

The use of the lifted representation of the system dynamics is useful to derive the convergence condition and to investigate the properties of the algorithm in the iteration domain. Under Assumption 3, and using the usual ILC notation $\delta_j \mathbf{y}$ as introduced by Phan (1989), define the operator $\delta_j \mathbf{y} = \mathbf{y}_{j+1} - \mathbf{y}_j$. Then Equation (2.29) can be written in the lifted form as

$$\delta_j \mathbf{y} = \mathbf{P} \delta_j \mathbf{u}, \quad (2.31)$$

where the convolution sum in Equation (2.29) becomes the entries of the $N \times N$ matrix

$$\mathbf{P} = \begin{bmatrix} \mathbf{CB} & 0 & 0\dots & \dots & 0 \\ \mathbf{CAB} & \mathbf{CB} & 0\dots & \dots & 0 \\ \mathbf{CA}^2\mathbf{B} & \mathbf{CAB} & \mathbf{CB} & \dots & 0 \\ \vdots & \vdots & \vdots & \dots & 0 \\ \mathbf{CA}^{N-1}\mathbf{B} & \mathbf{CA}^{N-2}\mathbf{B} & \mathbf{CA}^{N-3}\mathbf{B} & \dots & \mathbf{CB} \end{bmatrix}. \quad (2.32)$$

The equation

$$\mathbf{u}_{j+1} = \mathbf{u}_j + \mathbf{L}\mathbf{y}_{e,j}, \quad (2.33)$$

where \mathbf{L} is $m \times q$ and is referred to as the learning matrix. The updated feedforward control signal of the next iteration \mathbf{u}_{j+1} has dimensions $m \times N$ and is based on the $q \times N$ dimensional history of the tracking error $\mathbf{y}_{e,j}$ of the previous pass.

Since $\delta_j \mathbf{y} = -\delta_j \mathbf{y}_e = \mathbf{P} \delta_j \mathbf{u}$ and $\delta \mathbf{u}_j = \mathbf{L} \mathbf{y}_{e,j}$, it follows that

$$\mathbf{y}_{e,j+1} = (\mathbf{I} - \mathbf{P}\mathbf{L})\mathbf{y}_{e,j}. \quad (2.34)$$

From the previous equation a necessary and sufficient condition for convergence to zero tracking error is that the eigenvalues of $(\mathbf{I} - \mathbf{P}\mathbf{L})$ are located inside the unit circle,

$$|\lambda_p(\mathbf{I} - \mathbf{P}\mathbf{L})| < 1 \quad \forall p. \quad (2.35)$$

Assuming that condition (2.35) is respected, recall from the notation in Equation (2.30) that $(\mathbf{I} - \mathbf{P}\mathbf{L})$ maps, point-by-point, each element of the error history in $y_{e,j}$ to a lower value in the next iteration. By repeating this process, each individual value of the error history therefore tends to zero.

In general, methods for designing the learning matrix make use of concepts originally proposed for feedback control in the time domain. Optimal design based on quadratic cost (Gunnarsson and Norrlöf, 2001), adaptive gain selection based on least-square regression (Chi et al., 2008), robust control (De Roover and Bosgra, 2000), and high-order pole-placement techniques (Phan and Longman, 2002) have all been proposed in the ILC context. Despite the availability of several model-based approaches, the PD-type learning function remains dominant (Longman, 2000).

The important characteristic of ILC when applied to excavation is that the design of the learning matrix \mathbf{L} does not depend on the dynamics of excavation for the algorithm to converge. Note from the matrix \mathbf{P} in (2.32) that the dynamics of the plant \mathbf{A} are contained in entries *under* the main diagonal but not in the diagonal itself. If the designer does not have a model of \mathbf{A} it is unclear if condition (2.35) can be satisfied. A property of interest often used in ILC is that the eigenvalues of a lower diagonal matrix are also the elements of the main diagonal. Thus, if \mathbf{L} is designed so that (a) the product \mathbf{PL} is lower diagonal and (b) \mathbf{A} is absent in the main diagonal entries, the condition (2.35) will be independent of \mathbf{A} . If \mathbf{L} is designed to be lower diagonal, condition (a) is satisfied as \mathbf{P} is also lower diagonal. Also, the elements in the main diagonal of \mathbf{PL} will be composed of the product $P_{(i,i)} \cdot L_{(i,i)}$ —where (i, i) is the row and column position index of the entry in the matrix—and the main diagonal of \mathbf{PL} becomes $\mathbf{CB} L_{(i,i)}$, satisfying condition (b).

In conclusion, a lower triangular learning matrix \mathbf{L} leads to a lower triangular product \mathbf{PL} where the eigenvalue condition is $1 - \mathbf{CB} L_{(i,i)}$.

To investigate the disturbance properties of ILC assume that the system in Figure 2.16 (b) is a linear time-invariant (LTI), single-input/single-output (SISO) system. Then

$$y_{j+1}(t) = T(z) (d_{j+1}(t) + u_{j+1}(t)) + T_r(z)r(t), \quad (2.36)$$

where $T = P/(1 + CP)$ is the load sensitivity function, and $T_r = (CP)/(1 + CP)$ is the complementary sensitivity function. Omitting the time index and using the generic ILC learning rule $u_{j+1} = u_j + Ly_{e,j}$ Equation (2.36) gives

$$y_{j+1} = Td_{j+1} + T(u_j + Ly_{e,j}) + T_r r. \quad (2.37)$$

From Equation (2.37), together with the fact that two consecutive error histories are related by the same reference input as $y_{e,j+1} = y_{e,j} + y_j - y_{j+1}$,

$$y_{e,j+1} = (1 - TL) y_{e,j} - T(d_{j+1} - d_j). \quad (2.38)$$

This equation shows that the error during iteration $y_{e,j+1}(t)$ does not vanish as long as the difference between two consecutive disturbances $d_{j+1}(t) - d_j(t)$ is non-zero. The error resulting from the non-repetitive parts of the disturbances is a lower bound of ILC performance usually known as the ILC baseline error. Equation (2.38) also shows that the differences between disturbances act as a forcing input that, when present, drives the error away from zero. When disturbances are repetitive and the condition (2.35) is satisfied the dynamics in the iteration direction become unforced and the error converges to zero at a rate that depends on the learning function.

2.3.2 Plant Inversion as Learning Function

The present work will make use of a particular type of learning function where L is an estimate of the inverse of the plant \hat{P}^{-1} . It is known (Moore, 1993) that the goal of ILC is to generate the output of the best possible inverse of the system to track a given reference. If the plant inverse is given as a learning function, one may wonder what the goal of ILC is in this case. The goal is that disturbance dynamics are usually not part of \hat{P}^{-1} and ILC learns to map those unmodeled disturbances as part of the feedforward command. In excavation, this means that if \hat{P}^{-1} is the inverse model of the arm, plant-inversion ILC will add the dynamics of the interaction with soil as a predictive part of feedforward action.

Using $L = \hat{P}^{-1}$ and rewriting Equation (2.33) with the feedback command explicitly

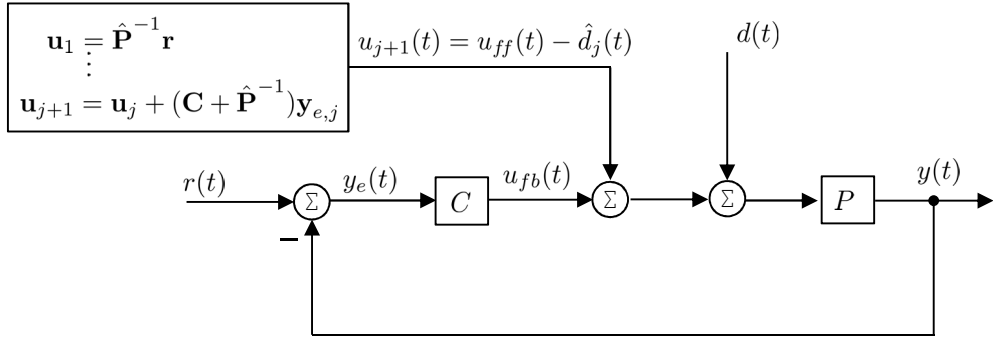


Figure 2.17 – Iterative learning control with plant inversion. This implementation achieves convergence in a single iteration by mapping the disturbances $d(t)$ onto the feedforward command $u_{j+1}(t)$.

appearing as the term Ce_j gives

$$\begin{aligned} u_{j+1}(t) &= u_j(t) + C(z)y_{e,j}(t) + \hat{P}^{-1}(z)y_{e,j}(t) \\ &= u_j(t) + [C(z) + \hat{P}^{-1}(z)]y_{e,j}(t). \end{aligned} \quad (2.39)$$

Taking $L' = (C + \hat{P}^{-1})$ as a learning function and substituting in Equation (2.38) we obtain

$$y_{e,j+1} = -T(d_{j+1} - d_j), \quad (2.40)$$

where the time index has been omitted. Comparison of Equations (2.38) and (2.40) shows that plant inversion as a learning function has the advantage that the error is dependent only on the disturbances, and not on the previous tracking error. Under iteration-repetitive disturbances, the learning process from zero disturbance knowledge to complete compensation is achieved in one iteration. Figure 2.17 shows the controller structure of the plant inversion implementation where the first iteration starts with reference compensation commands $\mathbf{u}_1 = \mathbf{P}^{-1}\mathbf{r}$.

2.3.3 Related Work: Inaccurate Prediction in ILC

Perhaps the main issue with ILC is that learning updates are known to be sensitive to non-repetitive disturbances. In terms of tracking error, the effect of non-repetitive disturbances was shown in Equation (2.40) where the difference between two consecutive disturbance histories are directly related to position errors. While in excavation the final position error is of secondary importance, non-repetitive disturbances generate inaccurate predictions during the important intermediate passes. Large inaccurate predictions does not allow the excavator to counteract disturbances with the best possible compensation action.

The Q -filter is perhaps the most general solution for counteracting the detrimental effects of non-repetitive disturbances in ILC. Norrlöf and Gunnarsson (2001) concluded that the relation between the cut-off frequency of the Q -filter and the frequency content of the disturbance determines the final performance of the controller. If it can be assumed that non-repetitive disturbances have significant power only at high frequencies $\omega > \omega_h$, which is usually the case of systems with noisy sensors, a low-pass filter Q with a cut-off frequency lower than ω_h will attenuate the detrimental effects of the noise from the learned signal. Low-pass filtering is also a condition for monotonic convergence and robustness in learning (Longman, 2000). Negative aspects of filtering are that the convergence rate deteriorates as the effective gain of the learning function is decreased (Norrlöf and Gunnarsson, 2001), and that full disturbance compensation can not be achieved. Low-pass filtering therefore involves a trade-off as the filter deliberately decreases performance in favour of robust learning in the presence of high-frequency disturbances. Clearly, low-pass filtering is not effective if the main non-repetitive components of the disturbance are present at low frequencies $\omega < \omega_h$.

Norrlöf (2004) investigated disturbance rejection in ILC based on the following vari-

ations of the plant-inversion learning function:

$$L = 1/G \quad (2.41a)$$

$$L = \mu/G \quad (2.41b)$$

$$L = 1/[(k + 1)G], \quad (2.41c)$$

where k is the iteration number, μ is a constant gain in the range $[0 \dots 1]$ and G is the plant model. Those functions were compared with both perfect and imperfect models resulting in six different updates. The interesting outcome of this comparison is that the best result was achieved with the learning function (2.41c) where G is a perfect model, while the worst result was obtained with the same function (2.41c), however with an imperfect model. This result shows that the optimal learning under ideal conditions is also the most fragile. The use of the pass number in (2.41c) acts as a derivative on the learned action. If the gradient is correct then prediction is favourable and the algorithm performs better than the usual plant-inversion learning (2.41a). On the other hand, with a wrong gradient (given by a plant with model error) prediction is worse than not using a derivative, and in this case the conventional (2.41a) performs better. For the same reason, the present work does not consider high-order ILC schemes; that is, schemes where more than one previous iteration is used during learning.

Chen and Moore (2002) explicitly addresses non-repetitive disturbances in ILC by exploring similar forms of learning functions and structures that are known to handle disturbances in the time domain. This approach uses the fact that ILC learning functions are analogous to feedback laws applied in the iteration domain, making the implementation intuitive and familiar. For the case where the repeating pattern is known, an implementation of the internal model principle (IMP) (Francis and

Wonham, 1976) in the iteration domain was proposed. In the case where the pattern is unknown a disturbance observer in the iteration domain was proposed. Chen and Moore (2002) noted that those schemes generate high-order ILC.

Chin et al. (2004) proposed eliminating the contribution of the non-repetitive disturbances by neglecting the feedback corrective action during learning. This is similar to updating the feedforward commands as if the previous iteration was in open-loop, as the effects of the disturbances do not show as non-causal actions. It should be noted, however, that feedback action is also a consequence of pure tracking error which can be present even in free motion. A possible drawback is that eliminating the feedback command during learning decreases the convergence rate.

Several approaches deal with non-repetitive disturbances by identifying and excluding the non-repetitive components of the learning signal rather than by attempting to compensate for them. In principle, this kind of approach is similar to low-pass Q -filtering (Longman, 2000; Norrlöf and Gunnarsson, 2001) where the non-repetitive parts of the disturbance are assumed to be contained in the frequencies beyond the cut-off of the filter. More sophisticated methods are needed, however, to identify non-repetitive disturbances that are present in the lower and mid frequency range.

One example of such identification is found in Mishra et al. (2007) where non-repetitive disturbances are identified in the tracking error of a silicon wafer positioning stage. The authors introduced the concept of segmented learning, where only output signals identified as repeatable are used to update the feedforward command. The nature of the process provided a good match to error segmentation since the repetitive segments—acceleration and deceleration of the stage—are also the segments that benefit the most from feedforward compensation. It was therefore possible to segment the error with physical observations of the process. In the case where segmentation

from physical observation is not obvious Mishra et al. proposed comparing repetitive R and non-repetitive NR metrics, where R is obtained by averaging the absolute values of the error profiles of several iterations, and NR is obtained by quantifying the variance of the error between iterations. The ILC update is of the form

$$u_{j+1}(t) = u_j(t) + \alpha(t)e_j(t) \quad (2.42)$$

where $t \in \{0, \dots, N - 1\}$ is the time index and $\alpha(t)$ is provided by a heuristic such that when the non-repetitive metric is larger than the repetitive metric the error at that sampling is skipped as

$$\alpha(t) = 0 \quad \text{if} \quad R(t) < f \cdot \max(NR) \quad (2.43)$$

where $f > 1$ is a safety factor.

Another segmentation approach was proposed by Tzeng et al. (2005) using wavelet filtering to identify the learnable parts of the output signal. The wavelet transform was used to decompose the signal into low resolution signals, and each individual signal was compared against a desired control profile. The signals with the desired profile were then used to reconstruct a filtered output error. The reconstructed signal was then used to update the feedforward input as usual. The method was tested on a single-axis rotary motor with unmodelled friction and backlash dynamics. The authors reported better convergence rate with wavelet segmentation when compared to conventional ILC learning. The wavelet technique was also used by Merry et al. (2006) for controlling a printer head. The flexible belt used to drive the head introduces dynamic effects that are difficult to model, presenting a suitable application for ILC. Experimental results showed that wavelet filtering led to smaller tracking error

than conventional ILC.

2.3.4 Related Work: ILC and H_∞ Control Design

Motivated by precision control of nano-positioning devices, Helfrich et al. (2010) introduced a systematic feedforward-feedback design with ILC and H_∞ control. This work also identifies the repeatable and non-repeatable components of the error, similar to the work of Mishra et al. (2007). Unlike Mishra et al., Helfrich et al. use the frequencies of the non-repetitive components of the tracking error to tune the design of an H_∞ feedback controller. The approach adopted in the present work is related to the work of Helfrich et al. in regards to the design of a feedback controller aiming at compensating for ILC limitations.

Helfrich et al. propose the segmentation of repetitive and non-repetitive components with the repetitive to non-repetitive (RNR) ratio metric

$$\text{RNR}(\omega) = 20 \log_{10} \left(\frac{R}{NR} \right) = 20 \log_{10} \left(\frac{|FFT[S(z)(r(z) - d(z))]|^2}{\sum_{j=1}^N |FFT[S(z)(d_j(z))]|^2} \right) \quad (2.44)$$

where FFT is the Fast-Fourier-Transform, and S , r , d , d_j are respectively the sensitivity of the feedback controller, the reference signal, the repetitive disturbance, and the non-repetitive disturbance. Figure 2.18 (a) sketches a possible form of the metrics R and NR . Figure 2.18 (b) shows how the relation would appear in the form of the ratio proposed by Helfrich et al. In this particular case, the repetitive parts have positive gain in the mid-frequency range. Helfrich et al. propose designing a feedback controller to attenuate the non-repetitive components with H_∞ design by means of weighting functions as shown in Figure 2.18 (c). In the example, the sensitivity of the H_∞ controller is specified to attenuate low-frequency disturbances. Frequencies

of repetitive content are learned using ILC by selectively filtering the learned signal with the Q -filter design. In this particular example learning is obtained by means of a band-pass filter as shown in Figure 2.18 (d).

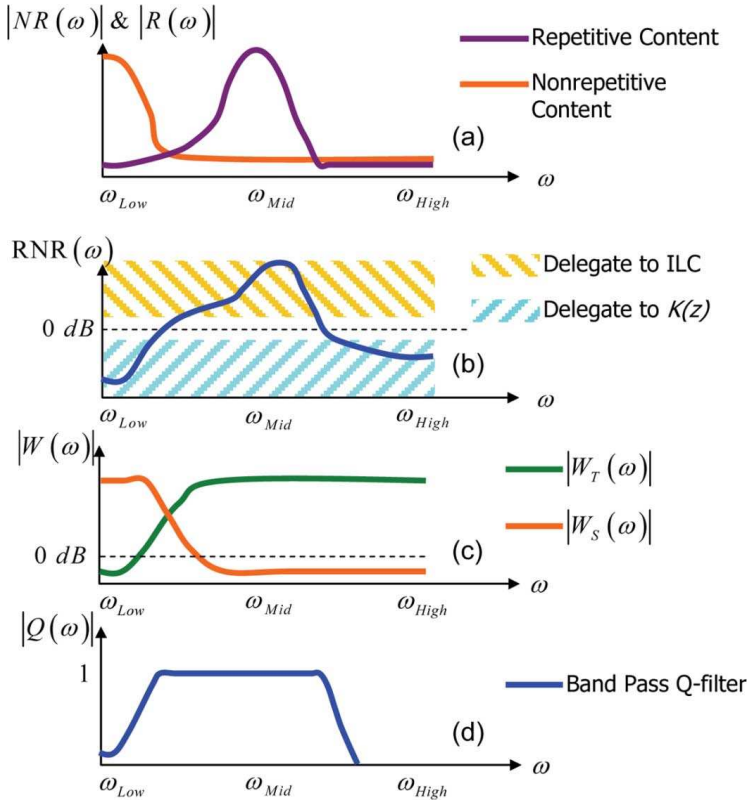


Figure 2.18 – An illustration of coordinated ILC and H_∞ design. (a) A hypothetical relation between the repetitive and non-repetitive contents of the error. (b) RNR ratio (c) Weighting functions during H_∞ design. (d) The Q -filter specification. From Helfrich et al. (2010).

As a designer can not separately access repetitive d and non-repetitive disturbances d_j , Equation (2.44) can not be implemented. Similar to the approach of Mishra et al., Helfrich et al. (2010) propose using the average of the tracking error $\bar{e}(z)$ as the repetitive component of the input signals in the numerator of the Equation (2.44), $\bar{e}(z) \cong S(z)(r(z) - d(z))$. The variance of the error $\tilde{e}(z)$ is used as the denominator of Equation (2.44), $\tilde{e}(z) \cong -S(z)d_j(z)$.

Note, however, that the repetitive to non-repetitive (RNR) ratio metric is also a function of the sensitivity S of the feedback controller, which is not yet designed, thus leading to an iterative design approach. In the first iteration a simple feedback controller is designed and executed a few times without ILC to obtain the statistics \bar{e} and \tilde{e} . The RNR ratio is then computed based on those errors from which the ILC can be designed in conjunction with the H_∞ feedback controller. As the new controller generates new sensitivities and new tracking errors, the process is repeated to recompute the RNR ratio and to refine the ILC and feedback designs, until convergence to the desired performance is achieved.

2.4 Conclusion

This chapter has reviewed the literature in autonomous excavation in Section 2.1 and organised the related work in three main different approaches: behaviour-based and task decomposition (Section 2.1.1), compliant and impedance control (Section 2.1.2), and predictive excavation (Section 2.1.3). This broad classification suggested that excavation control must present the ability to “accommodate” infeasible trajectories. For large machines, the infeasibility is presented in the form of tracking attempts where the excavation forces can be sufficiently large to damage the platform, and therefore the bucket motion must be adapted to limit forces to acceptable levels. It was also concluded from the literature that operators dig by making a series of shallow cuts, iterating until the desired shape is achieved.

Section 2.2 introduced the Bode integral and indicated that the performance of a feedback controller is fundamentally limited by the waterbed effect. For a system with side information Equation (2.23) showed by means of entropy measures that

the sensitivity can be decreased by a maximum amount given by the capacity of the channel C_p that transmits the preview. In Chapter 6, Equation (2.23) will be applied to excavation data to reveal the limitations of ILC and the FEE-based empirical model of Cannon and Singh (2000) in decreasing the magnitude of the sensitivity function.

Section 2.3 introduced ILC and discussed the advantages of ILC in excavation. The convergence condition, Equation (2.35), was derived and the effect of non-repetitive disturbances was given by Equation (2.38). Plant inversion as a learning function was discussed as a method for achieving fast convergence. The main issue of ILC regarding disturbances is that non-repetitive disturbances can not be learned, and this section also reviewed approaches proposed by other authors to overcome this problem.

Chapter 3

Experimental Platform and Excavation Strategy

This chapter introduces the experimental platform that was used in field trials to validate the proposed control methods. The chapter also discusses the differences between the body of work completed during the late 1990's using the same experimental platform and the present work¹. An excavation strategy will be devised in this chapter that takes into account the characteristics and limitations of the platform. The excavation strategy will be based on the studies of skilled operators that were reviewed in Section 2.1. This chapter also introduces two metrics that will be used to quantify excavation performance.

¹The experimental platform was not in use during the period between 2002 and 2009. In 2009 it was modified and re-commissioned by Maeda for the work presented here.

3.1 Experimental Platform

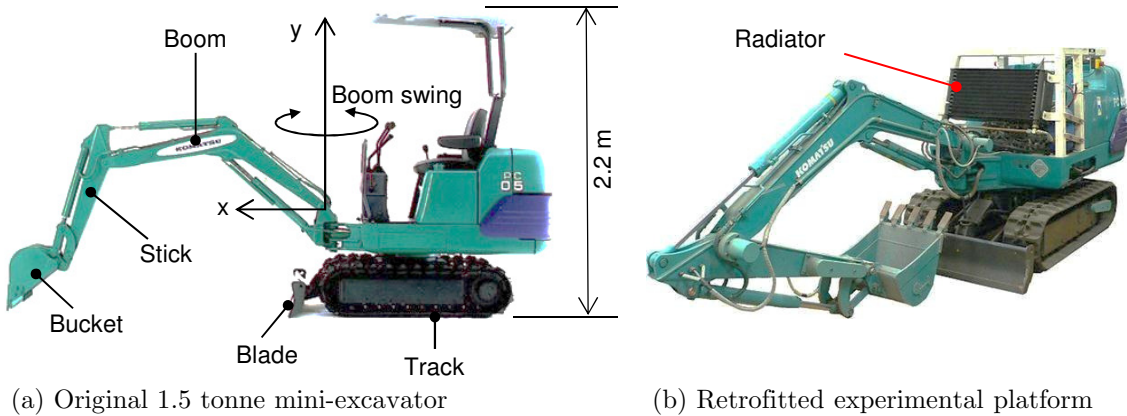


Figure 3.1 – The 1.5 tonne excavator used for the experimental work.

3.1.1 Original Modifications (1996–2000)

The experimental platform is based on a conventional 1.5 tonne Komatsu PC05-7 mini-excavator shown in Figure 3.1 (a). The arm has an experimentally-identified open-loop bandwidth of 3 Hz, weighs 150 kg and reaches 3 metres from the boom swing axis when fully extended. The platform was retrofitted by previous researchers at the Australian Centre for Field Robotics (ACFR) during the period between 1996 and 2000. Modifications included removal of the original seat, joysticks, and manual direction control (flow) valves, which were replaced with a hydraulic manifold assembly containing a flow-control servo-valve for each joint and track of the excavator. The manifold also contains transducers to measure pressure at the servo-valve ports. An oil-to-air radiator was installed at the front of the cabin to dissipate hydraulic fluid heat, as it can be seen in Figure 3.1 (b). Two 2-axis load pins were installed, replacing the original pins at the bucket pivot joint and the pin at the bucket cylinder

base. These load pins allow for the measurement of the bucket force and moment in Cartesian coordinates. In the present work load pins were used only for monitoring purposes, and were not connected to the control loop as a real-time feedback signal.

The retrofit done in late 1990's also included modification of the hydraulic supply. A compressed gas accumulator charged at 70 bar was included in the circuit to provide flow during peak demands and to damp pressure pulsations. The accumulator is shared by all joints and is charged by two hydraulic gear pumps, with each pump delivering a maximum flow of 11.9 l/min when the 9.7 kW (13 horsepower) diesel engine runs at a maximum speed of 2000 RPM. The platform is described in more detail in Appendix A.

Figure 3.2 shows a simplified diagram of the whole system; a more detailed diagram is presented as Figure A.2 in the Appendix. The system has seven identical Moog D633 servo-valves²—two are used to control the right and left tracks, three to control the cylinders of the arm, and the remaining two valves control the boom swing and the blade lift as indicated in Figure 3.1 (a). The tracks and the arm joints are fitted with absolute encoders with 12-bit resolution.

The programmable logic controller (PLC) block in Figure 3.2 comprises a stack of Moog M2000 controllers running at 100 Hz with the main purpose of decoding the CAN commands sent from the real-time controller and sending them as desired commands to the servo-valves in the form of 4-20 mA current signals. Although the servo-valve commands vary between 4-20 mA they are normalised to ± 10 mA in this document to facilitate visualisation. The PLC also encodes and transmits pressure measurements at the servo-valve ports and encoder measurements back to the controller in the form of CAN messages for real-time feedback. Physically the PLCs are

²An eighth servo-valve was installed to rotate the cabin, but this feature is currently disabled.

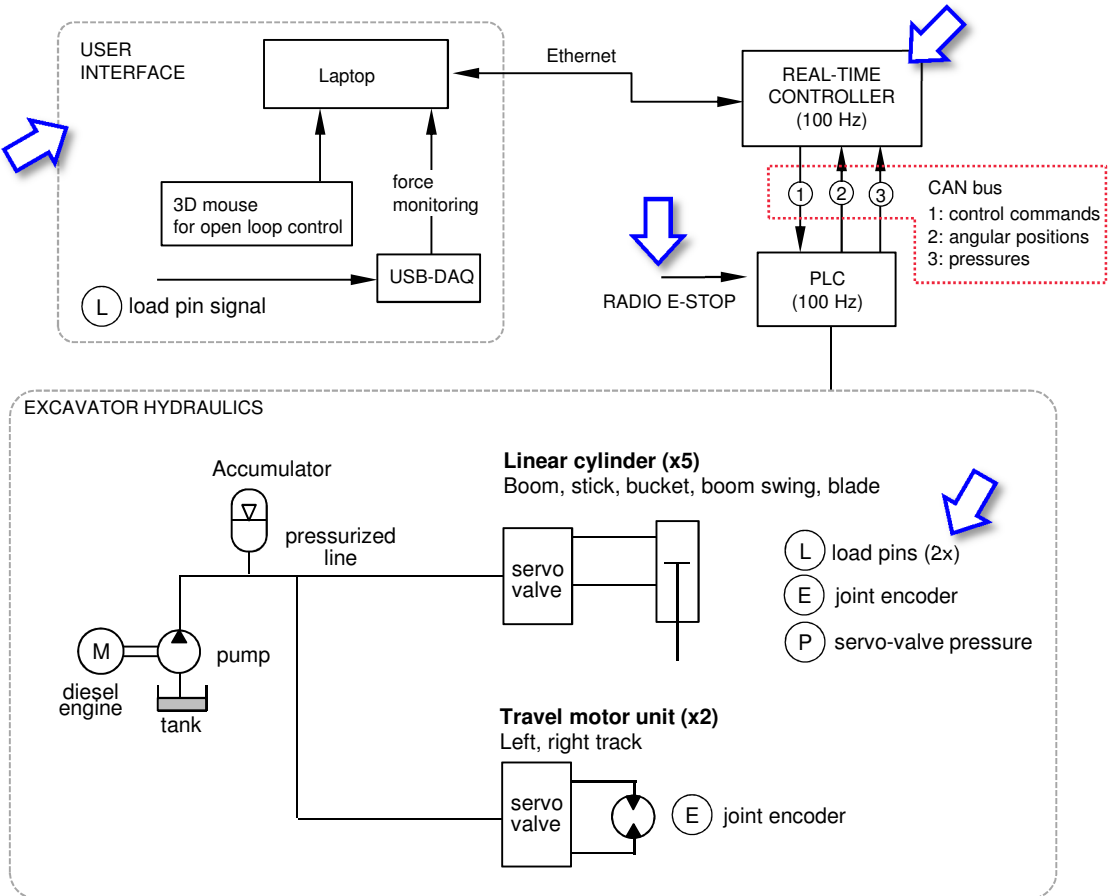


Figure 3.2 – A simplified schematic of the excavator system used in this work. The arrows indicate components that were modified for the present work.

mounted in an enclosure that sits on the top of the excavator.

In the original work, such as Le (1999) and Nguyen (2000), the real-time controller was an industrial PC. The PC was used to run the low-level motion/force control algorithms coded in C++ on Windows NT. The user interface consisted of a laptop with a joystick where two links could be controlled simultaneously in open-loop.

3.1.2 Current Configuration (2009–)

During the course of this work some modifications were made to subsystems indicated by the arrows in Figure 3.2. The load pins were upgraded from the original ± 1.5 tonne range to ± 3.0 tonne range to resolve saturation issues. The load pins are used in this work for implementing an off-line soil-tool interaction model that will be discussed in Chapter 6. They are not used for real-time control.

A fail-to-safe radio emergency stop system was added to the excavator, giving the capability of stopping the diesel engine and purging the accumulator. The industrial PC was replaced with a conventional desktop PC running a MATLAB® real-time xPC target, where core routines were coded in the C language and compiled. The new laptop uses a 3D mouse that allows for the simultaneous open-loop command of four links and the measurement of the load pin signals using a USB data acquisition board. Further details can be found in Appendix A

Note that during the excavation of soil, only the servo-valves of the boom, stick, and bucket are active. These are the links for which the control methods proposed in this work are designed. The boom-swing servo-valve is controlled with a simple proportional controller to regulate the angle of the excavation plane during digging. The boom swing axis is also used to rotate the whole arm to dump excavated soil at a location to the side of the cut.

3.1.3 Differences in Approach to Previous Work at ACFR

The experimental platform was used in previous work at the Australian Centre for Field Robotics (ACFR) where impedance control (Ha et al., 2000b), sliding mode control (Nguyen et al., 2000), and robust observers (Ha et al., 2002) were investigated

as control approaches in autonomous excavation. Further publications where the experimental platform was used include Nguyen (2000), together with (Le et al., 1997) and Le (1999) where the excavator was used to study the mechanics of tracked vehicles.

The main difference in approach between the previous body of work conducted at the ACFR and the present work is that the former adopted a behavioural, sensor-based hierarchical planner for high-level control, and cylinder impedance control at the low level. In the present work, as will be discussed in Section 3.2, high-level planning is simplified to geometric design of the desired cut profile, which will then be excavated iteratively in the spirit of a classic position tracking control problem. At the low level, predictive joint position control will be adopted.

Specifically, the work of Ha, Rye and others at ACFR published during the period 1998–2002 focused on single-pass excavation where a high-level planner was used to decompose a pass into a sequence of primitive actions. Ha et al. (2002) describes the higher-level planner as a combination of behaviour-based and hierarchical architectures using state charts. Fuzzy reasoning was used to define the high-level state of the task based on information provided from joint positions, cylinder pressure and laser-scanning of the soil surface. At the low level, each cylinder was given a linear position set point that was tracked with the use of impedance control based on differential pressure at the cylinder. Under the impedance approach the maximum bucket cylinder force reported during experiments was of approximately 0.7 tonne (Nguyen et al., 2000; Ha et al., 2002).

In contrast, the present work focuses on multi-pass excavation. The adjustment of the motion due to excavation forces will be based on actuator saturation instead of impedance, simplifying the sensing to require only encoder positions. This strategy

based on actuator saturation will allow the controller to achieve forces exceeding 1.5 tonne at the bucket cylinder. Also, while previous work at ACFR focused on robust reactive excavation strategies, this work motivates and introduces the use of predictive compensation. This work emphasises the simplicity of implementation of the proposed solution with general position tracking control methods; apart from the trajectory design, the proposed controller will make no use of skilled behaviours or geometric soil mapping.

3.1.4 Excavator Joint Dynamics with Servo-Valves

In general the modelling and estimation of the parameters of a hydraulic excavator arm is a complex task. Amongst other factors, the complexity is due to the redundant serial-link structure, the pressure-coupled and flow-limited hydraulic source, and the variation of hydraulic parameters with temperature. As discussed in Section 2.1.5 dynamic modelling of the hydraulic system can not be achieved without error, and feedback control of hydraulic machinery have relied on robust feedback. In this work, instead of treating the nonlinear coupled dynamics of the three links as a single plant in the usual way, the dynamics that result from the coupling between the servo-valve input and the motion of the corresponding actuated link will be treated as the effective plant dynamics, for which control methods are designed. This approach results in three approximately linear and decoupled plants where feedback control and learning can be applied to individual joints.

Moreover, the use of servo-valves alleviates, to a great extent, the issues of dead zone and nonlinear flow rates that were discussed in Section 2.1.5. In a flow-control servo-valve the position of the spool is controlled in closed-loop (integrated into the valve) so that, under constant load and supply pressure, the volume flow maintains a linear

relation to the input command. Figure 3.3 shows the characteristic curve of the Moog D633 servo-valve used in the excavator, obtained from the manufacturer's data sheet (Moog, 2013).

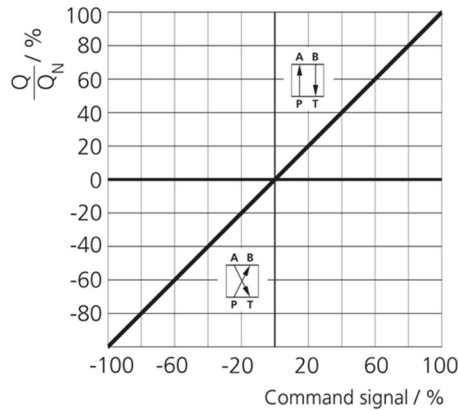


Figure 3.3 – Command to flow ratio characteristics of the Moog D633 servo-valve used in the experimental platform. The internal spool position controller linearises the flow under constant supply pressure and no load. From Moog (2013).

With the use of servo-valves it is straightforward to model the relation between the servo-valve input command and the velocity of the arm in *free motion*. Figure 3.4 (a) shows with the grey curve the experimental angular velocity³ of the bucket when tracking a “digging pass” in free motion. The black curve is the simulated response of a simple first-order model given by the transfer function

$$\dot{q}(s) = \frac{K_v}{\tau s + 1} u(s), \quad (3.1)$$

where $\dot{q}(t)$ is the Laplace transform of the joint velocity, K_v is the gain of the coupling between the servo-valve and the link dynamics comprising the inertial and frictional

³Precisely, the cylinder volume flow rate is proportional to the servo-valve command, and joint velocity is related to cylinder volume flow rate by the kinematic solution of three-and four-bar link mechanisms that are characteristic of hydraulic machines. It was noted that the non-linearity does not seem to be significant for the range of motion used in excavation, and the approximation error becomes negligible when compared to the flow disturbances caused by excavation forces.

forces due to the mechanism, τ is a time constant that accounts for response delay, and $u(s)$ is the servo-valve input, which will be also referred to as the plant input. The values of K_v and τ were found by least-square estimation over a full digging pass. The root-mean-square (RMS) error of the predicted velocity and the actual experiment in Figure 3.4 (a) was 4.1 deg/s when the arm was moved slowly with an average speed of 10 deg/s. The parameter values for each link are listed in Table 3.1.

Table 3.1 – Parameter values of the joint dynamics

Joint	K_v (deg/s mA)	τ (s)
Boom	5.20	0.10
Stick	3.95	0.10
Bucket	9.16	0.05

Figure 3.4 (b) shows, however, that the simple first-order model loses accuracy when the trajectory demands higher velocities; in this case the average speed was of 17 deg/s. The decrease in accuracy may be caused by the larger influence of inertial effects at higher speeds, reflected at the servo-valve as varying loads that degrade linearisation. In this experiment the RMS error increased from 4.1 deg/s to 6.5 deg/s, a degradation of 59%. Figure 3.4 (c) shows the case where the excavator contacts the soil. The linearity is clearly lost, providing evidence that disturbances from excavation have an impact on the flow control as the source of pressure is limited. The RMS error was 18.9 deg/s, a degradation of 360% relative to the original identification.

The fact that different velocities result in different errors—Figures 3.4 (a) and (b)—indicates that the excavator is, in fact, nonlinear. While the model can be refined by extending the system identification work, Figure 3.4 (c) shows that the dominant effect on the degradation of the linear model approximation is contact with the soil.

Following the approaches of Ha et al. (2000a) and Sirouspour and Salcudean (2001)

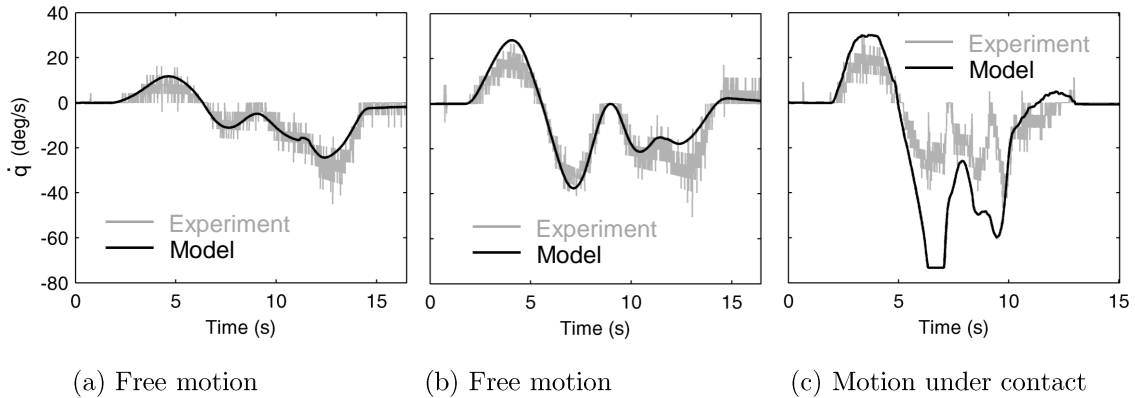


Figure 3.4 – Bucket dynamics approximated by a first-order model approximation based on the linear servo-valve characteristics. (a) In slow, non-contact “digging” motion the RMS velocity error between model and experiment was 4.1 deg/s. (b) Using a faster, non-contact “digging” motion the RMS error increases to 6.5 deg/s. (c) Under excavation forces the RMS error approximation error is 18.9 deg/s.

the first-order approximation in Equation (3.1) will be used for an approximate linearisation so that commands can be designed “as if” the system was linear. An observer will then be designed for compensating model deficiencies due to velocity effects and the reflection of excavation disturbance forces at the servo-valve command.

Care must be taken when interpreting the physical meaning of disturbance as used here. Each joint controller “sees” disturbances caused by external forces as deviations in the flow to the hydraulic cylinder that it controls. Interpretation of disturbances in the form of flow deviations leads to the compensation of the effect of the soil-tool interaction forces at the plant input (as matched disturbances) without the need for direct force sensing. For this reason figures showing disturbances in excavation will be given in milliamperes: the units of servo-valve commands. While disturbances arise due to the soil-tool interaction forces the reader should be aware that compensation provided by the controller is in the form of servo-valve commands.

3.2 Scope and Approach to Excavation

The aim of this section is to introduce a strategy for excavation that is compatible with the mini-excavator experimental platform and with the assumptions on expected excavation conditions.

Assumption 3.1 (Experimental Soil Conditions). The scope of this work is limited to excavation of soil, as opposed to excavation of fragmented rock. The soil to be excavated may present different resistive forces during a pass and between passes. Soil heterogeneity may be caused by the presence of rocks and by differences in composition and compaction of soil with depth. It is assumed that if there is an actuation margin (a) the soil can be sheared and (b) rocks present in the soil will be either left behind or captured by the bucket. Rocks are assumed to be small enough so that they do not stall bucket motion during a pass. In the case where actuators saturate or the controller does not generate enough command then under conditions (a) and/or (b) the bucket motion will deviate from the desired trajectory.

Note that under Assumption 3.1 large rock excavation as in (Lever, 2001) and (Marshall et al., 2008) is not addressed in the present work. Assumption 3.1 is, however, realistic in the context of the intended use of a 1.5 tonne backhoe-type mini-excavator.

3.2.1 Proposed Excavation Strategy

An approach to excavator motion control is devised based on some of the insights obtained from the literature reviewed in Section 2.1. Recall from the reviewed literature that a recurrent approach was to use an inner position control loop with an outer loop to control or modulate the maximum forces. This outer loop was sometimes regarded as a supervisory intelligent controller, as in the “dig by feel” in (Bernold, 1993) and

the behaviour-based control in Bradley and Seward (1998). Simpler forms of outer loop adjustment were given by the crowd arm retraction rule of Dunbabin and Corke (2006), the admittance behaviour in Marshall et al. (2008), the impedance matching in Tafazoli et al. (2002) and the target impedance control in Ha et al. (2000b). In large rock excavation (Marshall et al., 2008), impedance is used to naturally adjust the bucket to the contouring of rocks and to make the bucket “find its way” between rocks. In soil excavation, adjustment of the bucket motion to excessive forces is important to avoid damage to the arm.

In contradistinction to the situation that can arise with large excavators, the forces generated by the hydraulics of a mini-excavator are insufficient to damage the platform. Actuators of a mini-excavator saturate very quickly, limiting the maximum shear force that the bucket can apply to the soil before any structural damage can occur. Moreover, the present experimental platform also includes pressure relief valves that limit the maximum load on the engine. This suggests that saturation of the actuator itself naturally provides, in an unavoidable manner, the required adaptation of bucket motion to resistive soil forces, usually accomplished by an outer loop supervisory or impedance controller. When the resistive forces encountered during tracking of a reference trajectory cause one or more actuators to saturate, under Assumption 3.1 the bucket trajectory will deviate from reference trajectory. Excavation passes under actuator force saturation use the maximum force available from the hydraulics.

Returning to the skilled operator excavation passes investigated by Shao et al. (2008) and shown in Figure 2.6 (a), it is noted that the operator repeated several passes with similar motion profiles until the desired flat-bottomed cut was achieved. Here it is conjectured that the human operator has an image of the desired cut in mind and repeats passes that remove soil in layers, covering the whole length of the cut at

each pass until the desired cut is achieved. The work of Shao et al. (2008), however, did not use an outer loop controller to adapt the bucket motion to excessive forces, therefore requiring the design of several reference trajectories representing cuts with increasing depths that are tracked one by one. This strategy was also proposed in Bradley et al. (1989) where reference trajectories were given as “slices” as shown in Figure 2.6 (b). The obvious problem is how to specify the depth so that trajectories are feasible: that is, a trajectory depth that when tracked generates resistive soil-tool interaction forces that do not cause significant deviations to the motion of the bucket.

The excavation strategy used in this work is to repeat a sequence of excavation passes using a single reference trajectory that is defined by the final desired cut. This strategy eliminates the requirement for designing multiple intermediate reference trajectories for different pass depths. Initial passes will surely encounter sufficient resistance to saturate the actuators, and this will cause the bucket motion to deviate from the trajectory, leading to large soil residuals. A subsequent pass will be required, and the controller will iterate over the same reference trajectory. Due to the explicit use of iteration, a pass executed under saturated actuation is not regarded as a failure in tracking, but as an intermediate pass that makes use of the maximum output of one or more of the arm actuators.

In the case of larger machines the limitation is not on the actuator saturation but on the maximum allowable force that the arm can apply on the environment without causing significant cumulative (fatigue) damage to the platform. Here it is conjectured that the same excavation strategy is still applicable to larger machines by using, for example, a maximum allowable force measured at some location on the arm structure as a saturation signal.

3.2.2 Path and Trajectory Generation

The bucket tip path design is based on the trapezoidal profile observed from skilled operators (Shao et al., 2008) where the bucket is filled by horizontal dragging (Figure 3.5). It may be argued that this approach is inefficient as the bucket may be dragging soil over an unnecessary length. The findings in Bradley and Seward (1998), however, indicate that this is the most efficient strategy for digging in difficult conditions. The alternative approach, which consists of penetrating and curling the bucket while the boom and arm maintain a fixed position, seems to work only when the bucket can readily penetrate the soil, which may be insufficient in hard soil.

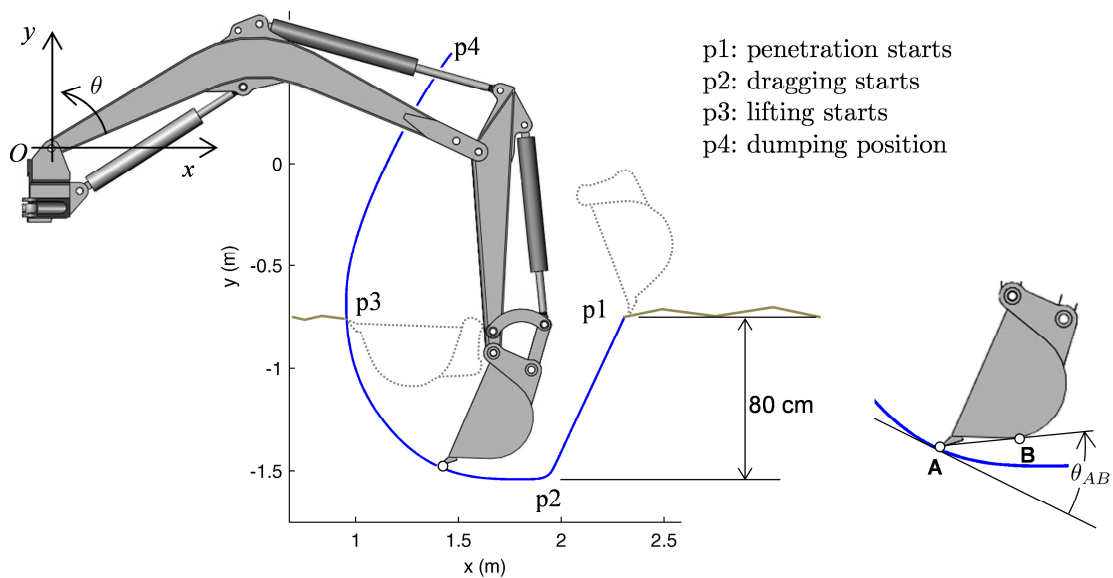


Figure 3.5 – The path defining an 80 cm deep cut used for evaluating controllers. Each controller has to achieve the desired cut by iteratively tracking a fixed reference trajectory, defined by the path of the cut and indexed uniformly by time. The orientation of the bucket is defined by an offset angle θ_{AB} between the segment AB and the path of the cut during penetration and dragging.

Referring to Figure 3.5, once the desired positions of the bucket tip are defined as a path, the orientation of the bucket relative to that path must be chosen. The choice of

bucket orientation is important because it defines the penetration angle of the bucket into the soil (angle of attack), which has a large influence on the force required to cut the soil. The excavation literature is, however, inconclusive regarding the best choice of bucket orientation. More than 50 empirical models have been reported (Blouin et al., 2001) for the penetration phase alone. Some empirical approaches such as that in Kuśmierczyk and Szlagowski (2008) recommend small angles of attack (approximately nine degrees) to minimise resistance to penetration. The disadvantage is that, although small angles of attack reduce the actuation forces required, they invariably lead to shallow cuts and slower material removal. Based on the analytical approach of Hemami (1993), in the present work the bucket orientation is designed so that the segment AB—starting at the bucket tooth tip and tangent to the bucket surface—is tangent to the path that defines the desired cut at point A. In theory, this condition minimises the force that arises through compacting the soil in front of the bucket, while maximising soil collection. In practice, however, adding an offset $\theta_{AB} \approx 5^\circ$ was shown to be effective in eliminating unnecessary sliding friction of the bucket surface against the bottom of the cut. During dragging, the bucket orientation gradually changes so that the bucket top becomes horizontal when the lifting phase starts at point p3 in Figure 3.5, minimising spillage.

The time on the path is defined to allow a large actuation margin relative to saturation. In a flow-controlled manipulator, actuation is minimised by slow joint velocities. The trade-off is that the duration of each pass may become excessively long. By observing operators digging in difficult conditions with a mini-excavator, a pass taking approximately 10 seconds from the penetration until the lifting phase seems to deliver an efficient excavation motion while allowing good actuation margins. When including the final dumping phase the whole pass takes approximately 14 seconds for an 80 cm deep cut. Previous work by Ha et al. (2002) using the same experimental

platform suggested that a 15 second cycle is in accordance with a human operator.

Finally, the servo-valve commands required to cause the bucket to track the reference trajectory were computed using the inverse of the first-order model of the arm, Equation (3.1). These commands are shown in Figure 3.6 for each of the links. To decrease the possibility of saturation the command peaks were reduced by smoothing the joint velocity profiles for each link of the arm. The starting points of the penetration, dragging, lifting and dumping phases are indicated in the figure as p1, p2, p3 and p4 respectively.

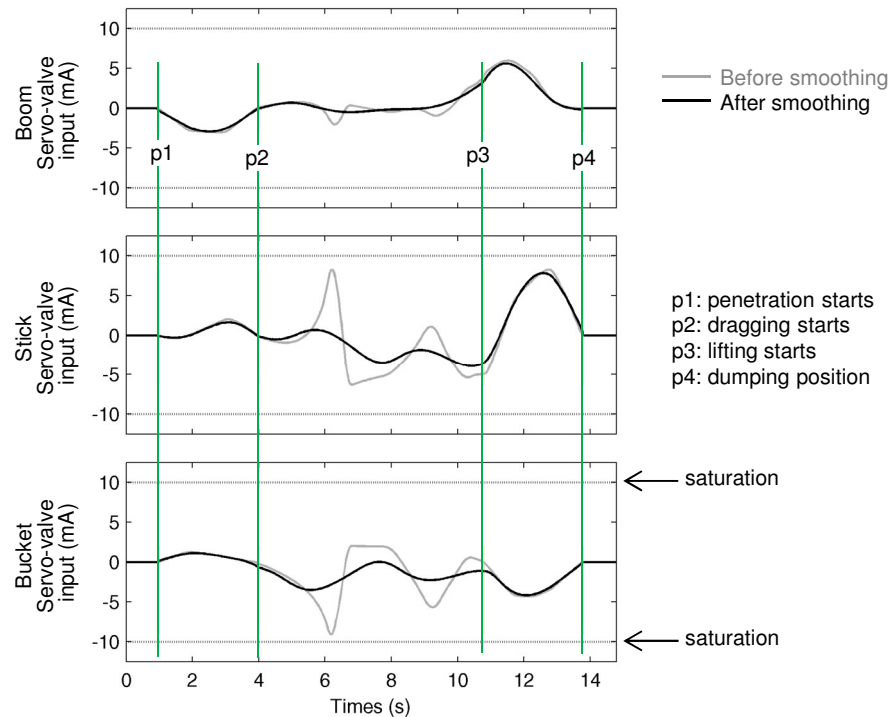


Figure 3.6 – Joint commands in free motion for tracking a final desired cut trajectory.

The grey curves represent the output commands from the inverse joint dynamics model. The black curves represent the commands after smoothing.

During experiments, the initial height of contact of the bucket teeth with the soil is defined by driving the arm in open-loop until contact with soil is made, indicated as point p1 in Figure 3.5. The encoder readings at that position are used to define the

origin of the trajectory for all subsequent passes of the cut.

It is often said that tracking a desired cut purely by means of position control can lead to a situation where the bucket becomes stuck when actuators saturate. Here, it is argued that under Assumption 3.1 there is always the possibility of lifting the bucket free of the soil, although saturation may compromise motion during the penetration and dragging phases. Recall the findings of Jarzebowski et al. (1995) that the cohesive strength of the soil in the direction of the shear band during lifting is near zero, as the soil above the bucket is already perturbed if not completely sheared, thus offering less resistance. The observations of Jarzebowski et al. on shear bands suggest that the forces required to pull the bucket out of the ground must be smaller than the forces that were required to move the bucket into the ground. As long as the trajectory ends above the current soil surface the bucket can be lifted free. During field trials more than 350 passes were executed by the excavator with the great majority of passes under flow saturation in one or more cylinders; there was no case where the bucket became stuck.

3.3 Definition of Performance Metrics

To quantify and compare the performance of different control methods the definition of a suitable accurate and unbiased metric is required. Since excavation is executed in a vertical plane, a natural metric for evaluating the tracking error is the x - y distance between the tip of the bucket and the desired cut, shown as d_{xy} in Figure 3.7 (a). This metric incorporates in a single value the error in all three joint angles of the arm at any point along the reference path, since the location of the bucket tip is

$$x = a_1 \cos(q_1) + a_2 \cos(q_1 + q_2) + a_3 \cos(q_1 + q_2 + q_3)$$

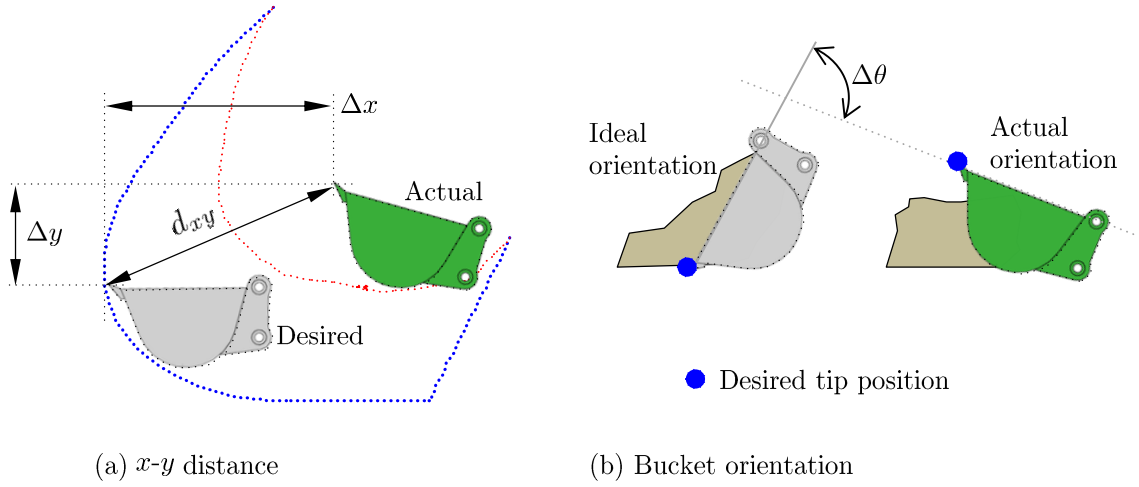


Figure 3.7 – Definition of performance metrics based on (a) bucket tip tracking error and (b) bucket orientation error.

$$y = a_1 \sin(q_1) + a_2 \sin(q_1 + q_2) + a_3 \sin(q_1 + q_2 + q_3),$$

where a_1 , a_2 and a_3 are respectively the lengths of the boom, stick and bucket links, and q_1 , q_2 , and q_3 are their respective joint angles measured in accordance with the Denavit-Hartenberg convention (Tsai, 1999, Ch. 2). A sufficient condition for a small bucket tip tracking error is that each joint has a small angular error at each step along the trajectory.

Over a whole pass, each sampling leads to a distance error value

$$d_{xy,j}(t) = \sqrt{(x_r(t) - x_j(t))^2 + (y_r(t) - y_j(t))^2} \quad (3.2)$$

where $t \in \{0, \dots, N - 1\}$ is the time index sampled uniformly during the pass up to a fixed number of samples N .

The RMS distance error will be used to form a metric that aggregates the total

deviation along a pass

$$d_{xy,j(RMS)} = \sqrt{\frac{1}{N} \sum_{t=0}^{N-1} (d_{xy,j}(t))^2}. \quad (3.3)$$

Although the RMS distance error will be adopted as a primary performance metric, it is useful to define a bucket orientation error as a secondary metric. Due to the three degrees of freedom of the arm, the same bucket tip position can be achieved with different bucket orientations. As illustrated in Figure 3.7 (b), the orientation is an indirect indicator of the efficiency of a pass in shearing soil with the correct tool angle. Large orientation errors indicate cases where soil is not being captured inside the bucket, but instead is pushed with the bucket face or back. The orientation error over a pass is aggregated as the RMS orientation error

$$\theta_{j,(RMS)} = \sqrt{\frac{1}{N} \sum_{t=0}^{N-1} (\theta_r(t) - \theta_j(t))^2}, \quad (3.4)$$

where $\theta = q_1 + q_2 + q_3$.

3.4 Limitations of a Position-Based Approach

Note that the strategy proposed in Section 3.2.1 effectively treats excavation as an iterative position-tracking problem under unusually large disturbances. Although not investigated in this work, in principle there is no reason why the proposed methodology could not be applied to force or impedance control. None of the elements that comprise the controller (the tracking controller, the observer, and ILC) are exclusive to position control. The main impediment to implementing force control in excavation

is practical: the installation and subsequent exposure to damage of load pins at the bucket joint and/or pressure transducers at the cylinder ports decreases the reliability of the system. Further, force or impedance control requires the treatment of noisy sensor data and additional high-bandwidth control loops which can be avoided in position control. Despite these factors, with suitable adaptations the control methodology proposed in this work could be used for learning force and impedance profiles. The learned force/impedance commands could then be used as feedforward inputs to improve feedback controllers already proposed in excavation—for example, it could be used in conjunction with the impedance methods in Ha et al. (2002) and Tafazoli et al. (2002).

The decision to use position as the variable of interest was based principally on the suitability of the available hardware for position control. The experimental excavator platform is provided with high-performance flow control servo-valves and reliable and robustly-enclosed encoders for position feedback. The position control approach also increases the applicability of the method to other hydraulic machinery as flow is the usual controlled variable.

Convergence of the bucket tip trajectory to the desired cut profile is directly related to the rate of soil removal, assuming that there is no spillage from the bucket and that the bucket does not compact the soil. The difference between the swept areas of two consecutive passes is then proportional to the volume of removed soil

$$V_{k+1} = W(A_{k+1} - A_k), \quad (3.5)$$

where A_k is the area swept during pass k , V_{k+1} is the swept volume, and W is the width of the bucket. In principle, the area can be computed using only joint encoders and forward kinematics. This idea is illustrated in Figure 3.8 (a). Using experimental

data, Figure 3.8 (b) illustrates the decrease in tracking error (3.3) and the swept volume relative to the volume of the desired cut.

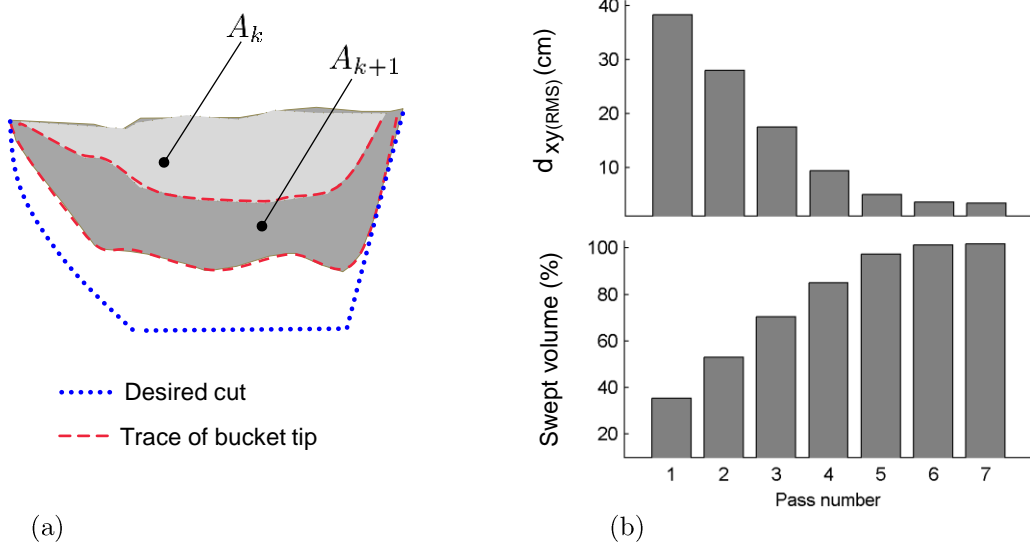


Figure 3.8 – Swept volume of material as a function of tracking error. (a) The conceptual use of tracking error to estimate the swept volume. (b) Swept volume computed experimentally.

Unfortunately, computation of the swept volume from kinematics introduced errors due to unexpected, and unmeasured, tilt of the excavator body (approximately $\pm 5^\circ$) during high-force penetration of the soil during some passes. Tilt of the platform means that the trace of the bucket tip projected with forward kinematics is not always aligned with the true world coordinates, making the computation of the area imprecise. Due to this issue, this work will use the proposed metrics (3.3) and (3.4) as they are relative to the arm base but independent of the platform orientation. Traces of the bucket tip as shown in Figure 3.8 are used in this work only for qualitative comparison or illustrative purposes. This technical issue can be resolved in future work with a platform tilt sensor, or by directly measuring removal of soil, for example with scales or visual information.

The adopted strategy of tracking a full pass at each iteration, although suitable for position-based control and ILC, is certainly inefficient in regards to actuation usage. While one would attempt to lift the bucket as soon as a full bucket condition is detected, the current strategy imposes the full tracking of the trajectory even when the bucket is already full. The implementation of such a detection system is, however, an open problem whose realisation involves profiling the bucket content while digging, for example by means of visual feedback, and it is beyond the scope of this work. Note that profiling on-line the soil captured by the bucket can be very difficult to achieve in practice due to the use of fragile optical sensors in the harsh, dusty excavation environments.

3.5 Conclusion

This chapter described the experimental platform, the scope of the excavation to be investigated, and proposed an excavation strategy and metrics for evaluating excavation performance. In the present work the control of the excavator is regarded as an iterative tracking problem based only on position error, where the single reference trajectory follows the desired path along an excavation cut. Iterative tracking is usual in iterative learning control and it is conjectured that it can provide a simple and straightforward solution to autonomous excavation. This strategy is one of the principal difference between the present work and previous related work in autonomous excavation—including the previous body of work conducted at ACFR—which had usually relied on behavioural, sensor-based hierarchical strategies.

The observations on skilled operators “slicing” soil and on trajectory adjustments with outer control loops made in literature reviewed in Section 2.1 were used here as the basis for devising an excavation strategy where a single reference trajectory is

tracked during all passes. Actuator saturation was proposed for naturally adapting bucket motion according to the maximum force capacity of the excavator and resistive excavation forces, from which slices are expected to become a natural consequence of position tracking deviations that occur when actuators saturate.

This chapter has also introduced distance and orientation error metrics that will be used to quantify excavation performance. The distance error metric will be used as a primary metric due to its clear quantification of tracking error. The orientation of the bucket will be used as an indicator of the efficient shearing of the soil.

Chapter 4

Feedback Disturbance Rejection

This chapter introduces feedback control of the hydraulic excavator arm and experimentally evaluates the performance achievable under this control. Despite the many solutions proposed for autonomous excavation that were reviewed in Section 2.1, this chapter adopts a simple proportional controller with feedforward reference compensation as the basic controller. This approach is motivated by two reasons. First, manipulator control methods based on proportional feedback and reference compensation are consolidated theoretically and widely accepted in practice. Moreover, it is argued that one of the reasons for the negligible industrial acceptance of the methods proposed in the literature is related to the relative difficulty in understanding and implementing them. Second, avoiding implementations that are particular to excavators maintains the proposed solution open to other applications.

Experimental evaluation of the proportional controller will show a lack of disturbance rejection, motivating the use of a disturbance observer to provide a form of virtual excavation force sensor. Although experiments will show that the observer increases the performance of the controller, the observer frequency response rolls off above

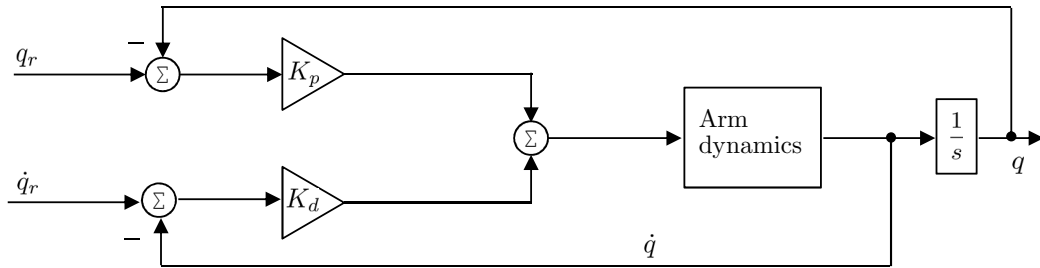
approximately 8 rad/s (15 rad/s for the boom) while excavation disturbances have significant power up to 20 rad/s indicating that disturbances can not be completely compensated at all frequencies.

4.1 Proportional Control in Excavation

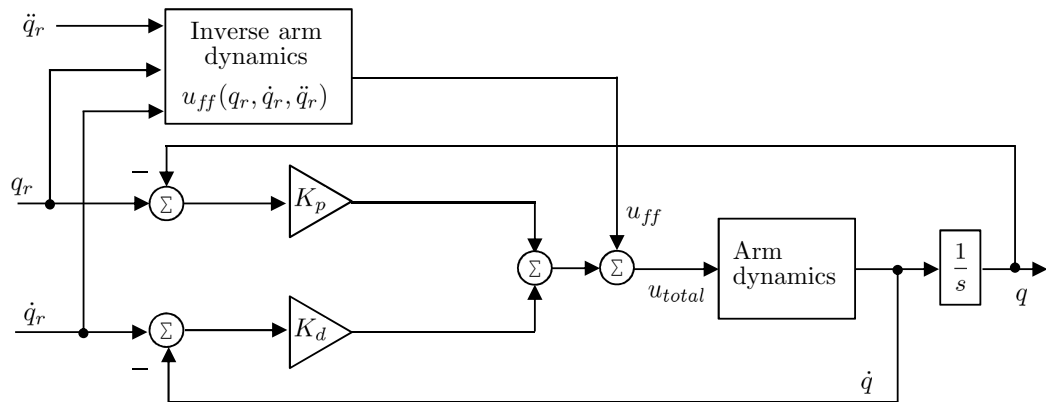
As it will be shown, a proportional feedback controller acting on flow-control servo-valves effectively implements a position proportional-derivative control law for each joint of the arm. According to Kelly and Salgado (1994), the proportional-derivative (PD) controller shown in Figure 4.1 (a) is the simplest controller that is adequate for manipulator control. The simple and intuitive structure of a PD controller makes parameter tuning easy and provides, in most cases, a reasonable amount of performance in relation to the amount of tuning effort required. It is also known, however, that serial link robotic manipulators with independent PD controllers at each joint rely on high gains to decouple the disturbances caused by the inertial effects of the other links. While high gear reductions in industrial manipulators minimise the effects of coupled dynamics, mechanisms with hydraulic cylinders usually have lever arm ratios that unfavourably amplify the load at the link end to the cylinder rod. This negative ratio suggests that dynamic compensation is important in hydraulic arms.

In free motion dynamic compensation can be achieved with a feedforward input containing the pre-computed commands required to move the arm over a given trajectory. This controller structure is shown in Figure 4.1 (b); the method is known as torque feedforward control (Corke, 2011) and the compensated control law is

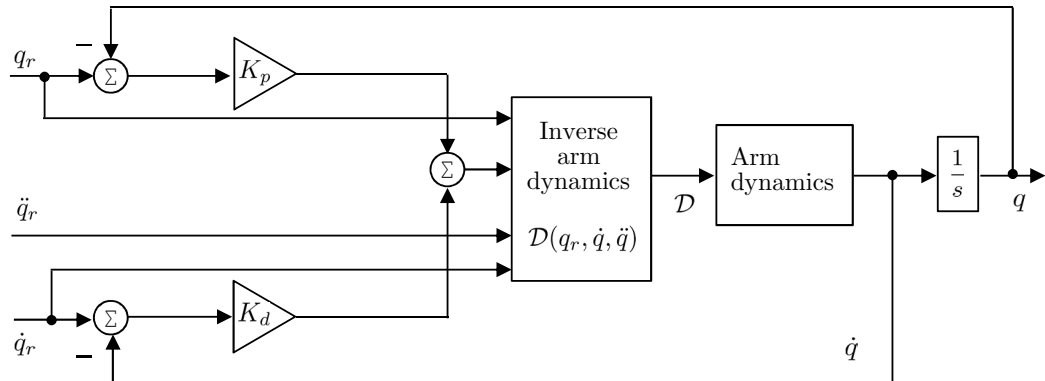
$$u_{total} = u_{ff}(q_r, \dot{q}_r, \ddot{q}_r) + \{K_d(\dot{q}_r - \dot{q}) + K_p(q_r - q)\}. \quad (4.1)$$



(a) Uncompensated dynamics



(b) Feedforward control



(c) Inverse dynamics control

Figure 4.1 – Three conventional manipulator control methods based on a linear PD controller; q_r is the position reference, q is the joint angle and K_p and K_d are respectively the proportional and derivative feedback gains. (a) Uncompensated dynamics. (b) Feedforward control. (c) Inverse dynamics control. After Corke (2011).

Another method of achieving dynamic compensation is by using the inverse model dynamics in feedback form. This method is known as inverse dynamics control and is represented in Figure 4.1 (c). The compensated control law is

$$u_{total} = \mathcal{D}\{q, \dot{q}, [\ddot{q}_r + K_v(\dot{q}_r - \dot{q}) + K_p(q_r - q)]\}, \quad (4.2)$$

where the function $\mathcal{D}(\cdot)$ implements the inverse dynamics commands. Note that in the feedforward case u_{ff} is dependent only on the reference trajectory while in the case of inverse dynamics control the output $\mathcal{D}(\cdot)$ is also a function of the current state.

Recall from Figure 3.4 (a) and (b) that the first-order approximation of the joint velocity dynamics $\dot{q}(s)/u(s) = K_v/(\tau s + 1)$ (Equation 3.1) is valid only in the neighbourhood of the trajectory used for parameter identification. Moving the arm at a higher speed showed discrepancies between the joint velocities predicted by the simple first-order model with fixed gain K_v and the experimental result. Figure 3.4 (c) showed that these discrepancies worsened further under the varying load conditions during excavation.

The effect of such parameter variation on the feedforward and inverse dynamics controllers is shown in Figure 4.2 with simulated examples comparing variations in the K_v value (listed in Table 3.1). To produce Figure 4.2, the same reference trajectory was tracked in simulation of free motion by the feedforward and inverse dynamics controllers. All simulated cases used the same proportional controller gains but different K_v values on the inverse model. In the feedforward case in (a), K_v errors of up to 15% cause biased motion but no instability. In the inverse dynamics case in (b), the same amount of error caused a much larger degeneration of performance. The amount of oscillation shown in simulation with the inverse dynamics method

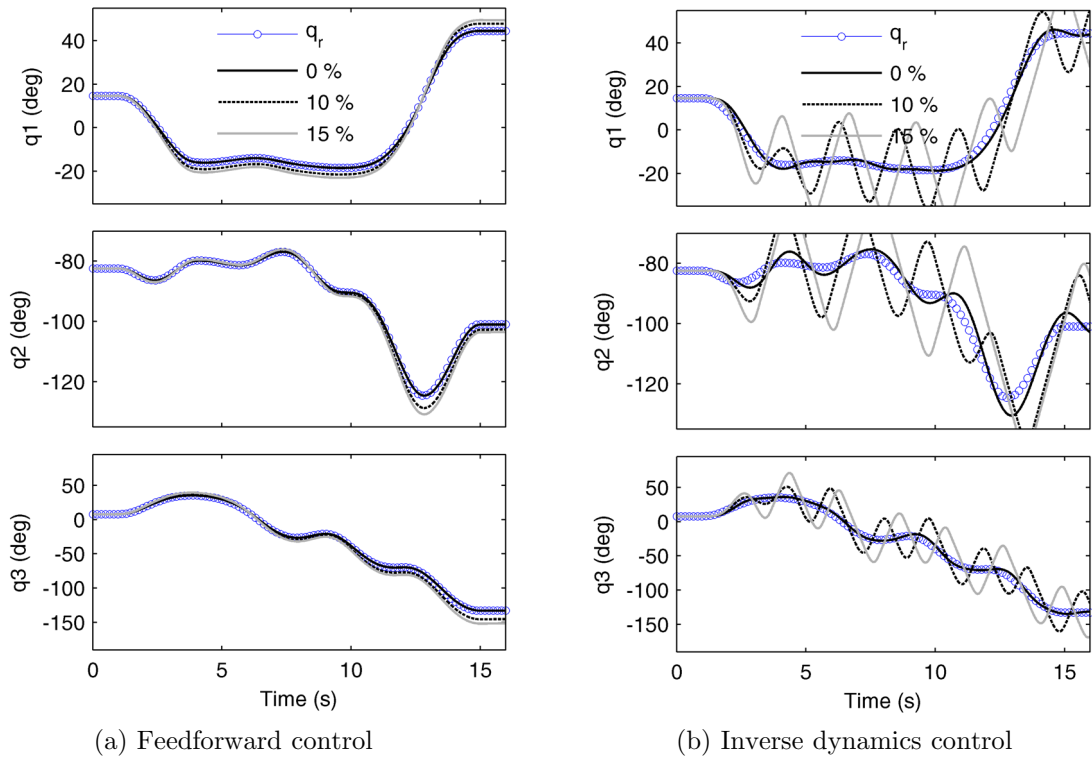


Figure 4.2 – Sensitivity of the first-order approximation of the joint dynamics to variation in the value of K_v . Simulated results with (a) feedforward control and (b) inverse dynamics control.

is unacceptably large for a real hydraulic arm, potentially leading to hydraulic and structural damage.

The issue of inverse dynamics control is that the feedback nature of the compensation increases sensitivity to modeling errors due to an increase in the loop gain. As indicated by Equation (4.2), compensation with inverse dynamics depends on the current state of the arm, and therefore model parameters must generalise for all possible arguments of the function $\mathcal{D}(\cdot)$. The lower sensitivity to parameter variation makes feedforward control more suited as a compensation method for excavation.

Also, note that feedforward control naturally fits the iterative excavation strategy of repeating bucket passes towards a fixed reference cut. Feedforward commands need

only be computed for the final trajectory, simplifying system identification to the task of finding suitable model parameters over the single desired trajectory. During the initial passes, when tracking deviations are large, the feedforward reference compensation biases the motion towards the desired final cut. In contrast, inverse dynamics control would require system identification of a larger range of achievable postures and velocities to cover the motion of different passes of a cut.

A simplified representation of the feedforward control with a proportional controller is shown in Figure 4.3, where P is the joint (plant) dynamics *in free motion*, \hat{P} is its estimated model given by Equation (3.1). The dynamics that arise during contact with the soil are assumed to enter the plant as load disturbances $d_j(t)$. The joint angle position reference is $q_r(t)$, and $q(t)$ is the current joint angular position, and $u_{ff}(t)$ is the feedforward reference compensation command. This controller will be referred to as the proportional controller with feedforward reference compensation, or simply as the proportional controller when convenient.

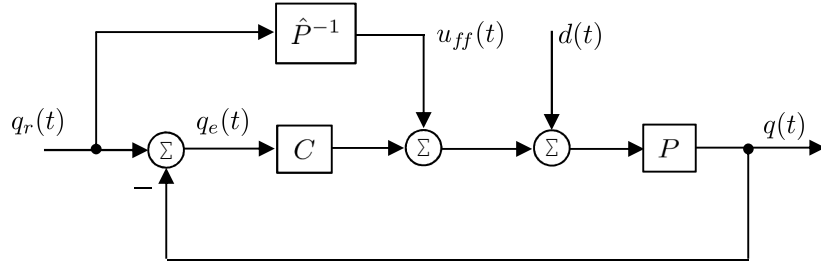


Figure 4.3 – The basic proportional controller for each joint of the excavator arm.

The block C is the linear compensator, P represents the joint dynamics *in free motion*, \hat{P}^{-1} is the estimated inverse model of the joint dynamics, q_r is the reference angular position, q is the current angular position of the joint, u_{ff} is the feedforward reference compensation command and d is the load disturbance from excavation.

Assumption 4.1 (Feedforward Reference Compensation). It is assumed that the residual disturbance from the mismatch between the feedforward command $u_{ff} =$

$q_r \hat{P}^{-1}$ and the ideal commands to drive the arm in free motion $q_r P^{-1}$ are negligible when compared to disturbances from the interaction with the environment. That is,
 $|d| >> |q_r(\hat{P}^{-1} - P^{-1})|$.

Remark. Although assumption 4.1 may seem strong for a complete model of a three-link hydraulic manipulator arm note that \hat{P} in this work is the first-order linear model given in Equation (3.1) representing a single joint of the arm driven by its respective servo-valve. As it was shown in Figure 3.4 (a) this simple model is a good approximation to predict the motion of the arm in free motion. Under Assumption 4.1 and considering that the disturbance from excavation enters the plant as the load disturbance $d(t)$

$$\begin{aligned} q &= \hat{P}^{-1} P q_r + CP(q_r - q) + Pd \\ q &= q_r + CPq_r - CPq + Pd \\ q - q_r &= P(1 + CP)^{-1}d \\ q_e &= -PSd, \end{aligned} \tag{4.3}$$

indicating that the only trigger for feedback action is the exogenous disturbance d . Notice specifically that under Assumption 4.1 the reference input q_r causes no feedback action. Whenever convenient throughout this thesis the reference input will therefore be disregarded when Assumption 4.1 is made so that it is clear that proposed methods will focus on compensating the disturbances from excavation $d(t)$ but not the reference $r(t)$, which can be compensated with an inverse model of the arm.

Experimental evidence that assumption 4.1 holds in the case of the excavator is seen by comparing Figure 3.4 (a), when the excavator moves in free motion driven by a feedforward command $q_r \hat{P}^{-1}$, with Figure 3.4 (c), when the excavator motion is

disturbed by soil interaction. Note the effect of the disturbance from excavation is clearly dominant when compared to the disturbances due to modeling error in \hat{P} .

In the case where assumption 4.1 does not hold—that is, when there is significant modeling error in \hat{P} —a large tracking error should be expected, imposing an extra load on the position feedback controller. As it will be shown in Section 4.2.1 for the disturbance observer and in Section 5.2 for the ILC cases, both observer and ILC do not address correction of tracking error as their only feedback measurement is the current position of the plant. The observer and the ILC will then compensate for the disturbances that arise during an erroneous motion driven by the inaccurate command u_{ff} . The performance of both observer and ILC are also dependent on the accuracy of the estimated plant inverse. Large inaccuracies in the plant model requires large correction gains for proper parameter observation and also increases the number of iterations for ILC convergence. Each component of the control system, the feedforward block, the observer and the ILC, heavily rely on the assumption that the plant in free motion can be properly identified, representing an important assumption of this work.

Preliminary Experiments

In this section, disturbance rejection aspects of the proportional controller will be discussed based on preliminary excavation results.

Substituting of $C = K_p$ in to the controller structure shown in Figure 4.3 leads to the closed-loop dynamics

$$\begin{aligned}\dot{\tilde{q}}_1(t) &= \tilde{q}_2(t) \\ \dot{\tilde{q}}_2(t) &= -\frac{K_v}{\tau}\tilde{q}_2(t) - \frac{K_v}{\tau}[K_p\tilde{q}_1(t)] + \frac{K_v}{\tau}u_{ff}(t),\end{aligned}\tag{4.4}$$

where q_1 is the angular position of the joint, q_2 is the angular velocity of the joint, $\tilde{q}_1 = q_r - q_1$ is the angular error, and $\tilde{q}_2 = -q_2$ is the velocity. Note that the term $-\frac{K_v}{\tau}\tilde{q}_2(t)$ represents the flow-control servo-valve effectively acting as a damper with gain $\frac{K_v}{\tau}$ on the velocity \tilde{q}_2 . The value of τ is a property of the coupling between the servo-valve and the arm link. Values of τ were previously given in Table 3.1. The second equation in (4.4) can be seen as an equivalent to a PD controller with a feedforward input.

To obtain the maximum possible disturbance attenuation by means of feedback, the proportional gain K_p of each joint was initially tuned with the arm executing a digging trajectory in free motion. The values of K_p were increased until oscillations were observed, indicating that the system was approaching instability. Oscillations are caused by gains exciting the resonant modes of the arm. Lower values were then selected as stable controller gains. The stable gain values used during experiments are given in Table 4.1.

Table 4.1 – Proportional gains

Joint	K_p
Boom	157
Stick	631
Bucket	986

Note that stability when digging should be expected upon first guaranteeing that the controller is stable in free motion, since bucket interaction with the soil highly damps the arm. The significant backlash present in the arm joints does not represent an issue as the arm is invariably loaded in the same direction, opposite to the motion.

Initial experiments were conducted on cohesive and approximately homogeneous soil¹,

¹ Visual inspection of the sub-soil shows that most of the material below 20 to 30 cm is composed of clay with scattered pieces of brick and roots.

as shown in Figure 4.4 using the iterative strategy proposed in Section 3.2.1 where the desired cut profile was used as a reference trajectory, marked in Figure 4.5 by circles. Soil collected in the bucket was dumped between passes at the side of the cut. The curves in Figure 4.5 show the path of the bucket tip for eight consecutive passes. The first pass is shown as the lightest grey curve. The colour of the lines is darker with the pass number. The sequence of trajectories shows that convergence was minimal during the last two passes.



Figure 4.4 – Visual inspection of the opened trenches shows that except for the initial few centimetres of dry top soil the dominant material was clay.

The initial experiments indicated that one issue with a conventional proportional controller is a lack of disturbance rejection provided by feedback. One would expect that if the gains could be increased arbitrarily, the iterative process of digging would converge towards the desired goal. Recall from Equation (4.3) that under an ideal reference compensation $q_e = PSd$, where $S = (1 + CP)^{-1}$ is the sensitivity function. To achieve the final trench iteratively, that is $q_e \rightarrow 0$, the sensitivity function must be small. As the plant P can not be modified, the magnitude of S can only be decreased at certain frequencies by increasing feedback gains. Increasing gains will, however lead to an increase of the sensitivity magnitude at other frequencies due to the Bode integral (Equation 2.4).

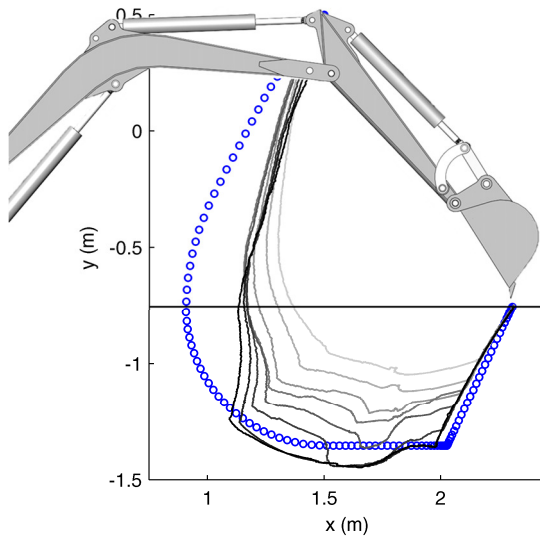


Figure 4.5 – Initial experiments using the basic proportional controller with a feedforward input based on the estimated internal dynamics of the plant.

The problem of heavy-duty manipulators is that high feedback gain values are usually not possible. Heavy manipulators such as those used in excavation, logging and concrete placement have low structural bandwidth due to the large inertia and long arm reach. Moreover, hydraulic systems have resonant modes caused by the compliance of flexible hydraulic hoses (Merritt, 1967), which decreases the effective bulk modulus of the hydraulic system.

Published examples suggest that a hydraulic excavator arm has an open-loop bandwidth between approximately 2 and 4 Hz, regardless of the size of the excavator. For example, Yoo et al. (2010) reported that a 30 tonne Doosan DX300LC excavator has a bandwidth of 4 Hz. In mini-excavators, a bandwidth of 2 Hz was reported by Dixon et al. (2005) and 3 Hz was identified on the experimental platform used in this work (Maeda et al., 2011). Feedback gains that cause motion at frequencies beyond the arm bandwidth can dangerously excite high frequency resonant modes of the arm or

hydraulic circuits.

A second issue of proportional control is related to the fact that feedback is based on position error. In forceful material removal, actuator output must maintain aggressiveness regardless of tracking error. An undesired effect of feedback on position is that actuation decreases as the system approaches the desired trajectory. Figure 4.6 intuitively illustrates this issue by portraying the control effort as the force in a stretched spring. When the end-effector is far from the desired trajectory the proportional spring is greatly extended, generating good control effort: that is $F = K_p\Delta Y$, where ΔY is large. As the bucket approaches the final trajectory the proportional spring is not deflected enough to generate the required control action for shearing the soil and convergence rate decreases proportionally. In the case the remaining soil imposes a resistance that equalises $K_p\Delta Y$ the convergence rate is theoretically zero.

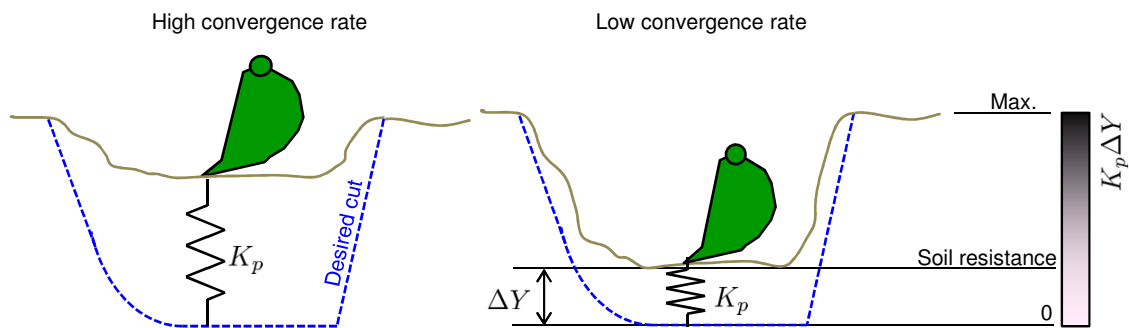


Figure 4.6 – The limitation of linear position error feedback is that control effort decreases as the end-effector approaches the trajectory. When the soil resistance equals the feedback output $K_p\Delta Y$ convergence vanishes.

4.2 Increasing Disturbance Rejection

This section investigates the use of a disturbance observer as an adaptive alternative to integral action to increase the disturbance rejection of the feedback controller.

Assuming that excavation forces can be represented as a slowly-varying disturbance due to the slow motion of the arm, the steady-state position error $Y_{E_{ss}}$ of a PI controller subject to a step disturbance of magnitude D is

$$\begin{aligned} Y_{E_{ss}}(s) &= \lim_{s \rightarrow 0} s \left[\frac{P}{1 + (K_p + K_i/s)P} \frac{D}{s} \right] \\ &= \lim_{s \rightarrow 0} s \frac{P}{s + (K_p s + K_i)P} D = 0, \end{aligned}$$

suggesting that the problem of persistent error caused by the remaining soil close to the desired trajectory that was illustrated in Figure 4.6 can be eliminated.

Stolt et al. (2012) showed that careful tuning of integral gains can, in fact, lead to a quantitative approximation to a known, slowly-varying disturbance force. While an integrator is usually a natural next step for increasing disturbance rejection, care should be taken with its use in autonomous excavation. In the work of Stolt et al. (2012), the ideal gain setting was possible because the integrator output was directly compared to measurements of the disturbance force. Note, however, that without such measurements it can be difficult to properly tune the integral gain. While proportional and derivative gains have a clear physical meaning as spring and damper whose effects can readily be observed even during the motion of the arm, the tuning of the integral gain depends on the disturbance forces, whose dynamics and magnitude are usually unknown.

Although heuristic methods for tuning a PI controller are available, with the most widely accepted being the Ziegler-Nichols method (Ziegler and Nichols, 1942), it is

also known that heuristic methods yield poor performance in comparison with modern auto-tuning PID methods (Åström et al., 1993; Åström and Hägglund, 2001). For the purposes of this work, however, two characteristics of excavation compromise the use of heuristics and auto-tuning methods. Firstly, changes in the excavation conditions require digging to be interrupted to set new PI gain values. Such interruptions may be unacceptably frequent if the soil conditions change constantly. Secondly, the tuning of the PI controller assumes that the system is working within the useful range of actuation. This is rarely the case in excavation which is characterised by severe saturation of the actuators.

For the experiments reported in Section 6, the PI controller was manually tuned by trial-and-error for the specific conditions of the field. As an anti-windup measure this work adopts a conditionally-freeze integrator (Hodel and Hall, 2001) which has only one tuning parameter. The method consists of an extra feedback loop that stops the integration of the error at the current value whenever the total actuation command exceeds a certain threshold, usually set to be the maximum actuator output. The rule has the form

$$\Delta u_i = \begin{cases} 0, & |u_p + u_i| \geq u_{tres} \text{ and } y_e \cdot u_i \geq 0 \\ y_e, & \text{otherwise,} \end{cases} \quad (4.5)$$

where Δu_i is the input of the integrator gain, and u_p and u_i are respectively the proportional and integral commands. The tracking error is y_e and u_{tres} is the threshold value. The sign of the product $y_e \cdot u_i$ is used to allow integration when the integral action saturates the actuator in the direction that decreases the tracking error.

4.2.1 Disturbance Observation

To avoid the issues of difficult tuning and windup with integrators an alternative for compensation of low frequency disturbance forces is a disturbance observer.

To motivate the use of an observer, initially assume the presence of a force sensor and a force control loop. One straightforward solution to compensating excavation forces would then be to feed the actuators with inputs that generate the opposite forces to the force sensor readings. In this hypothetical situation all disturbance rejection that was being allocated to the PI controller via position error is now being generated through force control. The burden on the PI controller is greatly reduced, and the PI gain values can be reduced.

Although force sensing seems to provide a direct solution for counteracting large forces under low-gain position feedback, there are technical issues with force sensing. In general, correct measurement of force values is problematic due to the presence of noise and calibration errors. In large heavy-duty manipulators, such as those used in mining, robust sensors with the required precision and large measurement range may not be available. The harsh conditions which sensors are exposed to also make their use difficult in practice².

An alternative to direct force measurement is to estimate forces using a virtual sensor. Here it is hypothesised that the performance of the proportional controller can be improved with a virtual disturbance sensor, in the same way it would be improved if direct force sensing was available. Although the method to be introduced is usually known as a disturbance observer (DOB), in terms of implementation it is no different

² Issues with durability and maintenance of the force sensors when installed directly in an exposed excavator arm seem to be the reason why estimation of excavated mass is done by weighing haul trucks using large scales. Information obtained by personal communication with mine operators, Pilbara, Western Australia.

from designing an estimator for an extra unmeasured state.

In the hydraulic control literature, disturbance observers have been mainly used for the compensation of cylinder friction (Friedland and Park, 1992; Tafazoli et al., 1998; Ha et al., 2000a; Bonchis et al., 2001). In general, disturbance observers are used for estimating forces, such as wind forces on unmanned aerial vehicles (Benallegue et al., 2007), that are difficult to measure with physical sensors. Observers are also used to overcome limitations of the physical sensors themselves, such as bandwidth, noise and compliance of the sensor structure (Katsura et al., 2007).

Figure 4.7 shows the structure of the proportional controller augmented with a DOB implemented by plant inversion (Kempf and Kobayashi, 1999). The observer output is $\hat{d}(t) = Cy_e(t) + u(t) - P^{-1}y(t)$ and, with an ideal inverted model, the observer estimate is exactly the disturbance at the plant input $\hat{d}(t) = d(t)$. The controller C consists only of a proportional control law as the role of the integral gain in compensating disturbances is now performed by the observer.

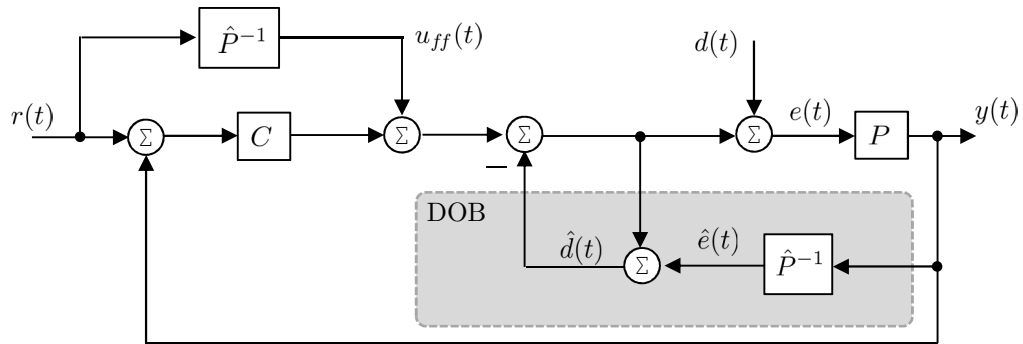


Figure 4.7 – Structure of the basic controller with feedforward reference compensation augmented with a disturbance observer (DOB). The block C is the controller, P is the plant, \hat{P} is the plant estimate, d is the disturbance at the plant input, \hat{d} is the disturbance estimated by the DOB, r is the reference, y is the output, e is the plant input and u_{ff} is the feedforward signal that compensates for reference changes.

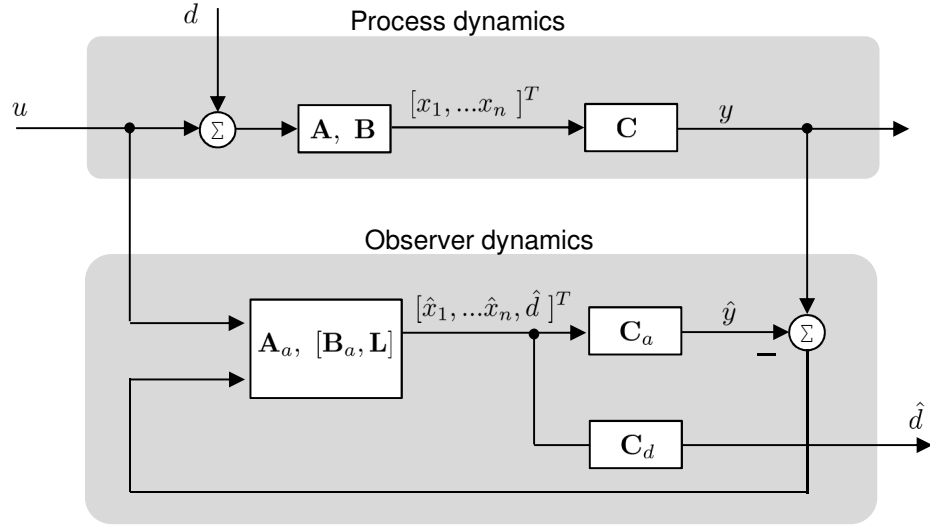


Figure 4.8 – Structure of the Luenberger observer as an estimator of disturbances.

Although the implementation in Figure 4.7 is intuitive, not only do errors in the inverse model \hat{P}^{-1} generate erroneous estimated disturbance values but the on-line inversion of the model is usually non-trivial. In general an observer is implemented as shown in Figure 4.8, where errors in the model are corrected by feedback and the internal model runs in forward simulation. The plant model is represented by the state matrix \mathbf{A} and the input matrix \mathbf{B} , with measurement given by the output matrix \mathbf{C} . The model of the augmented process given as $\mathbf{A}_a, \mathbf{B}_a, \mathbf{C}_a, \mathbf{C}_d$ contains an extra state representing the disturbance estimate \hat{d} . The process model runs in parallel with the real plant generating predictions $[\hat{x}_1, \dots, \hat{x}_n, \hat{d}]^T$. Since the disturbance is not part of the input of the observer model, the observed and predicted variables y and \hat{y} will differ. This error in prediction is corrected by the use of the gains \mathbf{L} to control the observer dynamics back to the true dynamics. Under perfect model assumptions, the amount of correction needed is the estimated value of the disturbance at the plant input \hat{d} .

The augmented observer model must include assumptions of the disturbance dynam-

ics. The usual assumption is that disturbances have slow varying dynamics, represented as $\dot{d} = 0$, suggesting that the observer is suitable for compensating slowly-varying disturbances. The augmented dynamics is

$$\begin{bmatrix} \dot{\mathbf{x}}(t) \\ \dot{d}(t) \end{bmatrix} = \begin{bmatrix} \mathbf{A} & \mathbf{B} \\ 0 & 0 \end{bmatrix} \begin{bmatrix} \mathbf{x}(t) \\ d(t) \end{bmatrix} + \begin{bmatrix} \mathbf{B} \\ 0 \end{bmatrix} \mathbf{u}(t)$$

$$\mathbf{y}(t) = [\mathbf{C} \quad 0] \begin{bmatrix} \mathbf{x}(t) \\ d(t) \end{bmatrix}.$$

The Luenberger observer (Luenberger, 1971) uses feedback to obtain the estimates

$$\begin{aligned} \dot{\hat{\mathbf{x}}}_a(t) &= (\mathbf{A}_a - \mathbf{LC}_a)\hat{\mathbf{x}}_a(t) + \mathbf{B}_a\mathbf{u}_a(t) + \mathbf{Ly}(t) \\ \mathbf{y}(t) &= \mathbf{C}_a\mathbf{x}_a(t) \\ \hat{d}(t) &= \mathbf{C}_d\mathbf{x}_a(t). \end{aligned} \tag{4.6}$$

Using the Laplace transform on Equation (4.6) leads to the observer transfer functions

$$\hat{\mathbf{x}}_a = \mathbf{B}_a(s\mathbf{I} - \mathbf{A}_a + \mathbf{LC}_a)^{-1}\mathbf{u} + \mathbf{L}(s\mathbf{I} - \mathbf{A}_a + \mathbf{LC}_a)^{-1}\mathbf{y}. \tag{4.7}$$

For a LTI system the estimator is stable if the observer gains $\mathbf{L} = [L_1, L_2, \dots, L_n]^T$ are selected so that the eigenvalues of $(\mathbf{A}_a - \mathbf{LC}_a)$ lie on the left side of the s plane.

In the case of the experimental platform, each joint of the excavator arm has an observer described by the matrices

$$\mathbf{A}_a = \begin{pmatrix} 0 & 1 & 0 \\ 0 & -1/\tau & K_v/\tau \\ 0 & 0 & 0 \end{pmatrix}, \quad \mathbf{L} = \begin{pmatrix} L_1 \\ L_2 \\ L_3 \end{pmatrix}, \quad \mathbf{x}_a = \begin{pmatrix} \hat{x}_1 \\ \hat{x}_2 \\ \hat{d} \end{pmatrix}, \quad \mathbf{B}_a = \begin{pmatrix} 0 \\ K_v/\tau \\ 0 \end{pmatrix},$$

$$\mathbf{C}_a = [1, 0, 0], \quad \mathbf{C}_d = [0, 0, 1], \quad (4.8)$$

leading to the linear system

$$\begin{aligned} \dot{\hat{x}}_1(t) &= \hat{x}_2(t) + L_1[x_1(t) - \hat{x}_1(t)] \\ \dot{\hat{x}}_2(t) &= (K_v/\tau)u(t) + (K_v/\tau)\hat{d}(t) - (1/\tau)\hat{x}_2(t) + L_2[x_1(t) - \hat{x}_1(t)] \\ \dot{\hat{d}}(t) &= L_3[x_1(t) - \hat{x}_1(t)], \end{aligned} \quad (4.9)$$

where \hat{x}_1 , \hat{x}_2 , and \hat{d} are respectively estimates of the position, velocity and disturbance.

While the linear DOB in Equations (4.9) will be useful for frequency analyses, in experiments a robust version of the observer will be used by replacing the correction term $L(x_1 - \hat{x}_1)$ with a switching function of the form $M\text{sgn}(x_1 - \hat{x}_1)$, where M is a large positive number. This method, reviewed in Section 2.1.5 as the variable structure observer (VSO) (Ha et al., 2000a) is known to be robust to model uncertainty by inducing a sliding behaviour on the error dynamics of the observer (Slotine et al., 1986). The VSO was shown to be particularly suitable with hydraulic actuators (Bonchis et al., 2001). In this work, to avoid the chattering typical of sliding modes the discrete switching is substituted by $M \tanh((x_1 - \hat{x}_1)/\gamma)$ as proposed by Ha et al. (2000a) leading to the dynamics

$$\begin{aligned} \dot{\hat{x}}_1(t) &= \hat{x}_2(t) + M_1 \tanh([x_1(t) - \hat{x}_1(t)]/\gamma_1) \\ \dot{\hat{x}}_2(t) &= (K_v/\tau)u(t) + (K_v/\tau)\hat{d}(t) - (1/\tau)\hat{x}_2(t) + M_2 \tanh([x_1(t) - \hat{x}_1(t)]/\gamma_2) \\ \dot{\hat{d}}(t) &= M_3 \tanh([x_1(t) - \hat{x}_1(t)]/\gamma_3). \end{aligned} \quad (4.10)$$

The values of M and γ were initially tuned in simulation, where the estimated value from the observer was compared to known disturbance inputs used as ground truth. The gains were later fine-tuned during field trials. The gains L_1 , L_2 , L_3 of the

equivalent linear DOB (4.9) were found by fitting the linear DOB output to the robust DOB response. The parameters of both observers are listed in Table 4.2 and their simulated response to step disturbances is shown in Figure 4.9.

Table 4.2 – Parameters of the disturbance observer.

Joint	K_v	τ	Linear DOB			Robust DOB (VSO)	
Boom	5.2	0.1	L_1	L_2	L_3	M	γ
Stick	3.95	0.1	6	300	2000	6000	0.45
Bucket	9.16	0.05	6	325	1200	8000	0.25
			10	300	800	4000	0.45

The robust observer will be used during experiments as previous works using the same experimental platform (Nguyen, 2000; Ha et al., 2002) showed that the method could successfully provide disturbance rejection. The linear observer in (4.9) with similar transient response will be used for frequency analysis. As both methods are disturbance observers the acronym DOB will be used to refer to both methods.

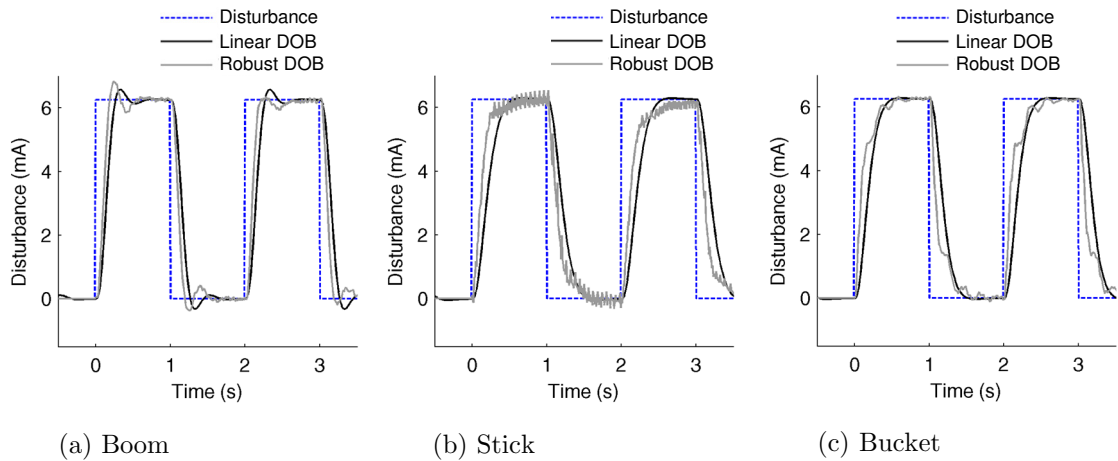


Figure 4.9 – The simulated response of the linear DOB and robust DOB (VSO) to step disturbances for each joint controller of the arm. The robust DOB was tuned on the experimental platform and used for experiments. The linear DOB with equivalent performance is used for frequency response analysis.

4.2.2 Stability Properties

A characteristic of disturbances in excavation, and of many material removal processes, is that forces that arise due to the interaction with the environment are reactive. For this reason, initial experiments with the proportional controller with bounded gains in section 4.1 did not disclose stability as a relevant concern as the reactive soil interaction forces increased the system damping. The use of the disturbance observer, however, requires a stability analysis as the observer estimates are used to compensate the dissipative forces from the soil and the interaction between the excavator and the environment loses the passive characteristic. The loss of passivity was reported by Le Tien et al. (2008) where an observer was used to compensate friction in a robotic arm; passivity was lost when the observer overcompensated, adding more energy than necessary to counteract friction.

Figure 4.10 presents the SISO controller structure for a single joint of the excavator arm. The reference and the feedforward reference inputs are omitted as it is assumed that excavation disturbances are significantly larger than the disturbance residuals caused by poor modeling of the arm in free motion (Assumption 4.1). In the usual Lyapunov stability analysis a model of the disturbance is required as part of the system. In the absence of an explicit disturbance model a Popov analysis (Slotine and Li, 1991) is used to investigate stability properties with an unknown disturbance function. Here disturbances are assumed to be a function of the arm motion and soil properties. In particular, disturbances are known to be reactive to the motion, and therefore have the opposite sign of the velocity.

Consider two linear functions are used to bound the unknown disturbance function. In Figure 4.10 the linear functions have slopes k_1 and k_2 , while the true disturbances

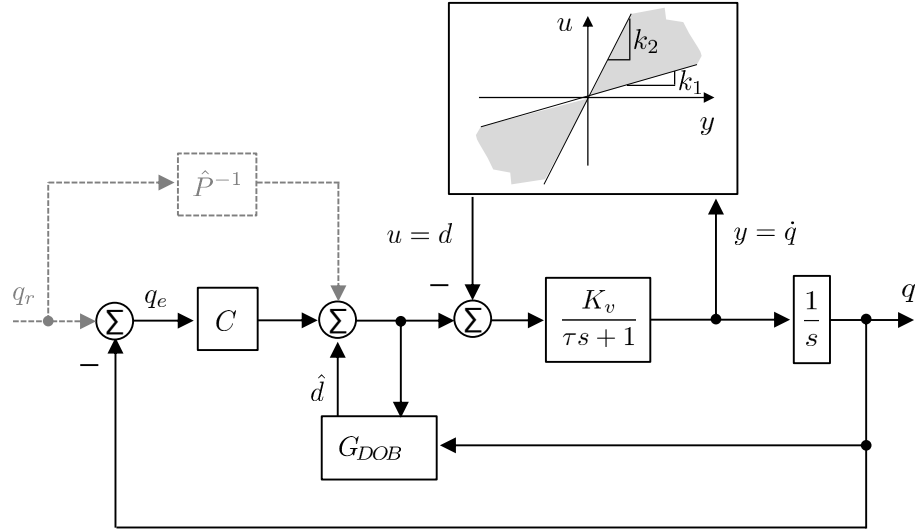
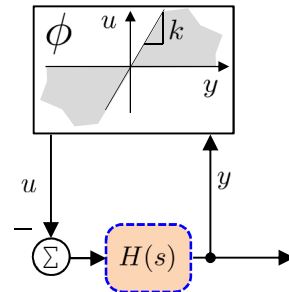


Figure 4.10 – Joint controller with DOB and unknown soil reactions. The dashed lines indicate that the reference input is assumed to be completely compensated by an ideal inverse model of the plant (Assumption 4.1).

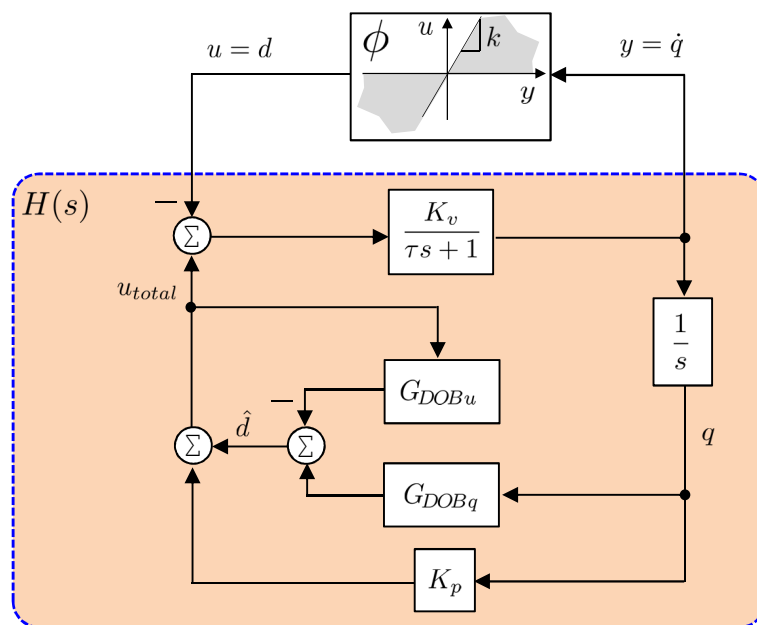
could be anywhere in the grey area. This is written as

$$k_1 y \leq d(y) \leq k_2 y \quad (4.11)$$

and it is said that the disturbance belongs to the sector $[k_1, k_2]$. Popov's criterion (Slootine and Li, 1991) states the sufficient and restrictive conditions at which the system is stable under the unknown disturbances bounded by the sector in Equation (4.11). For a canonical system as shown in Figure 4.11 (a) the conditions are that the system is autonomous; that the subsystem H , comprised of all known components of the system (that is, the controller and the plant), is linear and stable; and that the disturbance is memoryless and within the sector $[0, k]$. Under these conditions, the system is globally stable if the Popov plot—given by plotting $H(j\omega)$ in the s plane as $W(j\omega) = \text{Re}(H(j\omega)) + j\omega \text{Im}(H(j\omega))$ —is entirely contained at the right side of a line that crosses the real axis at $-1/k$.



(a) A generic system with a nonlinear function input



(b) Rearranged excavator joint controller

Figure 4.11 – Rearrangement of the excavator joint controller into the canonical form for a Popov stability analysis. (a) The canonical form where k is the slope that bounds the sector of the nonlinear function. (b) The rearranged joint controller.

In excavation, disturbances must be contained in the sector $[0, k]$ as the direction of any disturbance is necessarily opposite to the direction of the bucket velocity. Thus, although an explicit model of excavation disturbances is not available, it is known that it has the form of the block ϕ in Figure 4.11 (a). By rearranging the excavator joint controller in Figure 4.10 into the form of the canonical structure in Figure 4.11 (b),

the Popov plot of this new system indicates the stability of the joint control when the proportional controller with disturbance observer (P-DOB) is perturbed by the reactive soil-tool interaction forces.

The blocks G_{DOB_u} and G_{DOB_q} in Figure 4.11 (b) are the DOB transfer functions obtained by substituting the joint model parameters in (4.8) into Equation (4.7):

$$\begin{aligned} G_{DOB_u} &= \frac{K_v L_3}{\tau s^3 + (L_1\tau + 1)s^2 + (L_2\tau + L_1)s + K_v L_3} \\ G_{DOB_q} &= \frac{L_3\tau s^2 + L_3}{\tau s^3 + (L_1\tau + 1)s^2 + (L_2\tau + L_1)s + K_v L_3}. \end{aligned}$$

The Popov plot $W(j\omega) = \text{Re}(H(j\omega)) + j\omega \text{Im}(H(j\omega))$, where $H(s)$ is the new subsystem in Figure 4.11 (b) is shown in Figure 4.12 for each joint of the arm. Part (a) of Figure 4.12 shows the cases where the proportional feedback controller is disabled and part (b) when they are enabled, using the excavator arm joint parameters given in Table 4.3.

Table 4.3 – Parameters of the joint controller

Joint	K_p	K_v	τ	Linear DOB		
				L_1	L_2	L_3
Boom	157	5.2	0.1	6	300	2000
Stick	631	3.95	0.1	6	325	1200
Bucket	986	9.16	0.05	10	300	800

From Figure 4.12 (a) it is observed that when the position feedback is disabled each joint is passive, since the plots are entirely contained on the positive side of the real axis. In Figure 4.12 (b) the proportional gain has a value different than zero. When the disturbance observer (DOB) is active the system loses the passivity property and the curves enter the negative side of the imaginary axis. When the DOB is inactive, the controller is again passive, as a proportional controller alone can not add energy to

a system. Note from both figures that at high frequencies the curves of the controller with the active DOB asymptotically approach the straight lines representing the case when the DOB is inactive, indicating that attenuation of disturbances due to the presence of the observer becomes negligible at high frequencies.

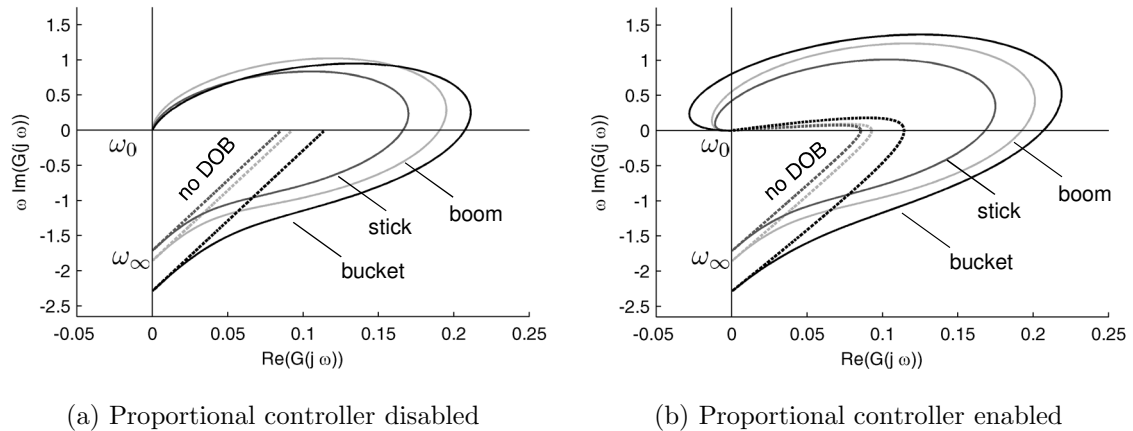


Figure 4.12 – The Popov plot where disturbances enter the system at the servo-valve input. The dotted lines represent the stability of the controller without DOB.

When Assumption 4.1 does not hold and the estimated plant presents significant modeling errors the Popov analysis is not applicable. It is still possible, however, to analyse the robustness numerically by means of integral quadratic constraints (IQC) (Megretski and Rantzer, 1997). In fact, Megretski and Rantzer (1997) show that the Popov criterion is a particular case of IQC analysis where the memoryless nonlinear disturbance is contained in a sector.

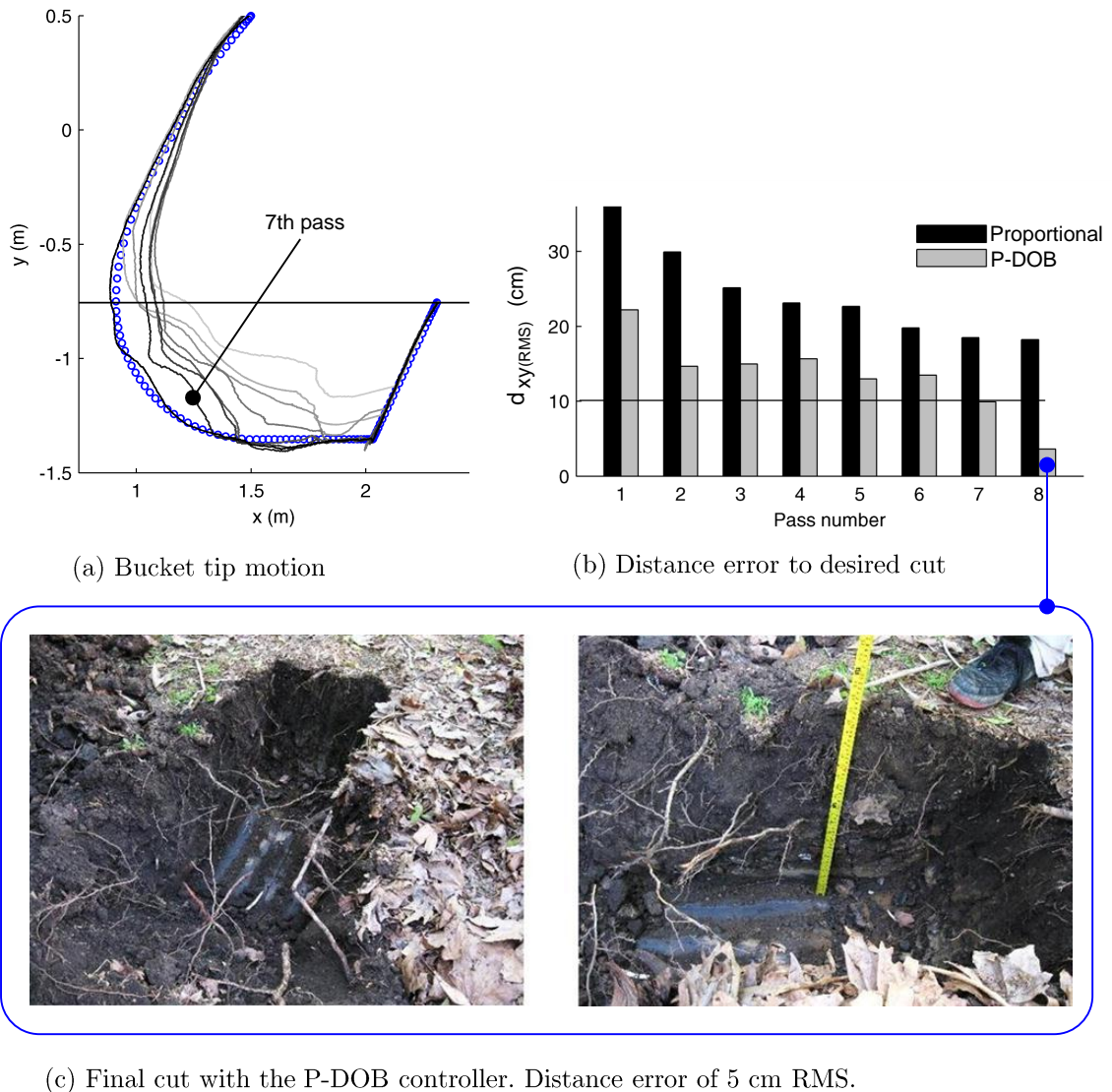
4.2.3 Excavation with Disturbance Estimation

To evaluate the excavator controller with the observer, the same procedure used in the experiments reported in section 4.1 was repeated at the same location, under the same soil conditions. The proportional controller was used again with the difference being that each joint now includes its own robust disturbance observer.

Qualitative results of this experiment are shown in Figure 4.13 (a) in the form of paths of the bucket tip. In comparing this figure with Figure 4.5, note that the original controller could not achieve the final cut by the end of the eighth pass. The disturbance estimates provided by the observer produced compensation commands that allowed the cut be completely finished with the same number of passes, under the same feedback gain values.

The bars in the plot in Figure 4.13 (b) represent the RMS distance error metric $d_{xy(RMS)}$ of the bucket tip in relation to the desired cut trajectory during each of the eight passes. The $d_{xy(RMS)}$ metric was defined in Section 3.3. The black bars indicate the proportional controller used in the previous experiment and the grey bars represent the proportional controller with disturbance observer (P-DOB). In the case of the P-DOB controller, the RMS distance error between the desired cut and the trajectory of the eighth pass was less than five cm. A photograph of the final cut is given in Figure 4.13 (c).

The significant improvement of the proportional controller with disturbance observer (P-DOB) compared to the proportional controller alone supports the hypothesis that sensitivity to disturbances can be improved by using an estimator as a virtual sensor. Disturbance forces could be counteracted by estimating their effects at the plant input, which in the case of a hydraulic arm represents deviations in the expected flow (or deviations in the expected position of the valve spool). The disturbance observer provides a general method of improving disturbance rejection of feedback controllers with insufficient position gains even when direct access to force or torque disturbance measurements is not available.



(c) Final cut with the P-DOB controller. Distance error of 5 cm RMS.

Figure 4.13 – The experiment with a proportional controller reported in Section 4.1 is repeated with the proportional controller augmented with the robust DOB. (a) The trace of the motion of the bucket tip in Cartesian coordinates. (b) Distance error per pass (c) Final appearance of the cut using the P-DOB controller. The seventh pass is indicated in (a) for presenting a 10 cm RMS error. This error value will be used in Chapter 6 as an indication of a typical coarse cut.

4.3 Disturbance Rejection Beyond Feedback Limits

Although the experiments described in Section 4.2.3 showed that the inclusion of a disturbance observer improved the performance of the proportional controller, the effectiveness of the compensation depends on how fast the state estimates in Equation (4.6) converge to the true values. Slow convergence means that the estimator will present long transients when tracking the true disturbance values, during which time disturbance forces are not correctly compensated.

The frequency response of the linear observer (Equation (4.9)) for each link of the arm is shown in Figure 4.14. The responses show that the observers act as low-pass filters on the true disturbance values and roll off above approximately 8 rad/s (15 rad/s in the case of the boom). The time response of the linear observers was shown in Figure 4.9; each joint disturbance observer has a settling time of approximately 0.5 seconds. Experimental results will show (Figure 5.9 on page 148), however, that disturbances have significant power up to 20 rad/s (3 Hz) indicating that disturbances with frequencies in the band between 8 to 20 rad/s can not be properly estimated, and therefore compensated.

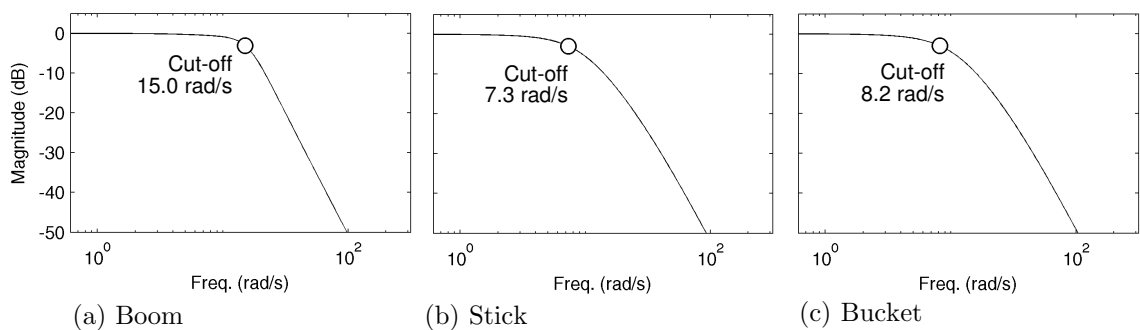


Figure 4.14 – The frequency response of the linear disturbance observer for each joint of the arm shows that the estimated value is a low-pass filtered version of the true disturbance. The -3 dB cut-off frequencies are marked with circles.

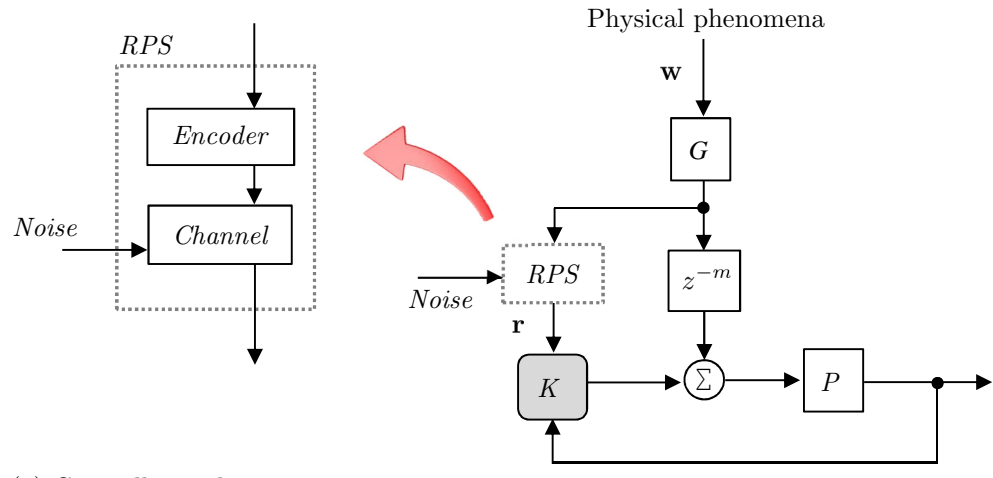
It is intuitive to think that if disturbances could be estimated with an observer having higher bandwidth, controller performance would be improved, response to soil reaction forces would be reduced and each excavation pass would remove more material. To some extent, the observer bandwidth could be improved by optimising its correction gains and refining its internal disturbance model. While those measures may provide a remedial solution, the fundamental limitation of linear closed-loop systems that incorporate feedback is that disturbance rejection can not be achieved at all frequencies due to the limitations of the Bode integral in Equation (2.4). This means that any “improvement” that extends the observer bandwidth causes deterioration at other frequencies. In general practical cases, due to limitations in bandwidth controllers and actuators are only effective in attenuating low-frequency disturbances meaning that high-frequency disturbances are usually amplified.

Figure 4.15 (a) replicates the generic control system with side information that was reviewed in Section 2.2. For such system, Martins et al. (2007) showed that Equation (2.23) — transcribed here for an open-loop-stable plant as

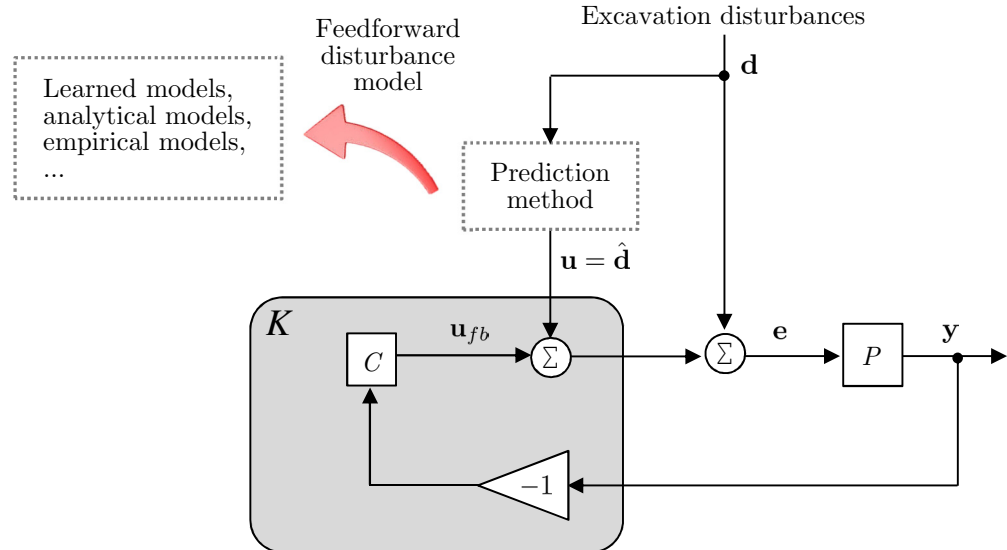
$$\frac{1}{2\pi} \int_{-\pi}^{\pi} \log |S_{\mathbf{d},\mathbf{e}}(\omega)| d\omega \geq -C_p, \quad (2.23 \text{ revisited})$$

where $C_p = \max_{\mathbf{p}_r} I_\infty(\mathbf{r}; \mathbf{d})$ —is an indication that a limited preview of the disturbance as side information can decrease the value of the Bode integral, increasing disturbance rejection beyond the limits of the feedback controller K .

Interpreting the side information that might be provided by a remote preview system (RPS) as the feedforward action provided by a disturbance model in excavation suggests that, if augmented with prediction capabilities, the excavator controller can achieve performance beyond the limits of its current feedback configuration. As it was suggested by Equation (2.17) (on page 42) the amount of improvement is quan-



(a) Controller with preview



(b) Controller with feedforward model of the disturbance

Figure 4.15 – Prediction of excavation forces as side information. (a) The original general controller with a remote preview system. (b) The actual controller where the prediction used to generate feedforward inputs is regarded as the remote preview system. The predicted disturbance \hat{d} is assumed to be a corrupted version of the true disturbance d .

tifiable as the mutual information rate $I_{\infty}(\hat{\mathbf{d}}; \mathbf{d})$ between the true disturbance \mathbf{d} and its predicted value $\hat{\mathbf{d}}$ in the feedforward command. This information rate causes the maximum achievable amount of decrease of the sensitivity integral of the feedback controller when prediction is available.

This interpretation is shown in Figure 4.15 (b). Comparing Figure 4.15 (a) and (b), the physical phenomena that affect the plant are identified as the excavation disturbances during a pass. The encoder of the RPS block takes the form of the feedforward model that encodes excavation disturbances according to the particular predictive method that is used: as the parameters of a soil-tool interaction model; as learned commands; as look-up tables, etc. The limitation of the channel in transmitting information quantifies the inaccuracy of the predictive excavation model. This interpretation indicates that, even if inaccurate, non-causal compensation of disturbances in excavation can bring potential benefits in terms of disturbance rejection.

In this work iterative learning control (ILC) will be used as a predictive method to compensate disturbances in excavation. This choice leads to the analogy depicted in Figure 4.16. While in the aircraft case the preview of disturbance is given by a remote preview system (RPS), in excavation ILC will be used to estimate the time-history of the disturbances in the previous pass which will then be used as a preview of the disturbances in the next pass. This reasoning is supported by the results in Moore (2000) where a one-step-ahead minimum error predictor control law—a RPS with a one-step look-ahead—is shown to be equivalent to ILC. The details of the learning rule for generating such preview estimates and the combination of ILC with the feedback controller will be discussed in Chapter 5.

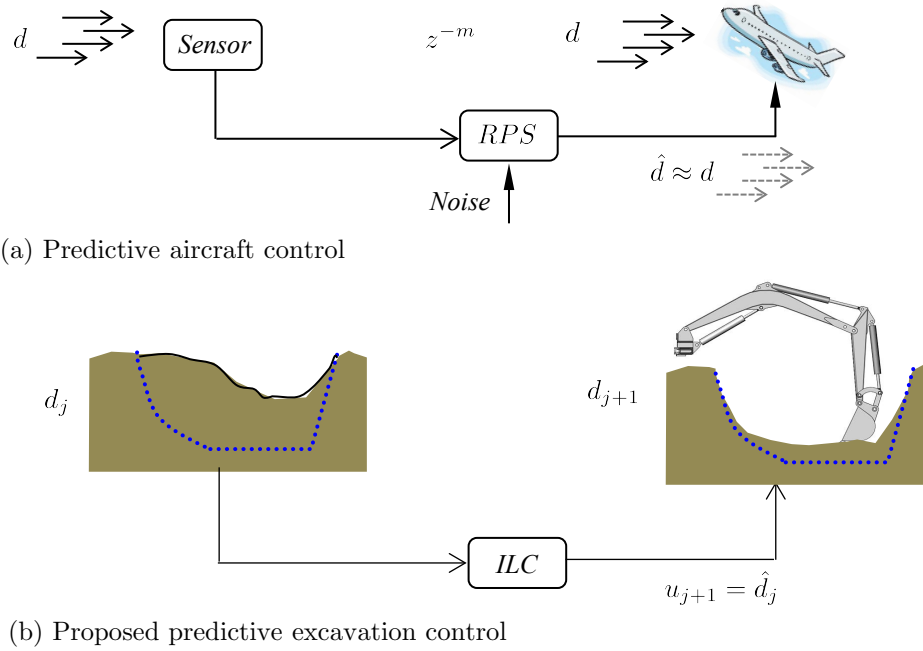


Figure 4.16 – Prediction of excavation forces as side information. (a) An aircraft controller with a remote preview system (RPS). (b) The proposed excavator controller with iterative learning control (ILC).

4.4 Conclusion

This chapter has proposed a proportional controller with feedforward reference compensation as the simplest adequate control method for a flow-driven hydraulic excavator arm. The choice of this control method, as opposed to other methods that are specific to excavation, was motivated by the fact that control methods based on linear feedback and dynamic compensation have been successful in a wide variety of applications, offering a well-known basic structure that can easily be implemented only with position feedback.

Dynamic compensation with feedforward control was adopted to dynamically compensate and decouple the joints of the excavator arm while avoiding the high sensitivity to parameter variation which is the main difficulty with inverse dynamics control. The feedforward control also simplified the system identification procedure as the model

needs only to capture the dynamics of motion of the final desired reference trajectory.

Initial experiments digging in near-homogeneous cohesive soil showed that disturbance rejection of the proportional controller was insufficient to maintain a satisfactory convergence rate towards a final cut. A disturbance observer was introduced to increase disturbance rejection of the proportional compensator as an adaptive alternative to integral action. Preliminary experiments indicated that this form of estimation was effective in increasing the disturbance rejection of the controller. In applications where direct force sensing is not available the observer provides a form of virtual sensor.

The plots of the frequency response of the linear observer (Figure 4.14) showed that the observer acts as a low-pass filter from the true disturbance and its estimate. The dynamics of the observer suggests that compensation can not be achieved completely as transient responses when tracking the true disturbance are inevitable. Fundamentally, the problem is related to the causality of the proposed methods. Results related to side information in preview control suggests that non-causal action can improve the performance of a feedback controller. Re-framing this result in the context of feedforward disturbance models in excavation suggests that the limitation of the proportional controller with disturbance observer (P-DOB) in providing disturbance rejection to the hydraulic manipulator can be overcome with the use of prediction, thus motivating the use of ILC as a predictive method in the next chapter.

Chapter 5

A Predictive-Reactive Controller in Excavation

This chapter proposes a predictive-reactive controller that uses the accurate parts of predicted disturbances with the goal of increasing disturbance rejection of the excavator controller by preemptive compensation. At the same time, to account for the fact that inaccuracies in prediction are inevitable, the controller uses a disturbance observer to estimate the prediction error. The general properties of the controller will be discussed and evaluated with excavation data. The chapter illustrates the performance of the proposed controller in simulation by using a simplified 1D tillage scenario to compare the controller with other control methods discussed in this work. Finally, the chapter discusses the proposed method in relation to published methods of iterative learning control (ILC) in the presence of non-repetitive disturbances.

5.1 Disturbances in Excavation

Using the data from the preliminary experiments reported in Section 4.2.3, Figure 5.1 shows the disturbance histories of typical excavation passes \mathbf{d}_j plotted in the same sequence for each of the actuators of the excavator arm. A simple observation from the plot is that disturbances decrease with the number of passes. Assuming that the soil was homogeneous, this corresponds to intuition since at each pass the bucket removes soil, decreasing the amount of material remaining to be sheared and dragged in the next pass. Despite the first and last passes being quite different, especially in the case of the boom, disturbances of consecutive passes show that there is some form of consistency in the *direction* of the disturbance, although not so much in the magnitude. The direction of disturbances is consistent because the same reference trajectory is being attempted at each pass, leading to similar tracking attempts.

In general disturbance histories between two consecutive passes seems to be reasonably consistent and well-behaved. Figure 5.1 (a) shows, however, that some transi-

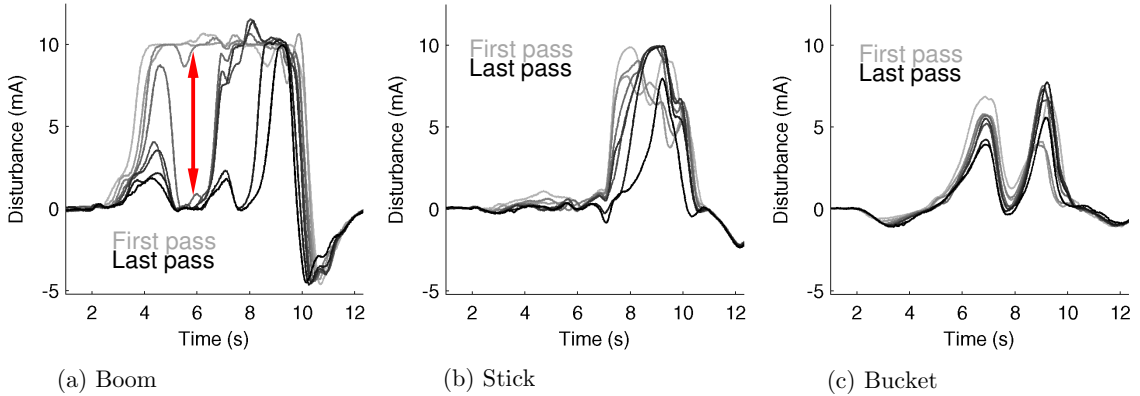


Figure 5.1 – Disturbances at the three servo-valves of the excavator arm during field experiments. The light grey curves show the first passes in undisturbed soil. The same controller then iterates seven more times towards the desired cut. The direction of the disturbance is approximately consistent from pass to pass, offering a structure that can be learned approximately.

tions may be unpredictably abrupt as indicated by the arrow. It is unclear what causes those abrupt changes: a previous pass may have fractured underlying soil, so that the disturbance in the next pass is much lower than would occur in un-fractured soil. Another possible cause is the dislodgement of lumps of compacted soil, or changes in soil compaction or composition (e.g. top-soil to sub-soil transition). Predicting such transitions seems difficult with analytical models and may be a source of large inaccuracies. The literature reviewed in Section 2.1.3 suggests that a disturbance predictor model is likely to be inaccurate, regardless of the prediction method selected. Cannon and Singh (2000) reported the same inaccuracy of 20% in force prediction using two models, an extended version of the original nonlinear fundamental equation of earthmoving (FEE) model and the FEE-based empirical model, both reviewed in Section 2.1.3. Tan et al. (2005) suggested that errors in identification of the parameters of soil-soil interaction models should be expected to be within the range of 20% to 30%. Althoefer et al. (2009) reported inaccuracy of 32% in soil density estimation using the hybrid Mohr-Coulomb and CLUB model.

Results, both from the experiments in Figure 5.1 and from the literature, suggest that an important feature of a predictive controller used in autonomous excavation is the ability to deal with large inaccuracies in prediction.

Here, a data-driven approach is proposed as a model-free¹ soil-tool interaction force predictor as an alternative to methods that require the explicit modelling of excavation forces. The choice of a data-driven approach is motivated by several factors:

1. A lack of experimental evidence that soil-tool interaction models can achieve the accuracy required for direct compensation in the lower level of motion/force control.

¹ The term “model-free” refers here to freedom from the knowledge encoded in an explicit soil-tool interaction model. The proposed method still requires a model of the arm dynamics.

2. Analytical soil-mechanics approaches to soil-tool interaction modelling introduce the issues of selecting and tuning an appropriate model, and ensuring that some minimal set of parameters is observed. This almost certainly requires the use of extra sensing to map soil surface geometry and to measure forces.
3. As Figure 5.1 suggests, a learning approach in excavation seems feasible, as some degree of similarity can be seen between disturbances generated by successive passes of a single cut.
4. A data-driven approach maintains a generic solution, leaving open the possibility of other applications.

5.2 Proposed Method

The proposed controller structure is shown in Figure 5.2 (a), where P represents the dynamics of the plant free from contact with the environment: that is, in free motion. The dynamics that arise during interaction with the environment are assumed to enter the plant as load disturbances $d_j(t)$. The estimated value of $d_j(t)$ is provided by a given predictive method as $u_j(t)$. The concept of the controller is to use the accurate parts of the predictive action $u_j(t)$ to increase disturbance rejection of the feedback controller as was suggested in Section 4.3. At the same time, as inaccurate predictions are expected in tasks like excavation, an observer is executed in the time domain to explicitly estimate the prediction error $(d_j(t) - u_j(t))$. The possibility of estimating the prediction error arises because the predicted disturbance $u_j(t)$ compensates the actual disturbance $d_j(t)$ before the observer input; what remains at the observer input is the disturbance residuals. For this reason, the structure in Figure 5.2 (a) subtracts the disturbance observer (DOB) output before the signal $u_j(t)$ is added to the loop.

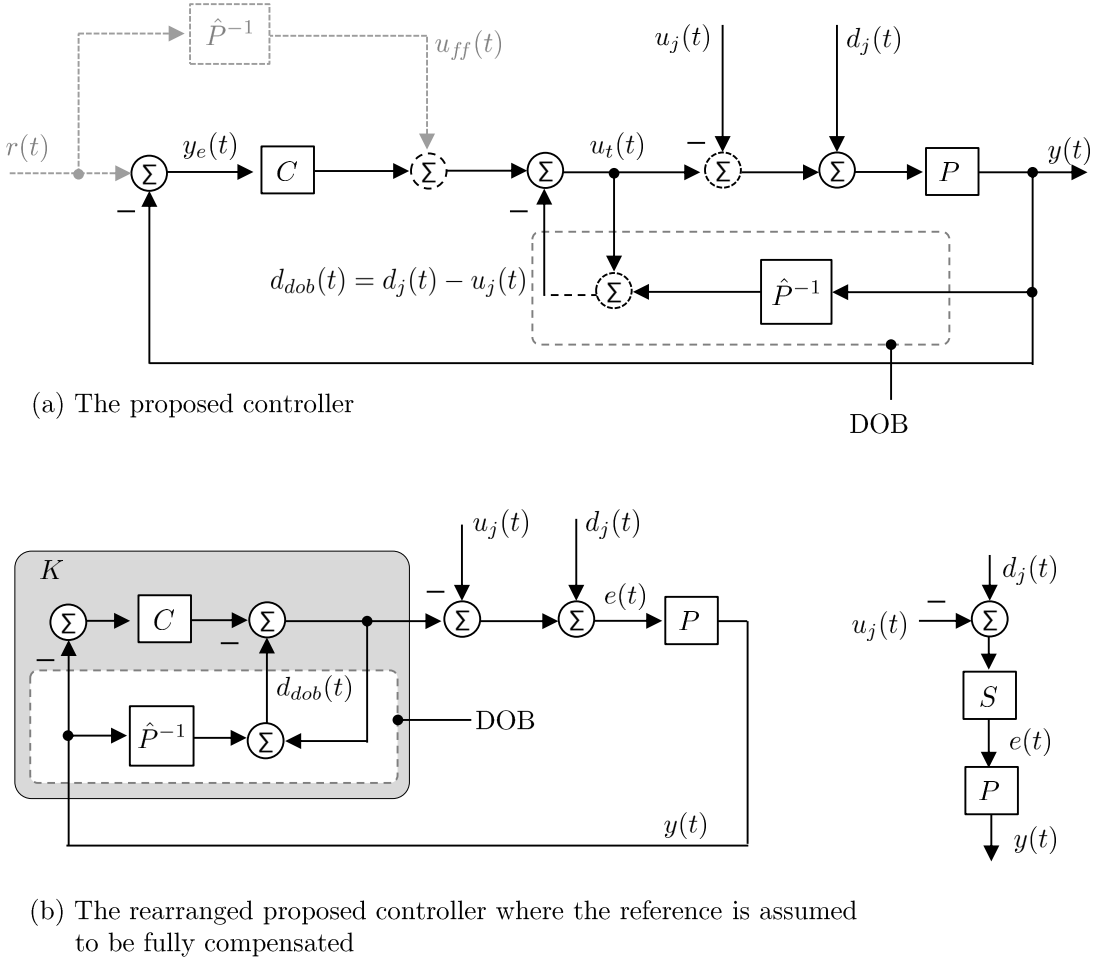


Figure 5.2 – Proposed predictive-reactive controller structure. The blocks P and \hat{P} are respectively the plant and the invertible plant estimate *in free motion*. The signals r , y , y_e and u_{ff} are the reference, the position output, the tracking error and the feedforward reference compensation command respectively. The terms d_j , u_j and d_{dob} are the disturbances arising from the interaction, the estimated disturbance and the DOB output, respectively. (a) The conventional representation with an ideal feedforward reference compensation (shown dashed). (b) At the left, the rearranged controller with the DOB and position feedback C grouped as a feedback controller K . Note from the representation on the right that the disturbance d_j is compensated preemptively by u_j before the feedback compensation.

Although the controller structure in Figure 5.2 is open to any predictive method that can provide an estimate of the disturbance, as was discussed in Section 2.3 this work adopts iterative learning control (ILC) to generate a history of disturbance compensation actions \mathbf{u}_{j+1} . The main motivation for this choice was that ILC is

a model-free approach that maintains the generality of the solution and requires minimal sensing.

This work proposes a variant of the plant-inversion ILC as

$$\begin{aligned} u_{j+1}(t) &= Q(z)[C(z)y_{e,j}(t) + u_j(t) - P^{-1}(z)y_j(t)] \\ &= \hat{d}_j(t). \end{aligned} \quad (5.1)$$

To understand the meaning of the update in Equation (5.1) notice that the output of the disturbance observer in Figure 5.2 (a) is $\hat{d}(t) = C(z)y_e(t) + u_t(t) - P^{-1}(z)y(t)$. In comparison, when $Q = 1$ Equation (5.1) is the implementation of the same observer in the iteration domain. The main difference between this update and a conventional ILC update with plant inversion (reviewed in Section 2.3.2) is that the controller does not learn the reference history \mathbf{r} , but only the disturbance compensation commands \mathbf{d}_j . This is essential to separate the feedforward input $u_{ff}(t)$ from $u_{j+1}(t)$, allowing inclusion of the time-domain DOB.

A characteristic of the proposed controller is that disturbances are counteracted twice. One compensation occurs between iterations when the update rule in Equation (5.1) uses the disturbance of the previous pass to compensate the disturbance of the next pass. A second compensation is made during execution when the time-domain DOB estimate is used to compensate for the error in predicted disturbances ($d_{j+1}(t) - u_{j+1}(t)$). This controller will be referred to as the predictive-reactive controller since the first counteraction on disturbances is predictive, and the second is reactive.

5.2.1 General Properties

The general properties of the proposed predictive-reactive controller are given in this section.

Under Assumption 4.1 the reference input is assumed to be exactly followed using $u_{ff}(t)$ and the controller can be rearranged as shown in Figure 5.2 (b), where the block K is comprised of the position feedback compensator C and the disturbance observer. The position $y_j(t)$ is

$$y_j(t) = -K(z)P(z)y_j(t) + P(z)[d_j(t) - u_j(t)] \quad (5.2)$$

$$= P(z)[1 + K(z)P(z)]^{-1}[d_j(t) - u_j(t)], \quad (5.3)$$

and, since $y_e = -y$ and $S = (1 + KP)^{-1}$,

$$y_{e,j}(t) = -P(z)S(z)[d_j(t) - u_j(t)], \quad (5.4)$$

indicating that the position error is independent of the reference $r(t)$ and due only to the prediction error $[d_j(t) - u_j(t)]$. The block representation is on the left in Figure 5.2 (b). Equation (5.4) suggests that the tracking error is decreased by compensating the disturbance d_j either by predictive action u_j or by the feedback attenuation S .

As in the case of a controller without ILC, errors in reference compensation due to a poor inverse model lead to additional tracking errors which must be compensated by the feedback controller as extra disturbances. In distinction from a conventional ILC based on tracking error, the update in Equation (5.1) does not have access to the reference command and consequently it does not improve reference tracking but only excavation disturbance rejection. As a result poor reference compensation from the

inverse plant will be a persistent source of disturbance. For this reason, it is important that a good estimate of the dynamics of the plant in free motion is available.

Assumption 5.1 (Ideal Disturbance Estimate). During the update of Equation (5.1) the Q -filter is set to unity and an invertible and ideal model of the plant P^{-1} is available. Under this assumption the disturbance history of a pass can be fully recovered from Equation (5.1); that is $\mathbf{u}_{j+1} = \mathbf{d}_j$.

Remark 1. The use of $Q \neq 1$ in Equation (5.1) has the same effect on the output error as in a conventional ILC. The filter may be used to avoid learning of non-repetitive disturbances in certain frequency bands, with the disadvantage that complete disturbance compensation becomes unachievable as $(\mathbf{d}_{j+1} - \mathbf{u}_{j+1}) \neq \mathbf{0}$ even in the case of iteration-repetitive disturbances. In practice, the Q -filter is usually used as a low-pass filter to attenuate high-frequency noise-like disturbances. This also guarantees monotonic convergence (Longman, 2000). Note that the on-line DOB also acts on non-repetitive disturbances. As the observer can only lead to attenuation over a certain limited low-frequency band, a plausible combination is to use the Q -filter to attenuate the noise-like high-frequency components of the non-repetitive disturbances during off-line updates, and to use the on-line DOB to attenuate the low-frequency components of the non-repetitive disturbances during the execution of the controller.

Theorem 5.1 (One-Iteration Convergence). *Assuming that the feedforward command u_{ff} in Figure 5.2 causes the plant exactly to follow a desired reference in the absence of disturbances, and that disturbances are iteration-repetitive; that is, $\mathbf{d}_{j+1} = \mathbf{d}_j$, the proposed controller converges in one iteration.*

Proof: When the reference is tracked by predicted values from an estimated plant

inverse Equation (5.4) holds

$$y_{e,j+1}(t) = -P(z)S(z)[d_{j+1}(t) - u_{j+1}(t)]. \quad (5.5)$$

Due to Assumption 5.1 the ILC update (5.1) is the disturbance of the previous pass $\mathbf{u}_{j+1} = \mathbf{d}_j$ so that

$$y_{e,j+1}(t) = -P(z)S(z)[d_{j+1}(t) - d_j(t)]. \quad (5.6)$$

Because disturbances are assumed repetitive $\mathbf{d}_{j+1} - \mathbf{d}_j = \mathbf{0}$ and

$$y_{e,j+1}(t) = 0. \quad (5.7)$$

Equation (5.7) shows that the tracking error goes to zero with one update of the control command. **QED.**

Remark 2. Under repetitive disturbances, if Assumption 5.1 is not respected the update Equation (5.1) generates a disturbance estimate that differs from the true disturbance $\mathbf{d}_{j+1} \approx \hat{\mathbf{d}}_j$. In this case it is clear that the error does not vanish in a single iteration. If the model error is systematic, the error becomes part of the actual repetitive disturbance which can be compensated in subsequent iterations. The number of subsequent iterations required for complete disturbance compensation will depend on the amount of modelling error in \hat{P}^{-1} .

Regardless of the inaccuracy of the estimated plant, the condition for the ILC convergence given by Equation (2.35) must be respected. In the case the uncertainty in the model is large enough such that (2.35) can not be respected the learning function has to be replaced from \hat{P}^{-1} with a less aggressive learning function. This explains the popularity of simple PD-type learning functions where the gain can be controlled

at will, usually leading to slow, however stable, learning rates.

Remark 3. The magnitude of the tracking error is decreased at all frequencies when the magnitude of the disturbance prediction error of a controller using ILC is lower than the magnitude of the disturbance itself. This can be written as

$$|D_j(e^{j\omega}) - U_j(e^{j\omega})| < |D_j(e^{j\omega})| \quad \forall \omega. \quad (5.8)$$

This can be seen by referring to right-most structure in Figure 5.2 (b): the tracking error of a controller with ILC prediction is related to disturbances by

$$|Y_E(z)| = |P(z)S(z)[D_j(z) - U_j(z)]|, \quad (5.9)$$

while the tracking error of the same controller without ILC prediction is

$$|Y_E(z)| = |P(z)S(z)D_j(z)|. \quad (5.10)$$

Equation (5.8) in the excavation context will be discussed in Section 5.2.2.

5.2.2 Properties in Excavation

Convergence of ILC under Excavation Disturbances

Consider that x_j represents the current state of an excavation cut and $V(x_j)$ is a quantity that represents the remaining amount of soil that must be sheared and removed to complete the cut. $V(x_j)$ will subsequently be regarded as a Lyapunov candidate function.

Assumption 5.2. The excavation process does not remove more soil than necessary to complete the cut

$$V(x_j) > 0 \quad \forall x_j \neq 0, \quad V(0) = 0. \quad (5.11)$$

Assumption 5.3. Each pass reduces the amount of soil remaining

$$V(x_{j+1}) < V(x_j) \quad \forall x_j \neq 0. \quad (5.12)$$

Assumption 5.4. Disturbances are bounded according to

$$\|d_j\|_2 \leq \alpha V(x_j), \quad (5.13)$$

where α is a positive constant.

Assumption 5.5. Position tracking error is caused only by excavation disturbances and is independent of the reference input such that the following relation holds

$$y_{e,j}(t) = -P(z)S(z)[d_j(t) - u_j(t)], \quad (5.14)$$

where u_j is the ILC input.

Theorem 5.2 (Convergence to Zero Tracking Error). *Under assumptions 5.2, 5.3, 5.4, and 5.5 the excavation process converges to zero tracking error:*

$$y_{e,j} \rightarrow 0 \text{ as } j \rightarrow \infty.$$

Proof: From the discrete-time version of the Lyapunov theorem, assumptions 5.2 and 5.3 imply that

$$x_j \rightarrow 0 \quad \text{as} \quad j \rightarrow \infty. \quad (5.15)$$

From assumption 5.4 and Equation (5.15)

$$\|d_j\|_2 \rightarrow 0 \quad \text{as} \quad j \rightarrow \infty, \quad (5.16)$$

indicating that disturbances tend to zero as soil is removed.

Since ILC estimates zero values when disturbances are zero; that is, $u_j = 0$ for $d_j = 0$, using Equation (5.16) and assumption 5.5 gives

$$y_{e,j}(t) \rightarrow 0 \quad \text{as} \quad j \rightarrow \infty \quad (5.17)$$

indicating that the excavation process converges to zero tracking error. **QED.**

Although Equation (5.17) shows that ILC converges, note that during intermediate passes two different passes will undergo different disturbance histories as disturbances are reactive to their respective motion. Monotonicity can not be guaranteed as the difference $(\mathbf{d}_j - \mathbf{u}_j)$ can increase between consecutive passes.

Experimental Excavation Data

During field trials to be reported in Chapter 6, a total of 162 passes were executed with predictive ILC commands. Since each pass requires three independent ILC updates (one for each joint controller), in total, $3 \times 162 = 486$ updates were made using Equation (5.1). There was no case where joint tracking errors using ILC diverged, despite the presence of rocks and differences in soil composition from place to place on the experimental site.

Using a data set of 335 excavation passes obtained during from field trials, Figure 5.3 shows the mean value of the 335 computations of the power spectral density (PSD) of

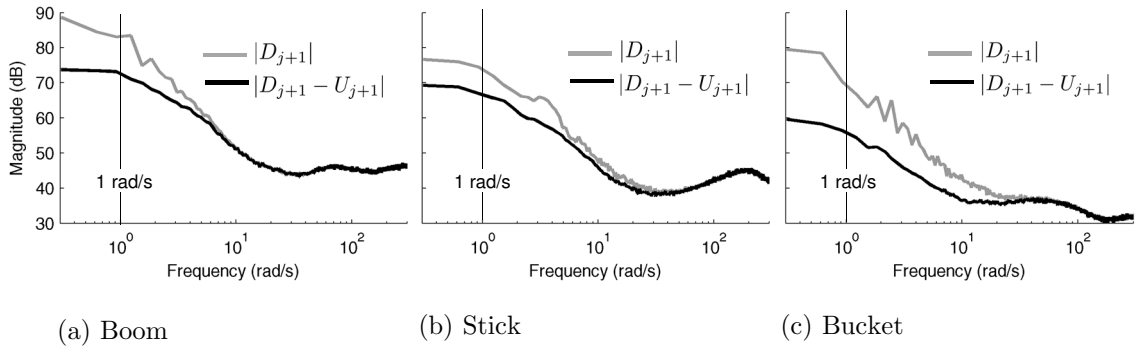


Figure 5.3 – Evaluating the validity of Equation (5.8) using real excavation data. . .

$(\mathbf{d}_{j+1} - \mathbf{u}_{j+1})$ for each joint controller of the excavator arm. The difference was obtained by calculating \mathbf{d}_{j+1} as the disturbance of the current pass and $\mathbf{u}_{j+1} = \mathbf{d}_j$ as the predicted disturbance based on data from the previous pass, both from Equation (5.1). The decrease in disturbance magnitude is most significant at low frequencies, $\omega < 1$ rad/s. The fact that, on average, the magnitude of the prediction error has a smaller value than the magnitude of the disturbance provides evidence that ILC updates are, in fact, preemptively decreasing the effect of disturbances in the tracking error. This shows that Equation (5.8) holds in the excavation case.

As a typical example, Figure 5.4 shows in the form of disturbances in the time domain a set of seven excavation passes required to open a cut during field experiments. The difference ($d_j(t) - u_j(t)$) is shown as the black curve and is overlaid with the uncompensated disturbance $d_j(t)$ in grey. The figure shows the significant reduction that can be achieved when the ILC update is used to reduce the disturbance load on the feedback controller by means of feedforward compensation. Residuals due to the non-repetitive disturbances seem, however, inevitable. In fact, in excavation one should not expect the history of the difference ($\mathbf{d}_j - \mathbf{u}_j$) to be zero as this would require the dynamics to be static in the iteration direction. Rogers et al. (2007) reported that the dynamics of material removal in repetitive processes propagate in

the iteration direction.

Using again data from the set of 335 experimental passes, Figure 5.5 shows in grey the mean value of the prediction error $|D - U|$ compared with the attenuation provided by the feedback $|S(D - U)|$. In the figure $|S|$ was obtained as the impulse response of the predictive-reactive controller in Figure 5.2 using the model of the excavator and the proportional controller and robust observer used during experiments. Figure 5.5 provides evidence that the feedback controller is effective in attenuating the great majority of the low-frequency components of the ILC prediction error.

As a typical example, Figure 5.6 shows the attenuation of the prediction error per pass when the excavator opened a cut with a sequence of eight passes. The black bar represents the non-attenuated case: that is, the error of ILC prediction quantified as the root-mean-square (RMS) value of $[d_j(t) - u_j(t)]/d_j(t)$. The grey bar represents the attenuated case when the prediction is simulated as the input disturbance of the predictive-reactive controller, quantified as the RMS value of $S(z)[d_j(t) - u_j(t)]/d_j(t)$. The average decrease in disturbance compensation error over all passes and joints was of 28%. During field trials to be reported in Chapter 6, the decrease of the compensation error will be reflected as passes with less overshoot and lower tracking error.

Further decrease is not possible due to the large residual power of the attenuated prediction error. This residual is noticeable from Figure 5.5 where the power of $S(D_j - U_j)$ is still significant, with an average value of approximately 40-50 dB over the whole spectrum.

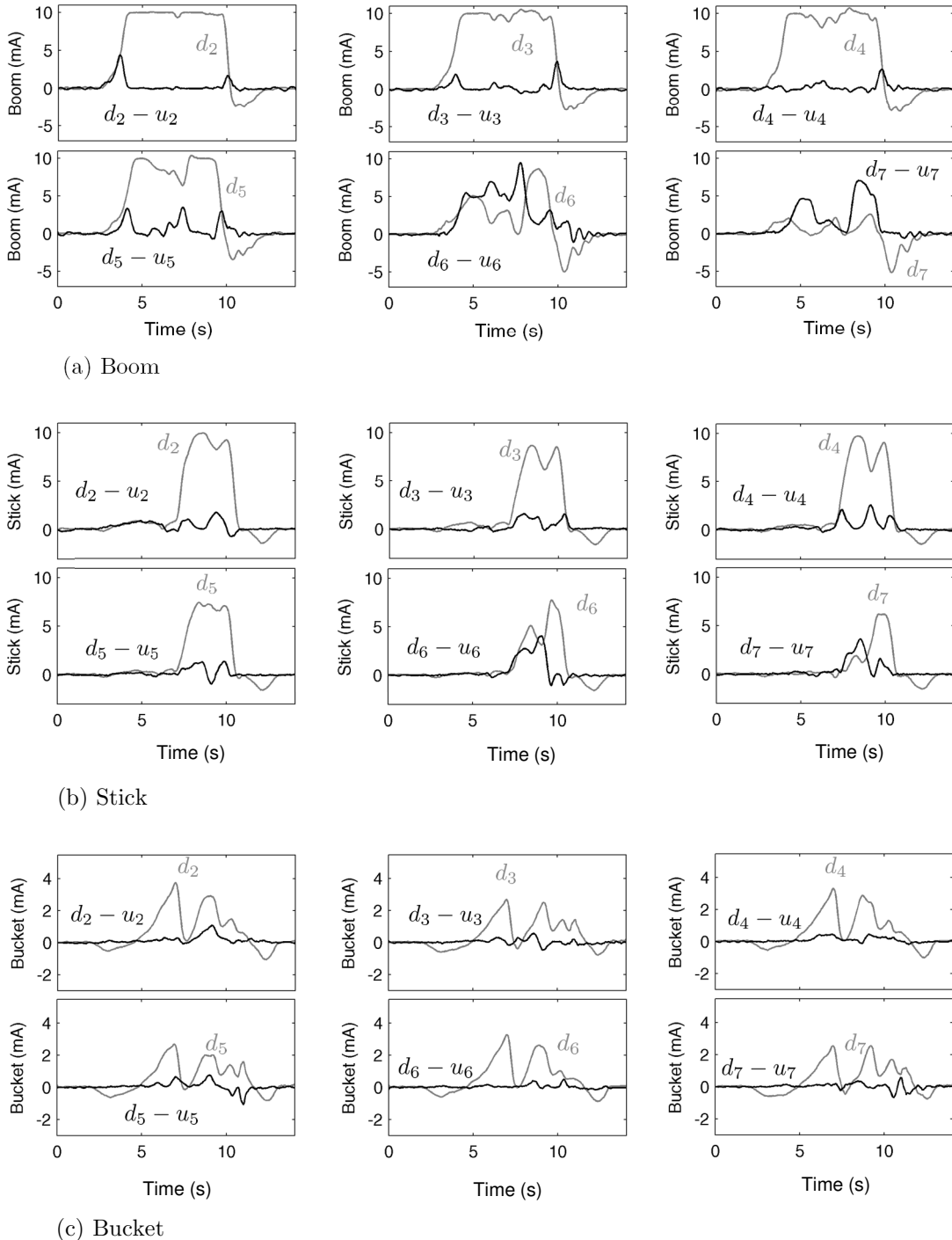


Figure 5.4 – A comparison of typical disturbances as seen at the plant input when the prediction from the previous pass is used (black curves) and is not used (grey curves). Clearly, for most of the passes shown in the plots, making use of the prediction greatly decreased the effective disturbance that enters the plant.

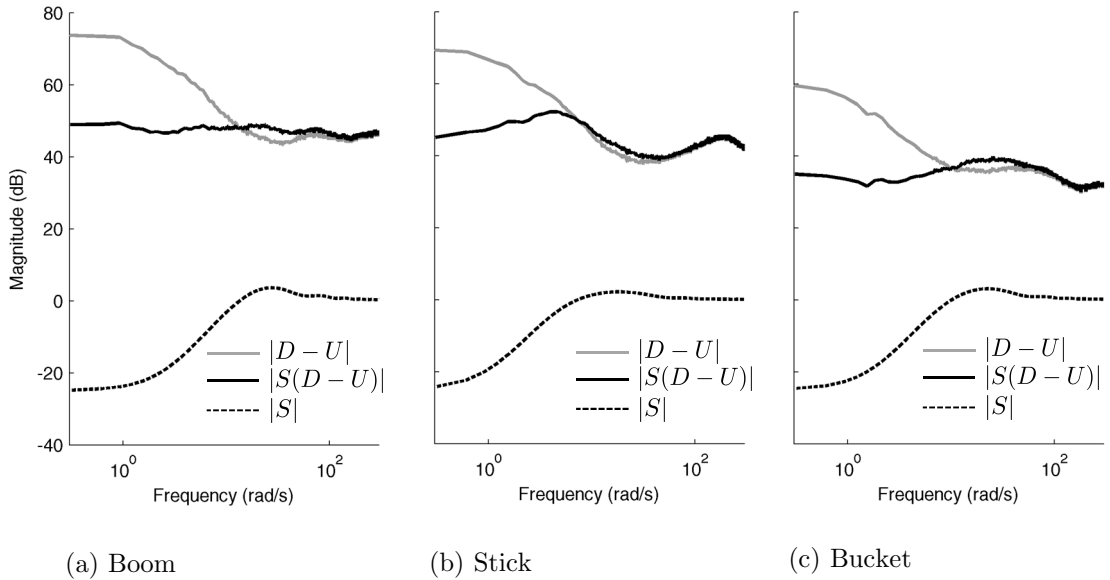


Figure 5.5 – Attenuation of the disturbance prediction error by the sensitivity function of the feedback controller. At each joint the value of D and U represents the average over 335 passes.

5.3 Simulations in 1D

This section utilises a simple 1D simulation that approximates a case of tillage to systematically illustrate the proposed predictive-reactive controller. Simulation not only makes it possible to cover systematically a variety of situations that are not encountered in excavation experiments, but also allows for the interpretation of the results to be free from the complexities of the real hydraulic excavator and the unknown characteristics of the soil being excavated.

To make the following explanations concise and unambiguous two definitions are introduced.

- *Reactability* characterises the ability of a feedback controller to reject disturbances when following a trajectory within a pass; that is, its performance in the time domain.

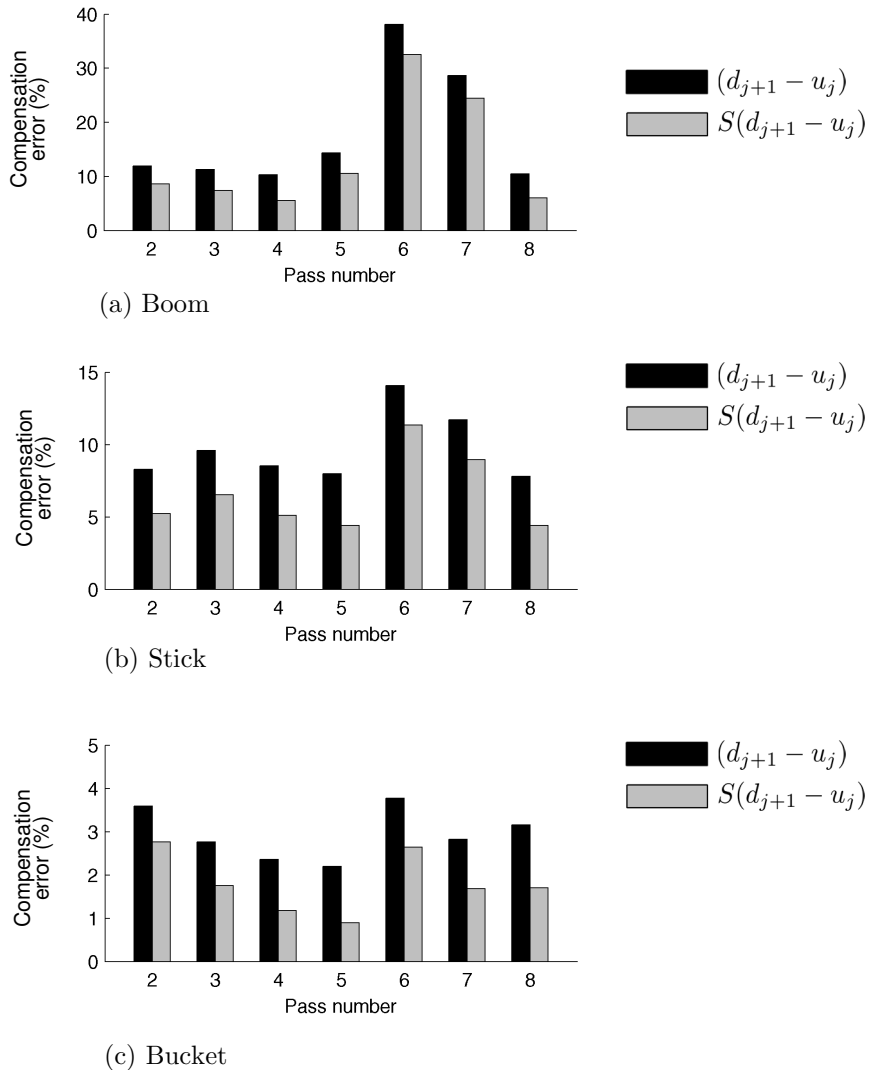


Figure 5.6 – Comparison of compensation error using only the predictive ILC and the proposed predictive-reactive controller. The predictive update was obtained with Equation (5.1) from which the difference between consecutive disturbance passes $d_j - u_j$ was computed. The same difference was used as the input for control system using an excavator model. The average decrease in disturbance compensation error due to the feedback was 28%. The experimental data were obtained from the experiments reported in Section 4.2.3, here used as a typical example of excavation disturbances.

- *Predictability* characterises the ease in predicting the true disturbance between passes by making use of past data. In the ILC case it is related to the ability to predict disturbances in the next iteration.

Clearly, reactability and predictability can be readily changed in simulation, but not easily controlled in the real world. Analytical models in excavation that assume soil homogeneity can only address the case of high predictability and high reactability as variations are smooth in both the time and iteration directions.

Care must be taken to distinguish between the definition of predictability used in this work and learnability as defined in Arimoto and Naniwa (2000). As defined by Arimoto and Naniwa, learnability is “one of system’s characteristics of capability of learning any type of a desired output via repeated practices”. Learnability is a qualitative property that indicates the existence of a function norm $\|\cdot\|$ such that $y_e \rightarrow 0$ as $k \rightarrow \infty$; it does not quantify the convergence rate or the robustness of the algorithm. A learning function that does not respect the ILC convergence property (2.35) leads to a system with no learnability. Arimoto and Naniwa show that for a SISO linear system learnability is equivalent to a system being stable. While learnability is a property exclusive to ILC, predictability characterises the degree of non-repetitiveness of the disturbance field and is independent of the control method.

To define the simulation scenario, consider a tillage process where a tool moves along a surface in the horizontal direction as shown in Figure 5.7 (a). One motion from 0 to 3 metres in the x-direction represents one pass, or iteration. For the next iteration the tool is moved in the vertical (depth) direction. Assume that once the new depth is defined the tool is locked in the vertical direction. The depth of the tool is defined by the lines labelled by the pass number as shown in Figure 5.7 (a). The disturbance force in the horizontal direction is assumed to be given by a “stiction field” defined by

$$d = -\text{sgn}(\dot{x})d_{\text{stiction}}(x, y), \quad (5.18)$$

where d_{stiction} is the magnitude of the stiction at position (x, y) . Different stiction

fields are shown in Figure 5.7 (b), (c), and (d) where stiction magnitudes are indicated by the grey scale.

Notice that in this simulation the disturbance counteracted by the controller is the simulated interaction force (measured in Newtons), in contradistinction to the real excavation case where disturbances are referred to the servo-valve input and measured in milliamperes. In simulation, directly compensating interaction forces is straightforward since no real sensing is required. In excavation practice, however, direct force compensation relies on the installation of load cells and inner force-control loops while compensation of disturbances at the servo-valve input makes the implementation much simpler to achieve.

The stiction values in the disturbance fields were generated by convolving a two-dimensional matrix with normally-distributed random values with a 2D Gaussian acting as a filter. A filter with small kernel widths in both dimensions generates a field that is noisy and disturbances are consequently difficult to compensate in both the time (x-direction) and iteration (y-direction) domains. Filters with large kernel widths in the x-direction generate fields that have smooth disturbances along the pass, and therefore high reactability. Large kernel widths in the y-direction generates fields with smooth transitions between passes, therefore high predictability. As the x- and y-kernel widths of the filter are changed independently different disturbance fields can be created.

As examples, Figure 5.7 (b) shows a case of low reactability and high predictability, which is favourable for ILC. Figure 5.7 (c) shows a case of high reactability and low predictability, which is favourable for DOB. Figure 5.7 (d) shows a case of high reactability and high predictability, where transitions are smoother in both directions which is favourable for both ILC and DOB.

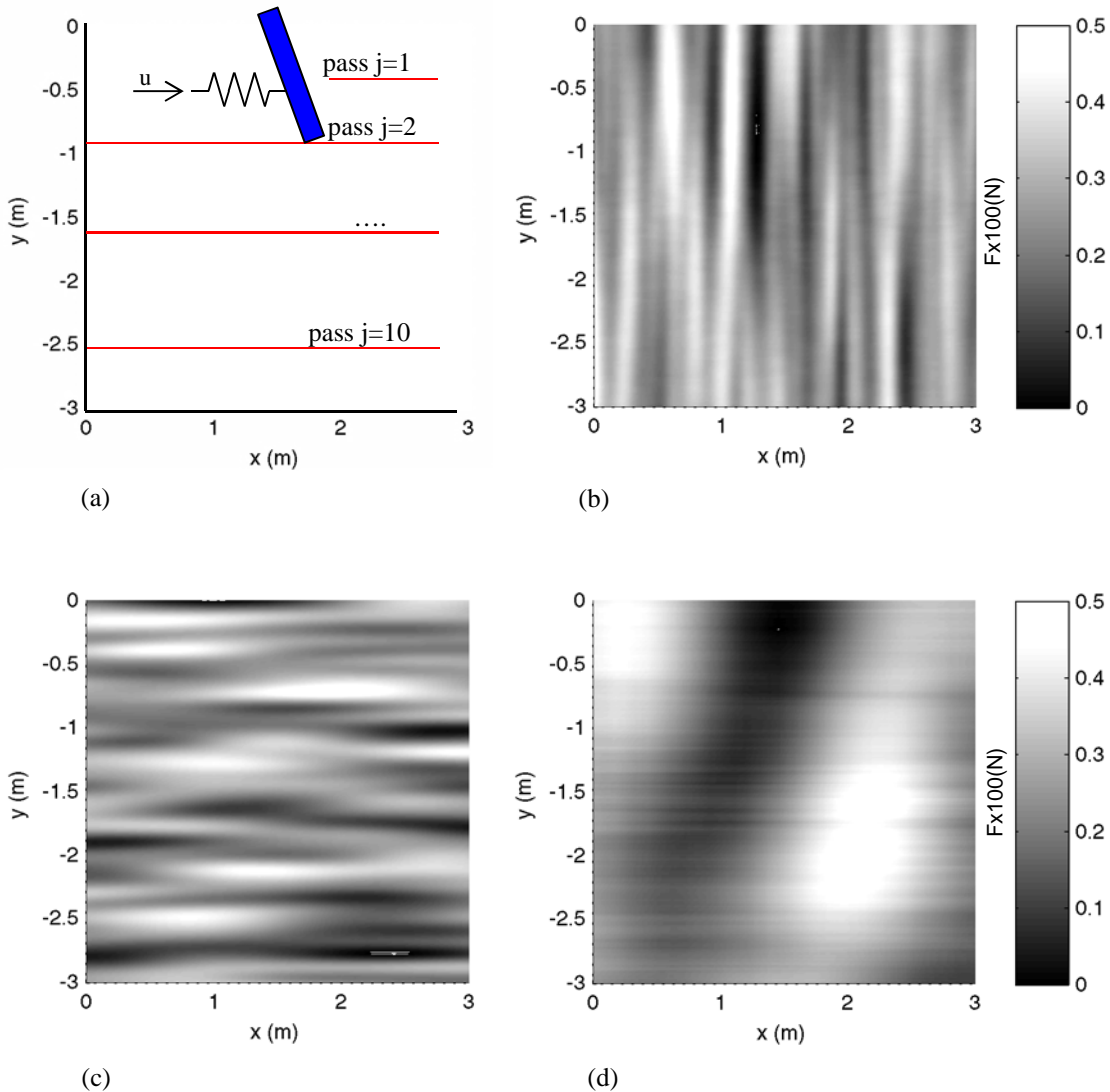


Figure 5.7 – (a) The one dimensional tillage-like scenario used for simulation. (b) An example of high predictability generated with a Gaussian filter with large kernel width in the y direction. (c) An example of high reactability generated with a Gaussian filter with large kernel width in the x direction. (d) An example with large filter kernel widths in both directions generating a field with smooth transitions.

The controllers used in simulation are added with derivative action to emulate the presence of flow control servo-valves in the real excavator. Therefore the controllers are referred to as proportional-derivative (PD), proportional-integral-derivative (PID), proportional-derivative with disturbance observer (PD-DOB), proportional-derivative

with ILC prediction (PD-ILC), and the proposed predictive-reactive controller is designated as PD-DOB-ILC. All controllers are listed and briefly described in Table 5.1. All controllers have an ideal feedforward reference compensation (Assumption 4.1) such that the only trigger for feedback action are forces from the field of disturbances. The actuator compliance shown in Figure 5.7 (a) was used to impose a limit on feedback gains where the spring has a natural frequency of 25 rad/s in series with the tool mass of 50 kg. The basic PD controller has proportional and derivative gains of 2567 and 70 respectively.

Table 5.1 – Controllers evaluated in 1D simulation

Controller	Description
PD	PD feedback controller
PID	PD controller with anti-windup integral action
PD-DOB	PD controller augmented with DOB for direct disturbance estimation
PD-ILC	PD controller with plant inversion ILC
PD-DOB-ILC	The proposed predictive-reactive controller

In the case of the PID controller the integral gain was tuned by increasing its value to achieve a fast response when tracking a step disturbance. The gain was upper bound limited by to the compliance of the actuator. To address the problem of overshoot caused by integrator windup when varying disturbances are present, the same anti-windup method used for excavation experiments and discussed in Section 4.2 was also applied to the 1D system.

Disturbance fields were created by systematically sweeping through the x and y variances of the filter generating a total of 4,112 different field patterns. For each field, each controller was run over 10 iterations so that the ILC had 10 opportunities of learning. When a new field was used, the previous ILC command was reset to zero. The results are summarised in Figure 5.8 where the RMS tracking error in the x direc-

tion is plotted as a function of the reactability and predictability of the disturbance field.

Shown in Figure 5.8 (a), a PD controller with limited gains led to the worst performance, where the error was independent of the reactability and predictability. When the integrator was added—with the conditionally frozen integrator (4.5) as an anti-windup measure—the overall performance improved considerably as shown in plot (b). With the PID controller the lowest tracking errors were obtained when reactability was high, as disturbances were slowly varying. As the PID controller did not use previous information, changes in predictability had no effect in performance.

In plot (c) of Figure 5.8 the PD controller was augmented with the DOB and the trend was the same as the PID controller, where predictability had no effect and high reactability lead to smaller error. The DOB presented lower error than the PID, in part because it did not suffer from the windup effect that often caused overshoot, but also because the DOB generated adaptive compensation, in contrast to the fixed gains of the integral compensator. Improvement in the anti-windup rule and the use of adaptive integral gain could potentially bring both controllers to the same performance level.

Plot (d) of Figure 5.8 shows that the ILC had the opposite behaviour to the PID and DOB compensators. Reactability changes only affected the feedback action provided by the PD controller but not ILC compensation. The tracking was not affected by different kernel widths on the x-axis. On the other hand, the plot shows that performance improved as predictability increased. Figure 5.8 (e) shows that the combined PD-DOB-ILC controller achieved the lowest error amongst all methods across a wide range of reactability and predictability values. The worst performance was, as expected, at the low reactability and low predictability corner, a condition

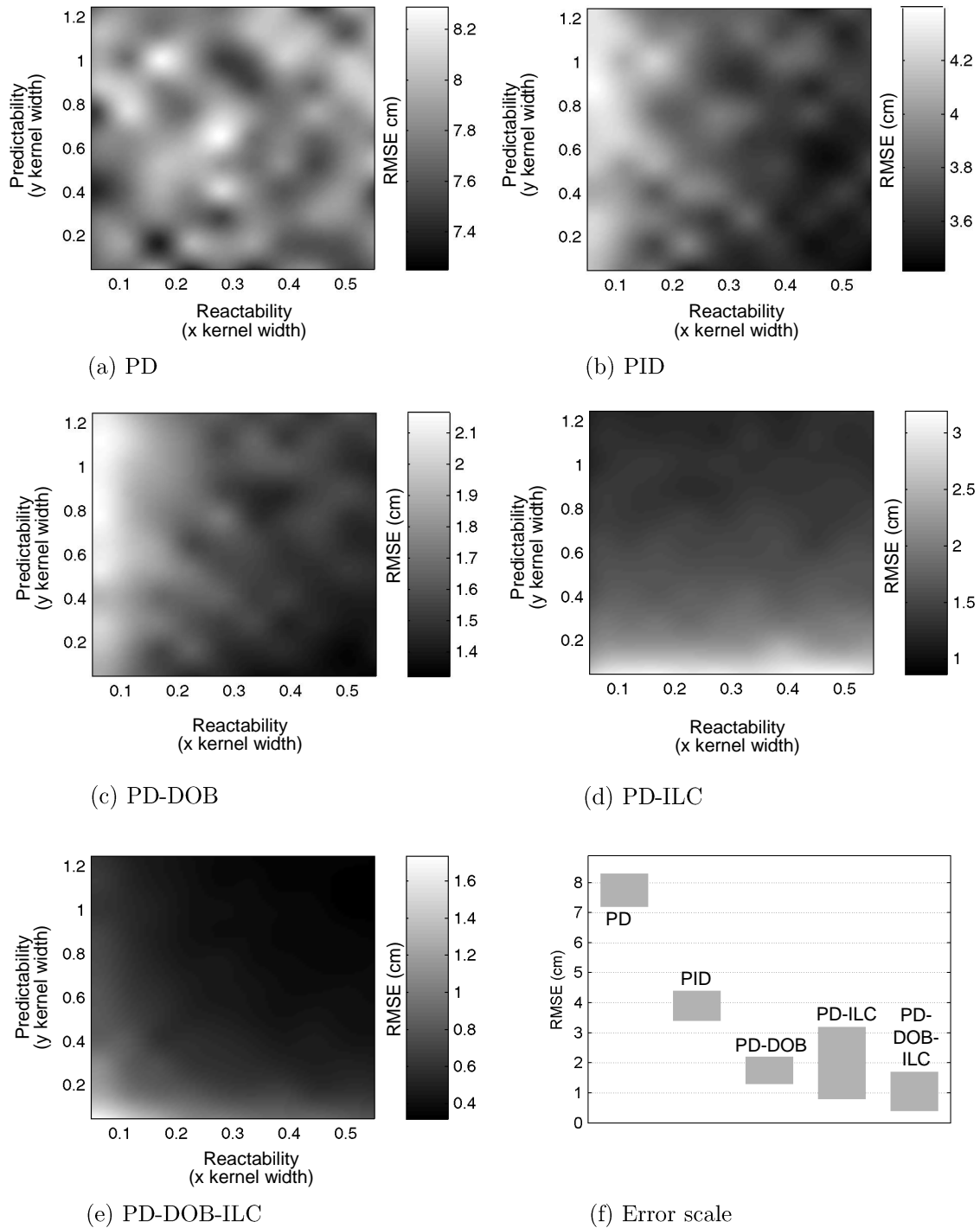


Figure 5.8 – (a-e) Simulated results as a function of different combinations of predictability and reactability. Note that different gray intensity scales have been used in each sub-plot to maximise legibility. **(f)** The range of tracking errors.

where both DOB and ILC performed poorly.

Figure 5.8 (f) shows the range of RMSE tracking of each controller over the whole simulation set. The PD controller tracking error was considerably worse than all of the other methods, with a minimum error of 7.2 cm and maximum error of 8.3 cm. Note that the error range was larger in the PD-ILC case than in the PD-DOB case: the worst case with the PD-ILC was worse than the PD-DOB, while the best case with the PD-ILC was also better than the PD-DOB. This shows that while the controller with DOB does not always outperform ILC, the observer allows more consistent compensation as it is always reactive to the disturbances. In contrast, predictive ILC action can certainly improve performance when the conditions are favourable, but it can also make results worse when predictability is low. Figure 5.8 (f) shows that the advantage of the proposed PD-DOB-ILC combination is that the on-line DOB compensation alleviates the worst-case scenario of the ILC prediction. The worst tracking error of the PD-DOB-ILC controller was close to the worst case of the PD-DOB, representing the condition where predictability is low and therefore the effect of the ILC prediction was negligible. Conversely, when predictability is high the best case of the PD-ILC controller is comparable to the best case with the proposed PD-DOB-ILC controller; feedback action from the PD-DOB is negligible and ILC prediction provides the main source of compensation.

Finally, Table 5.2 qualitatively summarises the controller performances as a function of the observed tracking error. Notice that the proposed PD-DOB-ILC controller is the only method that can profit from high levels of both predictability and reactability. Also, while all controllers have a degraded performance under low predictability or reactability, the proposed controller can still decrease the tracking error in low predictive/reactive conditions as long as the other condition is favourable.

Table 5.2 – 1D simulation results in terms of tracking error.

Method	Predictability		Reactability	
	Low	High	Low	High
PD	\emptyset	\emptyset	\emptyset	\emptyset
PID	\emptyset	\emptyset	–	+
PD-DOB	\emptyset	\emptyset	–	+
PD-ILC	–	+	\emptyset	\emptyset
PD-DOB-ILC	r	+	p	+

Legend:

\emptyset	Inensitive.
+	Positive effect.
r	Depends on the reactability.
p	Depends on the predictability.
–	Negative effect.

5.4 Discussions of the Method

5.4.1 Relation to Other Approaches

A characteristic of the methods used to address the problem of non-repetitive disturbances in ILC, reviewed in Section 2.3.3, is that the great majority focus on the off-line part of the algorithm, essentially changing the way that the update rule works. This was achieved either by identifying and then filtering or segmenting the learning signal (e.g. Mishra et al. (2007)), by avoiding learning the feedback action as in Chin et al. (2004), or by introducing disturbance methods in the iteration domain (Chen and Moore, 2002). Essentially, these are all attempts to decrease the effect of the non-repetitive disturbances during learning, thus leading to better prediction.

Figure 5.9 shows, however, that segmentation is not possible in excavation. In the figure the grey curves on the upper row show the power spectral densities of excavation disturbances, $PSD(d_j)$, at each of the three servo-valve inputs over a set of 40 excava-

tion passes obtained from field trials to be described in Chapter 6. The black curves represent the mean and the dashed curves the standard deviation. DC disturbances contain the most power, which decreases with frequency, reaching a minimum shown as the vertical line at approximately 20 rad/s or 3 Hz. This frequency characteristic should be expected as excavation disturbances are reactive, thus reflecting the arm dynamics which has a bandwidth of approximately 3 Hz. Clearly, the use of ILC is advantageous only if it can be used to compensate the significant low-frequency disturbances. The bottom row shows, however, that the non-repetitive disturbances, plotted as $\text{PSD}(d_j - u_j)$, from the same data are also significant at lower frequencies. Under the segmentation approach (Tzeng et al., 2005; Mishra et al., 2007; Helfrich et al., 2010) the Q -filter would be of high-pass characteristic. This would, however, eliminate the possibility of ILC in learning the low-frequency disturbances that, although erroneous, contain the most significant disturbance components as the plots on the upper row show. The essential problem is that disturbances in excavation are reactive to the motion of the arm, and therefore have a bandwidth that matches the bandwidth of the arm motion. As a consequence both repetitive and non-repetitive disturbances are present in the same low-frequency band, eliminating the possibility of segmentation. The proposed predictive-reactive controller is an alternative to segmented learning for systems where the identification of frequencies is not possible, or is difficult to achieve, as in applications where reactive disturbances are dominant.

Disregarding high-order ILC schemes, since plant inversion estimates the repetitive disturbance in a single iteration (Theorem 5.1) it can be said that, in excavation, the predictive part of the proposed predictive-reactive controller is already performing at the limits of the accuracy achievable by ILC. For this reason, the on-line DOB was introduced to handle the expected inaccuracies of ILC prediction in the time domain. Under this view, the method of Helfrich et al. (2010), discussed in detail in

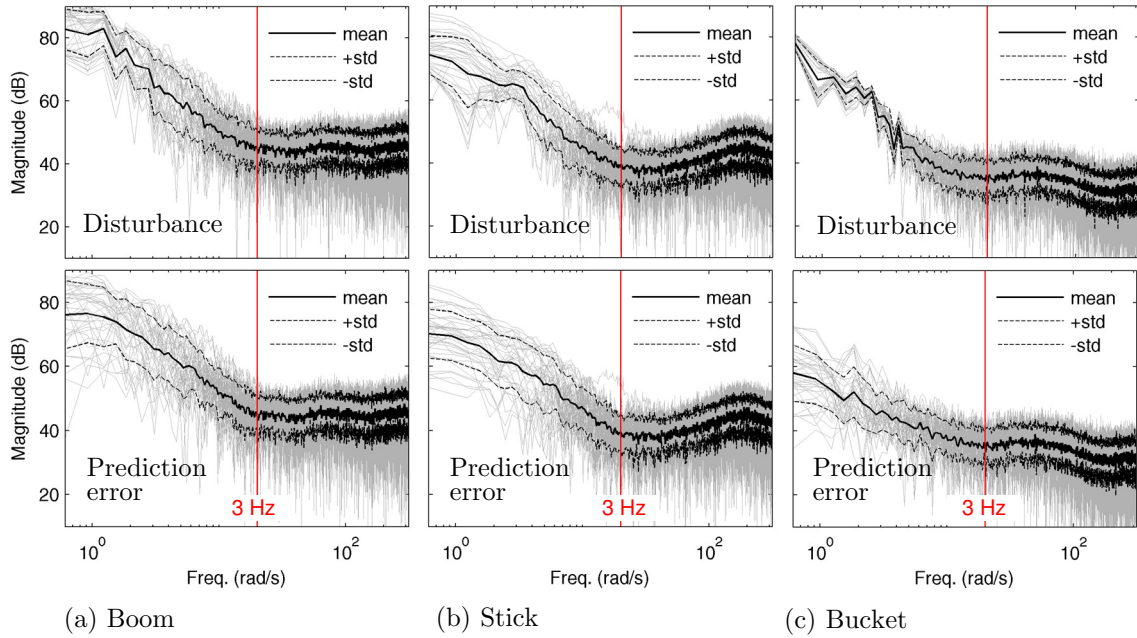


Figure 5.9 – The power spectrum of excavation disturbances over 40 passes is shown by the grey curves in the top row. The bottom row shows the ILC prediction error. The dominant and non-repetitive disturbances are contained in the small bandwidth of the excavator dynamics, showing that segmentation can be difficult to achieve in systems with slow dynamics.

Section 2.3.4, is related to the proposed predictive-reactive controller in regards to the combination of ILC with feedback action. In the work of Helfrich et al. (2010) the design specification of a H_∞ feedback controller was based on the non-repetitive frequencies of the disturbances. This specification was coordinated with the design of a Q -filter for learning the repetitive components of the disturbance. This controller is shown in Figure 5.10 (a) where the arrows indicate components responsible for counteracting disturbances. The coordinated design required the generation of output errors to segment disturbance frequencies. The issue is that to generate output errors a feedback controller must be designed, and its sensitivity influences the segmentation as indicated by Equation (2.44). Dependence on the sensitivity of the previous controller to provide data for segmentation led to the need for an iterative de-

sign approach where the coordinated design process was repeated to simultaneously refine the ILC and feedback controller, until convergence was achieved. The proposed predictive-reactive controller does not require the generation of tracking errors to segment disturbance frequencies as disturbances are estimated by Equation (5.1) during the ILC updates and by the on-line observer during the controller execution as indicated by the arrows in Figure 5.10 (b).

Notice that the observer approach proposed here is parallel to the problem of designing a feedback controller to compensate disturbances as discussed in Chapter 4. The conventional feedback illustrated in Figure 5.10 (c) shows that the block responsible for counteracting disturbances was the compensator C . As was discussed in Section 4.2, the observer was used directly to estimate excavation disturbances instead of compensating them by means of position feedback, which would otherwise require unachievable feedback gain values. The benefit of using the observer, illustrated in Figure 5.10 (d), was to decouple the design of C from the disturbance compensation, in the same way that the observer was useful in decoupling the compensator C from the ILC prediction in Figure 5.10 (b).

5.4.2 A Note on Implementation

Assuming that a feedback controller C is already designed, for example as a conventional proportional controller, the general guidelines for the design of the proposed predictive-reactive controller follows a two-step procedure.

- First, an ILC system is designed using an appropriate learning function to estimate disturbances of the process, which is most probably the plant inversion itself or some variant of plant inversion (Norrlöf, 2004). The controller is executed iteratively, while experimental data are recorded, on the task of interest

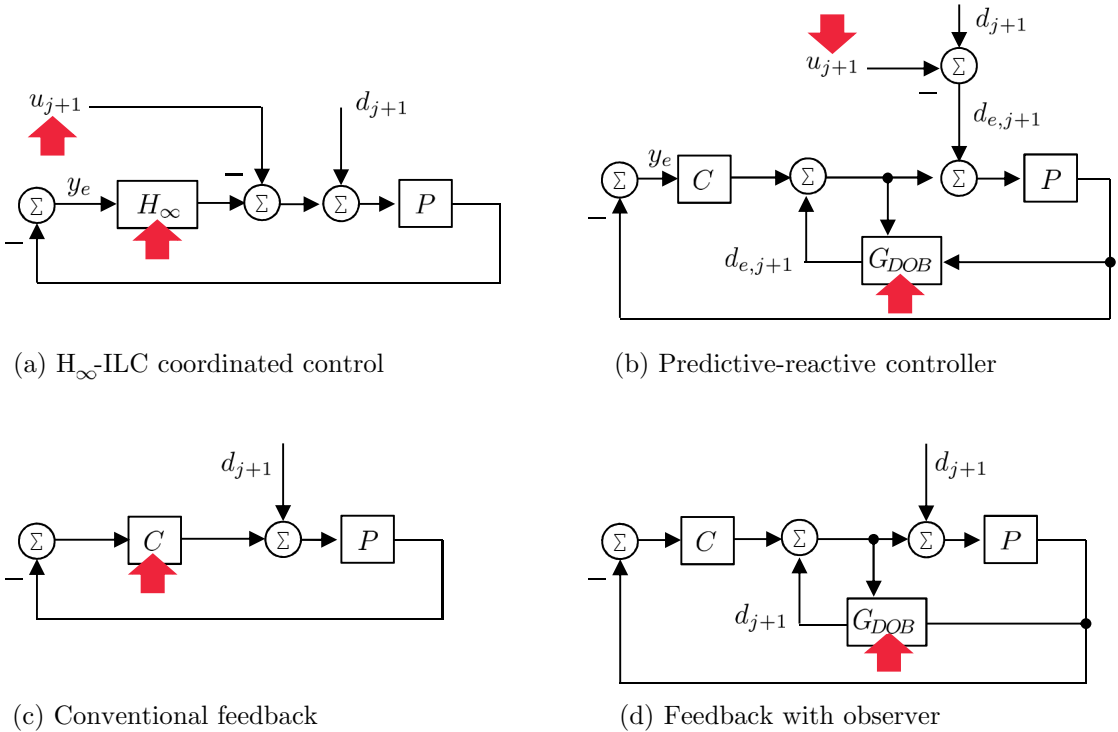


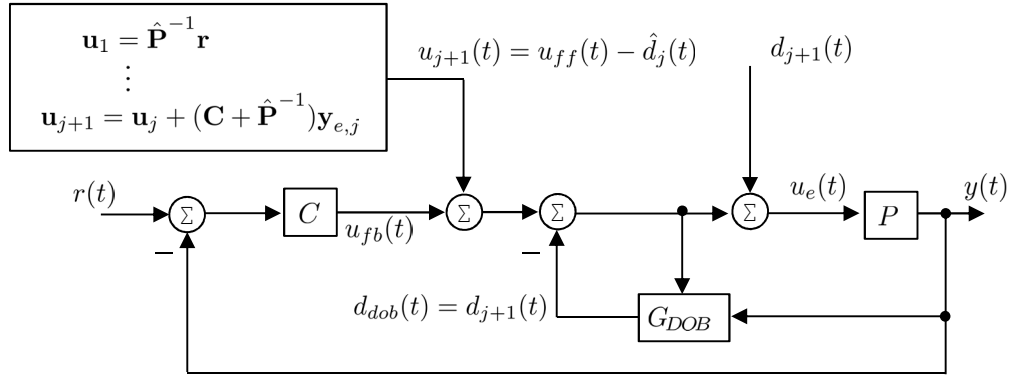
Figure 5.10 – The use of the observer in the reactive and predictive cases. The arrows indicate the blocks responsible for counteracting disturbances.

with the updates given by the selected ILC method and without a disturbance observer. The collected data are used to characterise the error in ILC prediction, for example in the form of power spectrum plots as was shown in Figure 5.9.

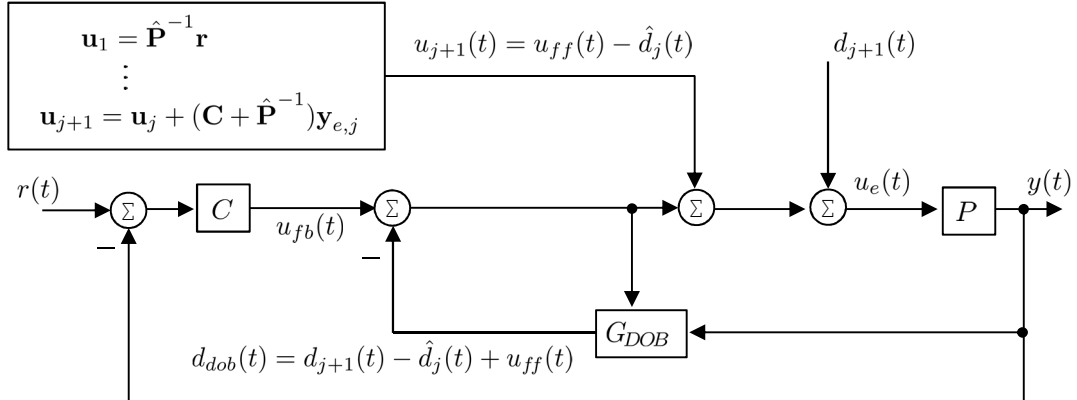
- Second, a DOB-based feedback is designed to compensate for the error in ILC prediction characterised in the previous step. These data are also useful for tuning the Q -filter. In the excavator case, the bottom row of Figure 5.9 shows that the DOB must track low-frequency disturbances, and that a plausible Q -filter is a low-pass filter designed to cut the high-frequency noisy measurements beyond 3 Hz.

Care should be taken in the implementation of the controller regarding the compensation of the exogenous reference input r . As discussed, the use of the observer is possible because the structure of the proposed predictive-reactive controller in Figure 5.2

decouples the feedforward reference compensation u_{ff} from the ILC disturbance update u_{j+1} . As the update rule in Equation (5.1) is based on plant inversion, one could consider simply augmenting the conventional plant inversion ILC structure in Figure 2.17 (a) with a DOB, leading to the two hypothetical controllers in Figure 5.11. Both implementations, however, lead to incorrect compensation. In Figure 5.11 (a)



(a) ILC input before DOB



(b) ILC input after DOB

Figure 5.11 – Examples of hypothetical implementations when a DOB is used to augment an existing ILC controller. (a) DOB signal added after the ILC input. (b) DOB signal added before the ILC input. Both controllers lead to erroneous compensation.

the signal to the plant u_e is given by

$$u_e(t) = u_{fb}(t) + u_{ff}(t) - \hat{d}_j(t) - \hat{d}_{dob}(t) + d_{j+1}(t)$$

where \hat{d}_j is the ILC estimate of the disturbance based on the data from pass j and d_{j+1} is the true disturbance that enters the plant during the next iteration $j + 1$. Considering that all estimates are perfect; that is, $d_{j+1}(t) = \hat{d}_j(t) = \hat{d}_{dob}(t)$, leads to

$$u_e(t) = u_{fb}(t) + u_{ff}(t) - d_{j+1}(t)$$

and the disturbance $d_{j+1}(t)$ is still present at the plant input. The issue is that the ILC update with plant inversion \mathbf{u}_{j+1} contains its own estimate of the disturbance based on the previous pass $\hat{\mathbf{d}}_j$ which overlaps with the on-line DOB compensation.

Adding the ILC input after the DOB as shown in Figure 5.11 (b) also leads to erroneous compensation

$$\begin{aligned} u_e(t) &= u_{fb}(t) - [d_{dob}(t)] + u_{ff}(t) - \hat{d}_j(t) + d_{j+1}(t) \\ &= u_{fb}(t) - [d_{j+1}(t) + u_{ff}(t) - \hat{d}_j(t)] + u_{ff}(t) - \hat{d}_j(t) + d_{j+1}(t), \end{aligned}$$

and considering that all estimates are perfect, $u_e = u_{fb}$, showing that the feedforward reference compensation u_{ff} was compensated as if it was disturbance. In this case the issue is that the observer compensates for any signal between its own input and the plant input. Thus, the ILC must not contain the reference compensation command.

5.5 Conclusion

This chapter proposed a predictive-reactive controller with the goal of using the accurate parts of the predictive action to increase disturbance rejection of a feedback controller. The feedback part of the controller accounts for compensating the prediction errors of the predictive method. Focusing on the simplicity of implementation and general use of the solution this chapter proposed the use of iterative learning control (ILC) for disturbance prediction as a method that does not require explicit modelling of the soil-tool interaction force.

General properties of the controller were investigated. Under certain assumptions, the proposed controller maintains the single iteration convergence of conventional plant-inversion ILC, while minimising the errors in prediction compensation. The controller has the property to improve the prediction accuracy of an ILC controller as well as the disturbance load of a feedback controller. The controller was shown to converge to zero tracking error, although not monotonically. The assumptions were investigated and confirmed to hold with real excavation data.

Simulation in 1D was used to compare all discussed methods with a simple tillage-like case. The results showed that the predictive methods with ILC achieved better performance when predictability was high, although predictive methods also showed the largest variation between the worst and best cases as a result of wrongly predicted preemptive action. The next chapter will evaluate the same controllers in extensive field trials using the experimental platform.

Finally, this chapter discussed the use of the proposed method as an alternative to segmented ILC learning for applications where disturbances are reactive to the applied force. Reactive repetitive and non-repetitive disturbances have a bandwidth that reflects the bandwidth of the arm dynamics making the segmentation technique difficult to apply.

Chapter 6

Field Experiments

This chapter describes and discusses experiments that were done to evaluate the proposed predictive-reactive controller by means of a direct comparison with other control methods discussed in this work. The excavation experiments were done under “real conditions”, meaning that the soil at the experimental site was undisturbed before the experiments and therefore subject to natural compaction and consolidation; the soil was heterogeneous, containing in some places a large number of small rocks. Soil conditions were in accordance with Assumption 3.1 (on page 76) under which the excavation strategy in Section 3.2.1 was proposed.

This chapter quantifies disturbance attenuation provided by ILC during the experiments by using the sensitivity-like function $S_{d,e}$ given in Equation (2.22). Also by means of the sensitivity-like function, this chapter will compare the attenuation provided by the FEE-based empirical model of Cannon and Singh (2000) with the attenuation provided by ILC under the same disturbances. Finally, the proposed predictive-reactive controller will be used to open a 3.6 m long trench as a proof-of-concept demonstration of a controller in autonomous excavation.

6.1 Experimental Procedure and Soil Conditions

Experiments were conducted at a farm near the town of Marulan, New South Wales on sandy clay loam soil. The area used for experiments (shown in Figure 6.1) was selected for having soil with relatively high cohesion and low fraction of sand in relation to other locations in the farm.



Figure 6.1 – Location of field experiments.

Visual inspection of finished cuts showed evidence that the soil was heterogeneous in relation to topsoil/subsoil composition and also in relation to the incidence of rocks. The gradual change in the colour of the wall of a typical cut, shown in Figure 6.2 (a), indicates that the subsoil layer was reached after approximately 40 cm of digging. This verification is important to confirm that the excavator was digging beyond the topsoil which is usually softer. In the experimental area of approximately 40 x 40 m different concentrations of rocks, up to 15 cm in size, were observed at the bottom of the cuts as shown in Figure 6.2 (b).

A soil cone penetrometer (Figure 6.3) was used as a tool to estimate¹ the shear resistance of the soil to penetration. The penetrometer is used by manually pushing a calibrated conical tip into the soil and reading the pressure displayed on the

¹ Characterisation of soil-tool parameters is highly desirable to evaluate the control performance, however even the measurement of simple soil properties like cohesion and friction angle are impractical in the field. Collecting soil for later laboratory analysis does not capture the real excavation condition since it perturbs the soil from the natural compacted state.

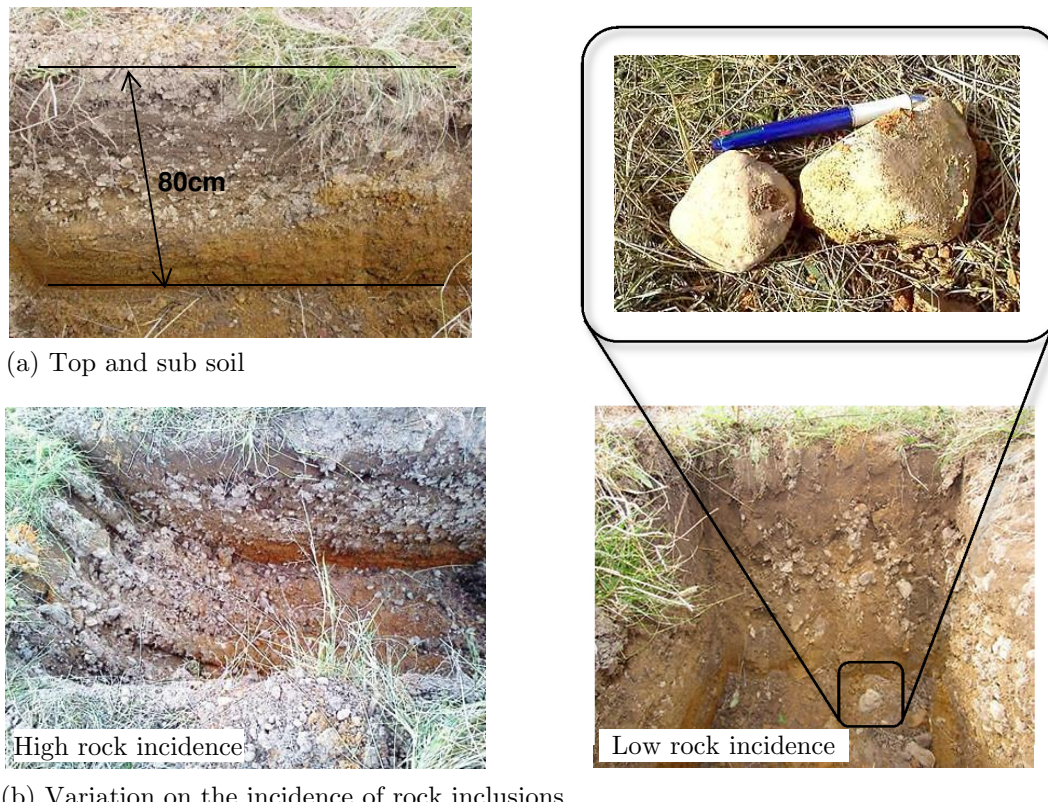


Figure 6.2 – Heterogeneous soil conditions during experiments. (a) The wall of a cut shows changes in soil composition with depth. The topsoil is approximately 40 cm deep. (b) Different areas presented different incidence of rocks.

manometer as a function of the depth of penetration. The plot shows a total of 106 measurements made over the excavated area. Repeated measurements at the same depth but at different locations show the high variability of resistive pressure as an indication of the high dispersion of soil strength. The cross symbols in the figure represent additional measurements that were taken at the bottom of an 80 cm deep cut. The higher resistance to penetration at the bottom surface of the cut is evidence that the subsoil was more difficult to dig than the topsoil.

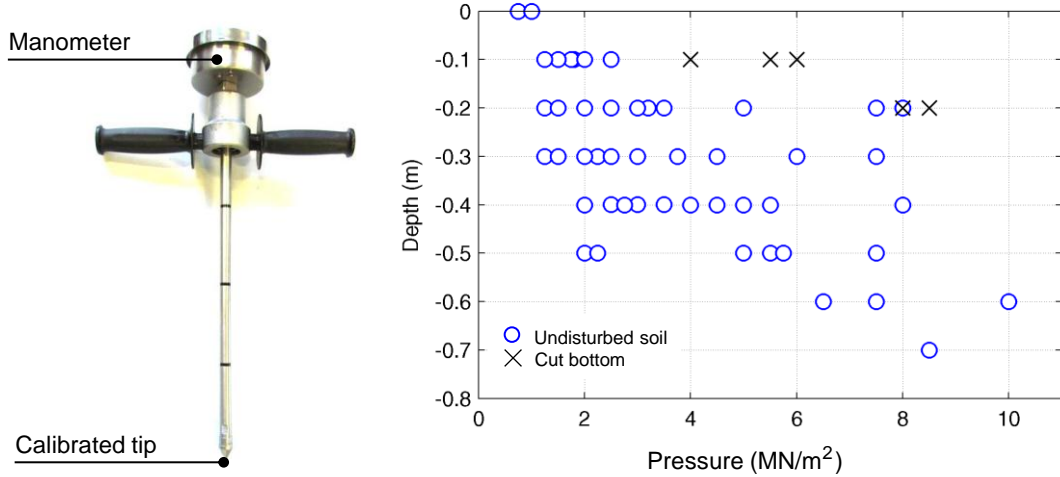


Figure 6.3 – Measurements of the soil shear resistance made using a penetrometer (left). The cross marks are additional measurements taken at the bottom of a cut after the digging was completed, indicating that the soil shear strength increased with the depth, even on the fractured surface.

6.2 Results

The controllers evaluated in field experiments are listed in Table 6.1.

Table 6.1 – Controllers evaluated in field trials

Controller	Description	Structure
Proportional	Proportional feedback controller	Fig. 4.3
PI	Proportional controller with anti-windup integral action	Fig. 4.3
P-DOB	Proportional controller augmented with a disturbance observer	Fig. 4.7
P-ILC	Proportional controller with plant inversion ILC	Fig. 2.17
P-DOB-ILC	The proposed predictive-reactive controller	Fig. 5.2

Apart from the integral gain of the proportional-integral (PI) controller, all controllers were designed and tuned before deployment; parameters were not changed during experiments.

The PI controller required fine-tuning in the field before experiments were conducted. The integral gain was increased by trial-and-error between passes, aiming to achieve small tracking errors during the dragging phase, which is the phase that requires the most aggressive actuation. At the same time the integral gain had to be limited to ensure that overshoot of the bucket during the final lifting phase did not cause excessive soil spillage. The integrator was conditionally frozen as an anti-windup measure using the method described in (Hodel and Hall, 2001) and given in Equation (4.5).

The procedure used to evaluate all control algorithms consisted of iteratively digging a cut 80 cm deep and 1.2 m long designed according to the method described in Section 3.2. As in the previous experiments, only the final trajectory of the desired cut was given to the controller. Successive cuts were made parallel, and were spaced approximately one metre apart in an attempt to place cuts sufficiently close that soil variation was minimal within a set of experiments, yet were spaced widely enough to avoid digging in previously-disturbed soil. This process required translating the excavator using “parallel parking” manoeuvres. Although more time-consuming than simply rotating the boom, the additional manoeuvres ensured that each cut was made with identical excavator poses where the arm, cabin and tracks are aligned.

6.2.1 General Results

The two metrics used to quantify performance are the RMS distance error between the bucket tip and the desired cut and the RMS orientation error of the bucket. Both metrics were defined and discussed in Section 3.3 and are rewritten here for convenience. The RMS distance error $d_{xy,j}(RMS)$ was defined as

$$d_{xy,j}(RMS) = \sqrt{\frac{1}{N} \sum_{t=0}^{N-1} (d_{xy,j}(t))^2}, \quad (3.3 \text{ revisited})$$

where $d_{xy,j}(t) = \sqrt{(x_r(t) - x_j(t))^2 + (y_r(t) - y_j(t))^2}$. This metric represents the tracking error in Cartesian coordinates and also the final precision and finish of the trench. The orientation error of the bucket during a pass is quantified by $\theta_{j,(RMS)}$ as

$$\theta_{j,(RMS)} = \sqrt{\frac{1}{N} \sum_{t=0}^{N-1} (\theta_r(t) - \theta_j(t))^2}, \quad (3.4 \text{ revisited})$$

where $\theta = q_1 + q_2 + q_3$. Recall that the orientation error is an indirect indicator of the efficiency of a pass in shearing soil with the correct bucket angle.

To quantify the relative performance of two controllers, define the relative improvement $RI(A, B)$ as the average improvement of controller A in relation to controller B in terms of the distance error metric $d_{xy,j,(RMS)}$ over a sequence of passes to open identical cuts as

$$RI(A, B) = \frac{1}{M} \sum_{j=2}^M \frac{d_{xy,j,(RMS),B} - d_{xy,j,(RMS),A}}{d_{xy,j,(RMS),A}} \quad (6.1)$$

where M is the last pass. Intuitively this metric indicates, on average, how much closer to the desired cut the controller A was in relation to the controller B .

Figure 6.4 summarizes a total of 245 passes where each of the Proportional, PI, P-DOB, P-ILC, and the P-DOB-ILC controllers dug seven cuts at different locations covering the approximate 40 x 40 m experimental area. Figure 6.4 (a) shows the $d_{xy,j,(RMS)}$ metric. During the first pass the Proportional and P-ILC controllers showed approximately the same tracking error as the ILC input was zero during the first pass. For the same reason, the P-DOB showed the same error as the P-DOB-ILC during the first pass. At the last pass, the Proportional, PI, P-ILC, P-DOB, and P-DOB-ILC controllers achieved a final average tracking error $d_{xy,j,(RMS)}$ of 11, 3, 2,

4 and 1 cm respectively.

The Proportional controller showed the largest tracking error, with unacceptably low convergence for practical excavation purposes. The PI controller produced the most aggressive initial passes, however convergence was low after the fourth pass and the PI controller performance then became worse than all other methods except the Proportional controller. The P-ILC controller achieved faster convergence when compared to the P-DOB controller due to the preemptive disturbance compensation. The proposed predictive-reactive P-DOB-ILC controller achieved the fastest convergence.

Figure 6.4 (b) shows the orientation error of the bucket as measured by $\theta_{j,(RMS)}$. The predictive-reactive P-DOB-ILC controller clearly outperformed all other controllers. Curiously, the Proportional controller showed an increase in the $\theta_{j,(RMS)}$ error during intermediate passes. This is an indication that, although the bucket tip was getting closer to the desired cut (indicated in Figure 6.4 (a)), the resistive excavation forces also increased, possibly due to the transition from soft topsoil to rocky subsoil, generating a larger resistive moment at the bucket tip and worsening the orientation tracking performance during intermediate passes.

Considering a realistic use of the proposed methods, some applications such as in mining or mass excavation may require a faster cycle rather than a precise cut. In this case, the most important characteristic is the ability of the controller to maintain a high convergence rate towards the rough cut. Referring back to Figure 4.13 (a) and (b), note that during the seventh pass a 10 cm RMS distance error lead to coarse tracking, where most soil from the cut was removed despite poor tracking of the reference trajectory. In Figure 6.4 (a) a rough cut is therefore represented by the 10 cm line as an example. On average, the methods augmented with ILC prediction—P-ILC and P-DOB-ILC—achieved the 10 cm mark during the fourth pass. The

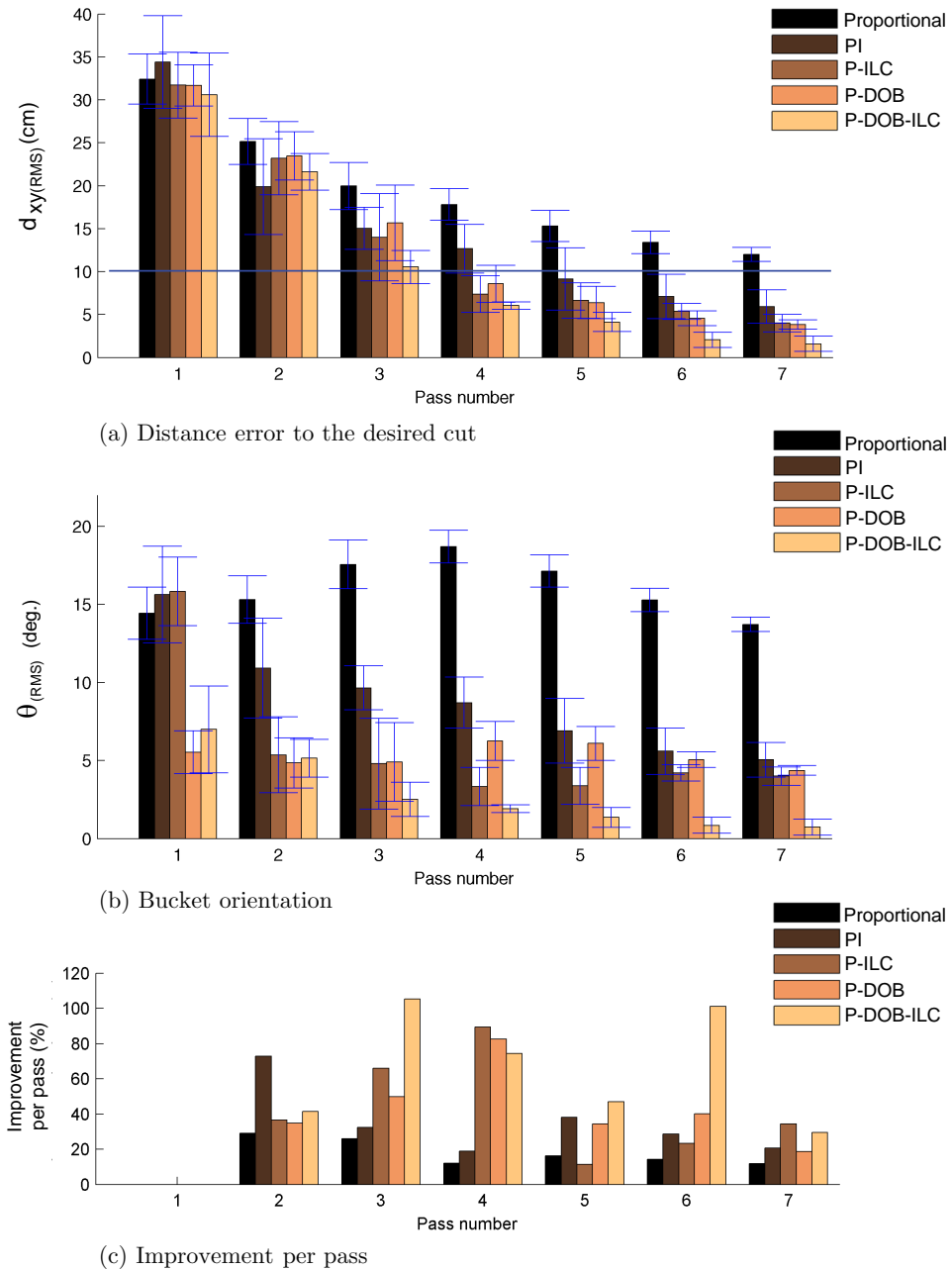


Figure 6.4 – Comparison of the performance of the Proportional, PI, P-DOB, P-ILC, and P-DOB-ILC controllers in terms of the distance error and orientation error metrics. (a) The $d_{xy,j}(RMS)$ metric is the RMS distance error over the cut. (b) The $\theta_{(RMS)}$ metric is the RMS orientation error of the tool angle (bucket). (c) Improvement of the $d_{xy,j}(RMS)$ metric in relation to the previous pass. In all metrics the predictive-reactive P-DOB-ILC controller outperformed all other controllers.

P-DOB controller took one extra pass, the PI controller took two extra passes, and the Proportional controller did not achieve a rough cut by the end of the seventh pass. As expected, predictive methods tend to achieve higher convergence rates due to the preemptive disturbance compensation. In applications such as in mining aggressive performance is reflected as less passes per cut, potentially improving the production cycle and operation profitability.

Figure 6.4 (c) shows the decrease of the $d_{xy,j}(RMS)$ metric in relation to the previous pass as an indicator of the controller improvement per pass. In this metric only the proposed predictive-reactive P-DOB-ILC controller could generate an improvement of more than 40% during six of seven passes. Note that although the PI controller made a second-pass improvement of nearly 80% over the first pass, the controller could not maintain this ratio for the remaining passes.

Taking the proposed predictive-reactive controller commands as an example, Figure 6.5 shows the actuation commands to each link during the seven passes required to open a cut. The free motion commands (circle marks) are shown to emphasise the additional commands that were required to overcome disturbances. The boom actuator required the most additional drive and showed periods of full flow saturation up to the fourth pass. The stick actuator was partially flow-saturated up to the third pass and the bucket required the least additional drive. Although the boom has very limited motion during an excavation pass, it is typically the only link positioned to exert downward force and so defines the amount of penetration that the arm can achieve during the pass. Saturation of the boom actuator during the penetration phase causes bucket depth deviation from the desired trajectory which compromises the depth achievable during the remainder of the cut.

Figure 6.6 shows examples of cuts made with the P-DOB, P-ILC, and P-DOB-ILC

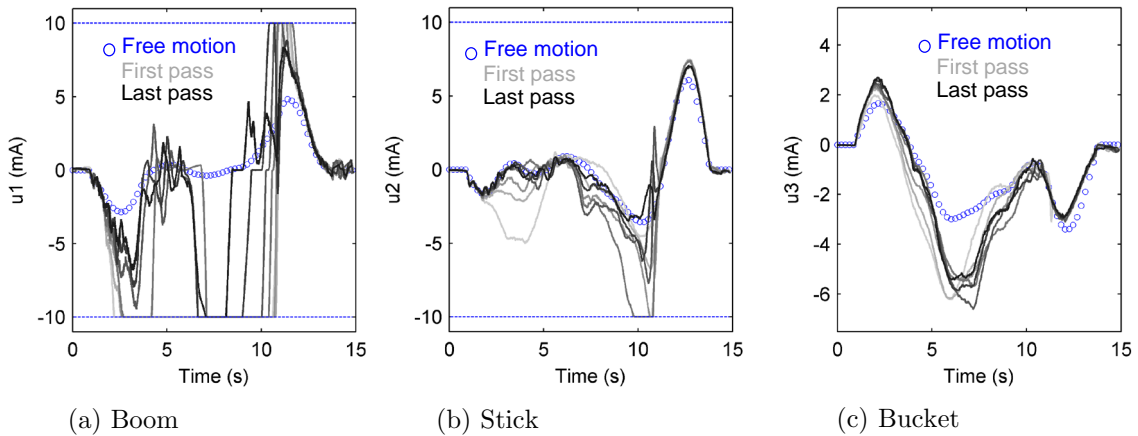


Figure 6.5 – Servo-valve commands of each cylinder link when using the P-DOB-ILC controller for iteratively cutting the desired profile. The first pass is shown in light grey. The passes were repeated seven times, with the last pass shown in black. The undisturbed free motion command is shown as the circle marks and gives an idea of the additional command drive required due to the disturbances.

controllers as plots of the Cartesian coordinates of the bucket tip. Note that a natural consequence of flow saturation in the actuators is that shallow cuts are generated. A sequence of shallow cuts resemble the “slicing” passes (Figure 2.6) observed by Bradley et al. (1989). This result supports the hypotheses that saturation provides a natural motion adaptation to resistive soil forces for a mini-excavator, and that repeated attempts to track the same reference lead to a sequence of slicing passes.

6.2.2 Predictive and Reactive Compensation

The introduction of either the DOB estimates or the predictive ILC action significantly improved the performance of the Proportional controller. As discussed in Chapter 5, however, ILC action is prone to inaccurate prediction, resulting in effects such as those which can be observed qualitatively in Figure 6.6 (b) where the bucket tip overshot the desired trajectory during several passes when using the P-ILC controller. The tendency of the P-ILC controller to overshoot may have practical con-

sequences, for example if digging close to infrastructure. Visually it is clear that the P-DOB controller shown in Figure 6.6 (a) digs with less overshoot as compensation is purely reactive. The disadvantage of the P-DOB is that convergence and tracking error in Figure 6.4 was worse due to the typical phase lag of reactive controllers. In Figure 6.6 (c) the observer was used to attenuate prediction errors from ILC and the improvement is reflected in trajectories that showed less overshoot. From this result it is concluded that when careful cut execution is important and overshoot must be avoided, for example when digging close to underground structures, the use of a pure reactive P-DOB controller is preferable. As the precision of the excavation task becomes less important a controller with ILC is preferable as it achieves faster convergence. Note that a future work could address the modification of ILC-based controllers with the addition of simple rules to monitor and counteract overshoot by measuring distance between the position of the bucket in relation to the path. This extension would improve the overshoot issue while maintaining the fast ILC convergence.

In Figure 6.7 the tracking distance error $d_{xy,j}(RMS)$ of Equation (3.3) is separated into two sub-plots according to the control method:

- The Proportional and the P-ILC controllers; and
- The P-DOB and the predictive-reactive P-DOB-ILC controllers.

The sub-plots show the improvement provided by predictive action when using the same feedback controller. The results are shown from the second pass, since the first pass has no preview. The improvement provided by ILC is most notable in Figure 6.7 (a). Using the relative improvement metric defined in Equation (6.1), the average distance error improvement of P-ILC compared to the Proportional controller was 45%, indicating that the P-ILC controller was, on average, 45% closer to the

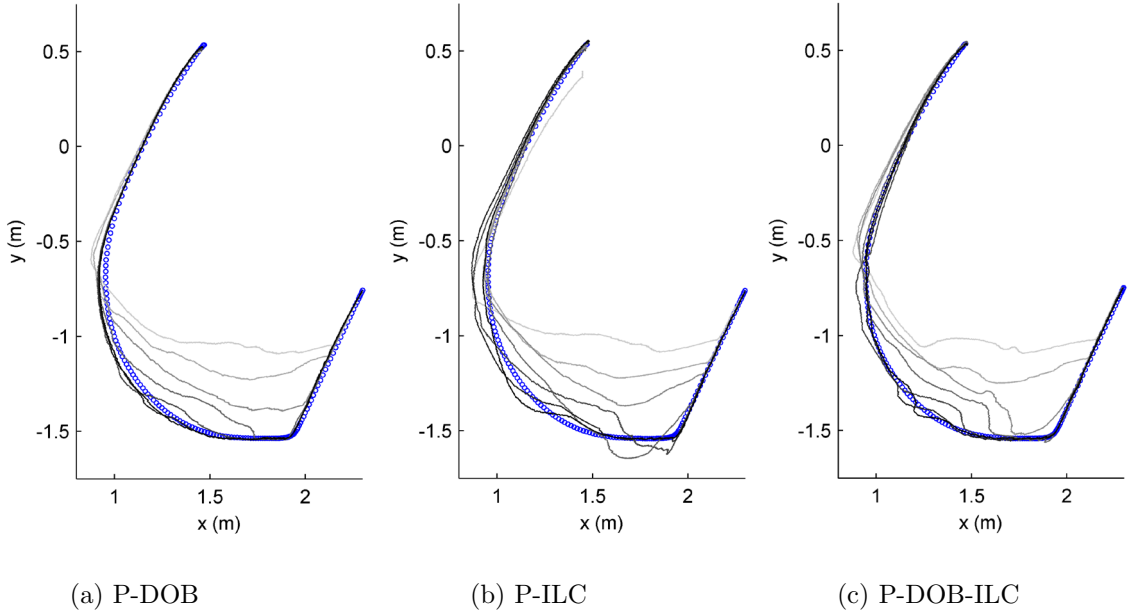


Figure 6.6 – Motion of the bucket tip with the P-DOB, P-ILC, and P-DOB-ILC controllers. (a) The reactive P-DOB showed the best contouring of the final profile, without overshooting the trajectory. (b) The erroneous ILC compensation tended to overshoot the trajectory. (c) The use of the DOB combined with ILC seemed effective in using the aggressiveness of prediction while attenuating the overshooting.

desired cut in relation to the Proportional controller over a sequence of passes to open similar cuts. The improvement of the P-DOB-ILC in relation to the P-DOB was 29%. These results experimentally support the use of prediction, suggested in Section 4.3, to improve disturbance rejection beyond the feedback limitations of the Proportional and the P-DOB controllers.

Figure 6.8 compares the improvement provided by the on-line DOB in terms of the tracking distance error $d_{xy,j}(RMS)$. Using the relative improvement metric defined in Equation (6.1), the average distance error improvement of the P-DOB-ILC controller compared to the P-DOB controller was 25%. This result shows that the DOB was effective in compensating for the erroneous predictions of ILC.

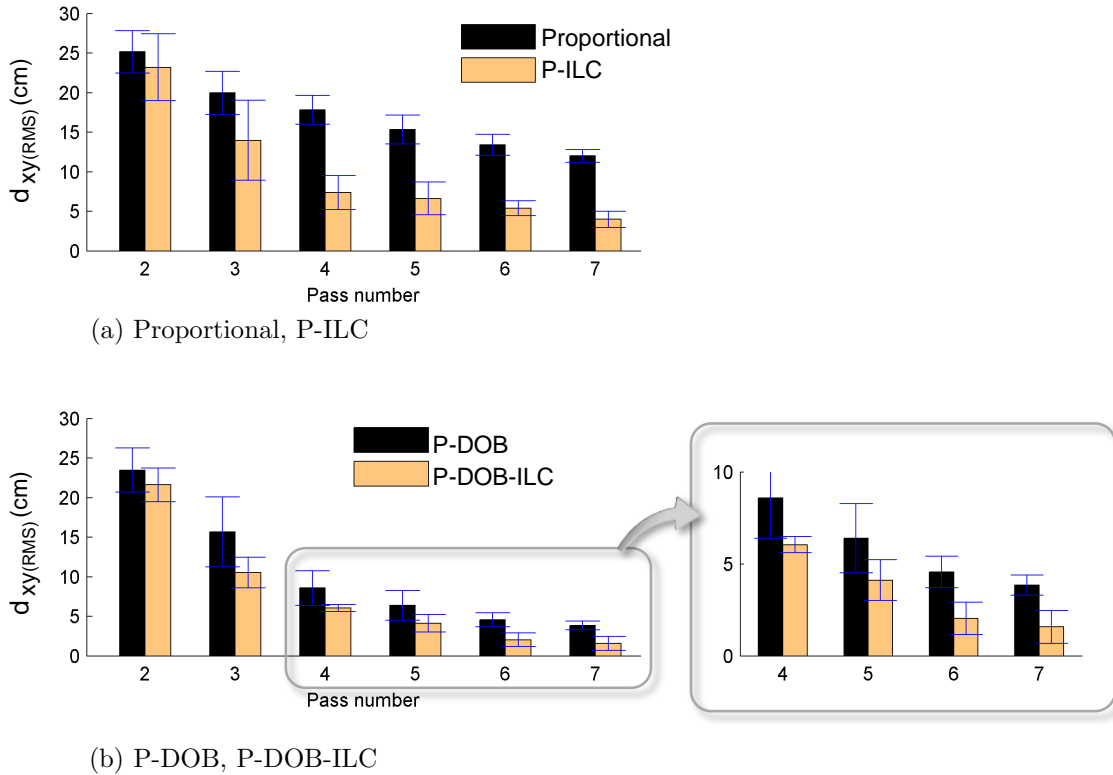


Figure 6.7 – A comparison between the experimental performance of controllers with and without preview. (a) The Proportional controller compared with its predictive version with ILC. (b) The P-DOB controller compared with its predictive version with ILC. Despite inaccuracies in prediction, performance of a manipulator in excavation can be improved with the use of predictive action.

6.2.3 Sensitivity-Like Function in Experiments

As suggested in Section 4.3, in this work ILC is regarded as a source of side information that adds disturbance previews to the basic Proportional feedback controller via feedforward input. This interpretation provides metrics that quantify the effect of inaccurate prediction on the sensitivity function of the excavator controller. The metric used in the following is the “sensitivity-like” function (Martins et al., 2007), which is the sensitivity of a system containing both feedback and feedforward preview

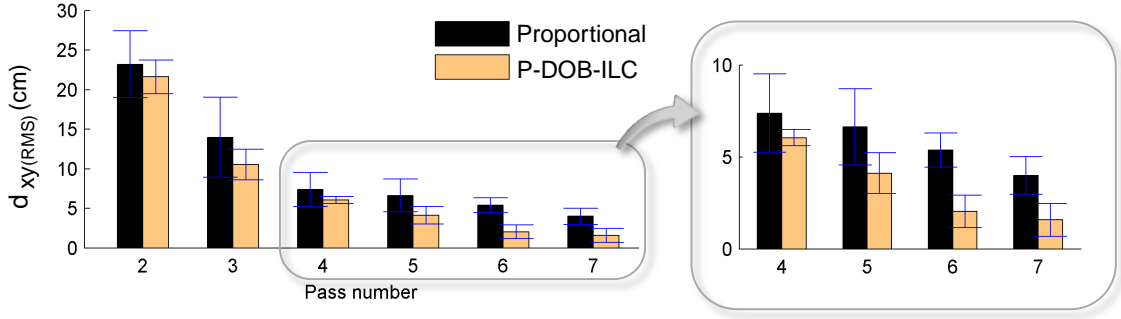


Figure 6.8 – The effect of the DOB in decreasing prediction error is reflected in lower tracking error.

parts

$$S_{\mathbf{d}, \mathbf{e}} = \sqrt{\hat{F}_{\mathbf{e}}(\omega)/\hat{F}_{\mathbf{d}}(\omega)}. \quad (2.22 \text{ revisited})$$

The degree of inaccuracy that ILC shows in excavation can be visualised by plotting $S_{\mathbf{d}, \mathbf{e}}$. The same plot also functions as a layer of abstraction whereby different predictive methods in excavation can be compared in relation to their ability to providing sensitivity attenuation. Here, the FEE-based empirical model of Cannon and Singh (2000) is compared with ILC.

Figure 6.9 shows the disturbance attenuation provided by ILC in the form of the sensitivity-like function obtained from a set of 84 passes. Each pass is represented by a grey curve obtained with Equation (2.22) where $\hat{F}_{\mathbf{d}}(\omega)$ was calculated from experimental data with Equation (5.1). To calculate the value of $\hat{F}_{\mathbf{e}}(\omega)$, refer back to Figure 4.15 (b) and note that the total plant input \mathbf{e} is obtained by adding the experimental feedback input \mathbf{u}_{fb} and predictive ILC commands $\mathbf{u}_j = \hat{\mathbf{d}}$ to the estimated disturbance \mathbf{d} .

The solid black line in Figure 6.9 is the mean of the sensitivities over all 84 passes. The

dashed black lines show plus and minus one standard deviation. The figure also shows the sensitivity of the Proportional controller, labelled as S . The fact that, on average, the sensitivity-like function of the controller with the predictive ILC was lower than the sensitivity transfer function of the pure feedback proportional controller indicates that ILC prediction was effective in improving disturbance rejection at each joint controller of the arm. This hypothesis was supported by the improvement in tracking in Figures 6.7. Here, it is also demonstrated in the form of sensitivity attenuation.

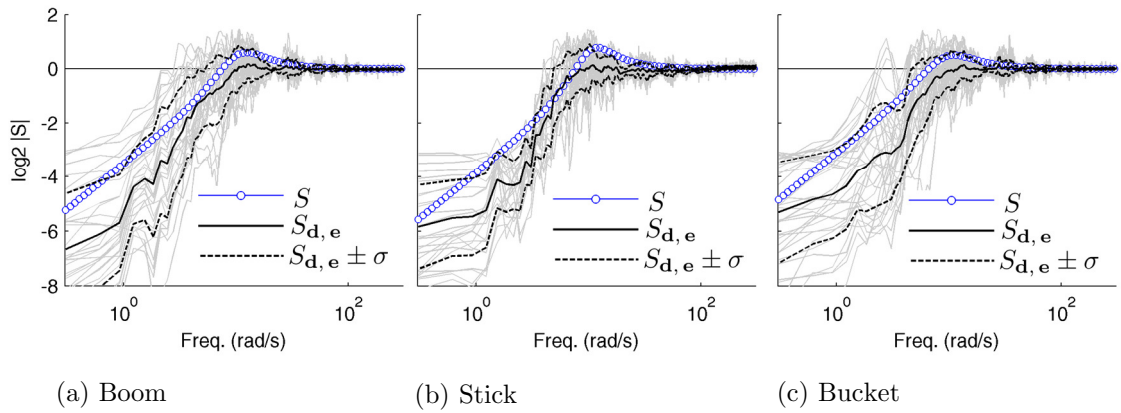


Figure 6.9 – Sensitivity attenuation achieved experimentally with the ILC feedforward action as a disturbance preview. (a) Boom sensitivity attenuation. (b) Stick sensitivity attenuation. (c) Bucket sensitivity attenuation.

Similar to the example in Section 2.2.3 using a noisy channel, a comparison between the sensitivity reduction and the maximum achievable reduction quantified by the channel capacity is useful to evaluate the loss of disturbance preview during the execution of the controller. To compute the channel capacity note that, according to the interpretation presented in Section 4.3, the remote preview system (RPS) is given by the ILC. As such, the interpretation of the noise channel \mathbf{c} is the ILC prediction error $\hat{\mathbf{d}} = \mathbf{d} + \mathbf{c}$. Thus, the power spectral density ratios between the disturbance input \mathbf{d} and the “noise” ($\mathbf{c} = \hat{\mathbf{d}} - \mathbf{d}$) provides the effective signal-to-noise ratio (SNR) of the communication channel. Figure 6.10 shows that the noise is coloured, so that

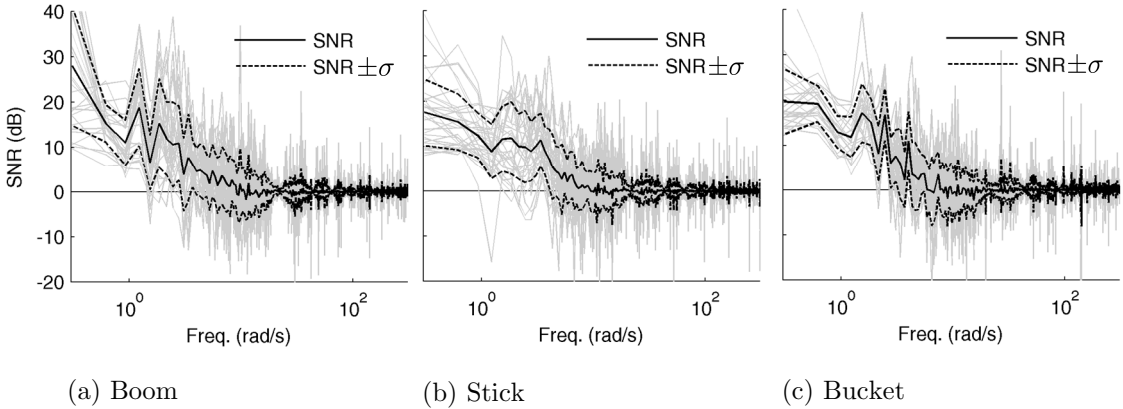


Figure 6.10 – Signal-to-noise ratios of the ILC regarded as a remote preview system in excavation. The noise of the “ILC channel” which quantifies prediction error is coloured.

the capacity of the continuous channel can be computed by integrating the SNR over the spectrum (Cover and Thomas, 2006) as

$$C_{cont} = \int \frac{1}{2} \log_2 \left(1 + \frac{PSD(\mathbf{d})}{PSD(\hat{\mathbf{d}} - \mathbf{d})} \right) df \quad [\text{bits/second}]. \quad (6.2)$$

Assuming that each sampling of the controller transmits one complete message, the average capacity per message is $C_p = C_{cont}/F_s$ where F_s is the controller sampling frequency.

Recall from Equation (2.23) that for an open-loop stable plant the attenuation of the sensitivity is bounded by the channel capacity as

$$\int_{-\pi}^{\pi} \log |S_{\mathbf{d}, \mathbf{e}}(\omega)| d\omega \geq -2\pi C_p. \quad (6.3)$$

Empirical evaluation of Equation (6.3) using experimental data is summarised in Table 6.2. The column labelled *Attenuation* represents the left side of Equation (6.3) and was computed empirically by integrating the actual sensitivity reduction previously shown in Figure 6.9. The column *Lower bound* represents the right side of

Equation (6.3), and was computed using Equation (6.2).

Table 6.2 – Experimental ILC sensitivity attenuations in bits/message

	<i>Attenuation</i>	<i>Lower bound</i>
Boom	−0.48	−0.54
Stick	−0.37	−0.34
Bucket	−0.35	−0.45

Note that while *Attenuation* is the decrease in the sensitivity function achieved by the controller in the presence of ILC preview, *Lower bound* quantifies the channel capacity; that is, the maximum amount of information that can be transmitted in the presence of noise. In the ideal case a controller that is fully effective in using the predicted disturbance would achieve an attenuation that is equal to the lower bound. For the boom and the bucket the attenuation achieved corresponds to 89% and 79% of the theoretical bound indicating that the real system contained losses. Sources of loss may include components of the feedforward signal whose bandwidth are beyond the actuator reproducibility and noise in measurement and servo-valve commands. In the case of the stick axis, the fact that the attenuation is larger than the theoretical bound may be attributed to the large variance of the results.

Prediction with the FEE-Based Empirical Model

Here a possible implementation of a soil-tool interaction force model is considered as an alternative to ILC in excavation. The FEE-based empirical model presented in Cannon and Singh (2000) is chosen as it has a reduced number of parameters in comparison with other soil-mechanics models. As discussed in Section 2.1.3 the empirical model of Cannon and Singh has the form

$$F = \Psi_1 \Gamma_1 + \Psi_2 \Gamma_2 + \dots, \quad (2.3 \text{ revisited})$$

where the form of the basis function $\Gamma = (d^2, \cos(\rho), \alpha, V_s)$ was motivated by the fundamental equation of earthmoving (FEE). The method uses measured data from a bucket force sensor, together with measured or estimated values of the four basis parameters, to fit least-squares values of Ψ_i over a window of past data.

To compare the attenuation of disturbances provided by the FEE-based empirical model with the attenuation provided by ILC the “sensitivity-like” function in Equation (2.22) was used. Recall that the sensitivity-like function is a ratio of the PSDs of the disturbance \mathbf{d} and the plant input signal \mathbf{e} . The disturbance \mathbf{d} can be estimated from Equation (5.1) using experimental data. Note, however, that to obtain the plant input $\mathbf{e} = \mathbf{u}_{fb} + \mathbf{d}$ requires the controller feedback signal \mathbf{u}_{fb} . As the model was implemented off-line, the response of the feedback controller was obtained by simulation using the first-order model of the servo-valve controlled joint dynamics, Equation (3.1), where the parameter values of the Proportional controller were set to those used for the experimental controller. To provide a fair basis for comparison, this first-order simulator and the same disturbances were also used with the ILC controller to obtain the feedback response \mathbf{u}_{fb} due to prediction error from which the sensitivity-like function was computed.

In the case of the empirical model, the values of F in Equation (2.3) were obtained as forces at the bucket tip, which were estimated during experiments from forces measured at the load pins (see Appendix A). Both observed and predicted disturbances were projected as disturbances at the joint controllers by using the Jacobian of the arm $F = J^{-1}\tau$ so that a direct comparison with ILC was possible.

Figures 6.11 shows several sensitivity curves for the boom, stick, and bucket. In each plot, the sensitivity of the pure feedback controller is indicated as \mathbf{S} . The sensitivity-like function of the simulated controller with ILC is indicated as $\mathbf{Sde_ILC}$. The remain-

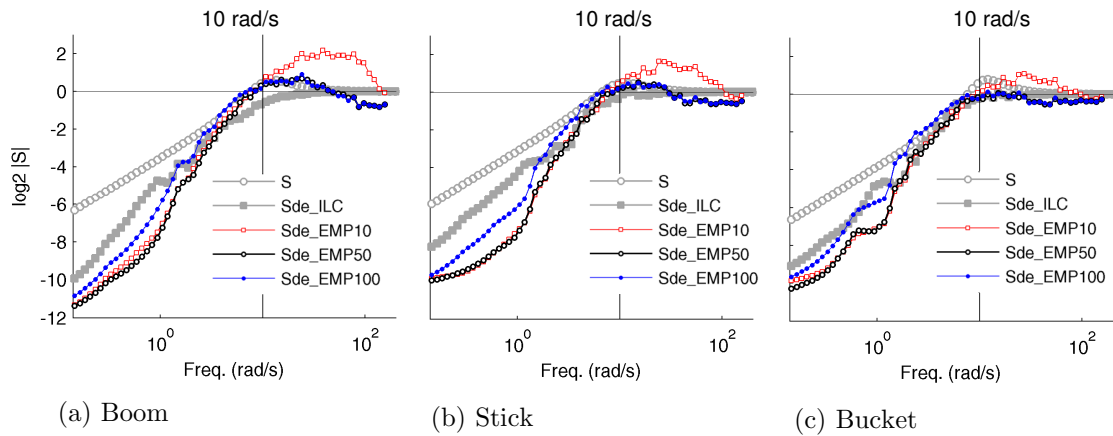


Figure 6.11 – Disturbance attenuation provided by the empirical model proposed of Cannon and Singh (2000). The empirical method achieves more disturbance attenuation than the ILC, however it depends on the proper choice of the size of the window containing past data points for regression and requires direct force sensing.

ing curves show the sensitivity-like function of the empirical model for window size values of 10, 50, and 100 points labelled as **Sde_EMP10**, **Sde_EMP50**, and **Sde_EMP100**, respectively. The number of points refers to the amount of past data that was used in the FEE-based empirical model for least-squares regression on the measured data.

The plots show that a small window size of 10 points achieves good attenuation at lower frequencies, and prediction deteriorates above approximately 10 rad/s. In fact, for frequencies above 10 rad/s the sensitivity of the controller with preview is worse than that of the feedback controller alone. This is a powerful result of the side information in the excavation context: it indicates the frequencies and magnitudes where the possible use of the preview provided by the FEE-based empirical model is, in fact, detrimental to performance due to erroneous prediction. In practice, this result suggests that better disturbance rejection (at least at higher frequencies) can be obtained by simply not using prediction at all.

Changing the amount of past data for regression impacts the sensitivity. A larger

window size of 100 points leads to better attenuation at higher frequencies but the attenuation deteriorates in the low frequency range. A window size of 50 points seems to achieve the best overall attenuation.

Table 6.3 quantifies and compares the attenuation provided by ILC with the best attenuation provided by the FEE-based empirical model which occurs for the model **Sde_EMP50**. The values of the sensitivity are computed by integrating the curves in Figure 6.11. For the ILC and empirical model the sensitivities are computed as $\int_{-\pi}^{\pi} \log |\text{Sde}_\text{ILC}(\omega)| d\omega$ and $\int_{-\pi}^{\pi} \log |\text{Sde}_\text{EMP50}(\omega)| d\omega$, respectively.

Table 6.3 – Attenuation of sensitivity function using the FEE-based empirical model and ILC.

Sensitivity integral in bits/message		
	Sde_EMP50	Sde_ILC
Boom	-0.635	-0.538
Stick	-0.652	-0.404
Bucket	-0.836	-0.436

The tabulated results suggest that, with an appropriate choice of the window size, the empirical model can provide more disturbance rejection than ILC. This result should be expected since models with structure, such as the FEE-based empirical model, contain more information and make direct use of disturbance measurements. The main disadvantage of the empirical model is, perhaps, the need of force sensors, whose calibration and maintenance can be impractical for large machines like mining excavators. An inner force loop for force control must also be designed. Other issues are the size of the window, which is a parameter that may require re-tuning according to changes in excavation conditions. ILC does not require force sensing and extra control loops as the disturbances are estimated at the plant input. The result shows

that the use of ILC involves a trade-off between simplicity of the implementation and achievable sensitivity attenuation. Both methods have equivalent and low computational cost: ILC is computed between iterations, and the empirical model is solved with simple least-square regression.

6.2.4 Trenching

Experiments in this work focused on the opening of a single cut where the position of the excavator was fixed and only the arm moved. There are three reasons for choosing the single cut experiment. First, single cut opening is central to excavation. Even during the opening of long trenches the tracks are not designed to move when dragging or shearing soil with the arm (Komatsu, 1991); single cuts are supposed to be concatenated to achieve larger holes. Second, by ensuring that a controller can reliably open a single cut the extension to the process of opening a long trench, which is perhaps the most typical excavation operation, follows naturally. Third, the choice allowed for the design of a straightforward experimental procedure for the comparison of different control methods.

Figure 6.12 (a) shows a proof-of-concept experiment where the proposed predictive-reactive controller was used for trenching. The trenches were 3.6 m in length and 80 cm deep and the finish quality defined by the RMS distance error was set as 5 cm. The appearance of a trench is shown as a photograph in Figure 6.12 (b). The experiment consisted of digging a cut iteratively, in the same way as the previous experiments, until the first cut achieved the desired RMS value. Then the excavator trammed backwards 90 cm, which was enough to re-start a cut overlapping with the flat bottom of the previous cut. The feedforward disturbance compensation of the ILC was reset to zero after each tramping. This procedure was repeated three

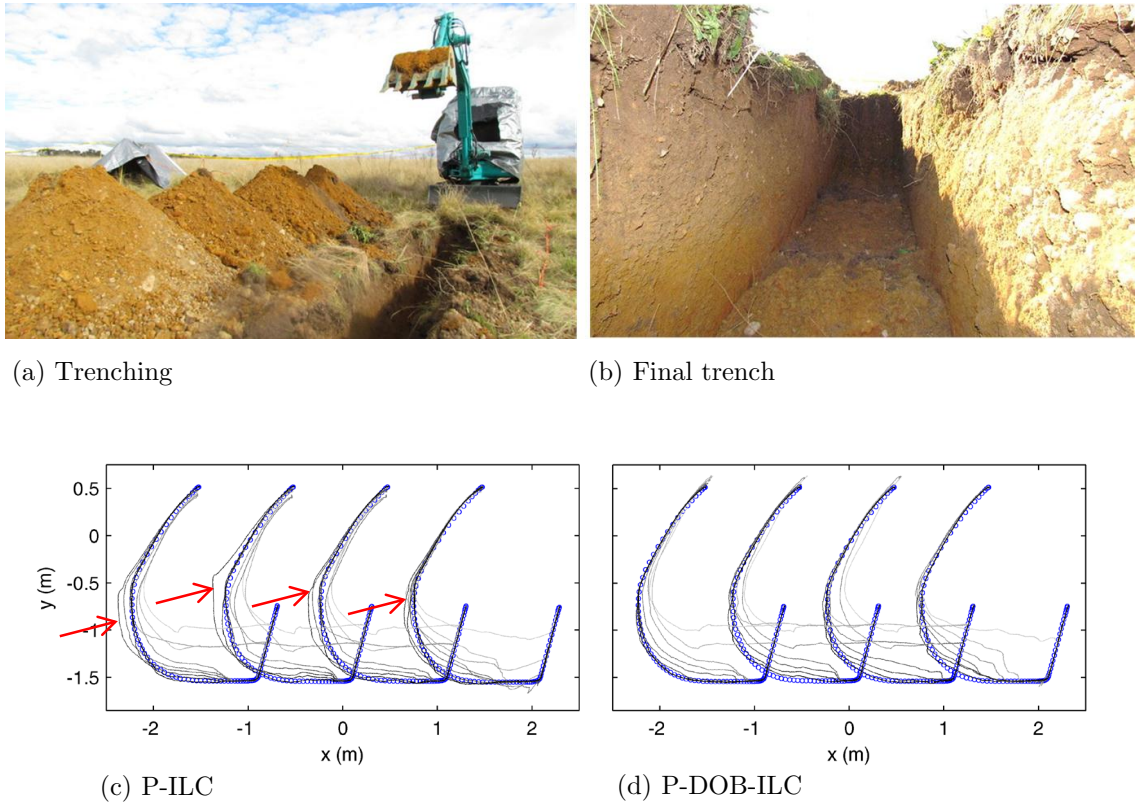


Figure 6.12 – Trenching with the P-ILC and P-DOB-ILC controllers. The controllers took 34 and 30 passes respectively to achieve a final trench profile with quality given by an RMS distance error of 5 cm. (a) Trenching experiment. (b) P-ILC controller with the expected overshoots caused by the inaccuracies in prediction due to the non-repetitiveness of disturbances. Overshoots are indicated by arrows. (c) P-DOB-ILC controller shows less overshoot as the observer counteracts prediction errors.

times. The P-ILC and the predictive-reactive P-DOB-ILC controller took a total of 34 and 30 passes, respectively. Figure 6.12 (c) shows the effect of the inaccuracies in ILC prediction causing trajectory overshoot (indicated by arrows). Figure 6.12 (d) shows that the on-line DOB produced less overshooting as the observer attenuates ILC inaccuracies.

6.3 Conclusion

This chapter presented extensive field experiments using the mini-excavator robotic platform. The Proportional, PI, P-DOB, P-ILC, and the proposed predictive-reactive P-DOB-ILC controllers were evaluated and compared side-by-side using the strategy proposed in Section 3.2. Together with the trenching experiment the field trial resulted in more than 300 passes in undisturbed and heterogeneous soil.

Several hypothesis were validated in this chapter. First, the iterative excavation strategy proposed in Section 3.2.1 where motion adaptation to infeasible passes is a natural consequence of actuator flow saturation. The proposed strategy also led to passes resembling the “slicing” reported by Bradley et al. (1989) in manned excavation.

Second, the preliminary experiments reported in Chapter 4 in approximately homogeneous soil were extended in real heterogeneous excavation conditions. It was shown (Figure 6.4) that a disturbance observer acting as a virtual sensor of excavation disturbances could significantly improve the tracking metric of a proportional controller as an alternative to integral action. In fact, the performance obtained with the DOB was, for the majority of passes, superior to the PI controller which had to be tuned specifically for the conditions of the field trial.

Third, Figure 6.7 supported the hypothesis that the addition of disturbance previews provided by ILC decreases the tracking error of a pure feedback controller, potentially leading to less passes to complete a cut. This hypothesis was also supported by the comparison of the sensitivities of the proportional controller with its predictive version.

Fourth, the use of a DOB to improve the performance of an inaccurate predictive controller by compensating prediction error was validated experimentally. This hy-

pothesis was supported by the results in Figure 6.8 where the predictive-reactive P-DOB-ILC controller achieved 25% better tracking than the predictive P-ILC controller. This improvement was also observed qualitatively in terms of the bucket tip paths shown in Figure 6.6 and Figure 6.12, where the P-DOB-ILC showed less overshoot than the P-ILC controller.

Finally, with the use of the experimental data and the sensitivity-like function the FEE-based empirical model was implemented and compared with ILC by means of simulated response of the feedback controller. The results showed that although in practice the empirical model may achieve better rejection than ILC, its implementation depends on the correct setting of the size of regression data, the installation of load cells, and the design of force control loops. The use of ILC is therefore a trade-off between the simplicity of implementation and achievable performance.

Chapter 7

Summary and Conclusions

The work presented has addressed the fundamental control problem of limited disturbance rejection in feedback control systems, motivated by the practical problem of autonomous excavation. In excavation the limited amount of disturbance rejection provided by feedback was reflected in low convergence rates when iteratively repeating excavation passes towards a desired cut. An interpretation of side information in controllers with preview motivated the use of predictive action also providing metrics to quantify the sensitivity of controllers with feedforward action. The literature showed, however, that prediction of disturbance forces in autonomous excavation is prone to error due to complexity of soil-tool interaction forces.

This work used ILC as a feedforward model of disturbances in excavation. A disturbance observer was used to estimate and counteract ILC prediction error. Extensive field trials quantified by means of tracking error and sensitivity plots, provided the evidence that the proposed method resulted in an increase of disturbance rejection while minimising the detrimental effects of inaccurate prediction caused by the non-repetitive components of the disturbance. The method emphasised the imple-

mentability of the solution to real excavator platforms with only joint position as the required feedback signal.

The experimental platform demonstrated the ability to autonomously excavate a deep cut with aggressive preemptive disturbance compensation. The method is independent of the initial feasibility of the desired cut in relation to actuator saturation. Feedforward commands were adapted to different soil conditions using ILC and passes were repeated without operator intervention until a specified precision of the cut was achieved.

7.1 Summary of Main Results

This section summarises the main contributions and results contained in this thesis.

Excavation Strategy. An iterative excavation strategy was proposed in Section 3.2.1 by considering observations of skilled operators (Shao et al., 2008; Bradley et al., 1989) and inspired by the strategies for accommodating large disturbance forces reviewed in Section 2.1. Due to the limited power of the mini-excavator platform, actuator flow saturation was used as a natural method of adapt bucket motion to infeasible reference trajectories. Saturated actuators generated trajectories that approximately resemble the observation by Bradley et al. (1989) of skilled operators digging in “slices”. The proposed behaviour and results of related work are summarised in Figure 7.1.

DOB as a Virtual Sensor. In Chapter 4 the use of a disturbance observer was proposed as an alternative to integral action to increase disturbance rejection of the proportional controller during excavation. In the hydraulic control literature the use of disturbance observers has mainly been focused on compensation of internal

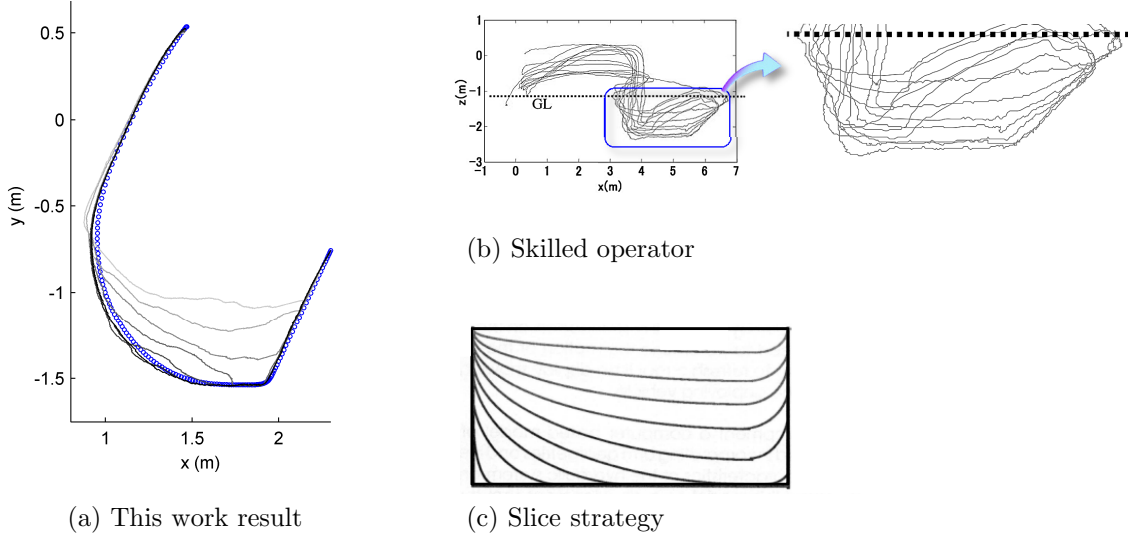


Figure 7.1 – (a) Excavation paths using the strategy proposed in this work. (b) An excavation strategy used by skilled operators. From Shao et al. (2008). (c) Digging in “slices”. From Bradley et al. (1989).

frictional forces of the cylinder. This work made extensive use of the observer as a virtual sensor of soil reaction forces during excavation. As shown in Figure 7.2, after the same number of eight passes the P-DOB controller was able to achieve the desired cut while the conventional proportional controller was still far from finishing the cut.

Predictive Excavation. In Chapter 2.2 the information-theoretic result in Equation (2.23) (on page 43) for systems with side information was interpreted as a feed-forward model of disturbances in excavation. This interpretation motivated the use of prediction in excavation as a method to overcome the limitations of the Bode integral, and also provided ways to quantify disturbance attenuation in terms of the sensitivity-like function.

Under the application of interest, difficulties associated with the selection, measurement and estimation of parameters using analytical models led to a data-driven regression approach based on iterative learning control. Using the boom controller as

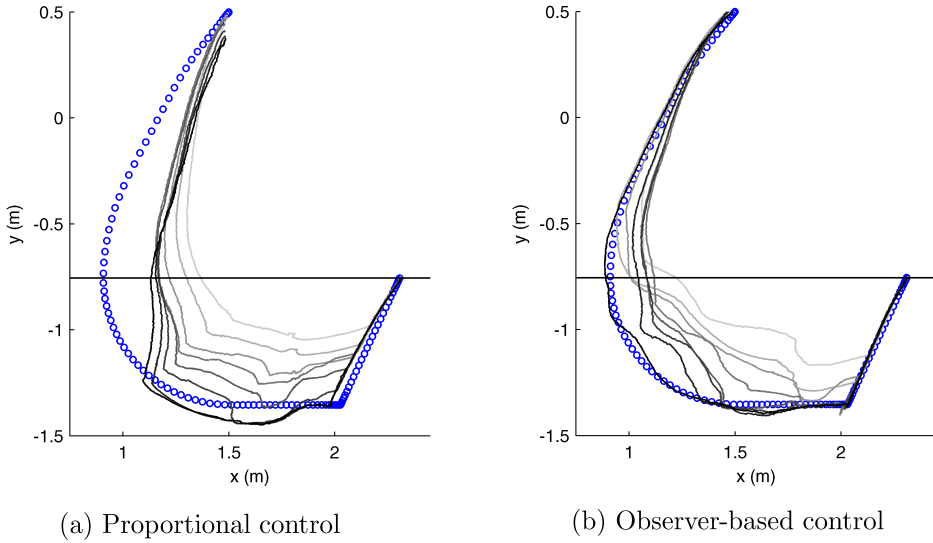


Figure 7.2 – The use of a disturbance observer as a form of virtual sensor of excavation disturbances was used to increase the disturbance rejection of a proportional controller as an alternative to integral action.

an example, Figure 7.3 (a) shows the sensitivity S of the original proportional controller compared with the plot of the sensitivity-like function $S_{d,e}$ of the proportional controller with ILC prediction (P-ILC). The fact that the controller with ILC has a lower sensitivity magnitude shows that the predictive system improved the disturbance rejection of the feedback controller. Also, recall from Table 6.2 that the negative value of the integral of the sensitivity indicates that the *waterbed effect was overcome through the preview of disturbances via ILC*. During field trials, disturbance rejection was also quantified in the form of the reduction in tracking error as shown in Figure 7.3 (b). On average, the distance between the bucket and the final cut during a sequence of seven passes decreased by 45% (metric (6.1)) with the use of ILC when compared to a proportional controller. In practice this reduction means that the bucket could achieve the desired cut precision with less passes.

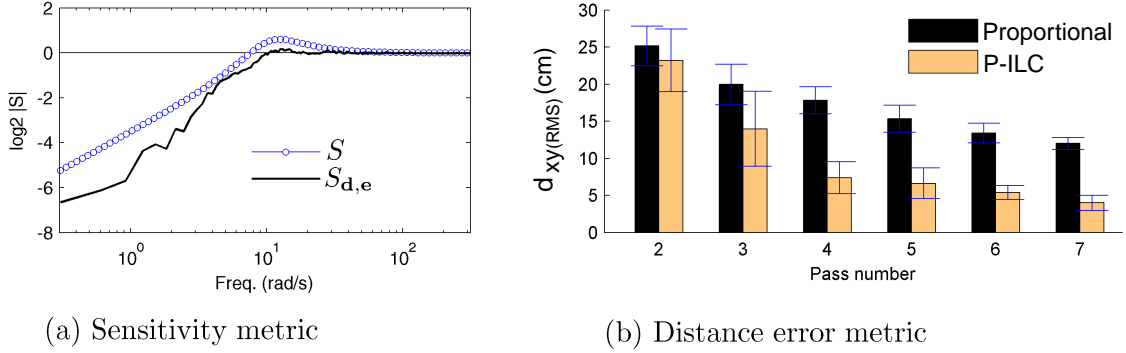


Figure 7.3 – The use of ILC prediction improved disturbance rejection as shown by the sensitivity-like function in (a), leading to aggressive passes that decreased the distance error per pass between the bucket and the final cut (b).

Reacting on Prediction Error. The aim in proposing the predictive-reactive controller in Figure 5.2 was to use the accurate parts of ILC prediction to improve disturbance rejection by preemptive compensation while attenuating inaccuracies in prediction with an on-line observer. The use of the observer required an alternative structure which drives the observer with the disturbance prediction error rather than with the full disturbance as is usual. As a result, Figure 7.4 (a) shows an example of a cut where the error in ILC prediction generates overshoot. In Figure 7.4 (b) the use of the observer attenuates the prediction error so that the final trajectory shows less overshoot while maintaining the aggressiveness of predictive action. Results from field trials showed that the average tracking error per pass decreased by 25% with the combined predictive-reactive P-DOB-ILC controller relative to the predictive P-ILC controller.

Simplicity of Implementation. As mentioned in the introduction to this thesis, control for autonomous excavation is one of the oldest challenges in field robotics: despite three decades of research, no commercial deployment of a fully-autonomous excavator has been reported to date. This work has argued that one of the issues inhibiting industrial acceptance is related to the difficulty of implementation of the

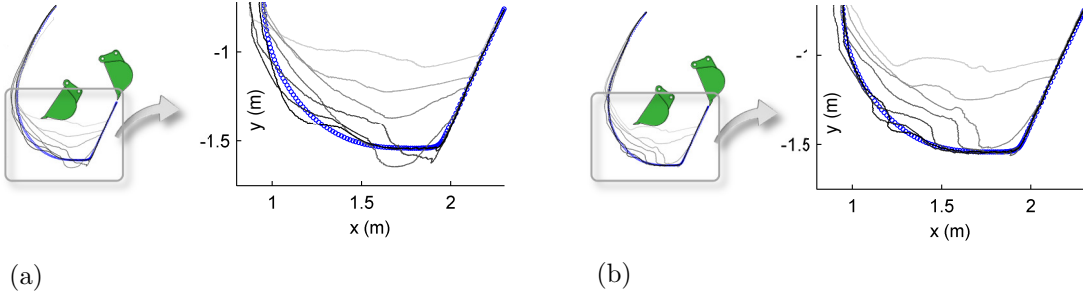


Figure 7.4 – The use of the observer to estimate inaccurate predictions resulted in less overshooting of the reference trajectory as shown by the bucket tip motion. (a) Controller without observer (P-ILC). (b) Controller with observer (P-DOB-ILC).

various solutions that have been proposed. Solutions sought in the present work relied only on feedback from joint encoders, and the control design was focused on straightforward reference tracking methods rather than excavation-tailored formulations. Two benefits of this approach are that the proposed controller has potential applications to general scenarios where a plant undergoes large and approximately repetitive disturbances, and that it can be applied with minimal sensing. The final proposed predictive-reactive controller was presented in Figure 5.2.

Previous control solutions to autonomous excavation have relied on force sensing and direct force control; this leads to implementation difficulties as the great majority of hydraulic machines are flow-controlled. In principle, however, the proposed method could be applied to the control of force or impedance. The proportional tracking controller, the DOB, and ILC are general methods where the control variable is not limited to position or velocity. A detailed discussion can be found in Section 3.4.

7.2 Limitations and Future Work

Iteration-Invariant ILC Trajectories. In this work one of the main assumptions was that the reference trajectory was iteration-invariant. While this assumption made

the application of ILC straightforward, repetitive tasks often can be accomplished faster by time optimisation. Shao et al. (2008) suggested that the initial passes of an excavator should have higher speeds than the final passes, when the finishing quality becomes important. In surgical manipulation, Van Den Berg et al. (2010) proposed a variant of ILC update where the trajectory duration was updated at each iteration. Van Den Berg et al. showed, however, that aggressive time step reductions can lead to poor convergence. In a flow-controlled excavator arm it is conjectured that decreasing time is non-trivial as faster trajectories demand higher flow commands which in turn decreases the actuation margin available to counteract excavation disturbances. One possible solution would be to divide a trajectory in the time domain into several segments. Each segment would then have its duration adjusted according to the level of disturbance, the amount of required actuation, and the error in tracking.

Excessive dragging can be avoided in the case where real-time feedback of bucket fill is available. Although this strategy may improve efficiency in terms of actuation usage, iteration-variant trajectories invalidate the use of ILC as the reference trajectory becomes non-repetitive. For the predictive part of the controller, other forms of disturbance prediction—for example by soil-mechanics models—may be necessary.

Control Design with Sensitivity-Like Functions. Using the experimental data collected during field trials plots of the sensitivity-like function, Equation (2.22), provided visual information regarding the sensitivity attenuation of the joint controller as a result of ILC prediction. This information could be used further to tune the feedback controller or to design a new controller based on sensitivity-like curves. Unfortunately, a design method based on plots of sensitivities is not scalable or generalisable. The quantification of a predictive controller with sensitivity-like functions should also take advantage of systematic and scalable design techniques, for example, within the frameworks of preview control (Takaba, 2003) and H_∞ loop-shaping

(McFarlane and Glover, 1992).

Ideal Reactive-Predictive Controller. This work addressed the problem of using inaccurate predictions by incorporating a plant inversion ILC update rule so that the prediction error becomes available to a disturbance observer as shown in Figure 5.2. The use of ILC for prediction was motivated by its simplicity and generality. A proportional controller was chosen as the feedback controller as it is the simplest feasible method to control a flow-driven hydraulic arm, and the use of a disturbance observer for attenuation of prediction error was motivated by robustness and consolidated use in hydraulic system motion control.

There is clearly an infinity of other possible predictive and reactive methods that may fit the proposed predictive-reactive controller structure. For example, results in Chapter 6 suggested that a specialised candidate for excavation is the FEE-based empirical model. The method of Helfrich et al. (2010) for designing robust feedback could be an alternative to the proposed P-DOB feedback controller in systems with high bandwidth. Rather than providing a final answer, the present work foreshadows future investigations of a class of problem where predictions are useful to overcome poor feedback performance, although they are intrinsically inaccurate due to the uncertain and complex nature of the interaction.

Integration with High-Level Planners. The controller proposed in the present work addressed the problem of achieving a desired cut by forceful material removal, which is regarded as the lowest level of capability for autonomous excavation. A natural next step towards a complete autonomous excavation system would be to integrate the proposed controller with planners and other high-level decision structures. High-level planning in excavation is usually addressed as a task decomposition problem, where the environment is mapped geometrically and divided in a sequence

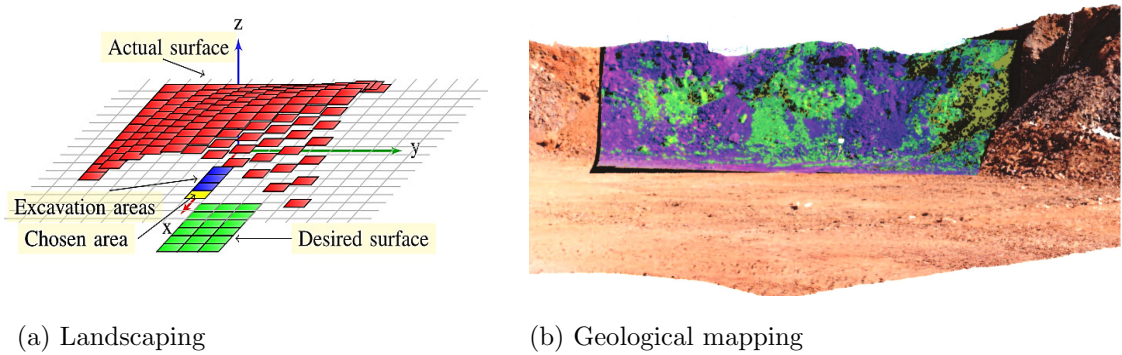


Figure 7.5 – Examples of potential use of high-level excavation planners with the controller proposed for autonomous excavation. (a) The landscaping planner of Schmidt et al. (2010) indicates the location of cuts for the autonomous excavator. From Schmidt et al. (2010). (b) 3D geological maps could be used to indicate the areas to be dug according to their mineral content. From Nieto et al. (2010).

of small cuts to achieve a desired landscape (Romero-Lois et al., 1989; Schmidt et al., 2010) as shown in Figure 7.5 (a).

In mining applications, data fusion of hyperspectral and laser images are used to form a 3D geological map of the mine face as shown in Figure 7.5 (b) (Nieto et al., 2010). This geological map could then be used to decompose the mine face in a sequence of selective reference cuts, tagged according to the mineral content. Those cuts could then be used by the autonomous excavator controller presented in this work as desired profiles for the generation of reference trajectories.

Towards Commercial and Industrial Application. Although technological efforts towards mining automation have been increasing during the last decades, autonomous excavation seems to have received scant attention in relation to other mining processes. Autonomous haul trucks, blast-hole drills and ore trains are already a reality in contemporary mines. The commercial deployment of autonomous excavators is, however, unheard of. This discrepancy is due to two related factors: the number of excavators in a mine is usually small compared to other types of mining machinery, and

the excavation process dictates the production pace of the entire mine. Experienced excavator operators can judge and impose a certain rhythm on the mine to achieve a desired target of material removal: a valuable reasoning that mining companies may be reluctant to put at risk or to delegate to a single fully-autonomous excavator. For this reason, here it is envisioned that the first deployment of the methods proposed in this work would be in the form of an assistance tool: the expert human operator would retain responsibility for high-level and high-risk reasoning, while the methods proposed in this work would be utilised in the low-level control actions. One could imagine an interface as simple as a button which, when pressed, would execute a single pass under feedback control where actions are predicted by ILC on the basis of the previous pass. Such a simple and minimal implementation would remove the burden from the operator of controlling the excavator arm during a pass. This form of semi-automation has been the model adopted by Caterpillar Inc., where part of the results from collaboration with the Carnegie Mellon University Robotics Institute have been commercialised under the name Aggregate Autodig for the automation of the scoop cycle of wheel loaders.

List of References

- Ahn, H., Chen, Y., and Moore, K. (2007). Iterative learning control: brief survey and categorization. *IEEE Transactions on Systems, Man, and Cybernetics, Part C: Applications and Reviews*, 37(6):1099–1121.
- Alleyne, A. and Liu, R. (2000). A simplified approach to force control for electro-hydraulic systems. *Control Engineering Practice*, 8(12):1347–1356.
- Althoefer, K., Tan, C., Zweiri, Y., and Seneviratne, L. (2009). Hybrid soil parameter measurement and estimation scheme for excavation automation. *IEEE Transactions on Instrumentation and Measurement*, 58(10):3633–3641.
- Arimoto, S., Kawamura, S., and Miyazaki, F. (1984). Bettering operation of robots by learning. *Journal of Robotic Systems*, 1(2):123–140.
- Arimoto, S. and Naniwa, T. (2000). Equivalence relations between learnability, output-dissipativity and strict positive realness. *International Journal of Control*, 73(10):824–831.
- Åström, K. and Canudas de Wit, C. (2008). Revisiting the LuGre friction model. *IEEE Control Systems Magazine*, 28(6):101–114.
- Åström, K., Hägglund, T., Hang, C.-C., and Ho, W. (1993). Automatic tuning and adaptation for pid controllers-a survey. *Control Engineering Practice*, 1(4):699–714.
- Åström, K. J. and Hägglund, T. (2001). The future of pid control. *Control engineering practice*, 9(11):1163–1175.
- Benallegue, A., Mokhtari, A., and Fridman, L. (2007). High-order sliding-mode observer for a quadrotor UAV. *International Journal of Robust and Nonlinear Control*, 18(4-5):427–440.
- Bernold, L. (1993). Motion and path control for robotic excavation. *Journal of Aerospace Engineering*, 6(1):1–18.

- Bessa, W., Dutra, M., and Kreuzer, E. (2010). Sliding mode control with adaptive fuzzy dead-zone compensation of an electro-hydraulic servo-system. *Journal of Intelligent and Robotic Systems*, 58(1):3–16.
- Blouin, S., Hemami, A., and Lipsett, M. (2001). Review of resistive force models for earthmoving processes. *Journal of Aerospace Engineering*, 14(3):102–111.
- Bode, H. W. (1956). *Network analysis and feedback amplifier design*. Van Nostrand Reinhold.
- Bonchis, A. (2001). *Modelling and control of hydraulic servo systems*. PhD thesis, The University of Sydney.
- Bonchis, A., Corke, P., and Rye, D. (1999). A pressure-based, velocity independent, friction model for asymmetric hydraulic cylinders. In *Proceedings of the 1999 IEEE International Conference on Robotics and Automation*, volume 3, pages 1746–1751.
- Bonchis, A., Corke, P., Rye, D., and Ha, Q. (2001). Variable structure methods in hydraulic servo systems control. *Automatica*, 37(4):589–595.
- Bradley, D. and Seward, D. (1998). The development, control and operation of an autonomous robotic excavator. *Journal of Intelligent and Robotic Systems*, 21(1):73–97.
- Bradley, D., Seward, D., Bracewell, R., Chaplin, R., and Widden, M. (1989). Control and operational strategies for automatic excavation. In *Proceedings of the 5th International Symposium on Automation and Robotics in Construction*, pages 237–244.
- Bristow, D., Tharayil, M., and Alleyne, A. (2006). A survey of iterative learning control. *IEEE Control Systems Magazine*, 26(3):96–114.
- Bu, F. and Yao, B. (2000). Nonlinear adaptive robust control of hydraulic actuators regulated by proportional directional control valves with deadband and nonlinear flow gains. In *Proceedings of the 2000 American Control Conference, 2000*, volume 6, pages 4129–4133.
- Bullock, D. and Oppenheim, I. (1989). A laboratory study of force-cognitive excavation. In *Proceedings of the Fifth International Symposium on Automation and Robotics in Construction*.
- Cannon, H. (1999). *Extended earthmoving with an autonomous excavator*. PhD thesis, Carnegie Mellon University.
- Cannon, H. and Singh, S. (2000). Models for automated earthmoving. In *Lecture Notes in Control and Information Sciences - The 6th International Symposium Experimental Robotics*, pages 163–172. Springer.

- Chen, Y. and Moore, K. (2002). Harnessing the nonrepetitiveness in iterative learning control. In *Proceedings of the 41st IEEE Conference on Decision and Control*, volume 3, pages 3350–3355.
- Chi, R., Hou, Z., and Xu, J. (2008). Adaptive ilc for a class of discrete-time systems with iteration-varying trajectory and random initial condition. *Automatica*, 44(8):2207–2213.
- Chin, I., Qin, S., Lee, K., and Cho, M. (2004). A two-stage iterative learning control technique combined with real-time feedback for independent disturbance rejection. *Automatica*, 40(11):1913–1922.
- Clark, M., Magstadt, C., Mettlach, G., Price, R., and Alshaer, B. (2011). Velocity based control process for a machine digging cycle. US Patent 7,979,181.
- Cohen, A. and Shaked, U. (1997). Linear discrete-time H_∞ -optimal tracking with preview. *IEEE Transactions on Automatic Control*, 42(2):270–276.
- Corke, P. (2011). *Robotics, Vision and Control: Fundamental Algorithms in MATLAB*. Springer.
- Cover, T. and Thomas, J. (2006). *Elements of Information Theory*. Wiley-Interscience.
- De Roover, D. and Bosgra, O. H. (2000). Synthesis of robust multivariable iterative learning controllers with application to a wafer stage motion system. *International Journal of Control*, 73(10):968–979.
- Dixon, R., Taylor, C., and Shaban, E. (2005). Comparison of classical and modern control applied to an excavator-arm. In *Proceedings of the IFAC 16th Triennial World Congress*, pages 4–8.
- Duff, E., Caris, C., Bonchis, A., Taylor, K., Gunn, C., and Adcock, M. (2010). The development of a telerobotic rock breaker. In *Field and Service Robotics*, pages 411–420. Springer.
- Dunbabin, M. and Corke, P. (2006). Autonomous excavation using a rope shovel. *Journal of Field Robotics*, 23(6-7):379–394.
- Francis, B. and Wonham, W. (1976). The internal model principle of control theory. *Automatica*, 12(5):457–465.
- Friedland, B. and Park, Y. (1992). On adaptive friction compensation. *IEEE Transactions on Automatic Control*, 37(10):1609–1612.
- Gay, J. (2004). Method for developing an algorithm to efficiently control an autonomous excavating linkage. US Patent 6,691,010.

- Gunnarsson, S. and Norrlöf, M. (2001). On the design of ilc algorithms using optimization. *Automatica*, 37(12):2011–2016.
- Ha, Q., Bonchis, A., Rye, D., and Durrant-Whyte, H. (2000a). Variable structure systems approach to friction estimation and compensation. In *Proceedings of the 2000 IEEE International Conference on Robotics and Automation*, volume 4, pages 3543–3548.
- Ha, Q., Nguyen, Q., Rye, D., and Durrant-Whyte, H. (2000b). Impedance control of a hydraulically actuated robotic excavator. *Automation in Construction*, 9(5-6):421–435.
- Ha, Q., Rye, D., and Durrant-Whyte, H. (1999). Fuzzy moving sliding mode control with application to robotic manipulators. *Automatica*, 35:607–616.
- Ha, Q., Santos, M., Nguyen, Q., Rye, D., and Durrant-Whyte, H. (2002). Robotic excavation in construction automation. *IEEE Robotics and Automation Magazine*, 9(1):20–28.
- Haga, M., Hiroshi, W., and Fujishima, K. (2001). Digging control system for hydraulic excavator. *Mechatronics*, 11(6):665–676.
- Helfrich, B., Lee, C., Bristow, D., Xiao, X., Dong, J., Alleyne, A., Salapaka, S., and Ferreira, P. (2010). Combined H_∞ feedback control and iterative learning control design with application to nanopositioning systems. *IEEE Transactions on Control Systems Technology*, 18(2):336–351.
- Hemami, A. (1993). Study of bucket trajectory in automatic scooping with load-haul-dump loaders. *Transactions of the Institution of Mining and Metallurgy. Section A, Mining industry*, 102:37–42.
- Hemami, A. and Hassani, F. (2009). An overview of autonomous loading of bulk material. In *Proceedings of the 26th International Symposium on Automation and Robotics in Construction*, volume 4, pages 405–411.
- Hodel, S. and Hall, C. (2001). Variable-structure PID control to prevent integrator windup. *IEEE Transactions on Industrial Electronics*, 48(2):442–451.
- Hogan, N. (1984). Impedance control: an approach to manipulation. In *American Control Conference, 1984*, pages 304–313.
- Hou, Z., Xu, J.-X., and Zhong, H. (2007). Freeway traffic control using iterative learning control-based ramp metering and speed signaling. *IEEE Transactions on Vehicular Technology*, 56(2):466–477.
- Huntsberger, T., Stroupe, A., and Kennedy, B. (2005). System of systems for space construction. In *Proceedings of the IEEE International Conference on Systems, Man, and Cybernetics, 2005*, volume 4, pages 3173–3178.

- Iglesias, P. (2001). An analogue of Bode's integral for stable nonlinear systems: relations to entropy. In *Proceedings of the 40th IEEE Conference on Decision and Control, 2001*, volume 4, pages 3419–3420.
- Jarzebowski, A., Maciejewski, M., Szyba, D., and Trampczynski, W. (1995). The optimisation of tools shapes and trajectories in heavy machines. In *Proceedings of the 12th International Symposium on Automation and Robotics in Construction*, pages 159–166.
- Kale, S., Ingram, R., and Sergott, K. (2011). System for automated excavation control based on productivity. US Patent 7,917,265.
- Katsura, S., Matsumoto, Y., and Ohnishi, K. (2007). Modeling of force sensing and validation of disturbance observer for force control. *IEEE Transactions on Industrial Electronics*, 54(1):530–538.
- Kelly, R. and Salgado, R. (1994). PD control with computed feedforward of robot manipulators: a design procedure. *IEEE Transactions on Robotics and Automation*, 10(4):566–571.
- Kempf, C. and Kobayashi, S. (1999). Disturbance observer and feedforward design for a high-speed direct-drive positioning table. *IEEE Transactions on Control Systems Technology*, 7(5):513–526.
- Kim, D., Kim, J., Lee, K., Park, C., Song, J., and Kang, D. (2009). Excavator tele-operation system using a human arm. *Automation in Construction*, 18(2):173–182.
- Koivo, A. (1994). Kinematics of excavators (backhoes) for transferring surface material. *Journal of Aerospace Engineering*, 7(1):17–32.
- Koivo, A., Thoma, M., Kocaoglan, E., and Andrade, J. (1996). Modeling and control of excavator dynamics during digging operation. *Journal of Aerospace Engineering*, 9(1):10–18.
- Kojima, A. and Ishijima, S. (1999). LQ preview synthesis: optimal control and worst case analysis. *IEEE Transactions on Automatic Control*, 44(2):352–357.
- Kojima, A. and Ishijima, S. (2003). H_∞ performance of preview control systems. *Automatica*, 39(4):693–701.
- Komatsu (1991). *Operation and Maintenance Manual. PC05-7 Hydraulic Excavator, SEAM020M0700*. Rev. 05-91(01-2).
- Kuśmierczyk, J. and Szlagowski, J. (2008). Automated excavation process analysis for given trajectory and soil parameters. In *Proceedings of the 25th International Symposium on Automation and Robotics in Construction*, pages 95–99.

- La Hera, P., Mettin, U., Manchester, I., and Shiriaev, A. (2008). Identification and control of a hydraulic forestry crane. In *Proceedings of the 17th IFAC World Congress*, pages 6–11.
- Le, A., Rye, D., and Durrant-Whyte, H. (1997). Estimation of track-soil interactions for autonomous tracked vehicles. In *Proceedings of the 1997 IEEE International Conference on Robotics and Automation*, volume 2, pages 1388–1393.
- Le, A. T. (1999). *Modelling and control of tracked vehicles*. PhD thesis, The University of Sydney.
- Le Tien, L., Albu-Schaffer, A., De Luca, A., and Hirzinger, G. (2008). Friction observer and compensation for control of robots with joint torque measurement. In *Proceedings of the 2008 IEEE/RSJ International Conference on Intelligent Robots and Systems*, pages 3789–3795.
- Lee, S. and Chang, P. (2002). Control of a heavy-duty robotic excavator using time delay control with integral sliding surface. *Control Engineering Practice*, 10(7):697–711.
- Lever, P. J. A. (2001). An automated digging control for a wheel loader. *Robotica*, 19(5):497–511.
- Lischinsky, P., Canudas de Wit, C., and Morel, G. (2002). Friction compensation for an industrial hydraulic robot. *IEEE Control Systems Magazine*, 19(1):25–32.
- Longman, R. (2000). Iterative learning control and repetitive control for engineering practice. *International Journal of Control*, 73(10):930–954.
- Luenberger, D. (1971). An introduction to observers. *IEEE Transactions on Automatic Control*, 16(6):596–602.
- Luengo, O., Singh, S., and Cannon, H. (1998). Modeling and identification of soil-tool interaction in automated excavation. In *Proceedings of the 1998 IEEE/RSJ International Conference on Intelligent Robots and Systems*, volume 3, pages 1900–1906.
- Lupashin, S., Schollig, A., Sherback, M., and D’Andrea, R. (2010). A simple learning strategy for high speed quadrocopter multi flips. In *Proceedings of the 2010 IEEE International Conference on Robotics and Automation*, pages 1642–1648.
- Maciejewski, J. and Jarzebowski, A. (2002). Laboratory optimization of the soil digging process. *Journal of Terramechanics*, 39(3):161–179.

- Maeda, G., Singh, S., and Rye, D. (2011). Improving operational space control of heavy manipulators via open-loop compensation. In *Proceedings of the 2011 IEEE/RSJ International Conference on Intelligent Robots and Systems*, pages 725–731.
- Malaguti, F. (1994a). Soil machine interaction in digging and earthmoving automation. In *Proceedings of the 11th International Symposium on Automation and Robotics in Construction*, pages 187–191.
- Malaguti, F. (1994b). Variable structure control in excavator robot. In *Proceedings of the 11th International Symposium on Automation and Robotics in Construction*, pages 263–267.
- Malaguti, F. (1999). Improved model of soil for environment-robot excavator interaction. In *Proceedings of the 16th International Symposium on Automation and Robotics in Construction*, pages 523–527.
- Malaguti, F. (2005). Cutting and impedance model of soil-excavator interaction. In *Proceedings of the 22nd International Symposium on Automation and Robotics in Construction*, pages 1–4.
- Marshall, J. (2001). Towards autonomous excavation of fragmented rock: experiments, modelling, identification and control. Msceng, Queen's University.
- Marshall, J., Murphy, P., and Daneshmend, L. (2008). Toward autonomous excavation of fragmented rock: full-scale experiments. *IEEE Transactions on Automation Science and Engineering*, 5(3):562–566.
- Martins, N. and Dahleh, M. (2008). Feedback control in the presence of noisy channels: “Bode-like” fundamental limitations of performance. *IEEE Transactions on Automatic Control*, 53(7):1604–1615.
- Martins, N., Dahleh, M., and Doyle, J. (2007). Fundamental limitations of disturbance attenuation in the presence of side information. *IEEE Transactions on Automatic Control*, 52(1):56–66.
- McFarlane, D. and Glover, K. (1992). A loop shaping design procedure using H_∞ synthesis. *IEEE Transactions on Automatic Control*, 37(6):759–769.
- McKyes, E. and Desir, F. (1984). Prediction and field measurements of tillage tool draft forces and efficiency in cohesive soils. *Soil and Tillage Research*, 4(5):459–470.
- Megretski, A. and Rantzer, A. (1997). System analysis via integral quadratic constraints. *Automatic Control, IEEE Transactions on*, 42(6):819–830.
- Merritt, H. (1967). *Hydraulic Control Systems*. John Wiley & Sons.

- Merry, R., van de Molengraft, R., and Steinbuch, M. (2006). Removing non-repetitive disturbances in iterative learning control by wavelet filtering. In *American Control Conference, 2006*, pages 6–pp.
- Middleton, R., Chen, J., and Freudenberg, J. (2004). Tracking sensitivity and achievable H_∞ performance in preview control. *Automatica*, 40(8):1297–1306.
- Mintah, B., Price, R., and King, K. (2011). Semi-autonomous excavation control system. US Patent 7,934,329.
- Mishra, S., Coaplen, J., and Tomizuka, M. (2007). Precision positioning of wafer scanners segmented iterative learning control for nonrepetitive disturbances [applications of control]. *IEEE Control Systems Magazine*, 27(4):20–25.
- Moog (2013). D633 and D634 series direct drive servo-proportional valves. <http://www.moog.com/literature/ICD/D633seriesvalvesE.pdf>. Rev. H 1005 CDL6581, accessed 13 March 2013.
- Moore, K. (1999). Iterative learning control – an expository overview. *Applied and Computational Control, Signals, and Circuits*, 1:151–214.
- Moore, K. L. (1993). *Iterative Learning Control for Deterministic Systems*. Springer, London.
- Moore, K. L. (2000). On the relationship between iterative learning control and one-step ahead minimum prediction error control. In *Proc. of the Asian Control Conference*, pages 1861–1865.
- Moore, K. L., Chen, Y., and Ahn, H.-S. (2006). Iterative learning control: A tutorial and big picture view. In *Proceedings of the 45th IEEE Conference on Decision and Control*, pages 2352–2357. IEEE.
- Nguyen, H. (2000). *Robust low-level control of robotic excavation*. PhD thesis, The University of Sydney.
- Nguyen, Q., Ha, Q., Rye, D., and Durrant-Whyte, H. (2000). Force/position tracking for electrohydraulic systems of a robotic excavator. In *IEEE Conference on Decision and Control*, volume 5, pages 5224–5229.
- Nieto, J. I., Monteiro, S. T., and Viejo, D. (2010). 3D geological modelling using laser and hyperspectral data. In *IEEE International Geoscience and Remote Sensing Symposium (IGARSS)*, pages 4568–4571.
- Norrlöf, M. (2004). Disturbance rejection using an ILC algorithm with iteration varying filters. *Asian Journal of Control*, 6(3):432–438.
- Norrlöf, M. and Gunnarsson, S. (2001). Disturbance aspects of iterative learning control. *Engineering Applications of Artificial Intelligence*, 14(1):87–94.

- Papoulis, A. and Pillai, S. (2002). *Probability, Random Variables, and Stochastic Processes*. McGraw-Hill.
- Parker, N., Salcudean, S., and Lawrence, P. (1993). Application of force feedback to heavy duty hydraulic machines. In *Proceedings of the 1993 IEEE International Conference on Robotics and Automation*, pages 375–381.
- Perruquetti, W. and Barbot, J. (2002). *Sliding Mode Control in Engineering*. Marcel Dekker.
- Phan, M. Q. (1989). *A mathematical theory of learning control*. PhD thesis, Columbia University.
- Phan, M. Q. and Longman, R. W. (2002). Higher-order iterative learning control by pole placement and noise filtering. In *Proceedings of the IFAC World Congress*, pages 1899–1904.
- Reece, A. (1964). The fundamental equation of earth-moving mechanics. *Proceedings of the Institution of Mechanical Engineers*, 179:16–22.
- Richardson-Little, W. and Damaren, C. (2008). Position accommodation and compliance control for robotic excavation. *Journal of Aerospace Engineering*, 21(1):27–34.
- Rocke, D. (1995). Automatic excavation control system and method. US Patent 5,446,980.
- Rocke, D. (1996). Control system for automatically controlling a work implement of an earthworking machine to capture material. US Patent 5,528,843.
- Rocke, D., Devier, L., and Herget, D. (1996). Teaching automatic excavation control system and method. US Patent 5,493,798.
- Rogers, E., Galkowski, K., and Owens, D. (2007). *Control Systems Theory and Applications for Linear Repetitive Processes (Lecture Notes in Control and Information Sciences, 349)*. Springer.
- Romero-Lois, H., Hendrickson, C., and Oppenheim, I. (1989). A strategic planner for robot excavation. In *Proceedings of the Sixth International Symposium on Automation and Robotics in Construction*.
- Rowe, P. and Stentz, A. (1997). Parameterized scripts for motion planning. In *Proceedings of the 1997 IEEE/RSJ International Conference on Intelligent Robots and Systems*, volume 2, pages 1119–1124.

- Sakaida, Y., Chugo, D., Yamamoto, H., and Asama, H. (2008). The analysis of excavator operation by skillful operator-extraction of common skills. In *Proceedings of the 2008 International Conference on Instrumentation, Control, Information Technology and System Integration*, pages 538–542.
- Salcudean, S., Tafazoli, S., Lawrence, P., and Chau, I. (1997). Impedance control of a teleoperated mini excavator. In *Proceedings of the 8th IEEE International Conference on Advanced Robotics*.
- Sarata, S., Koyachi, N., and Sugawara, K. (2008). Field test of autonomous loading operation by wheel loader. In *Proceedings of the 2008 IEEE/RSJ International Conference on Intelligent Robots and Systems*, pages 2661–2666.
- Sarata, S., Osumi, H., Kawai, Y., and Tomita, F. (2004). Trajectory arrangement based on resistance force and shape of pile at scooping motion. In *Proceedings of the 2004 IEEE International Conference on Robotics and Automation*, volume 4, pages 3488–3493. IEEE.
- Satoh, S., Fujimoto, K., and Hyon, S. (2006). Gait generation for passive running via iterative learning control. In *Proceedings of the 2006 IEEE/RSJ International Conference on Intelligent Robots and Systems*, pages 5907–5912.
- Schmidt, D. and Berns, K. (2010). An autonomous excavator for landscaping tasks. In *Proceedings of the 41st Internationel Symposium on Robotics (ROBOTIK)*, pages 1–8.
- Schmidt, D., Proetzsch, M., and Berns, K. (2010). Simulation and control of an autonomous bucket excavator for landscaping tasks. In *Proceedings of the 2010 IEEE International Conference on Robotics and Automation*, pages 5108–5113.
- Schoellig, A., Mueller, F., and D Andrea, R. (2012). Optimization-based iterative learning for precise quadrocopter trajectory tracking. *Autonomous Robots*, pages 1–25.
- Seiler, P., Ozdemir, A. A., and Balas, G. J. (2012). Performance limits with preview information and actuator rate constraints. In *Proceedings of the 2012 American Control Conference*, pages 5532–5537. IEEE.
- Seo, J., Lee, S., Kim, J., and Kim, S. (2011). Task planner design for an automated excavation system. *Automation in Construction*, 20(7):954–966.
- Seron, M., Braslavsky, J., and Goodwin, G. (1997). *Fundamental Limitations in Filtering and Control*. Springer.
- Shannon, C. E. (2001). A mathematical theory of communication. *ACM SIGMOBILE Mobile Computing and Communications Review*, 5(1):3–55.

- Shao, H., Yamamoto, H., Sakaida, Y., Yamaguchi, T., Yanagisawa, Y., and Nozue, A. (2008). Automatic excavation planning of hydraulic excavator. In Xiong, C., Liu, H., Huang, Y., and Xiong, Y., editors, *Intelligent Robotics and Applications*, volume 5315 of *Lecture Notes in Computer Science*, pages 1201–1211. Springer, Berlin and Heidelberg.
- Shi, X., Lever, P., and Wang, F. (1996). Experimental robotic excavation with fuzzy logic and neural networks. In *Proceedings of the 1996 IEEE International Conference on Robotics and Automation*, volume 1.
- Singh, S. (1995). Learning to predict resistive forces during robotic excavation. In *Proceedings of the 1995 IEEE International Conference on Robotics and Automation*, volume 2, pages 2102–2107.
- Sirouspour, M. and Salcudean, S. (2001). Nonlinear control of hydraulic robots. *IEEE Transactions on Robotics and Automation*, 17(2):173–182.
- Slotine, J., Hedrick, J., and Misawa, E. (1986). On sliding observers for nonlinear systems. In *American Control Conference, 1986*, pages 1794–1800.
- Slotine, J. and Li, W. (1991). *Applied Nonlinear Control*. Prentice-Hall, Englewood Cliffs, USA.
- Sohl, G. and Bobrow, J. (1999). Experiments and simulations on the nonlinear control of a hydraulic servosystem. *IEEE Transactions on Control Systems Technology*, 7(2):238–247.
- Song, B. and Koivo, A. (1995). Neural adaptive control of excavators. In *Proceedings of the 1995 IEEE/RSJ International Conference on Intelligent Robots and Systems*, volume 1, pages 162–167.
- Stentz, A., Bares, J., Singh, S., and Rowe, P. (1999). A robotic excavator for autonomous truck loading. *Autonomous Robots*, 7(1):175–186.
- Stolt, A., Linderoth, M., Robertsson, A., and Johansson, R. (2012). Force controlled robotic assembly without a force sensor. In *Proceedings of the 2012 IEEE International Conference on Robotics and Automation*, pages 1538–1543.
- Tafazoli, S., de Silva, C., and Lawrence, P. (1998). Tracking control of an electrohydraulic manipulator in the presence of friction. *IEEE Transactions on Control Systems Technology*, 6(3):401–411.
- Tafazoli, S., Salcudean, S., Hashtrudi-Zaad, K., and Lawrence, P. (2002). Impedance control of a teleoperated excavator. *IEEE Transactions on Control Systems Technology*, 10(3):355–367.

- Tahara, K. and Arimoto, S. (2011). Iterative learning scheme for a redundant manipulator: skilled hand writing motion on an arbitrary smooth surface. In *Proceedings of the 2011 IEEE International Conference on Robotics and Automation*, pages 4682–4687.
- Takaba, K. (2003). A tutorial on preview control systems. In *Proceedings of the International Conference on Instrumentation, Control, Information Technology and System Integration*, volume 2, pages 1388–1393.
- Tan, C., Zweiri, Y., Althofer, K., and Seneviratne, L. (2005). Online soil parameter estimation scheme based on Newton-Raphson method for autonomous excavation. *IEEE/ASME Transactions on Mechatronics*, 10:221–229.
- Tomizuka, M. (1975). Optimal continuous finite preview problem. *IEEE Transactions on Automatic Control*, 20(3):362–365.
- Tsai, L. (1999). *Robot Analysis: The Mechanics of Serial and Parallel Manipulators*. Wiley-Interscience.
- Tzeng, K., Tzeng, D., and Chen, J. (2005). A wavelet-based iterative learning control scheme for motion control systems. In *Proceedings of the 16th IFAC World Congress*.
- Vähä, P. (1993). Cognitive force control of excavators. *Journal of Aerospace Engineering*, 6:159.
- Vähä, P. and Skibniewski, M. (1993). Dynamic model of excavator. *Journal of Aerospace Engineering*, 6(2):148–158.
- Van Den Berg, J., Miller, S., Duckworth, D., Hu, H., Wan, A., Fu, X., Goldberg, K., and Abbeel, P. (2010). Superhuman performance of surgical tasks by robots using iterative learning from human-guided demonstrations. In *Proceedings of the 2010 IEEE International Conference on Robotics and Automation*, pages 2074–2081.
- Wang, F. (2004). Agent-based control for fuzzy behavior programming in robotic excavation. *IEEE Transactions on Fuzzy Systems*, 12(4):540–548.
- Wang, Y., Dassau, E., and Doyle, F. (2010). Closed-loop control of artificial pancreatic beta-cell in type 1 diabetes mellitus using model predictive iterative learning control. *IEEE Transactions on Biomedical Engineering*, 57(2):211–219.
- Westerberg, S., Manchester, I., Mettin, U., La Hera, P., and Shiriaev, A. (2008). Virtual environment teleoperation of a hydraulic forestry crane. In *Proceedings of the 2008 IEEE International Conference on Robotics and Automation*, pages 4049–4054.

- Yamaguchi, T. and Yamamoto, H. (2006). Motion analysis of hydraulic excavator in excavating and loading work for autonomous control. In *Proceedings of the 23rd International Symposium on Automation and Robotics in Construction*, pages 602–607.
- Yoo, S., Park, C., Lim, B., Lee, K., and Park, F. (2010). Bandwidth maximizing design for hydraulically actuated excavators. *Journal of Vibration and Control*, 16(14):2109–2130.
- Yousefi Moghaddam, R., Kotchon, A., and Lipsett, M. (2012). Method and apparatus for on-line estimation of soil parameters during excavation. *Journal of Terramechanics*, 49(3–4):173–181.
- Zeng, H. and Sepehri, N. (2006). Adaptive backstepping control of hydraulic manipulators with friction compensation using LuGre model. In *American Control Conference, 2006*, pages 3164–3169.
- Zhang, D., He, Q., Hao, P., and Zhang, H. (2005). Modeling and controlling for hydraulic excavator’s arm. In *Proceedings of the 22nd International Symposium on Automation and Robotics in Construction*, pages 1–7.
- Ziegler, J. and Nichols, N. (1942). Optimum settings for automatic controllers. *Transactions of the ASME*, 64(11).

Appendix A

Experimental Platform

Kinematics and rigid-body dynamics modelling of a hydraulic excavator arm can be found in early works in the autonomous excavation literature, for example Vähä and Skibniewski (1993); Koivo (1994) and Koivo et al. (1996).

The lengths, positions of centre of mass, and moments of inertia of the links of the PC05-7 mini-excavator arm are given in Table A.1. The values of the positions of centre of masses are approximate, estimated by assuming a uniform material distribution where the total mass is equal to the manufacture's specification, and computed using CAD models. The coordinates of the centre of mass are given in relation to each link coordinate frame, defined according to the Denavit-Hartenberg convention (Tsai, 1999, Ch. 2). The estimated moments of inertia are given at the centre of mass position.

General dimensions of the excavator are shown in Figure A.1 where the bold values indicate dimensions in millimetres. In the figure, locations of encoders for measuring joint angles are indicated by E1, E2 and E3 for the boom, stick and bucket joints respectively. L1 and L2 represent the location of the two load pins. L1 measures

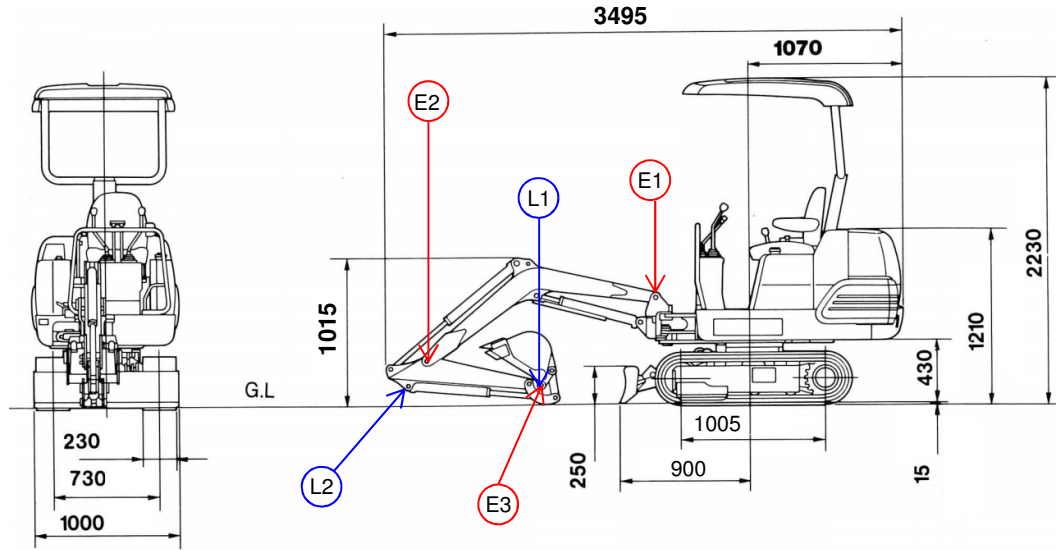


Figure A.1 – Excavator dimensions (in mm) and location of encoders and load pins.

Table A.1 – Arm link parameters of interest.

Link	Boom	Stick	Bucket
Piston rod diameter (mm)	30	30	30
Cylinder head diameter (mm)	55	50	50
Piston stroke (mm)	354	442	385
Estimated link+cylinder assembly (kg)	71	42	35
Link length (mm)	1730	930	545
Centre of mass position X (mm)	795	368	207
Centre of mass position Y (mm)	226	67	132
Estimated moment of inertia I_{zz} (kg·m ²)	47.94	5.58	2.21

the XY forces acting at the bucket joint and L2 measures the force at the cylinder. Those three measurements can be used to monitor the force and moment acting on the bucket, allowing measurement of the Cartesian forces at the bucket tip.

A general schematics of the whole system is shown in Figure A.2. The user access the system using a laptop running MATLAB®. A 3D mouse allows open-loop control of up to four servo-valves simultaneously. Measurement from the load pins are provided

by a data acquisition board connected to the laptop through (asynchronous, non-real time) USB communication. The load pins are used for monitoring purposes, and were not used to provide feedback signals.

The laptop is connected to the closed-loop real-time controller using Ethernet communication. The controller is executed on a conventional desktop PC running a MATLAB® xPC target, where core routines such as forward and inverse kinematics and inverse dynamics were coded in the C language and pre-compiled for efficiency. The real-time controller communicates via controller area network (CAN) bus to a series of Moog M2000 PLC's mounted in an isolated enclosure that is located on the top of the excavator.

The same enclosure also contains additional safety cards designed during the late 1990's by previous staff at the ACFR. The safety cards control the signals A, B, C, and D indicated by the arrows in Figure A.2, which are activated by a radio emergency stop circuit. The command A re-directs flow to discharge at the tank, de-pressurising the accumulator and hydraulic supply lines. Signal B locks all joints, C disables the servo-valves returning the spools to their spring-centred positions, and D stops the diesel engine.

In normal operation the diesel engine drives a pump at maximum rotation (2000 RPM) which pressurises the hydraulic circuit. The pump charges the accumulator which is shared by all servo-valve units. Some values of interest are given in Table A.2.

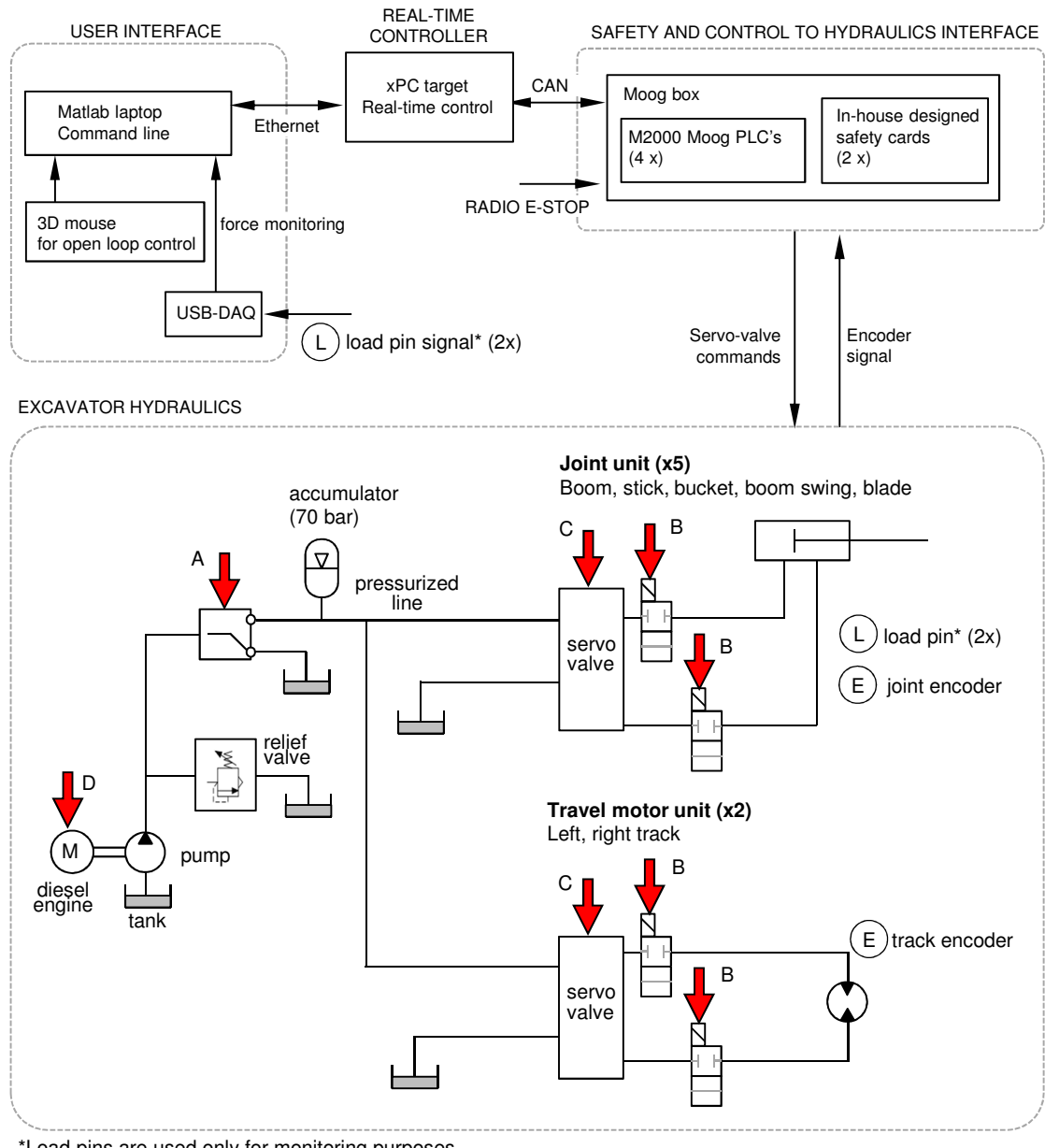


Figure A.2 – General schematic of the robotic excavator control and hydraulic systems.

Table A.2 – Experimental platform values of interest.

Parameter	Value/Description
Engine power	9.7 kW (13 horsepower)
Maximum travel speed	1.8 km/h
Estimated arm mass after retrofit	150 kg
Effective bulk modulus of oil	100 MPa
Maximum pump flow	Two at 11.9 l/min at 2000 RPM
Relief valve setting	18.6 MPa
Accumulator pre-charge	7 MPa
Encoders	Absolute 12 bit resolution
XY Load pins	Two at ± 3.0 tonne
Servo-valves	Moog D633
Real-time feedback controller	MATLAB® xPC target, 100 Hz (quad-core 3 GHz)
PLC CAN/actuator interface	Moog M2000, 100 Hz
CAN bus	250 kbit/s